OPTIMIZATION OF THE PRODUCTION OF CARBON NANOTUBE YARNS IN A CONTINUOUS CHEMICAL VAPOUR DEPOSITION AND APPLICATION IN INCANDESCENT BULB

Ezinne Igbokwe

A thesis submitted to the School of Chemical and Metallurgical Engineering, Faculty of Engineering and the Built Environment, University of the Witwatersrand, in fulfilment of the requirements for the degree of Doctor of Philosophy

September 2020

DECLARATION

I declare that this thesis is my own unaided work. It is being submitted for the Degree of Doctor of Philosophy in the University of the Witwatersrand, Johannesburg. It has not been submitted before for any degree or examination to any other university.

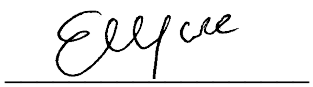

(Signature of Candidate) 24 day of September 2020

ABSTRACT

Incandescent light bulb technology in its current state is an embodiment of inefficient use of energy resources. Visible light is emitted from the tungsten wire used as filament in the incandescent bulb when it is heated to high temperatures by electrical energy. Less than 10% of the energy applied reaches the visible light wavelength. Most of the energy is radiated away in the infrared (IR) wavelength. To retain the incandescent light bulb technology, a new material with a high melting point, low vapour pressure, and the ability to radiate more in the visible light wavelength is required. Prospects of using carbon nanotubes (CNTs) as a replacement for tungsten filament in incandescent bulbs have inspired lots of research on the field emission properties of carbon nanotubes. However, a widespread application of CNTs in the macroscale has been limited because of the challenge involved in transferring its properties in the nanosize to the macroscale. The exciting prospect for the production of macroscopic CNT yarn in a continuous chemical vapour deposition (CVD) process for application in advanced technology is the focus of this study.

In this study, low-cost synthesis of spinnable CNT aerosol from methane carbon source and ferrocene catalyst in a floating catalyst chemical vapour deposition (FC-CVD) is presented. The direct spinning of as-synthesized CNT aerosol in the reactor system is used to produce macroscopic CNT yarn for application as a filament in incandescent light bulbs. The quality and quantity of CNT aerosol produced are influenced by many factors. A basic understanding of how these factors affect the quality and quantity of CNT yarns produced is an essential tool for the optimization of CNT yarn production. Statistical Design of Experiments was used to design and carry out experiments varying seven factors in two steps. From the experimental data, quadratic regression models were developed to explain the effect of synthesis conditions on the amount of CNTs produced (quantity) and oxidation temperature (quality). Consequently, optimal synthesis

parameters for the production of CNT yarns with a direct spinning system were determined. CNT yarns synthesized under the optimal conditions resulted in 3.23 g mass of CNTs produced with oxidation temperature of 438.26 °C.

Hydrogen co-feeding in CNTs synthesis from methane carbon source rarely considers the effect of the partial pressure of hydrogen, discounting it as insignificant in kinetic modelling. Therefore, to date, there is no derived kinetic model for the synthesis of CNT using methane as the carbon source with hydrogen co-feeding in an ideal plug flow reactor. In this study, the initial rate of decomposition of methane was derived as follows: $-\mathrm{r}_{CH_{4.0}} = \frac{6.475*10^{-2}e^{\left(-\frac{7330.99}{T}\right)}P_{CH_4}}{1+\sqrt{(1.28P_{H_2})}}$, where the catalytic decomposition of methane is the rate-limiting step. This indicates that an increase in the feed rate of hydrogen reduces the rate of reaction while an increase in the feed rate of methane increases the rate of formation of CNTs. The effect of temperature on the rate of reaction was obtained using Arrhenius and Eyring equations.

This study also investigated the light-emitting capacity and the mechanical properties of as-synthesized CNT yarns. It was established in this study that multi-walled CNTs were predominantly synthesized in the FCCVD system at the optimum conditions with an I_D/I_G ratio of about 0.3. A comparative study of the light emission capacities of the CNT yarn against commercial 60-Watt tungsten filament in an argon environment showed CNT yarns onset voltage to be twice lower, and the power consumption was about 5 times lower in CNT yarn. Consequently, as-synthesized CNT yarn from methane with Hydrogen co-feeding using ferrocene catalyst in a floating catalyst chemical vapour deposition reactor with direct spinning could be considered a viable blackbody material for replacement of tungsten filament in incandescent bulbs with high energy efficiency.

DEDICATION

To my Lord Jesus Christ whose love towards me is immeasurable.

To my parents, Jonathan and Chidinma Igbokwe

ACKNOWLEDGMENTS

I would like to take this opportunity to express my token of appreciation to the people who have helped me throughout this endeavour.

First, my gratitude goes to my supervisor Prof M. O. Daramola for his support, valued experience and motivations during this study.

Prof S. E. Iyuke, my co-supervisor for the technical expertise and set-up of the Swirled Floating Catalyst Chemical Vapour Deposition (SFC-CVD) reactor.

I would like to express my gratitude to the staff and students from the school of Chemical and Metallurgical Engineering, past and present, for the establishment of an enjoyable working environment. Special thank you is reserved for the workshop staff of the school, particularly Hopewell, for the construction and continued maintenance of the reactor for the duration of this study. Also, my thank goes to Motlatsi, Janet, Petra, and Letta for assistance with laboratory testing. Appreciation is expressed to the SEERU research group particularly Ugo Ikegwu and my laboratory "partner" Mr Thomas for their constructive criticism of this work throughout this study. To my office mates throughout my study for maintaining a conducive atmosphere for resourcefulness, I say a hearty thank you.

Sincere acknowledgements to Dr Rudolph Erasmus from the School of Physics for help with application studies and Raman Spectroscopy characterization of the samples. Thanks to the WITS Microscopy and Microanalysis Unit (MMU) for help with TEM characterization of the samples and to members Prof Bhattacharyya laboratory in the School of Physics for conductivity measurements.

Over and above, I recognise the financial support provided by the University of the Witwatersrand through the Postgraduate Merit Award (PMA) and National Research Fund (NRF), South Africa through the grant No: NRFCPRR106053.

I would not have been able to achieve this goal without the love and support of my family and friends. Special gratitude is expressed to my friends Saheed, Tina, Emem and Didi who stuck to me closer than a brother, you believed in me and showed it when and how it mattered most. To my sister and her husband who believed in me and has been one of my greatest fans, I bare my heart of gratitude. Last but most critical, I express my deepest thanks to my indefatigable admirers, my parents, Jonathan and Chidinma Igbokwe for the encouragements, prayers and understanding they have provided throughout my career. Your belief in me is such a source of strength for my journey thus far. I love you.

LIST OF REFEREED PUBLICATIONS

A list of publications in refereed journals and conferences is provided below. Copies of these publications are in Appendix C.

Igbokwe, E. C., Daramola, M. O., & Iyuke, S. E. (2019). Production of carbon nanotube yarns via floating catalyst chemical vapour deposition: Effect of synthesis temperature on electrical conductivity. *Results in Physics*, *15*, 1–7. https://doi.org/10.1016/j.rinp.2019.102705

Mahagani, N., **Igbokwe, E.,** Aberefa, O., Bodiba, V., Daramola, M. O., & Iyuke, S. E. (2019). Production of CNT Yarns from Methane Gas for Use as Filaments in Incandescent Bulbs: Thermodynamic Properties of As-spun CNT Yarns, *Journal of Physics: Conference Series 1378*, (2), p. 1-11.

Bodiba, V., **Igbokwe, E**., Mahangani, N., Aberefa, O., Daramola, M. O., & Iyuke, S. E. (2018). Production of CNT yarns for use as filaments in incandescent bulb: effect of carbon source and state of catalyst on the production of CNT. *IOP Conference Series: Materials Science and Engineering*, *413*(1), 1–7. https://doi.org/10.1088/1757-899X/413/1/012027

PRESENTATIONS AT CONFERENCES AND SEMINARS

Date	Name	Venue	Type
July 9 – 13, 2018	2nd International Conference on Engineering for Sustainable World (ICESW 2018)	Centre for Entrepreneurial Studies, Covenant University, Canaan Land, Ota, Nigeria	Paper
Aug 28, 2018	School of Chemical and Metallurgical Engineering Poster Day	University of the Witwatersrand	Poster
Oct 29 – 30 2018	9th Wits Cross-Faculty Post Graduate Symposium (Awarded 3rd prize in Faculty of Engineering and Built Environment)	University of the Witwatersrand	Flash Talk
July 3rd – 8th, 2019	3rd International Conference on Engineering for a Sustainable World ICESW 2019	Centre for Entrepreneurial Studies, Covenant University, Canaan Land, Ota, Nigeria	Paper
29 August 2019	School of Chemical and Metallurgical Engineering Poster Day	University of the Witwatersrand	Poster
3 – 4 Sept 2019	10th Wits Cross-Faculty Post Graduate Symposium	University of the Witwatersrand	Oral

TABLE OF CONTENT

LIST OF FIGURES

LIST OF TABLE

NOMENCLATURE

AC – alternating current

ANOVA – analysis of variance

BBD – box-Behnken design

CCD – central composite design

CNT/s – carbon nanotube/s

COST – change one separate factor per time

CVD – chemical vapour deposition

DC – direct current

DoE – design of experiment

DWCNT/s – double-walled carbon nanotube/s

FCCD – face centred composite design

FC-CVD – floating catalyst chemical vapour deposition

FID – flame ionization detector

GC – gas chromatography

HAZOP – Hazard and Operability

HiPCO – high-pressure catalytic decomposition

ID – internal diameter

LED – Light-emitting diodes

MWCNT/s – multi-walled carbon nanotube/s

OD – outer diameter

PECVD – plasma-enhanced chemical vapour deposition

PPE – personal protective equipment

RBM – radial breathing mode

RSM – Response surface methodology

SEM – Scanning electron microscopy

SWCNT/s – single-walled carbon nanotube/s

TCD – thermal conductivity detector

TEM – transmission electron microscope

TGA – thermo-gravimetric analysis

VACNTs – vertically aligned carbon nanotubes

VLS – vapour-liquid-solid

XRD – x-ray diffractometry

CHAPTER ONE

1. INTRODUCTION

1.1 Background and Motivation

Clean energy, responsible consumption and production, and industry innovation are part of the 17 Sustainable Development Goals (SDG) adopted by The United Nations (UN) member states in 2015 in a bid to eradicate poverty and ensure sustainability. Inefficient consumption in the energy sector has been a grave concern to various governments leading to the enactment of various acts like The United States of America (USA) ‘‘Energy Independence and Security Act of 2007’’. One of the missions of this Act is to improve the energy efficiency of products, specifically, all light bulbs are required to have a minimum of 25% efficiency between 2012 and 2014 and subsequently to have a 200% increase in efficiency of all light bulbs by 2020 (*Energy Information and Security Act of 2007*). The European Union (EU) Commission on another hand adopted a regulation in 2008 to phase out the conventional tungsten filament incandescent bulbs for households between 2009 and 2012 (“FAQ : phasing out conventional incandescent bulbs,” 2009). Africa was not left out as South Africa announced phase-out of conventional incandescent bulbs during a 2011 UN climate summit in Durban with a 2016 timeline for implementation (SAinfo & BuaNews, 2011). This phase-out became necessary as tungsten incandescent bulb is highly inefficient. It converts only about 10% of energy transmitted to it into visible light with the rest wasted as heat and infra-red (IR) radiation (Jacob, 2009; Lunk, 2015; Macisaac et al., 1999). Therefore the development of more efficient materials for use in the incandescent technology could significantly check the energy inefficiency in consumption and also reduce emissions.

The incandescent light bulb is the first commercialized light bulb in 1880 by Thomas Edison after getting a patent on it in 1879 (Matulka & Wood, 2013). It uses a very simple technology that has served humanity for over 120 years. It has become very ineffective with the exponential rise in energy consumption and global awareness on emissions. Various materials have been used as filament in incandescent light bulbs to improve energy efficiency and durability including carbon wire, osmium, tantalum and tungsten (Bowers, 2011; Lunk, 2015). Tungsten has been the most widely used because of its superior efficiency. However, its energy efficiency is lower than acceptable standards. Meanwhile, other lighting technologies have been developed including florescent lighting, and light-emitting diodes (LED). They, however, have a low quality of light and are produced from toxic materials that require special handling for disposal making the incandescent light bulb technology most desirable (Lim et al., 2013; Schleich et al., 2014). The effort to improve the widespread use of LED in South Africa is impeded by the high initial cost implications and variations in the efficacy of the products available in the market (Walsh et al., 2019).

In recent times, interest in the development of new materials to improve the energy efficiency of incandescent light bulbs has increased. Advantages of conventional incandescent bulbs include the low initial cost of production, simple technology, limited ultraviolet light produced, has wide light spectra, and good light colour performance (Cho et al., 2017; Macisaac et al., 1999). Given these advantages, it is critical to avoid the total phase-out of the incandescent light bulb technology. This research, therefore, seeks to develop a more energy-efficient material (CNT yarn) to replace tungsten filament in incandescent bulbs by valorising methane - a greenhouse gas, using a simple synthesis method.

With the advent of nanotechnology and the rediscovery of carbon nanotube, CNTs is being widely researched as the potential material to replace tungsten filament in incandescent bulbs (Jiang et al., 2004; Sharma & Kar, 2014; Wei et al., 2006). Carbon nanotubes are described as seamless cylinders of rolled-up graphene sheets (hexagonal arrangements of hybridized carbon atoms) with diameters in the nanoscale and approximate length to diameter ratio of 28,000,000:1 (Holban et al., 2016; Iijima, 1991). Their electrical conductivity and thermal conductivity are higher than that of copper (Alvarenga et al., 2010; Ebbesen et al., 1996; Wang et al., 2009), the tensile strength of about 150 Gpa and Young's modulus of over 1 Tpa (Peng et al., 2008; Wei et al., 2009; Yu et al., 2013). These make them applicable in electronics, hydrogen storage and fuel cells among others (Alvarez et al., 2019; De Volder et al., 2013; Peng et al., 2008).

A challenge to the widespread application of CNTs in electrical wiring in general and filament, in particular, is their nanosize. A long array of individual nanotubes is required to carry out spinning into its macroscopic size. The aspect ratio of CNTs is influenced by the carbon source, catalyst type and synthesis method (Bodiba et al., 2018; Moisala et al., 2006). In this research, methane gas was preferred over other hydrocarbons for two reasons. Firstly, methane gas was used as the carbon source in this research to valorise it. It is a greenhouse gas generally considered to be more dangerous than carbon dioxide. It is highly unreactive in the atmosphere therefore it is long-lived (Haskin & Edwards, 2013). Application of methane as the carbon source in this research provides a new avenue to drive the economic and political resolve to reduce gas flaring, thereby reducing the consequent pollution from its flaring. Secondly, it gave a better quality CNTs with a higher aspect ratio than acetylene (Bodiba et al., 2018). It is easier to handle than very toxic xylene which has been by other researchers for a similar application (Wei et al., 2006).

Spinnable CNT array or aerosol can be produced from methane gas using laser ablation, arc discharge and chemical vapour deposition (Aguiar-Hualde et al., 2017; Hou et al., 2001; Muñoz et al., 2000). Laser ablation and arc discharge are very expensive methods because of the high cost of generating laser and the high purity metal required as a source of electrodes (Agboola et al., 2007; Salvetat et al., 1999). Thermal catalytic CVD is found to be the cheapest technology for the production of high-performance CNTs (Mohammed et al., 2017; Prasek et al., 2011).

CNTs growth in a CVD is a chemical process consisting of the dissociation of carbon source, diffusion of carbon on the surface of the catalyst particle and the rate of nucleation (Iyuke & Simate, 2011). The delicate balance of the dissociation of carbon source, diffusion of carbon on the surface of the catalyst particle and the rate of nucleation control the growth mechanism of CNTs in a CVD (Yu et al., 2005). Temperatures in the system, the flow rates and concentration of the carbon source and catalyst are some of the parameters that influence the growth mechanism and the achievement of spinnable arrays (Jourdain & Bichara, 2013; Kukovecz et al., 2005; Lee et al., 2016). Statistical models were developed in this study to understand the main effect and the interactive effect of these parameters on the production of CNT yarn for a predetermined application. These models can be used to predict the synthesis parameters for CNT yarn production knowing the desired properties.

The assembly of spinnable CNT array or aerosol can be achieved by wet spinning or dry spinning (Behabtu et al., 2013; Hou et al., 2016). Wet spinning involves the dissolution of synthesized CNTs in a solvent, drawing and spinning the CNTs then evaporating the solvent causing additional costs for solvent and solvent removal. The solvent residue is left on the spun CNTs and adversely affects the properties (Behabtu et al., 2013). Dry spinning draws CNTs from an array of spinnable CNTs or directly from spinnable CNTs aerosol via the van der Waal attractions that exist between the

CNTs (Sundaram & Windle, 2017; Wang, 2014). Direct spinning into CNT yarn requires the synthesis of CNTs on a catalyst without catalyst support. The direct spinning of CNT aerosol was used in this research to produce CNT yarn thereby eliminating extra cost attached to post-production wet or dry spinning.

Catalyst type has various effects on the synthesis system for the production of CNTs (Moisala et al., 2003; Tripathi et al., 2017). Iron-based catalyst is found to be the cheapest and most effective of the three most common metal particles (Ni, Co and Fe) (Dasgupta et al., 2008; Ramirez et al., 2014). The state of catalyst is found to influence the quality of CNTs produced (Bodiba et al., 2018; Moisala et al., 2006). Ferrocene was chosen as the source of iron catalyst nanoparticle over the liquid iron pentacarbonyl and dissolved ferrocene because liquid catalyst decomposes quickly and dissipates faster, producing excessive catalyst nanoparticles resulting in short CNTs, therefore, are not adequate for continuous production of spinnable aerosol (Kuo et al., 2006; Moisala et al., 2006).

There is a strong need to develop theoretical and practical techniques for large scale production of macroscopic CNTs such as yarns and sheets with properties similar to the individual CNTs from which they are produced. High-quality CNTs using the CVD technique can be achieved (Aguiar-Hualde et al., 2017). The optimal parameters for the synthesis of CNTs with predetermined properties are not known yet (Bonadiman et al., 2006). However, kinetic and statistical models obtained from this research offer some understanding of the influence of various parameters on the CNTs quantity of CNTs produced and quality for predefined application and the CNTs growth mechanism. This is necessary for selecting the synthesis conditions for predetermined applications.

Given the above-detailed, floating catalyst CVD reactor was appropriate for the synthesis of spinnable CNT aerosol in this research. The synthesis of aerosol ensures the use of a direct spinning method for the assembly of CNTs to produce macroscopic CNTs. Floating catalyst chemical vapour deposition (FCCVD) reactor used in this research was developed in the University of the Witwatersrand. It was assembled and maintained by the School of Chemical and Metallurgical Engineering workshop providing an avenue for the application of purely African solution to global problems. Application of CNT yarn produced from FCCVD with direct spinning as a filament in incandescent bulbs without the necessity of post-production purification of CNTs for application in incandescent light bulbs significantly reduces the cost of production. Industries derived from this research will create jobs in a wide range of qualifications.

1.2 Statement of Research Problem

Consequent to the background and motivation, the objective of this research is to optimise the production of carbon nanotubes in an FCCVD system with direct spinning into macroscopic yarns for application as a filament in incandescent bulbs using methane as carbon source and ferrocene as a catalyst. Factors considered as influential to the growth mechanism of CNTs and their assembly into yarns were synthesis temperature, carbon source (methane) volumetric flow rate, carrier gas (argon and hydrogen) volumetric flow rates, promoter (thiophene) volume and catalyst vaporizer (ferrocene) temperature and the spinning rate.

1.3 Research Hypothesis

Therefore this research explored the development of a predictive model for the performance of the FCCVD reactor with the integration of the production of carbon nanotube aerogels and post-production spinning into macroscopic yarns with a view to its suitability as a filament in

incandescent bulbs. This is based on the premise that: i.) Statistical methods can be used to predict the quantity of CNTs produced and general quality of CNT yarns synthesized in an FCCVD reactor with direct spinning; ii.) Under optimal conditions, a spinnable array of CNTs is contained in the produced aerosol with a minimal amount of catalyst and carbonaceous residues; iii.) Adequate van der Waal attraction exists between the CNTs in the produced aerosol to cause desired assemblies forming macroscopic yarns with suitable strength and electron transferability.

1.4 Research Questions

To investigate these premises, the following research questions were posed and probed:

a) What are the main and interactive effects of the process conditions (temperature, methane volumetric feed rate, carrier gas feed rate, and spinning rates) on the quantity and quality of the CNT yarns produced in an FCCVD reactor using methane as carbon source and ferrocene as a catalyst?
b) What is the effect of synthesis temperature and hydrogen flow rates on the electrical conductivity of as-spun CNT yarns?
c) Can the production of CNTs using optimized conditions obtained in a) be explained with suitable kinetic models?
d) Can the produced CNT yarns using optimized conditions be suitable as a filament in the incandescent bulb?

1.5 Research Aim and Objectives

Experimental work is necessary to develop an understanding of how various factors influence the quality and quantity of CNT yarns produced in a CVD reactor. Analysis of the data obtained will define the optimum parameters required for the scale-up production of CNT yarns suitable for a pre-determined application. Therefore, the main objectives of this study are:

a) Optimize the process parameters of CNT yarns production in an FCCVD using 2^n factorial design to investigate the influence of synthesis conditions on the yield of CNTs;
b) Characterize and evaluate the performance of the effect of synthesis temperature and hydrogen flow rates on the electrical conductivity of as-spun CNT yarns;
c) Develop a kinetic model to understand the rates and mechanism of the formation of CNT aerogel and yarn in the FCCVD reactor using methane carbon source with Hydrogen co-feeding and ferrocene catalyst;
d) Assess as-synthesized and as-spun CNT yarns as a replacement for tungsten filament in incandescent bulbs.

1.6 Contribution to Knowledge

a) Establish the suitability of CNT yarn and understand the limitations and weak points that reduce its competence as incandescent bulbs filament;
b) Optimization of CNT yarn production in an FCCVD for incandescent bulb filament application;
c) Kinetic model for the synthesis of CNTs from methane with hydrogen co-feeding;
d) Proof of concept for the use of CNT yarns produced in a CVD by direct spinning as a filament for the incandescent bulb.

1.7 Thesis Outline

Chapter One covers the introduction to the thesis clarifying the background and motivation for the study. The hypotheses, aim and objectives of the study were also elucidated.

Chapter Two discusses the properties of materials used in incandescent light bulb technology and a review of literature on carbon nanotube synthesis methods and the effect of various parameters

on the quality and quantity of CNTs produced to tailor these properties to predetermined application.

Chapter Three details the experimental procedure of an FCCVD reactor set up devised for the synthesis of CNT aerosol with direct spinning into CNT yarns. Analytical techniques used to understand the qualities of samples in this study were described.

Chapter Four presents the statistical procedures used to understand the influences of operating variables on the synthesis of CNT yarn for application as a filament in incandescent light bulbs. Response surface methodology (RSM) was used to empirically optimize the synthesis of CNT yarns in an FCCVD reactor with direct spinning. The proposed regression model described the influence of the main and interactive effects of the synthesis conditions on the quantity of CNTs produced and oxidation temperatures of as-synthesized CNT yarns for application as a filament in incandescent light bulbs.

Chapter Five delves into the detailed study of the effect of synthesis parameters (synthesis temperature and hydrogen volumetric feed rate) on electrical properties of as-synthesized CNT yarns to compare it to the property of tungsten filament in the incandescent light bulb.

Chapter Six reports on a kinetic model developed for the production of CNTs from methane gas with hydrogen co-feeding to create an understanding of the collaborative effect of species in the FCCVD reactor production of CNTs.

Chapter Seven studies the mechanical properties of as-synthesized CNT yarns and compares the light emission of as-synthesized CNT yarn produced under the optimal conditions to commercial filament from 60 W incandescent light bulb.

Chapter Eight draws the conclusions of the findings in this research and recommendations for future research work.

CHAPTER TWO

2. LITERATURE REVIEW

2.1 Incandescent light bulb technology

Incandescent lamp technology was first invented early 19th century (Bowers, 2011; Chen & Murray, 1980). By definition and principle, incandescent light bulbs produce light by heating up thin conducting filament when an electric current is passed through it until it glows. Incandescent bulbs are the second commercial light source which quickly replaced the commercial oil lamps (Guarnieri, 2015). Various materials have been used in the manufacture of incandescent light bulbs since the invention of the technology. Improvements in the efficiency of incandescent bulbs were achieved with each material.

Tungsten was first used in the incandescent light bulb in 1904 (Chen & Murray, 1980; Guarnieri, 2015). It converts less than 10% of the electrical energy applied to it into light with the rest lost as heat (Macisaac et al., 1999). With the rising social and economic cost of energy and the development of more energy-efficient light bulbs, various governments of the world initiated a phase-out and outright ban of traditional tungsten incandescent bulbs. However, Harris (2009) and Lavelle (2014) documented significant resistance to these bans. They associated this with the advantages of incandescent light bulb technology (Harris, 2009; Lavelle, 2014) including their cheap and ease of manufacture, ease of disposal since it does not contain any toxic materials, has good colour rendering index, is tuneable, and compatible with alternating current (AC) and direct current (DC).

2.2 Materials for incandescent light bulbs

Various materials with incandescent properties have been employed over the 200-year history of incandescent technology (Bowers, 2011; Lunk, 2015). High melting point is one of the fundamental properties of materials used in incandescent bulbs because they operate by heating up the materials to high temperatures (Li et al., 2007). High vapour pressure of carbon filament led to blackening of the glass globe/flask which made carbon inadequate although it has a higher melting point (Bowers, 2011). Ductility of the filament was another important property. Platinum and iridium were one of the first materials used and later carbon threads and bamboos. Platinum was plagued with blackening of the bulbs and platinum was expensive. In 1879, Edison successfully created incandescent light bulbs using carbonized threads in a vacuum which lasted for up to 600 hours of lightening (Chen & Murray, 1980; Guarnieri, 2015). Widagdo (2006) reports a 100% increase in lamp efficiency when tungsten filament incandescent bulb when it was first developed in 1904. This improvement capped at about 10% of the electrical energy passed to the tungsten filament is converted to light and 90% lost as heat (Macisaac et al., 1999). Carbon thread is very brittle but Tungsten flexibility was achieved for by alloying at a low temperature making it more preferable to carbon (Lunk, 2015). The properties of the three main materials used for the commercial production of an incandescent light bulb are presented in Table 2.1.

Table 2.1. Comparison of the properties of materials used as filaments in commercial production of incandescent light bulbs

Property	**Tantalum**	**Carbon**	**Tungsten**
Melting point °C	2900	3500	3410
Thermal coefficient of expansion (/K)	6.5	2 – 6	4.3
Resistivity at 20 °C (μΩ-cm)	12.4	1000 – 7000	5.65
Temperature coefficient of resistance at 20 °C, (/°C)	0.0036	0.0002 – 0.0008	0.005
Specific gravity gm/cm^3	16.6	2.1	20
Luminescence efficiency (Lumens per watts)	3.6	4.5	12

Light generation by an incandescent body occurs by electrical heating of the material to high temperatures (Li et al., 2007). High light output is achieved at high temperature moving the radiation of the body from infra-red wavelength to visible light wavelength (400 – 800 nm) without melting the incandescent materials (Macisaac et al., 1999). The spectrum produced by incandescent materials is comparable to that of the sun though they are produced at a much lower temperature than the sun (Lunk, 2015). High-temperature radiation ensures blue light dominates (Zhao et al., 2005). Therefore materials with high melting points are required as incandescent materials. Incandescent materials with a higher melting point will ensure almost all the electrical energy inputted will be converted to light by shifting from lower wavelength to high visible

wavelength reducing to minimal the losses via convection and conduction. Individual SWCNT has been produced with a high melting point higher than that of tungsten (Wei et al., 2011) therefore, its application as a material for incandescent bulb lightning is explored.

2.3 Carbon nanotubes as material for incandescent light bulb

Tungsten filament used in incandescent light bulbs is inefficient and does not meet the standards therefore it has been phased-out for household lighting. The excellent mechanical electrical and mechanical properties of CNTs have made it a plausible replacement for incandescent bulb filament. The emission of light from individual and macroscopic CNTs (SWCNT, DWCNT and MWCNT) has been reported and some are presented in Table 2.2. Macroscopic CNTs reported thus far are either spun via wet spinning or from CNTs forest on a substrate. A cost-effective and continuous process like the FCCVD method with direct spinning used in this study offers enormous potential for transferring the properties of individual CNTs into macro-scale CNTs applicable as a filament in an incandescent light bulb. FCCVD process being a continuous one-step, homogenous gas phase process for bridging the gap between generating nano- and macro-scale CNTs material has made it the most attractive as an industrially scalable route.

Carbon nanotubes (CNTs) are unique nanostructures, with their diameter in the nano-dimension and length up to a few millimetres. Their outstanding electrical, mechanical and thermal properties (Fan et al., 1999; Li et al., 2005; Ren et al., 1998) have elicited great interest from researchers following its rediscovery in 1991 by Iijima (Iijima, 1991). Carbon nanotubes are made of effectively rolled-up graphene sheets therefore they derived their high mechanical properties from graphene. Like single, double or multi graphene sheets, they form single-walled, double-walled, or multi-walled carbon nanotubes respectively. They also consist mostly of the sp^2 carbon bonding

structure and are held by Van der Waals forces like the graphene sheets hold parallel to each other. Unlike graphene and courtesy of the rolled-up structure, carbon nanotubes form further three in-plane sigma (σ) bonds and an out of plane pi (π) bond perpendicular to the curved plane (Figure 2.1) causing them to have higher mechanical, electrical and thermal conductivities than graphene as well as more chemically stable (Meyyappan, 2004).

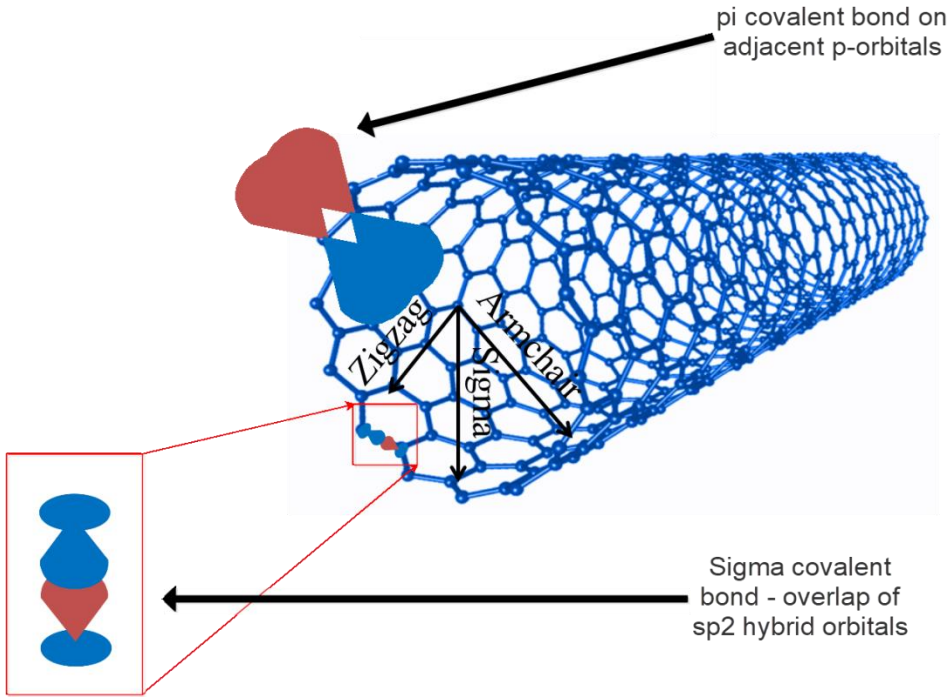

Figure 2.1 Bonding structures and chirality of carbon nanotubes adapted from (Meyyappan, 2004; Yu et al., 2013)

The curvature of the graphene sheet into CNTs could occur on the permitted wave vector directions or shift by a bandgap resulting in CNTs with different chirality (Kane & Mele, 1997). This is identified in single-walled carbon nanotubes (SWCNT). Depending on chirality, SWCNT can be metallic or non-metallic. Armchair chiral SWCNT are categorized as metallic while the zigzag and chiral as semiconductors.

Electrical and thermal properties of SWCNTs are dependent on chirality. MWCNT with usually larger outer diameter than SWCNT generally has a behaviour like metallic and semi-metallic conductors (Christen et al., 2004). There are strong indications that the electronic, thermal and mechanical properties depend on chirality and diameter of nanotubes (Collins & Avouris, 2002; Kim et al., 2001; Petit & Loiseau, 2003; Salvetat-delmotte & Rubio, 2002). Electrical conductivity has been observed to occur at room temperature in CNTs (Kociak et al., 2001; Tang et al., 2001). Electronic transport through metallic CNTs occurs without generation of heat due to the ballistic nature of transport throughout the 1D structure (Frank et al., 1998; Liang et al., 2001).

CNTs are, therefore, attractive for application as replacement of tungsten wire in incandescent bulbs. Some of the properties that make CNTs a potential for the replacement of tungsten in incandescent light bulb include a high melting point up to 3400 K (Wei et al., 2011), the high tensile strength of millimetre long CNTs averaging 0.85 Gpa, and Young's modulus approximately 34.65 Gpa (Kim et al., 2017) and low room temperature resistivity for SWCNT of about 10^{-6} Ω/cm and MWCNT of about 5.10^{-6} Ω/cm (Chiodarelli et al., 2011; Lekawa-Raus et al., 2014; Reich et al., 2008) have made it a potential target to replace tungsten filament in incandescent light bulbs. The resistance of MWCNT is found to decrease with an increase in temperature at low temperatures. Further increases above room temperature results in an increase in resistance this is consistent with the characteristics of tungsten (Lekawa-Raus et al., 2014; Zhao et al., 2011). A wide range of conductivities from 10000 S/cm to 67000 S/cm is reported due to the ranging purity of as-synthesized CNTs (Vigolo et al., 2000; Zhao et al., 2011). The vapour pressure of carbon nanotube is reported to be lower than that of tungsten (Li et al., 2003).

Carbon nanotubes have been shown to emit light when excited by both electric current and laser beams (Liu et al., 2009; Yeong & Thong, 2004). In light of these, diverse research has been carried

out to determine the properties of CNTs as incandescent light emitter. Table 2.2 presents some of these researches on both individual and macroscopic CNTs with emissions in a vacuum and in inert (argon) gas. Emissions at various onset voltages were observed from nanotubes produced from various production methods including the macroscopic types in various environments.

One of the major limitations for the application of CNTs as a filament in an incandescent bulb is the difficulty in extrapolating the excellent properties of individual nanotubes into the macro-scale material (Jourdain & Bichara, 2013). Ability to produce CNTs with identical properties under the same condition in varied batches is another challenge. Slight changes in the synthesis conditions significantly alter the quality of the CNTs produced (Dai, 2002). This research seeks to contribute to resolving these challenges.

Table 2.2 Some reported previous research on various carbon nanotubes applied as light illuminating materials, their method of production, and their operating environments

Nanotube type	**Post-production**	**Onset voltage, V**	**Illuminating Environment**	**References**
DWCNT Films	Densified in H_2O_2 and HCl	-	Vacuum	(Li et al., 2007)
CNTs coated carbon fiber	CVD with Carbon Fibre substrate	4.5	Argon	(Sharma & Kar, 2014)
SWNT filament	Spun in alcohol	5	Vacuum	(Wei et al., 2004)
suspended individual SWNT	Individual	1.4	Argon	(Mann et al., 2007)
DWNT filament	Spun in alcohol	3	Vacuum	(Wei et al., 2004)
DWNT filament	Spun from ethanol	6	Vacuum	(Wei et al., 2006)
MWCNT bundles	Direct bundles	11	Vacuum	(Li et al., 2003)
MWCNT sheets	Densified in water	2.4	Vacuum	(Zhang et al., 2005)
on-substrate individual SWNTs	Individual	7	Argon	(Mann et al., 2007)
MWCNT thread	Direct spinning	3	Vacuum	(Jayasinghe, 2011)
MWCNT Yarn	Direct spinning		Argon	This work

2.4 Techniques for the production of carbon nanotubes

Techniques for the production of carbon nanotubes are generally based on three factors: energy input source, carbon source and catalyst nanoparticles. The first discovery of carbon nanotubes is still been debated. However, there was a spike in the interest of researchers at the "re-discovery" by Iijima in 1991 (Iijima, 1991). This has led to the unearthing of various methods used in the synthesis of varieties of carbon nanotubes including single-walled, double-walled, multi-walled and branched carbon nanotubes. These synthesis methods include arc discharge (Krasnikov et al., 2019), laser ablation (Batani et al., 2014), chemical vapour deposition (CVD) (Li et al., 2010; Xia et al., 2005), electrolytic (Novoselova et al., 2008), hydrothermal (Gogotsi et al., 2000), and template (Jeong et al., 2002). Of these, arc discharge, laser ablation and chemical vapour deposition (CVD) are the most frequently used. They require a carbon source and heat source with or without a catalyst to meet CNTs synthesis condition (See & Harris, 2007). The carbon products obtained by these methods have their merits and demerits and they differ in their growth dynamics.

2.4.1 Arc Discharge

Arc discharge technique involves the use of two high purity graphite rods as anode and electrodes. Applied current discharges sparks between the electrodes encapsulated in a noble gas atmosphere at high temperature. The arc discharged between the electrodes by the dissolution of the anode creates carbon vapour which deposits on the cathode as carbon nanotubes and other carbonaceous substances (Sharma et al., 2015). The presence of carbonaceous deposits alongside carbon nanotubes necessitates product purification. Synthesis of SWCNTs is most effectively realized by arc discharge technique (Keidar, 2007). However, the tubes tend to be short with random sizes and directions. The type of CNTs produced is dependent on the temperature, the inert gas used, catalyst and current applied (Das et al., 2016). The arc discharge is an intermittent synthesis process as it

requires periodic shutdowns to enable the collection of product and the replacement of the electrode which is a major drawback (Zeng et al., 2006). This method is further limited by its complicated heat exchange systems and the maintenance of a vacuum (Jahanshahi & Dehghani, 2013)

2.4.2 **Laser Ablation**

In laser ablation, gas is produced as a result of laser pulses impact on a carbon target, commonly graphite, to produce SWCNTs (Muñoz et al., 2000). The basic principle of the laser ablation method involves the use of a laser source in a quartz tube reaction chamber sealed to a pump at one end and mounted in a tube furnace. Required gas flow is passed from the other end. A target rod is placed at a 1200°C temperature zone focused on the laser source operating at 532 nm to 1064 nm wavelength (Das et al., 2016). Carbon species produced from the target rods by the laser power are swept and deposited in a collector downstream by the gas flow allowing for continuous synthesis. This method requires an expensive laser to set-up, operate, and maintain. The efficiency of this method is reduced due to laser energy loss in the breakdown or ionization of the medium before hitting the target (Hamad et al., 2016). Operating under vacuum, however, eliminates this laser energy loss but it is limited to a low absorption rate because of low collision frequency and small electron density (Zhao & Shin, 2013). Maser et al (2002), opines that to achieve economically viable production of CNTs the following aspects are desired: continuous production; cheaper feedstock materials; and a more efficient process for the preparation of the target materials.

2.4.3 **Chemical Vapour deposition**

Chemical Vapour Deposition (CVD) technique operates by decomposing molecules of gaseous or gasified carbon-containing compounds (acetylene, methane, carbon monoxide or coal) over a

catalyst at elevated temperature (Bodiba et al., 2018; Moothi et al., 2015). These reactive radical carbon molecules then diffuse and bond on the catalyst leading to the formation of CNTs (Simate et al., 2014). CVD synthesis can be CNTs grown on typically Ni, Fe or Co supported catalyst or floating catalyst (Bayat et al., 2016; Igbokwe et al., 2019).

Spinnable CNTs forest is successfully produced using a floating catalyst CVD method with ferrocene dissolved in cyclohexane which also served as a carbon source (Zhang et al., 2010; Zhang et al., 2007). The simplicity of the equipment and low catalyst preparation are the main advantages of the floating catalyst method.

Gas decomposition is achieved in the plasma-enhanced CVD (PECVD) by the use of plasma and lower temperatures for catalytic growth (Bouts et al., 2017). Growth temperature, the chemical composition of catalyst film, and plasma power were found to influence morphology and structure of CNTs produced using nanocomposite nickel/carbon catalyst.

High-pressure catalytic decomposition (HiPCO) process is a variant of CVD for the synthesis of SWNTs from pressurized CO carbon source (Agboola et al., 2007; Nikolaev et al., 1999). An organometallic catalyst precursor is introduced into the reactor in the gas phase for the HiPCO, metal clusters are formed as catalyst decomposes. The SWNTs nucleates and grows on the decomposed catalyst.

Thermal chemical vapour deposition (CVD) grown CNTs are industrially considered as the most practical process for the synthesis of carbon nanotube (Schauer & White, 2015). Catalyst is a very important factor in this technique. It is responsible for nucleation and growth acting as seed particle and determining nanomaterial size (Gao & Yuen, 2012; Jourdain & Bichara, 2013). Catalyst is responsible for the dissociation of the carbon-containing compound, diffusion surface for carbon,

and maintained interactions at the rim (Iyuke et al., 2007). The combination of the transformation of gaseous carbon precursor into solid on the surface of catalyst particle and dissociation of carbon precursor ensures a continuous synthesis in a catalytic CVD until saturation (Jourdain & Bichara, 2013).

A cost-effective and continuous process like the floating catalyst CVD method with direct spinning used in this study offers enormous potential for transferring the properties of individual CNTs into macro-scale CNTs applicable as a filament in the incandescent light bulb. FCCVD process being a continuous one-step, homogenous gas phase process for bridging the gap between generating nano- and macro-scale CNTs material has made it the most attractive as an industrially scalable route.

2.5 Carbon Nanotubes (CNTs) yarn fabrication methods

Carbon nanotube yarns are a macroscopic assembly of one-dimensional carbon nanotube with the main axis along the nanotubes pulling path possessing axial strength, high aspect ratio and radial flexibility. Miao et al (2010) opined that carbon nanotube yarns can be varied by the twist inserted during spinning causing a variation in the porosity of the yarn and this, subsequently, has an effect on the mechanical properties of the yarns produced. The electrical conductivity and mechanical properties of carbon nanotube yarns are expected to be influenced by porosity or relative density, and the number of the nanotube-to-nanotube contact as is in other sintered materials (Behabtu et al., 2008; Bradford & Bogdanovich, 2008; Zhang et al., 2007; Zhong et al., 2010).

Assembly of CNTs into macroscopic dimensions like yarns while retaining the properties of the nanotubes remains challenging. Various methods have been used to fabricate carbon nanotube yarns. They are categorized broadly into the wet-spinning process and dry-spinning process.

2.5.1 **Wet Spinning**

Wet spinning involves the dispersion of synthesized CNTs into solution, conversion into yarns through spinning and subsequent removal of solvent (Zhang et al., 2008). Wet spinning can also be achieved by dispersing in a melt, aligned by flow, spun into yarns while cooling (Vigolo et al., 2000). Although Liu et al., (2010) determined that CNT yarns processed by wet methods have high impurities due to residue of dispersant and as a result, which reduces the electrical and thermal conductivities, they recognise that it is also dependent on the category: surfactant-based coagulation spinning, liquid crystalline spinning and polymer dispersion spinning.

Surfactant-based coagulation spinning is utilized for spinning polymer-free nanotubes. In the earlier version of this method, a polyvinyl alcohol solution was utilized as the coagulation solution (Vigolo et al., 2000). Kozlov et al (2005) in developing polymer-free surfactant-based coagulation spun yarn from 0.6 wt% carbon nanotubes dissolved in 1.2 % aqueous solution of lithium dodecyl sulfate surfactant. This low viscosity dispersion was introduced via spinneret into a flocculation bath containing 37 % hydrochloric acid and rotating at 33 rpm. Gel fibres were formed immediately contact between the solution and flocculation fluid was established. The gel fibre was dried under tension after it was washed with methanol. The spun yarn is well aligned with a diameter of between 10–50 μm (Kozlov et al., 2005). The electrical conductivity of yarn obtained is higher than the polymer coagulated yarns with lower mechanical properties.

A liquid-crystalline phase is formed by the dispersion of carbon nanotube in the acid solution above certain concentrations (Song et al., 2003; Song & Windle, 2005). Long orientational order is observed in this phase. The microstructure of dispersed nanotubes is observed to be similar to the original nanotubes after evaporation. Zhang et al (2008) to avoid the adverse effects of

concentrated acids on nanotube yarns, formed liquid-crystalline dispersion with ethylene glycol. The concentrated dispersion was extruded through a spinneret and flowed to coagulation bath containing diethyl ether where the ethylene glycol is displaced from the surface of the nanotubes. The fibres are heat-treated at 280 °C to remove the remaining ethylene glycol. The nanotubes within the fibre are highly aligned (Zhang & Kumar, 2008). Liquid crystalline spun carbon nanotube yarns have higher electrical and mechanical properties than surfactant-based spun yarns. These properties are further improved when the nanotubes are pre-purified before dispersion and spinning (Tsentalovich et al., 2017).

Polymer dispersion spinning method is another method of spinning carbon nanotube yarns using polymers in the melt or dissolved form. Petroleum pitch matrix was the first polymer used for melt-spun SWCNT composite fibre (Andrews et al., 1999) with improved mechanical and electrical properties at 1 % and 5 % nanotube loadings. Haggenmueller et al (2000) found yield strength and elastic modulus increased with increase in nanotube loading and draw ratio for nanocomposite of poly(methyl methacrylate) and SWCNT spun by a combination of casting and mixing methods. Excellent electrical properties and improvements were found consistent with the alignment of nanotubes in spun fibre (Haggenmueller et al., 2000).

2.5.2 **Dry spinning**

The dry spinning of nanotubes into yarns can be carried out from CNT forest of long arrays of CNTs deposited on the surface of a substrate or direct spinning from the aerosol in the reaction zone of a floating catalyst CVD.

Dry spinning from a substrate-based forest of MWCNTs as described by Zhang et al (2004) is affected by the degree of twist. Twist function includes reducing the inter-tube distance, producing

inter bundle lateral cohesion and increasing van der Waal attraction (Zhang et al., 2004). With an increase in the height of MWCNT in the forest, increases the stress transfer in the spun yarn and subsequently increases the yarn strength (Fang et al., 2010). Fang et al (2010), also observed a regressive linear dependence of yarn strength on yarn diameter.

Surface tension densification approach was applied by Ci et al (2007) in fabricating nanotube yarns from wet DWCNT. The wet forest promotes densification and stronger interactions between the nanotubes (Ci et al., 2007). The pulling and rotating align the CNTs in the direction of the pull.

The electrophoretic approach involves drawing nanotubes slowly from a dry dispersion of SWCNT with an electric field. Nanotube tips were drawn from the dispersion, assembled at the positively charged tips of subsequent tubes and spun (Gommans et al., 2000).

Direct spinning produces carbon nanotube yarns concurrently with synthesis from the furnace based on chemical vapour deposition technique. Yarn spun by direct spinning has better strength and electrical conductivity than yarns spun from the forest because direct spinning produces network aside the van der Waal forces (Zhang et al., 2006).

A large quantity of long spinnable CNTs is required to carry out the direct spinning of CNTs produced in chemical vapour deposition reactor into yarns. Various factors influence the quality and quantity of CNT aerosol produced in the catalyst CVD for direct spinning into CNT yarns (Kukovecz et al., 2005; Vanyorek et al., 2011).

2.6 Effect of operating variables on the quality and quantity of CNTs

Crucial to the spinnability of CNT yarns is to have strong van der Waals forces between individual CNTs in the grown CNT array. Before the growth of CNTs, decomposition of carbon precursor in

the presence of a catalyst and deposition of carbon atom on the surface of a catalyst takes place. However, if the appropriate conditions required for the growth of CNTs on the catalyst is not met, amorphous carbons are formed. Amorphous carbons are found to be responsible for the deactivation of catalysts and further hindering the growth of CNTs. Adequate control of reaction parameters is required to constrain the formation of amorphous carbon and enhance the growth of CNTs (Zhang et al., 2006). Adequate control of reaction conditions to enable the growth of well-aligned CNTs is necessary for spinnable CNT arrays (Zhang et al., 2009). Proper selection of the combinations of these parameters in line with the proposed application influence the quality and quantity of CNTs produced. These parameters include synthesis temperature, carbon source, catalyst and catalyst support, as well as promoters.

2.6.1 **Effect of temperature**

Following the rediscovery of carbon nanotubes by Iijima (Iijima, 1991) and further research on the carbon material comprising of graphene layers rolled into seamless concentric cylinders established their outstanding properties which made them desirable for applications in a wide range of areas including as composites for gas separation (Aberefa et al., 2019), as structural composites, (Li et al., 2013), in electronic devices (Baughman, 2002; Tans et al., 1998). Researchers have found synthesis temperature to be one of the most significant factors that affect the growth rate, morphology and structure of CNTs (Bodiba et al., 2018; Jeong, 2001; Kim et al., 2005; Ta et al., 2013) and they influence properties such conductivity, thermal stability, and tensile strength (Mittal et al., 2015). The bulk production of uniform CNTs with predetermined properties for specific applications still remains a challenge (Jourdain & Bichara, 2013).

Impact of synthesis temperature on the structure and morphology of carbon nanotubes is one of the parameters applicable to all the synthesis method therefore, it has been widely studied. Angulakshmi et al (2015) conclude CNTs growth rate and properties were highly dependent on the synthesis temperature in their study of the synthesis of multiwalled CNTs from *Zea mays* oil using Fe/Mo bimetallic catalyst (Angulakshmi et al., 2015). Kim et al (2005) observed an increase in growth rate with temperature in a CVD using ferrocene and acetylene. They attributed it to the provision of activation energy near the diffusion energy of carbon on iron from the catalyst (Kim et al., 2005). Jeong (2001) found a change in the surface morphology of the metal catalyst particle responsible for the growth of CNTs. The effect on the structure was studied by Ta et al (2013) where it was deduced that bamboo-like structures are produced at low temperatures and thin and regular structures are favoured at high temperatures. An increase in the diameter, density, and crystallinity of CNTs was observed to increase with an increase in synthesis temperature in a study using iron catalyst deposited on a silicon-oxide substrate (Lee et al., 2001).

Studies have shown synthesis temperature of CNTs to have effect in their application. Igbokwe et al (2019) observed a direct influence of the synthesis temperature of CNT yarns electrical properties for application as a filament in incandescent bulbs. They observed yarns produced at higher synthesis temperature possessed properties of a diode required for the predetermined application. This was attributed to the increase in the sp^2 content of the CNT yarn with an increase in synthesis temperature. However, Arjmand et al (2017) found that lower synthesis temperatures were favourable for the synthesis of CNTs for the production of polymeric nanocomposites for application in electromagnetic interference (EMI) shielding (Arjmand et al., 2017). This is credited to the formation of graphitic CNTs at higher synthesis temperatures while at lower temperatures lower diameter CNTs were formed resulting in better dispersion in a polymer matrix. Felisberto et

al (2017) also observed enhanced adhesion of low-temperature CVD synthesized MWCNT to polymers with improved mechanical performance.

Liu et al (2013) studied the effect of the calcination temperature of catalysts on the diameter of CNTs synthesized from methane over Fe_2O_3/MgO catalysts. Increase in calcination temperature was observed to increase the diameter of synthesized CNTs. Thermal post-treatment of CNTs have been seen to improve the electrical and mechanical application. Bulmer et al (2010) identified an increase in the I_G/I_D ratio with an increase in annealing temperature of CNTs and its effect on conductivity. They observed I_G/I_D ratio improved for annealing above 2000 °C in both argon and argon + Hydrogen environment consequently improving the specific conductance of CNT yarns (Bulmer et al., 2010).

2.6.2 **Effect of carbon source**

Carbon source has been found by researchers to have an influence on the quality and quantity of carbon nanotubes synthesized. Various carbon-containing compounds have been employed by various researchers ranging from organic to inorganic, hydrocarbons (linear or cyclic) and natural carbon sources using various catalysts and catalyst supports. SWCNTs have smaller diameters, the higher energy of formation and higher strain energy than MWCNTs, therefore, SWCNT are grown from high-temperature stable hydrocarbons like methane and carbon monoxide (Shah & Tali, 2016). Syntheses of CNTs from natural carbon sources such as oils have been reported to produce only MWCNTs without the production of VACNTs nor SWCNTs observed using various catalysts (Angulakshmi et al., 2015; Suriani et al., 2013). Plata et al (2010) reported that trace amount alkynes enhanced the formation of MWCNTs in an ethylene + Hydrogen system that had previously formed mostly volatile carbonaceous compounds(Plata et al., 2010). Using iron-

nanoparticles catalysts, Endo et al (1993) and José-Yacamán et al (1993) synthesized MWCNT and helical MWCNTs from benzene and acetylene carbon sources respectively. Bodiba et al (2018) investigated the yield and quality of carbonaceous species produced from acetylene and methane in a CVD under similar conditions. It was observed that acetylene yielded a large quantity of products but was largely nanoballs against the low yield consisting of mostly nanotubes from methane (Bodiba et al., 2018). In another study, Shirazi et al (2011) produced MWCNTs from cyclohexanol and xylene at 750°C in a CVD. Cyclohexanol was found to produce CNTs with higher purity which was attributed to the presence of oxygen in cyclohexanol (Shirazi et al., 2011). Lee et al (2017) used the I_G/I_D ratio to determine the effect of carbon source on of CNT fibres synthesized from acetylene, ethylene and methane under the same operating conditions with decreasing value respectively. Type, chirality and diameter of carbon nanotubes grown from methane, ethanol and toluene were studied in a floating catalyst reactor (Barnard et al., 2016). Narrow diameter SWCNT with armchair chirality were observed from ethanol and toluene precursor while methane-grown CNTs provided double-walled CNTs with broader diameter.

Hoecker et al (2017) investigated the different pyrolitic methane radical aerogel produced >1000 °C. These activated carbon species were later introduced to catalyst particles forming CNTs with different morphologies and crystallinity (Hoecker et al., 2017). In another study, Barreiro et al (2006) used ferrocene as both the carbon precursor and catalyst for the synthesis of SWCNTs in HiPco varying the pressure to produce varied diameter SWCNT without additional carbon source.

2.6.3 **Effect of catalyst type on CNTs production**

CNTs properties are also affected by the type of catalyst used during production. The most common metals used as catalysts include Fe, Ni and Co. A study by Suriani et al (2013) compared

the production of CNTs using Fe and Co catalysts. It was observed that CNTs produced by Co catalyst tends to have a larger diameter and lower quality than the one produced using Fe catalyst under the same conditions (Suriani et al., 2013). This is attributed to Fe catalytic stability and uniformity compared to cobalt for the production of CNTs. At lower temperatures between 500 °C – 650 °C, Ni shows higher activity and it is more efficient therefore it has the best growth performance (Allaedini et al., 2016). At temperatures above 750 °C, single-walled CNTs were easily synthesized using Fe catalyst on Al and Mo metal supports but could not be achieved with Ni catalyst under the same conditions (Shin et al., 2006). This is attributed to a higher diffusivity of Fe than Ni. Fe catalyst supported on activated carbon is reported to have a conversion rate of 98% for methane at 750 °C while Ni under same conditions converted only 42% (Sivakumar et al., 2011). Iron catalyst is seen to be the most effective of the three although CNTs deposits from Fe catalysts have the least graphitization (Dasgupta et al., 2008). Fe catalyst yield higher growth rate of vertically aligned CNT array than those of Ni or Co (Ramirez et al., 2014).

Iron catalyst nanoparticles sourced from different organometallic compounds under the same conditions were found to produce CNTs of varied quantity and quality. Moisala et al., (2006) in a study of the growth of SWCNT from CO carbon source using iron nanoparticles from ferrocene and iron pentacarbonyl ($FeCO_3$) catalysts observed low yield with $FeCO_3$ even under the best conditions. This was attributed to the lower decomposition temperature of $FeCO_3$ providing excessive catalyst nanoparticle.

2.6.4 **Effects of catalyst support on CNTs production**

Catalytic support is important in the production of carbon nanotubes (Mukesh & Jha, 2017). Properties of support materials that have considered in its selection include surface morphology,

pore size, substrate material, textural properties and dispersion of catalyst nanoparticles on the substrate. Lots of studies on the effect of catalyst support on the production of nanotubes have been carried out. The choice of catalyst support also has an impact on the production of CNTs. In CVD reactor the catalyst support are commonly used for the production are TiO_2, Si ZrO_2, MgO, SiO_2, CaO and Al_2O_3. Different catalyst support results in certain CNTs quality and also determines the production yield. Highly aligned carbon nanotubes can be grown using SiO_2 than when using Si as a substrate. When Si is used Fe particle tend to form stable $FeSi_2$ and Fe_2SiO_4 particles at a higher temperature which prevent the formation of CNTs (Jung et al., 2003). Oliviera et al (2012) in their study compared the effect of using 4% Co catalyst supported on Al_2O_3, SiO_2, TiO_2, and Nb_2O_5 in a CVD for the conversion of methane. They observed that textural properties of the support affected the particle size distribution of the catalyst and in turn the morphology of the nanotubes produced. A narrower particle size distribution is favourable to the production of SWCNT. Lee et al (2010) studied the effect of catalyst and its support on the characteristic of CNTs using CVD reactor. Both quartz plate and silicon wafer were used and compared as the catalyst support for Fe and Co. The results showed that CNTs grows better on a silicon wafer as compared to quartz substrate for both Fe and Co catalysts (Lee et al., 2010).

Using Fe film catalyst on SiO_2, Ta, Pd, and Cr support of different thicknesses, Wang et al (2006) found differences in the growth pattern with Ta support producing high density and uniformity in CNTs growth. Decomposition factor of catalyst support has also been found to be an important factor in the choice of support for CNTs synthesis given the need to easy purification of CNTs. Allaedini et al (2016) surmise that alkaline earth metal carbonates have the highest influence based on this factor.

Catalysts that are supported in an aerogel were discovered to be more productive than those supported on conventional supports (Su et al., 2000; Zheng et al., 2002). The reason being aerogel is known to possess very small density, very high porosity and also high surface area (Engel-Herbert et al., 2007; Hüsing & Schubert, 1998). High surface area is one key factor that made aerogel to gain more interest as catalyst support. Catalyst supported on aerogel was also found to not deactivate easily with time (Blanchard et al., 1982; Gao et al., 2019).

2.6.5 **Effect of promoters**

Various approaches have been explored to enhance products of CNTs synthesis by using promoters. The effect of promoters in CNTs synthesis is seen to be wide, ranging from affecting the general morphology and the number of walls, triggering branching, enhancing catalyst activity by fragmenting large particles of catalyst, and growth promoter (Ci et al., 2001; Devaux et al., 2012; Goyenola et al., 2012; Kucukayan et al., 2011; Liu et al., 2008; Sumpter et al., 2009). They achieve these by reducing the solubility of carbon in the catalyst, stabilizing the budding CNTs nucleus by reducing the energy at the interface between the catalyst particle and the CNTs edge (Rodiles et al., 2019). Sulfur is the most common promoter used according to literature. They are used in trace amounts in ratio to the catalyst as they could also poison catalysts (McRae et al., 2013).

Hydrogen gas could also fulfil the role of promoter as it has been found to enhance the quality of catalysts and modify the surface of synthesized CNTs (Behr et al., 2010; Ma et al., 2016). Regulation of hydrogen content for the production of CNTs could help regulate the morphology of synthesized CNTs as hydrogen has been found to initiate the reaction between carbon in methane and iron in ferrocene to form iron carbide in limited hydrogen supply (Behr et al., 2010).

At higher hydrogen concentrations, iron carbide is converted to iron, and etching of the forming CNTs occurs. It is known that hydrogen plays a role of the deoxidation of both the hydrocarbon and catalyst in the CVD system (Dichiara & Bai, 2012; He et al., 2010). Studies have reported elongation of catalyst activity by etching decomposed carbon from catalyst surface and synergetic activities of carbon source and hydrogen (Guellati et al., 2012; Wasel et al., 2007). Ma et al (2016) carried out a study on the effect of hydrogen in an FCCVD with different supports. They observed hydrogen has an effect on the decomposition of hydrocarbon and activation of catalyst (Ma et al., 2016).

Co-feeding of hydrogen during the production of CNTs has been reported to influence the morphology, electrical conductivity and mechanical properties of synthesized CNT yarns (Ma et al., 2016). Synthesis of aligned and spinnable CNTs that can be drawn and spun is desirable for the production of lightweight materials with high tensile and electrical properties. Formation of macroscopic CNTs such as yarn is achieved during the spinning of the aligned CNTs due to the attraction of Van der Waal forces (He et al., 2010).

All these studies stimulate the necessity for the investigation in an FCCVD system without support using a saturated hydrocarbon as a carbon source. To adequately optimize the production of CNTs in an FCCVD, these operating variables must be considered. Attention is therefore paid to their effects and interactions with other synthesis conditions in this work.

2.7 Process Optimization Methods

The parameters elucidated in Section 2.6 above have an influence on the determination of the optimum parameters for CNT yarn synthesis in FCCVD with direct spinning. Change one separate factor per time (COST) or Design of Experiments (DOE) can be used to understand the effect of

operating variables to optimize a process. The COST approach involves the change of one parameter per time with all other variables kept constant (Massart et al., 1978). The chosen response of the system is studied as a function of the varied parameter. Each parameter is skimmed and the blend of all the optimum parameters is acknowledged as the universal optimum. This approach is riddled with many disadvantages including the exponential rise in the number of experiments required with an increase in the number of parameters and the difficulty in getting a combination of optimum parameters for a universal optimum (Kukovecz et al., 2005). This is so because the COST approach assumes no interaction exists between the various parameters themselves making the parameters independent of each other. However, in real systems, there are varying levels of interactions between the parameters.

On the other hand, the Design of Experiments (DoE) is a statistical approach of acquiring the most possible amount of details about an operating system out of the least number of experiments (Goh, 2001). DoE is increasingly being implemented in catalytic systems and materials synthesis including in nanomaterials has also received widespread application (Kukovecz et al., 2005; Lee et al., 2016; Mohammed et al., 2017; Sharon et al., 2005; Vanyorek et al., 2011). Previous DoE and COST studies have considered the effect of a limited number of parameters in determining the optimum synthesis conditions. This is essentially acknowledged to be a result of the difficulty to vary a large number of parameters in the high-temperature process in which CNTs synthesis occurs (Gspann et al., 2014; Khavarian et al., 2011; Magrez et al., 2010). Derivation of universal optimum parameters has been elusive to the researchers. This could be because the interactions between the various parameters for the synthesis are not linear and their relationship to the quality and the quantity of CNT yarns produced is also not simple.

The effect of variables on chosen responses is described via response surface methodology (RSM). Face-centred composite design (FCCD), central composite design (CCD), and Box–Behnken design (BBD) are widely available for research. BBD is the most efficient of the other RSM as it has fewer experimental runs and expends less time (Rakić et al., 2014). It is commonly employed in industrial research with three process variables are involved (Onoji et al., 2017). 26 experiments are required in the BBD for four factors plus central points. It provides the same mathematical model as CCD. The localization of the experimental points is different from that of CCD because the extreme factor combinations are available in the CCD (Rakić et al., 2014). The absence of borderline regions on BBD makes it advantageous for this experimental problem given that the extreme points are physically unattainable.

2.8 Simple Kinetic Model Scheme

Process optimization can be based on the identified reaction kinetics of the system. Kinetic modelling of the system therefore serves to enable engineering scale-up and understanding the mechanism of the FCCVD system. The concentration and the chemical make-up of reactants and products, temperature, catalyst surface area control reaction kinetics. Kinetic study of CNTs formation over time can be deduced by the mechanism of the catalytic decomposition of hydrocarbon (Kristyan, 1997).

Catalytic growth of CNTs in a catalytic thermal CVD is based on the vapour-liquid-solid (VLS) mechanism and estimated to occur the three distinct steps: absorption of carbon atoms supplied by the feed gas, diffusion of adsorbed carbon atoms through the bulk catalyst metal, and formation of graphene layer and growth of CNTs from diffused carbon atom (Baker, 1972; Naha & Puri, 2008; Puretzky et al., 2005; Stadermann et al., 2009). VLS mechanism involves the absorption of the

vapour phase carbon source on high temperature liquefied catalytic particles to form a solid-state metal-carbon solution. The supersaturation of this solution precipitates stable carbon on the surface of the particle forming tubular carbon. The formation of carbonaceous platelets on the surface of the catalyst particle limits the further absorption of carbon atoms thereby terminating the growth of CNTs (Einarsson et al., 2008). Diffusion of carbon through iron for the formation of filamentous carbon is instigated by the concentration gradients created by the difference in solubility at the iron-gas and the iron-carbon interfaces (Audier & Coulon, 1985; Snoeck et al., 1997).

Several theoretical models have been proposed and used in describing CNTs growth using catalysts. The CVD process growth of carbon nanotubes occurs via the vapour-liquid-solid (VLS) model (Baker, 1972). This model proposes i.) catalyst particles are liquid; ii.) diffusion of the reactants occurs through the bulk of the particle. In this VLS model, the growth-limiting process is bulk carbon diffusion through the catalyst particle (Baker & Harris, 1978; Wirth et al., 2009; Wood et al., 2007).

Knowledge of the reaction mechanism, rate-limiting step, and overall rate equation for the synthesis of CNTs are necessary for the development of robust design methodology. Synthesis of CNTs in an FCCVD is carried out through various steps: adsorption of gaseous hydrocarbon on the surface of the catalyst; decomposition of carbon source (surface reaction) (Iyuke & Simate, 2011). The rate-limiting step is dependent on the conditions of the reaction (Yadav et al., 2019). Pirard et al., (2007), Ni et al., (2006), Liu et al., (2005) reported surface reaction of hydrocarbons as the rate-limiting step for the synthesis of MWCNT. However, adsorption of the hydrocarbon carbon source was reported as the rate-limiting step by Saraswat et al., (2016), Anisimov et al., (2010), and Baker (1989).

Attempt for the formulation of rate equations for the synthesis of MWCNT reported in the literature has been limited by various conditions. The influence of hydrogen partial pressure on the rate equations have not been considered by so many research groups including Saraswat et al., (2016) Abdullahi et al., (2012), Ni et al., (2006), Liu et al., (2005), Gommes et al., (2004), Qian et al., (2004) therefore causing a major limitation in the rate expressions formulated. In this research, the influence of the partial pressure of hydrogen on the synthesis of CNTs is considered in the rate equation.

Three individual runs of each flow rate were carried out. The total flow rate of each run was maintained within the laminar Reynolds number (Table 6.1) to improve the alignment or length of CNTs synthesized (Hong et al., 2005; Jin et al., 2007).

2.9 Concluding remarks

In considering carbon nanotubes as a viable material for replacement of tungsten in incandescent bulb technology, an exhaustive review of literature is presented in this chapter. A brief history of incandescent technology was presented and the materials used thus far are examined in their merits and demerits. Structure and properties relationships of carbon nanotubes necessary for its application in incandescent bulbs are scrutinized. Methods of production were surveyed for their quality of CNTs produced to ease of spinning into yarn. The focus was concentrated on arc discharge, laser ablation, and chemical vapour deposition since they are the most prevalent. The effects of operating parameters were researched to enable an informed decision on the variables and their ranges for optimization modelling. The general kinetic mechanism for thermal catalytic CVD using the vapour-liquid-solid model is highlighted.

Preliminary studies carried out indicate a higher yield of CNTs using acetylene as a carbon source in comparison with methane. However, they consist predominantly of nano balls which are not suitable for spinning into yarns. Nanostructures are produced at high temperatures from 700 °C. Synthesis temperatures above 900 °C tend to char the nanomaterials produced from acetylene while better quality nanotubes are produced from methane with increased temperature. Promoters were not used in these studies.

CHAPTER THREE

3. RESEARCH METHODOLOGY

3.1 Production of CNTs and CNT yarns

Production of CNTs and CNT yarn was carried out in a floating catalyst chemical vapour deposition (FCCVD) reactor with a direct spinning system. This unit was invented by Sunny E. Iyuke of the University of the Witwatersrand, South Africa (Iyuke, 2015). It involves the continuous feeding of vaporized floating catalyst and hydrocarbon under conditions suitable for the production of carbon nanotubes. Methane was the hydrocarbon used in this study with ferrocene as the floating catalyst. Figure 3.1 is a schematic of the system. Table 3.1 lists the components of the FCCVD system. Major segments of the system are described in the following sections. A detailed operation of the FCCVD system is presented in Appendix A.

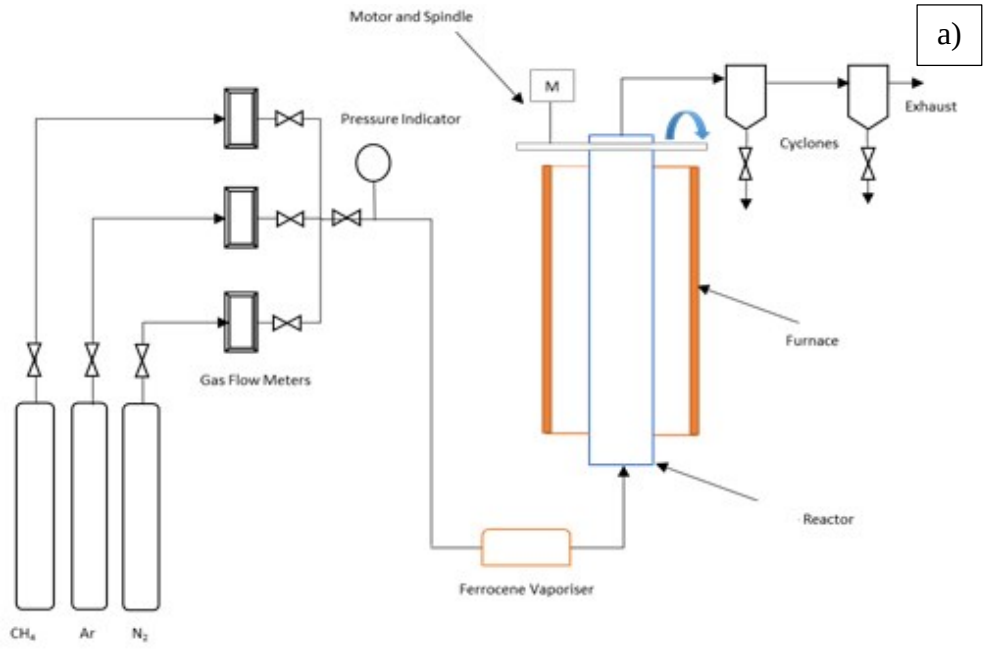

b)

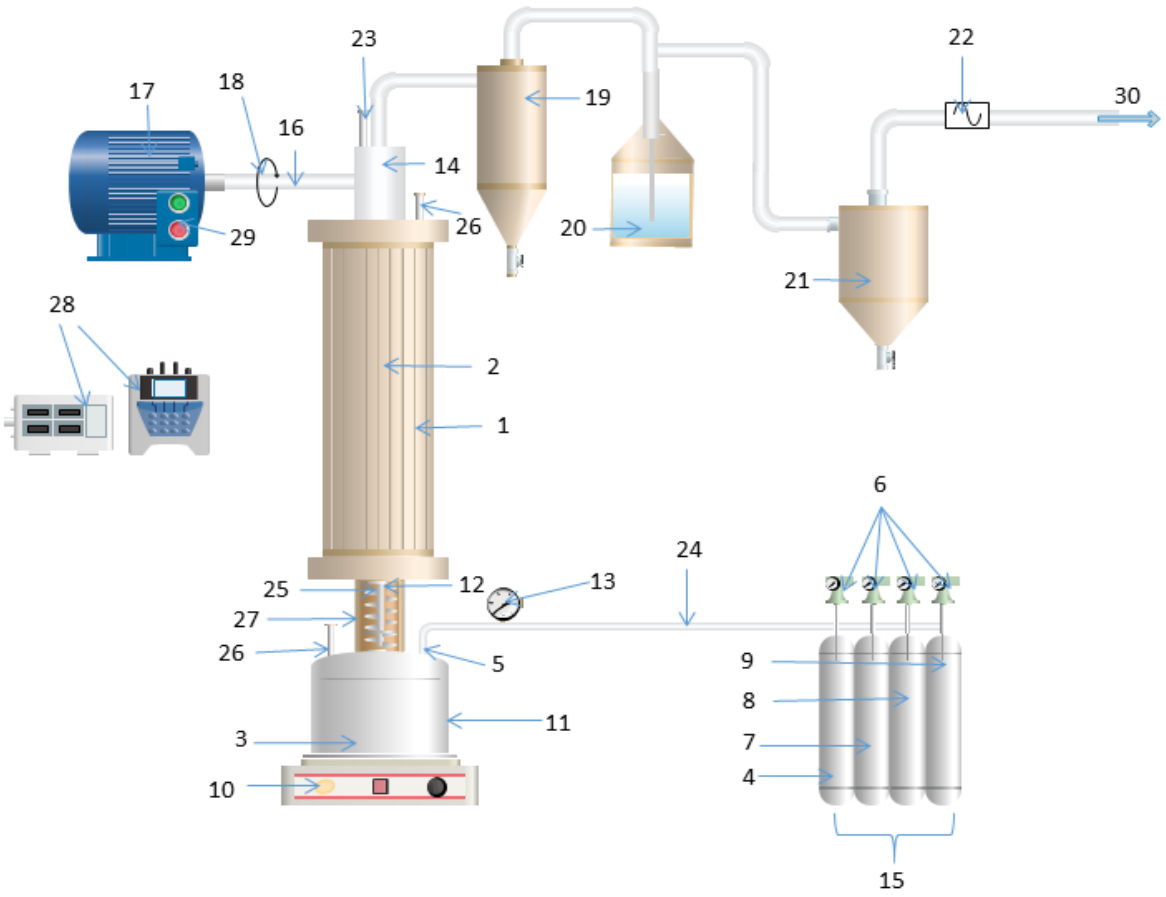

Figure 3.1. a) Process Flow Diagram of experimental set-up to produce CNT yarn; b) Schematic of the floating catalyst chemical vapour deposition (FCCVD) system

Table 3.1. Main components of the FCCVD system

No	Component Description	No	Component Description
1	Heating jacket/ furnace	16	Spindle
2	Reactor-cylinder section enclosed by furnace	17	Motor
3	Catalyst	18	Rotating motion
4	Hydrocarbon	19	Cyclone separator
5	The gas inlet to the vaporizer	20	Hydrocyclone separator
6	Gas flowmeters	21	Overflow cyclone
7	Argon	22	Filter
8	Hydrogen	23	Thermocouple
9	Nitrogen	24	Gas mixture delivery pipe
10	Hot plate	25	Spiral motion initiator
11	Vaporizer	26	Thermocouple
12	Inlet to reactor	27	Heating jacket
13	Pressure gauge	28	Temperature indicators
14	Outlet from reactor	29	Motor control
15	Gas cylinders	30	To exhaust

3.1.1 Catalyst vaporizer

The process occurring in the vaporizer is semi-continuous given that a fixed amount of catalyst is loaded into the chamber which is continuously carried into the reactor after vaporization until the catalyst is exhausted. The vaporizer is made up of an 8 mm thickness stainless steel pot, 150 mm high, and 120 mm outer diameter with a 100 mm swirled tube on the lid. It is heated by a hot plate to vaporize the catalyst placed into it. The vaporization temperature of solid ferrocene used in this study was varied between 120 °C to 180 °C. The temperature of the vaporizer was regulated and monitored using PT-100 thermocouples. The gases fed to the reactor are introduced via the vaporizer picking up the vaporized catalyst particles and carrying them into the pre-heated reactor where the conditions for the production of carbon nanotubes have been established. The gases feed to the reactor through the vaporizer include methane, a hydrocarbon, as a carbon source for the formation of carbon nanotubes; argon, inert gas, and hydrogen functioned as a carrier gases. The gases mix before being introduced into the vaporizer. The gas mixture and the vaporized ferrocene are carried to the reactor through the swirled tube maintained at 250 °C by a heating jacket.

3.1.2 Furnace section

The synthesis of carbon nanotubes is carried out in the furnace section of the floating catalyst chemical vapour deposition (FCCVD) system. It consists of a vertically oriented 800 mm long stainless steel pipe with an internal diameter of 60 mm and an outer diameter 75 mm. A part of the pipe where the reactions take place is encased in a 450 mm high furnace. The lower end of the tube is screwed onto the vaporizer lid connecting the vaporizer to the furnace. The reactor temperature was varied between 800 °C and 1000 °C (the maximum possible operating temperature of the furnace). Temperatures of the furnace and reaction tube were regulated and monitored using a temperature controller. The flow rate of the gas mixtures determines the

residence time of the reactants in the reactor since it operates as a plug flow reactor. The flow rate of the gas is measured using flow meters. The upper end of the stainless steel tube above the furnace leads to the spinning system, cyclone collector, and the exhaust system.

3.1.3 Product Collector and Exhaust system

A spindle connected to a motor is located at the upper end of the pipe for the spinning of CNTs from the aerosol formed in the furnace. CNTs are also deposited on the walls of the furnace. The rest passes through the pipe into the cyclone collectors and subsequently to the exhaust. In this study, the CNTs collected on the spindle and the tube walls are considered the quantity of CNTs produced as very little CNTs reaches the cyclone. This is because of the low quantity of CNTs produced from methane synthesis compared to synthesis from acetylene or other unsaturated carbons (Bodiba et al., 2018).

CNTs contained in the exit gas pass through the piping into the cyclone collector where it can be collected. The gas further passes through the hydro cyclone to dissolve in fluid before it is passed to another cyclone. The final portion of the gas is passed through a filter before being let out into the atmosphere via the exhaust.

3.2 Characterization of CNTs and CNT yarns

Techniques used in the characterization of as-synthesized CNTs and CNT yarns are described in this section. Characterizations of carbon-based nanomaterials were carried out by Scanning Electron Microscopy (SEM) (FEI FIB/SEM Nova 600 Nanolab), Transmission Electron Microscopy (TEM) (Joel JEM 4010) and Raman Spectroscopy (T-Y T64000). Thermo-gravimetric Analysis (TGA) of as-synthesized CNT yarns was conducted using a Perkin-Elmer

series STA 600. Gas Chromatography (GC) (Agilent Technology 6820) was used for gas analysis in this study.

3.2.1 Scanning Electron Microscopy

Geometric features, structural arrangements, spatial distribution as well as density of samples can be obtained using the scanning electron microscope with resolution as low as 1 nanometer (Xu et al., 2018). Micrographs of the surface morphology of CNT yarns can be generated by the SEM. SEM image is acquired by analysis of electromagnetic signals resulting from the interaction of an electron beam on the surface of the sample (Vida-simiti et al., 2004). With the advantage of a relatively wide range of magnification, the SEM technique allows for to easily focus with higher magnification on an area of interest of a sample originally scanned at a lower magnification (Wortmann & Fatikow, 2009). The sample preparation procedure is for SEM analysis of CNTs samples involves placing a few samples of CNTs powder on top of a carbon tape places on an aluminium stub holder (Lu et al., 1999). The sample is then double-coated with a 10 nm-thick 70/30 platinum/gold film to give it the electrical conductivity needed to avoid electrostatic charge (Vida-simiti et al., 2004). The sample holder is then placed into the SEM chamber. SEM images may be taken under desired magnifications and electron voltage between 15 keV and 30 keV.

SEM samples were prepared by mounting a small amount of as-synthesized CNT yarns onto a carbon tape stuck on an aluminium stub. The samples were then coated with double layers of 10 nm 60/40 gold/palladium in a Sputtercoater (EmiTech K550X Sputtercoater) and viewed in a scanning electron microscope (FEI Nova600 FIB-SEM) operated at 30 kV.

3.2.2 **Raman Spectroscopy**

Raman spectroscopy is inevitable for understanding the structure and the type of CNTs synthesized. This is critically important in deducing the quality of CNTs, the presence of defects and the level of graphitization. Characteristic one-dimensional peaks of SWCNT and MWCNT obtained by Raman spectroscopy distinguish them between each other and their types (Biró et al., 2002; Santangelo et al., 2006). It is a non-destructive analytical tool for CNTs' characterization. Laser generated photons scatter in-elastically, the Raman scattering, with excitations including phonons in the system. A shift in the energy of the scattered photons gives information about the phonon modes in the system (Costa et al., 2008; Dresselhaus et al., 2005).

Raman shift major features include (a) the radial breathing modes (RBM) found at the low-frequency peak region (100 – 400 cm^{-1}), typically significant in SWCNT and DWCNT as the frequency is dependent on diameter (Costa et al., 2008); (b) D-band region spanning between (1100 – 1500 cm^{-1}) activated by disordered graphite thus called disorder-induced band (Matthews et al., 1999); (c) G-band located between 1500 – 1600 cm^{-1}, a high-frequency bunch for ordered graphites not affected by the wavelength of the beam (Chipara et al., 2011; Dresselhaus et al., 1998); (d) Second-order mode observed between 2450 – 2650 cm^{-1} consisting of the overtone of the G-band commonly known as the G'-band or the 2D-band (Baranov et al., 1987).

The ratio of the intensities of the D- and G- bands serve to distinguish between SWCNT and MWCNT because the value is inversely proportional to the crystallite size of the nanotube graphites (Cançado et al., 2006). This ratio is also a measure of disorderliness within CNTs thereby determining the structural quality of a CNTs sample. The lower the I_D/I_G ratio the less the defects

in the CNTs structure, the lower the amount of atomic carbon indicating higher crystalline quality (Antunes et al., 2006).

No sample preparation is required for Raman Spectroscopy analysis. An analysis is carried out at room temperature with low laser power (<1.0 MW) to avoid localized heating and excitation of Fe-catalyst particles on the samples. The excitation wavelength of 514.5 nm was mostly applied.

3.2.3 **Transmission Electron Microscopy**

Morphology, crystal structure, and defects of CNTs are some of the critical information that can be obtained by the Transmission Electron Microscope (TEM). The qualitative characteristics such as dimensions including internal and external diameters and length can be determined using TEM. A high energy electron beam generated in the transmission electron microscope is used to obtain the microstructure of materials by transmitting it through a very thin sample to image on a fluorescent screen (Somani & Umeno, 2007). The tubular structure is visible in the TEM images, usually surrounded by distinguishable clusters of amorphous carbon and dark spots from the iron catalyst on the surface and inside the nanotubes. Sample preparation for TEM analysis involved putting a spatula tip of the sample into 5 mL of methanol and sonicated for 15 minutes. The resulting suspension is collected in a pipette and a drop is deposited onto a copper grid and allowed to air dry. The copper grid is loaded onto the sample holder and into the TEM chamber for investigation.

3.2.4 **Thermo-gravimetric Analysis**

Thermo-gravimetric Analysis (TGA) also called thermogravimetry is a technique in which the mass change of a material is monitored as the material is subjected to a controlled heating rate in a controlled environment (Sahle-Demessie et al., 2011). TGA is applied to characterize the thermal

decomposition of CNTs and their thermal stability under various heating and atmospheric conditions. The operation of TGA consists of programming the experimental run with sample heating rate and final temperature. The pre-determined mass of the sample is weighed into the sample pan and placed into the furnace chamber. The real-time data is recorded by the computer software for subsequent analysis. The experimental run system is then programmed giving the heating rate and the maximum temperature. The summary of the specifications of the TGA utilized is presented in Table 3.2.

Table 3.2. Specifications of Perkin-Elmer STA 600 TGA

Feature	Tolerance
Balance Sensitivity	10^{-3}mg
Balance Accuracy	0.1%
Temperature range	25 °C – 1000°C
Heating rate	0.1°C/min – 100°C/min
Temperature Precision	±2°C

Thermogravimetric analysis of carbon nanotubes in atmospheric air represents a measure for determining the thermal and oxidative stability of CNTs (Bom et al., 2002; Scheibe et al., 2010). Thermogravimetric analysis of the as-synthesized yarns was carried out under 25 mL/min air gas flow using a thermogravimetric analyzer (model SDT Q600). For each analytical run, approximately 5 mg of sample was placed in an aluminium crucible and loaded into the instrument. A second crucible was also placed in empty to serve as a reference. The loaded sample was heated

from ambient temperature to 900 °C at a heating rate of 10 °C/min. An increase in weight is observed in all the samples before a sharp decrease following the on-set of oxidation. Oxidation temperature was determined by Voigt fitting of the derivative weight curve from the TG analysis. The curve is derived from the thermogravimetric analysis of 5mg of CNTs sample in a DTA-Q600 SDT thermogravimetric analyser instrument heated in 25 mL/min airflow from room temperature to 900 °C with 10 °C/min heating rate.

3.2.5 **X-ray Diffractometry**

Phase identification of components is obtained by Powder X-ray Diffraction (XRD). The crystallographic phases and structural nature of the solid organic or inorganic samples are obtained with XRD. The crystalline and polycrystalline material even those in a mixture are capable of producing specific diffraction patterns when interacting with X-rays. The distinctive identification and characterization of these materials can therefore be obtained using XRD. The fingerprint of a substance is obtained by the diffraction pattern of the pure substance. Amorphous materials can also be identified in XRD by the random and disordered arrangement of atom in its diffraction. Bragg's equation ($d_{002} = \lambda/2 \sin \theta$) of the (002) diffraction peak which relates to the degree of graphitization of CNTs (graphite layers) is determined to be 0.34 nm (Gao et al., 2019).

Bruker D2 Phaser Powder XRD was used in this study. It uses Co-Kα irradiation with a 30 kV X-ray tube and a current of 30 mA over a $10° \leq 2\theta \leq 90°$ range (Mongwe, 2018). The XRD pattern of as-produced CNT yarns is generated by the Cu-Kα radiation source with wavelength λ=1.5406 Å. The detector moves in a circle around the sample. The detector position is recorded as the angle 2theta (2θ) while the detector records the number of X-rays observed at each angle 2θ. The X-ray intensity is also recorded.

3.2.6 **Gas Chromatography**

Gas chromatography (GC) is chemical analytical equipment used to determine the relative concentration of various gases contained in a sample (Rodiles et al., 2019). GC consists of a thermal conductivity detector (TCD) for detecting inorganic compounds and flame ionization detector (FID) for detecting organic compounds. Some GCs could consist of only one of the detectors. It generally operates by transporting the unknown gas mixture using a carrier gas through the tubular column. The adsorption coefficient of the constituent gases serves as the bases for GC analysis. Elution times for the constituent gases could be used when the oven temperature and detector temperatures are constant throughout the analysis. The retention time of the constituent gases is identified by generating a chromatograph. Outlined below are settings used for the operation of the HaysepQ 80/100 mesh 2 m x 1/8' gas chromatograph employed and Table 3.4 gives detailed information about the gas chromatograph column.

- Oven temperature 80 °C
- Nitrogen gas at 10 psi
- Initial Temperature – 35 °C
- Ramp rate – 20 °C/min
- TCD temperature at 250 °C
- Complete GC circle – 31 minutes

Table 3.3. Specifications of the column of Gas Chromatograph

Feature	Value
Length	2 m
Outer diameter	3.175 mm
Inner diameter	2.2 mm
Support	Carboxen-1000
Mesh range	80/100

3.3 Investigation of the effect of synthesis conditions

The effect of the synthesis conditions on the quantity and quality of as-synthesized CNTs and CNT yarns in the FCCVD reactor with direct spinning was studied in two categories. Statistical analysis was used in the first category and synthesis variables considered were synthesis temperatures, the volumetric flow rate of methane, the volumetric flow rate of hydrogen, the volumetric flow rate of argon, vaporizer temperature, spinning rate, and thiophene content. Oxidation temperature was used as the measure of the quality of produced CNTs because the material will operate at high temperatures while the quantity of CNTs produced was used as the measure of the quantity. A statistically designed experiment using fractional factorial was used to collect data. This data was used in developing regression models to explain the effect of synthesis variables on the quality and quantity of CNTs yarn. A detailed methodology for the statistical modelling is found in Section 4.2 of this thesis. An in-depth study of the effect of synthesis temperature and the effect of

hydrogen on the electrical property of as-synthesized CNTs was studied separately in the second category. A range of values was used to study its effect.

3.3.1 Effect of synthesis conditions on electrical properties

The electrical conductivity of the as-synthesized CNT yarns was obtained using a high field cryogen-free measurement system (Cryogenic Ltd) relating to a two-probe method test at room temperature. A small amount of sample containing nano yarns was pressed to form a thin film mat covering 5mm×5mm surface on the sample holder, was mounted using a nonconductive double-sided tape. Contact between the sample holder and the yarn was made by applying conductive silver paint from the four corners of the thin film onto the sample holder. After the paint dried, the sample holder was mounted and a two-point probe was used to take measurements at room temperature. Measurements at various voltages were taken between −0.1 V to 0.1 V and −2 V to 2 V with 5 μV steps passing through the sample in each measurement.

3.3.1 Analysis of exit gases from FCCVD reactor

The predominant gases shown by the GC analysis of the exit gases from the FCCVD reactor were methane and Hydrogen as well as carbon monoxide probably formed because of residual oxygen in the system. This is consistent over all the different flow rates. The compassCDS software incorporated into the GC was used to integrate the peak areas. The calibration of the GC is presented in Appendix B.

Analysis of the peaks shows hydrogen is had the most amount of product gas. The quantity of hydrogen increases as the flow rate of reactant gases increase. An increase in the flow rate of methane shows a decrease in the volume of methane at the exit of the reaction. This could be attributed to an increased flow velocity enabling a higher quantity of catalyst pick-up for the

reaction. This observation indicates a higher conversion of methane with an increase in pressure due to methane gas (Yadav et al., 2019). Zhang et al., 2004 observed that higher conversion for lower pressures at various temperatures of reaction (Zhang et al., 2004).

3.4 Testing of as-synthesized CNT-yarns as a filament in incandescent bulbs

The mechanical and electrical properties of the as-synthesized CNT yarns were determined in the study of the luminescence properties of CNTs. Tensile properties were acquired using micro tensile tester while the two-point probe was used to measure the electrical conductivity of as-synthesized yarn. Incandescence was studied under argon using a micro-Raman system.

3.4.1 Mechanical Properties

Measurement of the mechanical strength of as-synthesized CNT yarn was done using a Texture Analyzer, TA.XT Plus. CNT yarn was placed between two clamps and pulled until the break. 3 samples of various dimensions were successfully measured. The force [N] exerted on the CNT yarn and position of the moving grip [mm] were recorded at a 5milliseconds interval by the coupled Exponent Connect software. The strain of CNT yarn was calculated from this data.

3.4.2 Electrical Property

A two-point probe was used to measure the electrical conductivity of as-synthesized CNT yarn at room temperature in a high field cryogen-free measurement system (Figure 7.4a). A piece of yarn was mounted on a sample holder using a nonconductive double-sided tape. Contact between the sample holder and the yarn was made by applying conductive silver paint from the two corners of the yarn onto the sample holder to form a contact electrode. After the paint dried, the sample holder was placed in the cryogen chamber measurements were taken at room temperature. Measurements

of 2 samples were taken at various voltages between 0.1 V to 0.5 V with 5 μV steps passing through the sample in each measurement.

3.4.3 **Incandescent Properties**

Set up for light-emitting and spectra recording consisted of a micro-Raman system (Linkam TS1500) was used as a spectrometer (Figure 3.2) set up on a Raman system and an AC voltage meter as a power source. The micro-Raman was modified by fitting it with alumina slab and re-wiring to connect it to the AC voltmeter. CNT yarn was placed on an alumina slab. A silver paste was used to secure a connection between the yarn and the AC voltmeter connector on the alumina substrate and the micro-Raman covered. The CNT yarn is visible through a quartz window. The objective lens (a part of the Raman system) through which the generated spectra are collected is placed above the quartz window with its focal point set on the material to be tested. AC current and resistance of materials were measured using a multimeter. The objective lens was placed at a working distance of 10 mm from the quartz window. Argon gas was passed through the chamber of the micro-Raman at 4 mL/min for at least 10 minutes before taking readings to create an inert atmosphere and also passed throughout the experimental runs. Spectra are collected on the Raman system computer.

Some of the limitations in carrying out this study include low voltage capacity of the micro-Raman system (<12 V AC current); only one piece of yarn was successfully illuminated as the others had comparatively very high resistance for the low voltage system. The test could not be run for a long period to avoid the heating of elements beyond the heat capacity of the micro-Raman.

To measure the light spectra, the length of the material was determined as the length between the silver paste connections ~3.4 mm long. Light spectra of CNT yarn and 60W commercial tungsten

wire were measured. The room temperature resistance of the tested CNT yarns was 8.7 Ω while Tungsten was 6.8 Ω.

Figure 3.2 Photograph of the micro-Raman containing CNT yarn placed on alumina substrate and held on with silver paste

3.5 Safety, Health, and Environmental Assurance

Personal protective equipment (PPE), including laboratory coat, gloves, safety glasses, gas mask, must be worn throughout the operation of the equipment. Extreme care should be taken when working with the equipment as it works at very high temperatures. Highly inflammable gases, methane, and hydrogen are used in the synthesis of CNTs cause major concerns. The ferrocene catalyst used in the synthesis is also inflammable. Argon or other inert gas must be used in the synthesis process. Care must be taken to avoid leaks from the equipment before each run is made.

The operation of the equipment must be carried out in a well-ventilated environment. These safety issues were put into consideration throughout the experimental designs and the actual running of the experiments and data collections. Exit gases went through varying stages to ensure they were clean before being released to the environment.

Operability is considered as the ability of equipment or system or a whole industrial installation to operate in a safe and reliable condition without excessive problems in line with defined effectiveness in terms of performance, productivity, quality, and safety. Hazard and operability study (HAZOP) is a systematic technique planned to identify and evaluate operational problems and risks to personnel. HAZOP table for the FCCVD system with direct spinning is presented in Appendix A.

3.6 Concluding remark

An overview of the techniques employed in the synthesis and characterization of CNT yarns is presented in this chapter. Standard procedures were used for the characterization of produced materials. Procedures for the series of experiments conducted in this study are described. Some of the experimental procedures that are not described in detail in this chapter are discussed in subsequent chapters, where necessary. In subsequent chapters, results obtained from the experimental protocols described in this chapter are presented and discussed.

CHAPTER FOUR

4. OPTIMIZATION OF SYNTHESIS VARIABLES USING STATISTICAL DESIGN OF EXPERIMENTS

This chapter presents a predictive regression model that was employed to investigate the effect of operating conditions on CNT yarn production in FCCVD. Variables considered were synthesis temperature, Methane volumetric feed rate, Argon volumetric feed rate, Hydrogen volumetric feed rate, vapouriser temperature, thiophene volume, spinning rate and quantity of CNTs produced and oxidation temperature were considered as responses.

4.1 Experimental

4.1.1 Synthesis of CNT yarn

A detailed description of the working principles of the FCCVD reactor is presented in Chapter Three. Due to the limitations of the reaction unit, resources, and previous studies, seven experimental factors were considered as influential to the quantity and quality of CNT yarns produced in the FCCVD reactor with direct spinning. They are synthesis temperature, methane volumetric feed rate, argon volumetric feed rate, Hydrogen volumetric feed rate, vaporizer temperature, thiophene volume, and spinning rate. The volumetric flow rates of the gases in this study were measured at room temperature of 25 °C. Experiments were carried out under atmospheric pressure for 30 minutes each. Quantity of CNT yarns in this study was determined by the quantity of CNT yarns collected from the rotating spindle and the upper segment of the stainless

steel pipe wall above the part encased by the furnace measured in grams. SEM described in Section 3.2.1 was used in the identification of CNT yarn produced in FCCVD with direct spinning.

4.1.2 Defining the optimum process conditions using DoE

Two stages of DoE were performed. The first stage was the screening stage consisted of 2-level fractional factorial design (n^{k-3} type). k is the experimental variables and n is the level (Montgomery, 2005). The seven experimental variables and their value ranges are presented in Table 4.1. 16 experimental runs were determined from the factorial design using Design Expert® statistical software and executed. Table 4.3 lists the 16 different combinations of experimental conditions over the 2 levels and seven variables ($2^{7-3} = 16$) and the results. The results are designated based on ratings explained in Table 4.2. Optimization stage was the second stage and entailed a response surface analysis. In this stage, Box-Behnken design was applied to vary the four most significant variables (Perincek & Colak, 2013). Optimum synthesis conditions were determined using Design Expert® statistical software.

Table 4.1. Actual value of experimental ranges and levels of independent process variables of 2-level fractional factorial design

Independent Process Parameters	**Symbols**	**Actual Parameter Levels**		
		Low (-1)	Central (0)	High (+1)
Synthesis Temperature (°C)	X_1	800	900	1000
Methane volumetric feed rate (mL/min)	X_2	50	100	150
Argon volumetric feed rate (mL/min)	X_3	50	100	150
Hydrogen volumetric feed rate (mL/min)	X_4	0	75	150
Vapouriser temperature (°C)	X_5	120	150	180
Thiophene Volume (mL)	X_6	1	2	3
Spinning rate (rpm)	X_7	50	125	200

4.2 Results and Discussions

Physical appearance and quantity (mass, g) of CNT yarns collected on the rotating spindle after each run and subsequent cooling of the reactor system was used to develop a rating system. The rating key is presented in Table 4.2. SEM micrographs of various physical appearances of the as-synthesized CNTs are depicted in Figure 4.1. The dusty product is depicted in Figure 4.1a. At very high magnification compared to others, only a little string can sparsely be seen. They are rated 2 and 3 with the difference being the quantity produced. In Figure 4.1b, the nanotubes are clustered

together indicating a higher van der Waal attraction exists between the individual tubes than the dusty products. However, the clusters are irregular therefore they are not suitable for this application. Films are depicted in Fig 4.1c. They consist of CNTs held together by van der Waals attractions along the longer length of the nanotubes but they do not roll up fully. Fibres, on the other hand, are long macroscopic CNTs fully rolled up as seen in Fig 4.1d (Lee et al., 2016). The most significant factors that influenced the morphology of the as-synthesized CNT yarns were determined. The summary of the results is presented in Table 4.3.

Table 4.2. Appearances and Quantity used to conduct the initial screening of as-synthesized CNT yarns

Rating number	**Appearance**	**Quantity**	**Description**
1	Nothing	No CNTs	Light soot on the spindle
2	Dusty	Low	Less than 0.03 g soot collected from the spindle
3	Dusty	High	Carbon black soot >0.03 g collected from the spindle
4	Lumps	Low	Clusters of carbon collected from spindle <0.05 g
5	Lumps	High	Clumps of carbon >0.05 g collected from the spindle
6	Film	Wide ribbons	Loose ties of carbon fibres collected from the spindle
7	Fibre	Long fibre	Tight ties of carbon fibres collected from the spindle

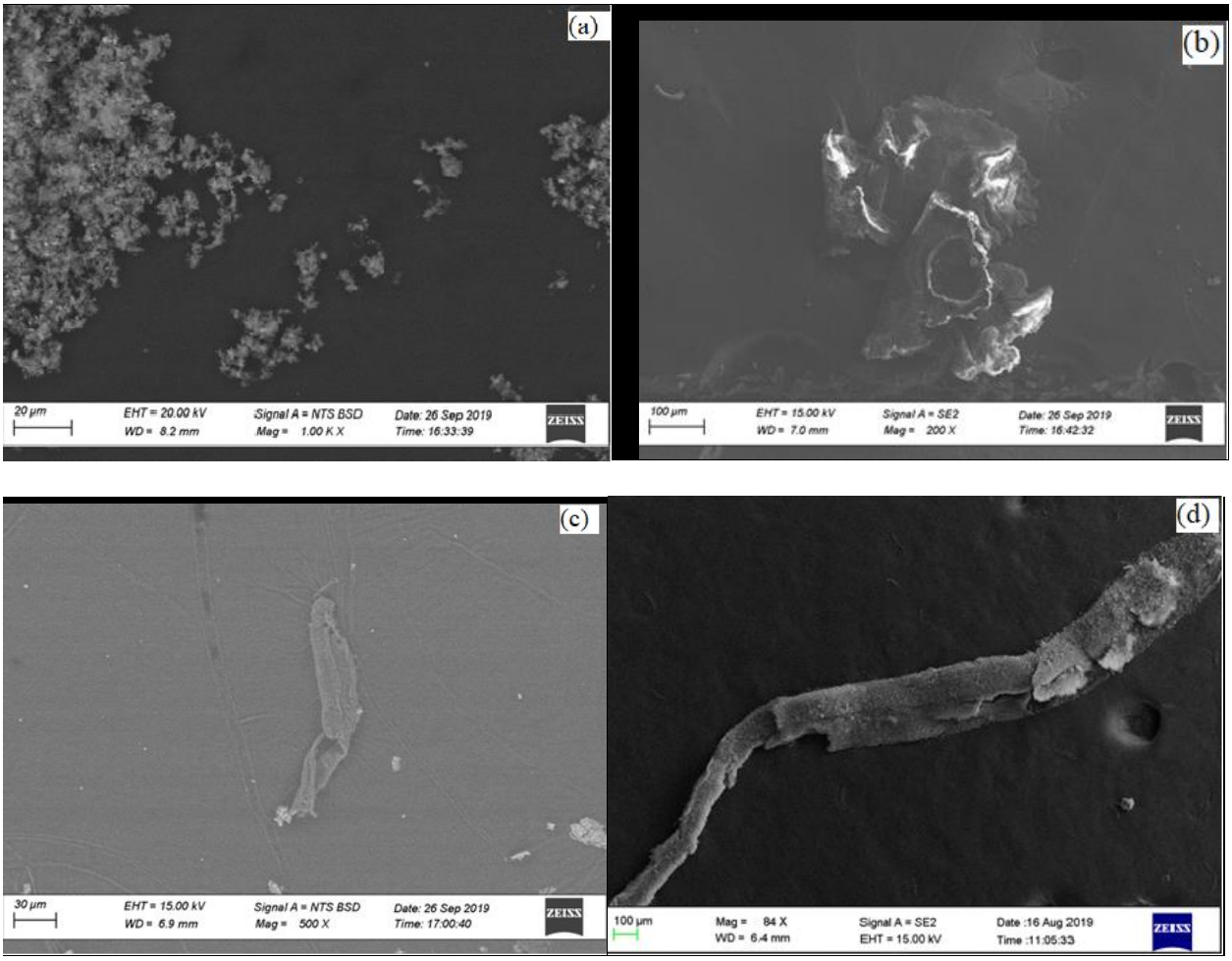

Figure 4.1. SEM images depicting the various appearances of as-synthesized CNT yarns under different synthesis conditions. a) Dusty; b) Lumps; c) Films; d) Fibre

Table 4.3. 2-level fractional factorial design (experimental runs and results).

Run	Synthesis Temperature, °C	Methane feed rate, mL/min	Argon feed rate, mL/min	Hydrogen feed rate, mL/min	Vaporizer temperature, °C	Spinning rate, rpm	Thiophene volume, mL	Rating
1	1000	150	150	150	180	200	3	7
2	800	50	50	0	120	50	1	1
3	800	150	50	150	180	50	3	4
4	1000	50	150	0	120	200	1	4
5	1000	50	50	0	180	50	3	3
6	800	50	50	150	120	200	3	2
7	800	150	50	0	180	200	1	4
8	1000	50	50	150	180	200	1	7
9	1000	150	50	0	120	200	3	6

10	1000	150	50	150	120	50	1	6
11	800	150	150	0	120	50	3	3
12	1000	50	150	150	120	50	3	5
13	800	50	150	150	180	50	1	5
14	1000	150	150	0	180	50	1	5
15	800	150	150	150	120	200	1	4
16	800	50	150	0	180	200	3	3

The most significant variables to the model were chosen as seen in the half-normal plot shown in Figure 4.2. The variables close to the zero on the normal % probability axes are less significant with the blue colour indicating negative effect while those close to 100 are the most significant. The four variables with the most positive effects were chosen: synthesis temperature, methane volumetric flow rate, hydrogen volumetric flow rate and vaporization temperature. Table 4.5 was used to inspect the p-values of the selected variables. All pass the 0.1 test indicating they were found to be normal at 90% confidence level (Lawson et al., 1998).

Table 4.4. ANOVA for the modified factorial model.

Source	**Sum of Squares**	**Degree of freedom**	**Mean Square**	**F-value**	**p-value**
Model	33.75	4	8.4375	9.5806	0.0014
A-Synthesis Temperature	18.0625	1	18.0625	20.5097	0.0009
B-Methane	5.0625	1	5.0625	5.7484	0.0354
D-Hydrogen	7.5625	1	7.5625	8.5871	0.0137
E-Vaporization Temperature	3.0625	1	3.0625	3.4774	0.0891
Residual	9.6875	11	0.8807		
Cor Total	43.4375	15			

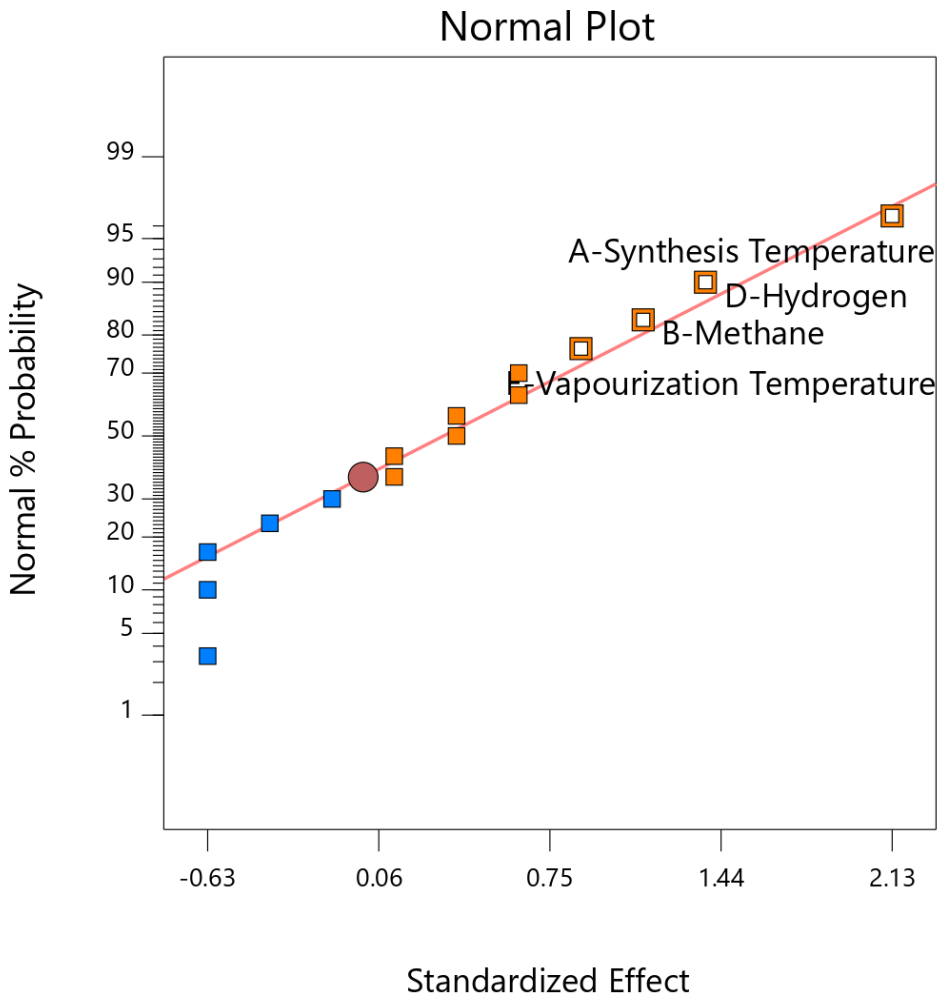

Figure 4.2. Normal probability plot of effects for the synthesis of CNT yarn in an FCCVD reactor (Blue cubes are factors that had a negative effect on the responses, the yellow cubes had a positive effect, while the yellow cubes with holes in them are the chosen factor with the most significant effects).

4.2.1 **Statistical Analysis**

The effects of synthesis temperature, methane flow rate, hydrogen flow rate, and catalyst vaporization temperature on the synthesis of CNTs from methane were studied using an RSM Box-Behnken design (BBD). A total of 26 runs were performed to study the effects on the quantity of CNTs produced and the oxidation temperature of CNTs. The ranges used were: synthesis temperature, 900 – 1000 °C; methane volumetric flow rate, 50 – 150 mL/min; hydrogen volumetric flow rate, 75 – 150 mL/min; and catalyst vaporization temperature 150 – 180 °C. The responses from the resulting 26 runs are shown in Table 4.5.

The responsibility of each factor to the quantity of CNTs produced and the Oxidation temperature is statistically discussed. They were fitted to linear, two factor-interaction (2FI), quadratic and cubic polynomial models, using DoE as shown in Table 4.6. It was observed that the linear, 2FI and quadratic models for the quantity of CNTs produced were significant as sequential p-values were less than 0.1. Comparing the coefficient of determination R^2 of the model, the quadratic model with 0.8772 is most preferred since it has the most acceptable R^2 (Khuri & Mukhopadhyay, 2010). Examination of the model for oxidation temperature shows only the linear model is significant with an R^2 value of 0.7298. However, this R^2 value is considered to be low and could not adequately describe the model.

Table 4.5. 2^4 Box-Behnken design matrix showing the actual values of independent variables, the quantity of CNTs produced and oxidation temperature of CNT yarns

Run	Factors				Responses	
	Temperature A_1, ^oC	**Methane A_2, mL/min**	**Hydrogen A_3, mL/min**	**Vaporization Temperature A_4, ^oC**	**Quantity of CNTs produced, g**	**Oxidation Temperature, ^oC**
1	900	100	75	165	0.0694	423.04
2	1000	100	150	165	0.1768	446.36
3	950	50	150	165	0.1049	420.15
4	1000	100	112.5	180	0.2015	450.22
5	950	150	112.5	150	0.0711	428.58
6	950	100	150	180	0.1094	427.63
7	950	50	112.5	150	0.0802	419.57
8	950	50	112.5	180	0.0585	419.69
9	900	100	112.5	180	0.0449	430.46
10	1000	100	75	165	0.0559	442.57
11	950	100	112.5	165	0.0437	424.48
12	1000	100	112.5	150	0.0955	432.29
13	950	100	112.5	165	0.0739	437.74

14	950	100	150	150	0.0817	432.11
15	950	150	150	165	0.1183	435.87
16	1000	50	112.5	165	0.0863	427.42
17	950	150	75	165	0.1053	420.60
18	950	100	112.5	165	0.0516	430.75
19	950	50	75	165	0.0669	418.90
20	900	100	150	165	0.0955	422.75
21	950	100	75	150	0.0517	424.57
22	900	100	112.5	150	0.0319	392.79
23	1000	150	112.5	165	0.2771	453.44
24	950	150	112.5	180	0.2862	437.02
25	950	100	75	180	0.0726	419.51
26	950	100	112.5	165	0.0712	433.00

Table 4.6. Model fit summary

Source	Quantity of CNTs			Oxidation Temperature		
	Sequential p-value	**Lack of Fit p-value**	**Adjusted R^2**	**Sequential p-value**	**Lack of Fit p-value**	**Adjusted R^2**
Linear	0.0017	0.0305	0.4578	0.0001	0.2887	0.7298
2FI	0.0689	0.0473	0.6217	0.6964	0.2418	0.5461
Quadratic	0.0811	0.0740	0.8773	0.6435	0.1983	0.4982
Cubic	0.1107	0.1260	0.9061	0.2639	0.1806	0.6921

The possible main effects and interactions of the models are: - synthesis temperature (A_1); methane volumetric feed rate (A_2); hydrogen volumetric feed rate (A_3); and vaporizer temperature (A_4). The interaction between synthesis temperature and methane volumetric feed rate (A_{12}); the interaction between synthesis temperature and hydrogen volumetric feed rate (A_{13}); the interaction between synthesis temperature and vaporiser temperature (A_{14}); the interaction between methane volumetric feed rate and hydrogen volumetric feed rate (A_{23}), the interaction between methane volumetric feed rate and vaporiser temperature (A_{24}), the interaction between hydrogen volumetric feed rate and vaporiser temperature (A_{34}).

One way analysis of variance (ANOVA) test informed the suitability and dependability of response fits for quadratic functions of the process variables (Abu Amr et al., 2014). These values give confidence to the comparisons of the experimental and predicted quantity of as-synthesized CNT yarns. The analyses of variance (ANOVA) for the quantity of CNTs produced and the oxidation

temperature are summarized in Table 4.7 and Table 4.8 respectively. The p-values indicate the significance of each term in the ANOVA. The terms (main and interaction) less than 0.1 in value are considered significant model terms and emerged as the major determinant in the models. Terms with p-values above 0.1 were not included in the models. The regression equations for the quantity of CNTs produced is a reduced quadratic equation is given by Equation 4.1. Multiple coefficients of determination; R^2 = 83.65% and adjusted R^2 = 75.96% summarizes the statistical significance of the model. The model for oxidation temperature is a reduced linear equation written as Equation 4.2. Multiple correlation coefficient; R^2 = 72.98% indicate a moderate correlation of the model. R^2 = 67.86% is close to the correlation coefficient gives good confidence to the comparison of experiment and predicted oxidation temperature of as-synthesized CNT yarns (Nagelkerke, 1991).

$$\text{Quantity (g)} = 0.0686 + 0.0369A_1 + 0.0338A_2 + 0.0221A_3 + 0.0301A_4 + 0.0616A_{12} + 0.0592A_{24} + 0.0288\,A_1{}^2 + 0.0438A_2{}^2 + 0.0098 \quad (4.1)$$

$$\text{Oxidation temperature (°C)} = 427.924 + 12.7412\text{A}_1 + 6.978\text{A}_2 + 4.55167\text{A}_4 + 1.56 \quad (4.2)$$

Table 4.7. One way ANOVA test for response surface for Reduced Quadratic model of quantity of CNT yarn produced in FCCVD

Source	Sum of Squares	Degree of freedom	Mean Square	F-value	p-value	
Model	0.0903	8	0.0113	10.87	<0.0001	Significant
A-Synthesis Temperature	0.0125	1	0.0125	12.00	0.0030	
B-Methane	0.0091	1	0.0091	8.80	0.0086	
C-Hydrogen	0.0058	1	0.0058	5.63	0.0297	
D-Vaporizer Temperature	0.0109	1	0.0109	10.46	0.0049	
AB	0.0061	1	0.0061	5.85	0.0271	
BD	0.0140	1	0.0140	13.50	0.0019	
A^2	0.0044	1	0.0044	4.25	0.0548	
B^2	0.0102	1	0.0102	9.85	0.0060	
Residual	0.0177	17	0.0010			
Lack of Fit	0.0170	14	0.0012	5.56	0.0917	not significant
Pure Error	0.0007	3	0.0002			
Cor Total	0.1080	25				

Table 4.8. One way ANOVA test for the response surface of the reduced linear model of the oxidation temperature of as-synthesized CNT yarn response factor.

Source	Sum of Squares	Degree of freedom	Mean Square	F-value	p-value	
Model	2333.94	3	777.98	12.44	< 0.0001	Significant
A- Synthesis Temperature	1598.40	1	1598.40	25.57	< 0.0001	
B-Methane	486.92	1	486.92	7.79	0.0107	
D-Vaporiser Temperature	248.61	1	248.61	3.98	0.0587	
Residual	1375.44	22	62.52			
Lack of Fit	1284.41	19	67.60	2.23	0.2790	not significant
Pure Error	91.03	3	30.34			
Cor Total	3709.38	25				

The value of R^2 indicates the congruence of the simulated model with experimental results (Sekoai et al., 2017). Figure 4.3 and Figure 4.4 are the graphical depictions of the congruence for the simulated values to the experimental results for the quantity of CNTs and oxidation temperature

of CNTs respectively. There is an adequate convergence between experimental and simulated values for the quantity of CNTs (R^2 = 0.8772) and oxidation temperature (R^2 = 0.7298). The residual plot shows the assumption of independence is not satisfied (Martin et al., 2017).

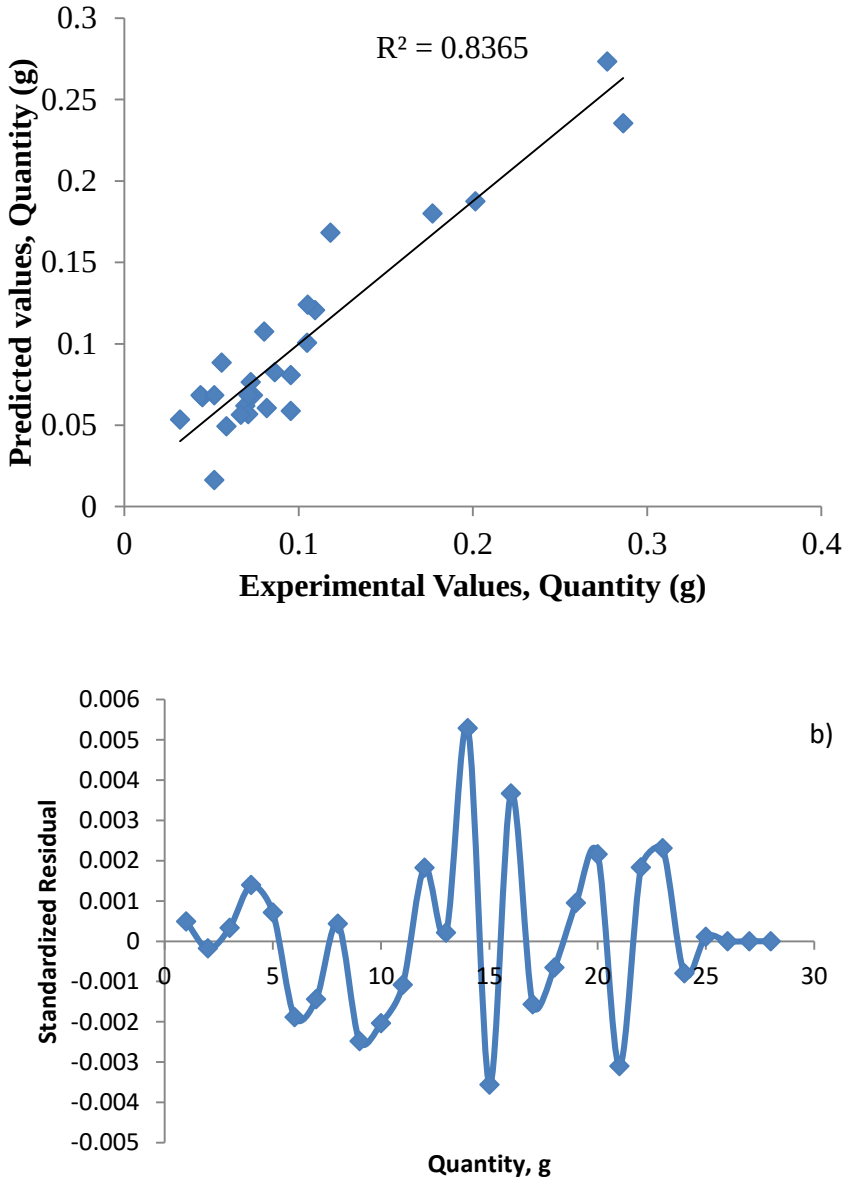

Figure 4.3. a) Experimental versus predicted quantity of as-synthesized CNT yarns b) Standardized residual as a function of quantity of as-synthesized CNT yarns.

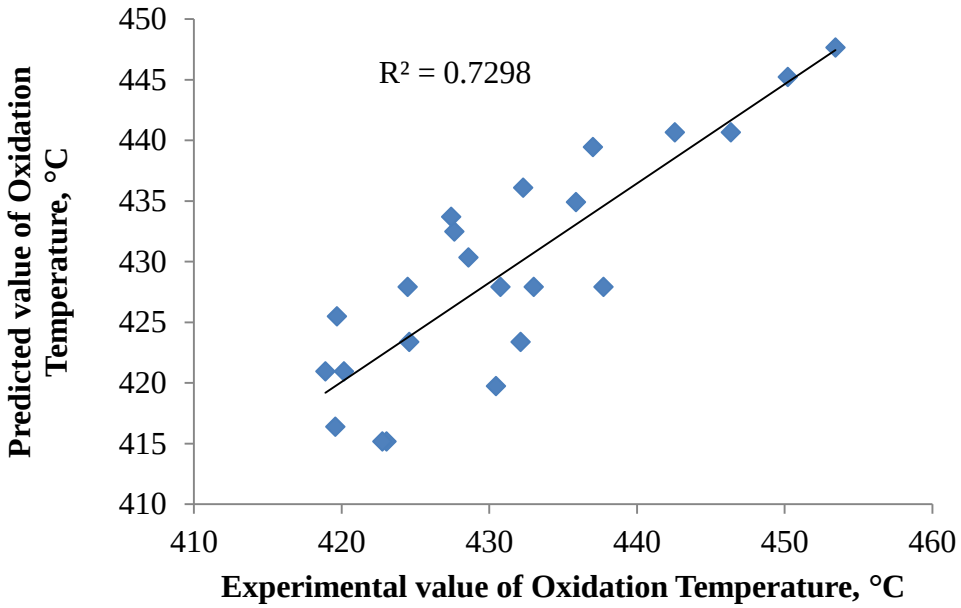

Figure 4.4. Experimental versus predicted oxidation temperature of as-synthesized CNT yarns

4.2.2 **The Interaction Effects among the Variables in the Regression Models**

Effect on quantity: Response surface methodology (RSM) is a common statistical technique used to catalyse investigations into the design and manufacture of processes and products. Several works have used RSM to optimize various parameters in the synthesis of CNTs (Kukovecz et al., 2005; Lee et al., 2016; Vanyorek et al., 2011). Figure 4.4 shows the main and interactive effects of two variables to the quantity of as-synthesized CNT yarn in an FCCVD. Quantity is on the z-axis of each plot. Quantity is maximized in the interaction of each variable at their maximum points. The surface response of the correlation of synthesis temperature, methane flow rates and their interactions indicates quantity initially decreases with increase in temperature and methane flow rate. Minimum values of quantity are reached at about 930 °C synthesis temperature and 70 mL/min methane flow rate. Further increase in synthesis temperature and methane flow rate, increases the quantity of CNT yarn. This is attributed to an increased rate of decomposition of

catalyst and high rate of carbon diffusion from the surface of the catalyst (Simate et al., 2014). Lee et al., (2016) found a comparable correlation. A similar relationship is observed in the relationship between the vaporization temperature and methane flow rate Figure 4.4E where quantity decreases initially with an increase in methane flow rate and vaporization temperature. Before reaching the midpoint, a sharp increase in quantity is observed (Kukovecz et al., 2005). No change in quantity is initially observed on the interaction between hydrogen flow rate and synthesis temperature. However, soon after the midpoint, quantity began to increase and reach its peak at the maximum values (Khuri & Mukhopadhyay, 2010). Similar responses are observed in the relationships between vaporization temperature and synthesis temperature (Figure 4.4C) and between hydrogen flow rate and methane flow rate (Figure 4.4D). In Figure 4.4F, there is a steady rise in the quantity from the interactions of vaporization temperature and hydrogen flow rate. This interaction has the least effect on quantity.

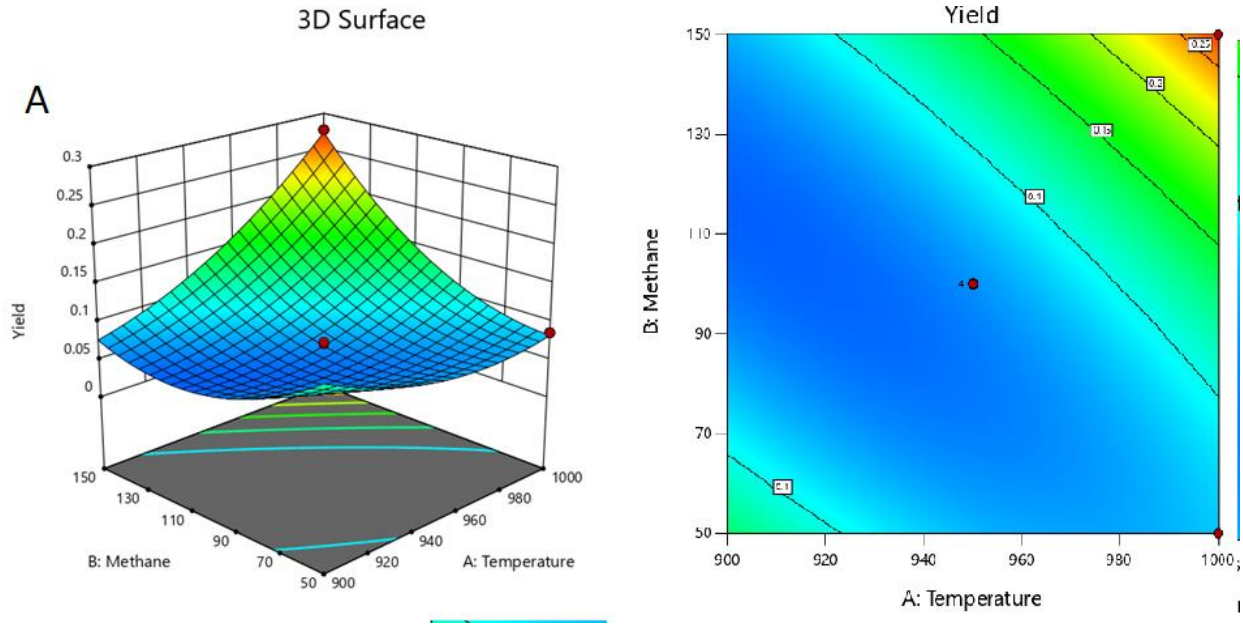

B

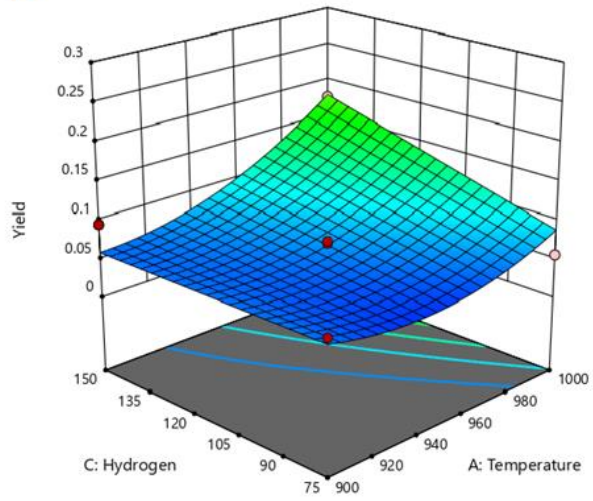
Yield
0.3
0.25
0.2
0.15
0.1
0.05
0
150
135
120
105
90
75
C: Hydrogen
900
920
940
960
980
1000
A: Temperature

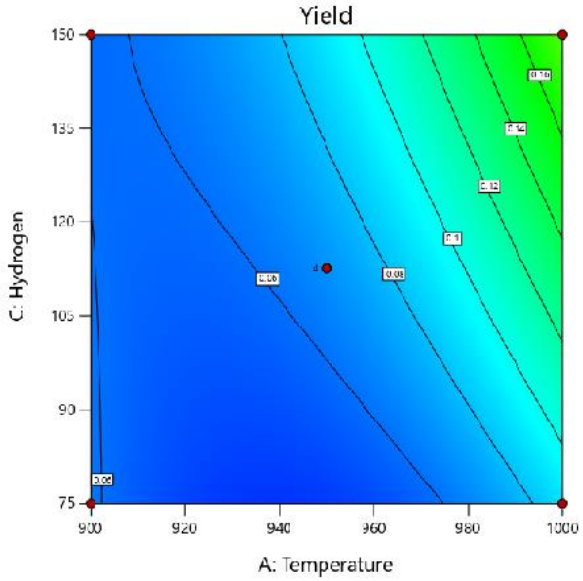
Yield
C: Hydrogen
150
135
120
105
90
75
900
920
940
960
980
1000
A: Temperature

C

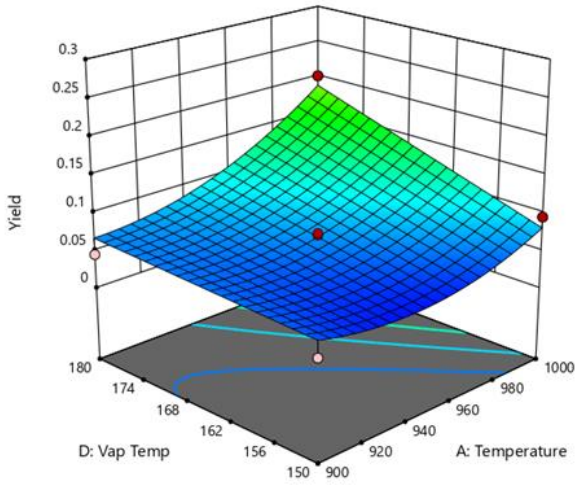
Yield
0.3
0.25
0.2
0.15
0.1
0.05
0
180
174
168
162
156
150
D: Vap Temp
900
920
940
960
980
1000
A: Temperature

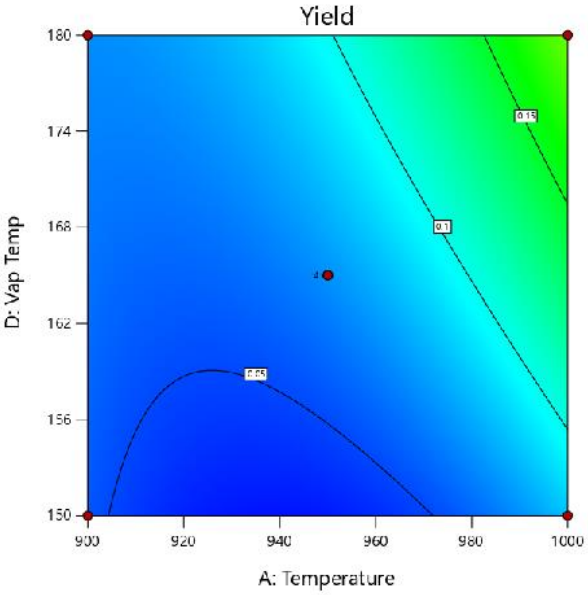
Yield
D: Vap Temp
180
174
168
162
156
150
900
920
940
960
980
1000
A: Temperature

D

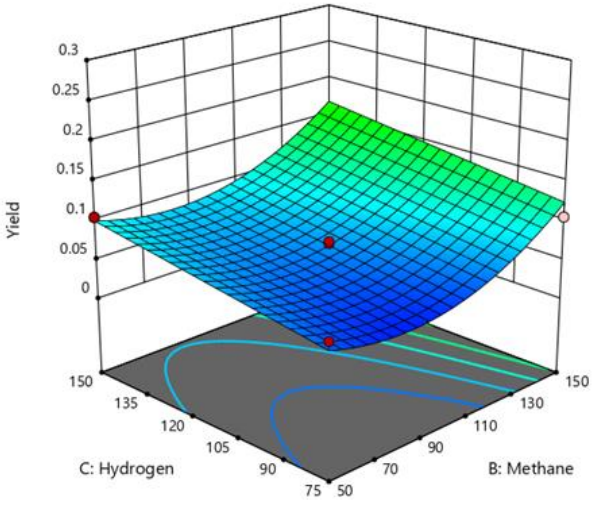
Yield
0.3
0.25
0.2
0.15
0.1
0.05
0
150
135
120
105
90
75
C: Hydrogen
50
70
90
110
130
150
B: Methane

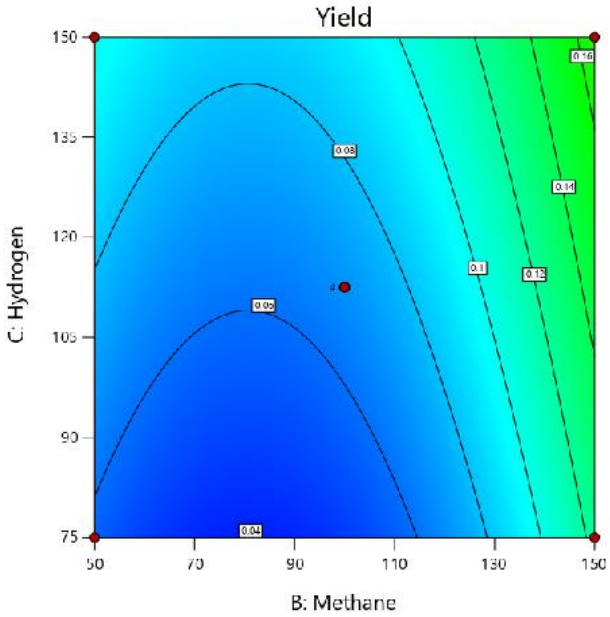
Yield
C: Hydrogen
B: Methane
150
135
120
105
90
75
50
70
90
110
130
150
0.08
0.14
0.1
0.12
0.05
0.04

E

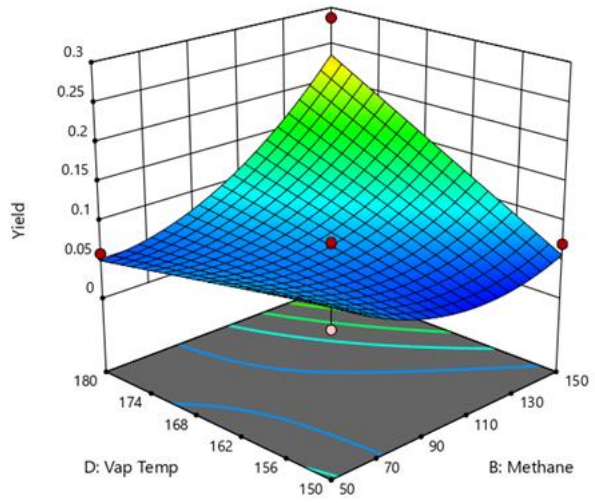
Yield
0.3
0.25
0.2
0.15
0.1
0.05
0
180
174
168
162
156
150
D: Vap Temp
50
70
90
110
130
150
B: Methane

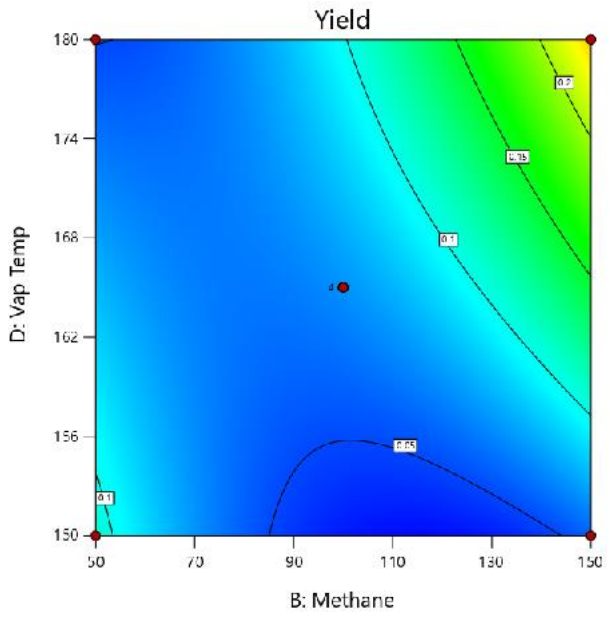
Yield
D: Vap Temp
B: Methane
180
174
168
162
156
150
50
70
90
110
130
150
0.2
0.1
0.05
0.1

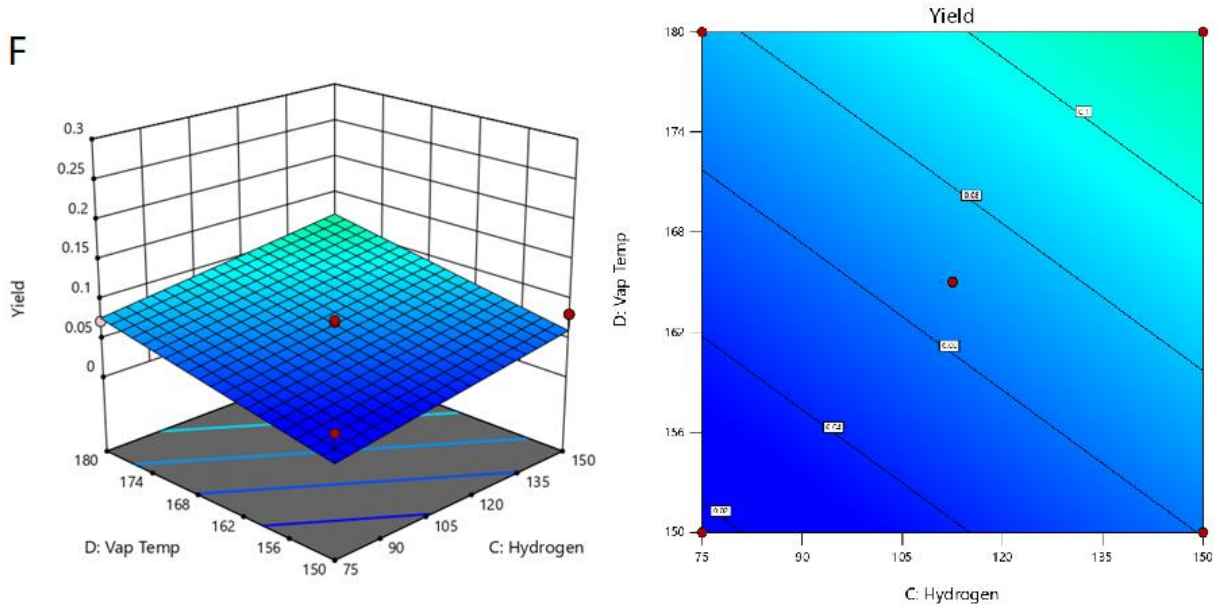

Figure 4.5. Response surface and contour plots of Box-Behnken design for the interactions of the process variables for the production of CNTs in an FCCVD on quantity. The interactions of (A) Synthesis temperature (°C) and Methane flow rate (mL/min); (B) Synthesis temperature (°C) and Hydrogen flow rate (mL/min); (C) Synthesis temperature (°C) and Vaporization temperature (°C); (D) Methane flow rate (mL/min) and Hydrogen flow rate (mL/min); (E) Methane flow rate (mL/min) and Vaporization temperature (°C); (F) Hydrogen flow rate (mL/min) and Vaporization temperature (°C).

Effect on oxidation temperature: Failure of hydrogen to meet this test could be attributed to the fact that hydrogen could cause CNTs to deform from hollow tubes to fibres (Behr et al., 2010). The hollow structure is necessary for its excellent properties. Synthesis temperature is seen to have the most effect on oxidation temperature. The catalyst particle diameter is modified by varying the vaporization temperature. The p-value of the effect of vaporization temperature on the quality of CNTs produced is not very statistically significant. This is in tandem with literature where the

correlation between catalyst particle and CNTs diameter was seen to be independent of experimental conditions (Nasibulin et al., 2005).

Response surface plots in Figure 4.6 show the main effects of two variables on the oxidation temperature of as-synthesized CNT yarns in an FCCVD (z-axis). Synthesis temperature and methane flow rate had the most pronounced effect on the oxidation temperature of as-synthesized CNT yarns. Figure 4.6A shows a steady rise in the value of oxidation temperature with increase in synthesis temperature and methane flow rate. Similar trends are observed in Figure 4.6C and Figure 4.6E for the interactions of synthesis temperature - vaporization temperature and methane flow rate-vaporization temperature respectively. In Figure 4.6B, the rise in oxidation temperature is occasioned only by the rise in synthesis temperature as hydrogen is not part of the model. This is also observed in Figure 4.6D and Figure 4.6F. The highest oxidation temperature (446 °C) is observed from BBD runs of 1000 °C, 150 mL/min methane volumetric flow rate and vaporization temperature of 180 °C. Plots with hydrogen volumetric flow rate show no effect of hydrogen flow rate on the oxidation temperature as it is not part of the model. Validation of optimal parameters resulted in oxidation temperature in the range of observed oxidation temperatures.

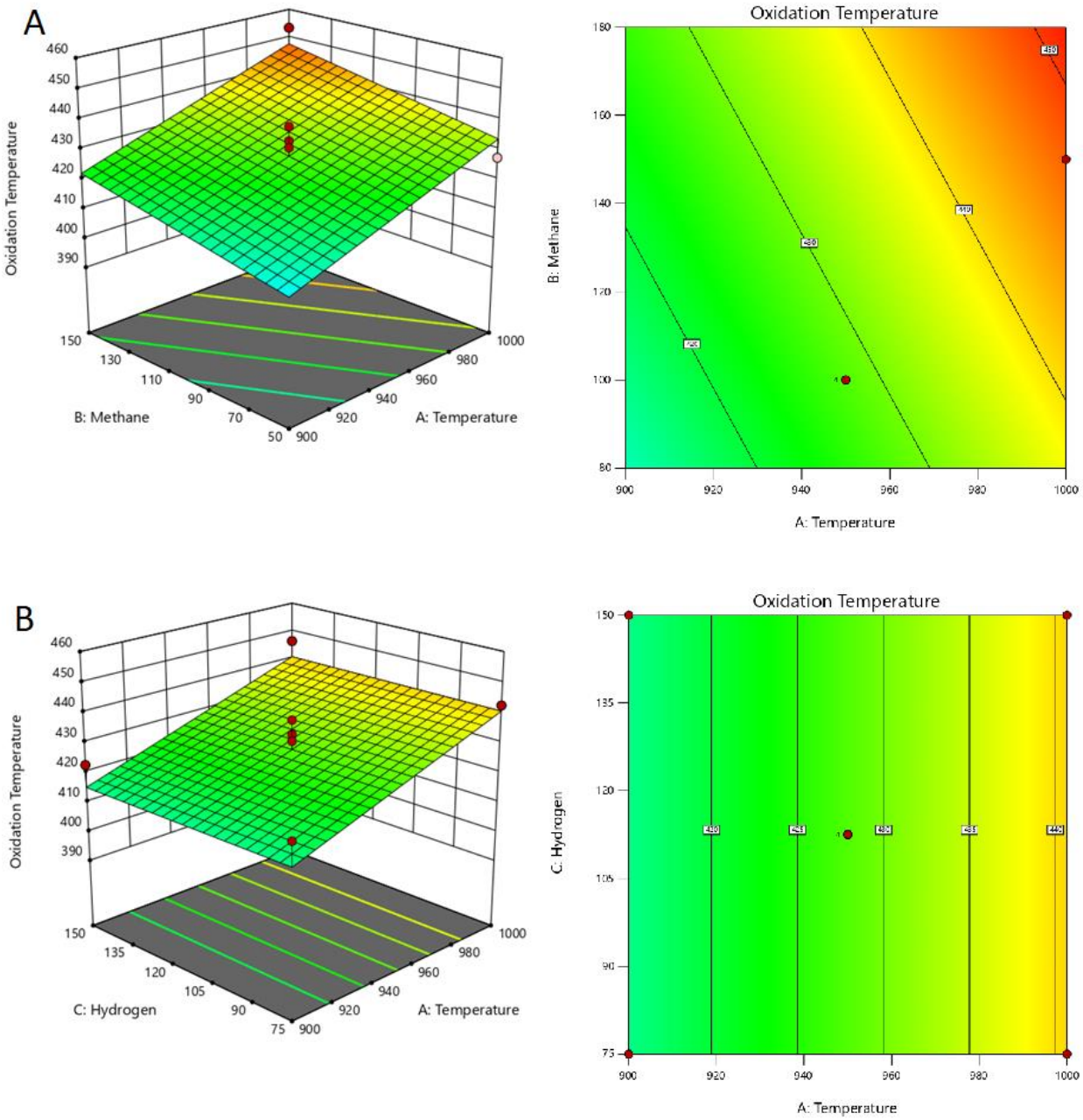
A
Oxidation Temperature
460
450
440
430
420
410
400
390
150
130
110
90
70
50
B: Methane
900
920
940
960
980
1000
A: Temperature
Oxidation Temperature
180
160
140
120
100
80
B: Methane
900
920
940
960
980
1000
A: Temperature
B
Oxidation Temperature
460
450
440
430
420
410
400
390
150
135
120
105
90
75
C: Hydrogen
900
920
940
960
980
1000
A: Temperature
Oxidation Temperature
150
135
120
105
90
75
C: Hydrogen
900
920
940
960
980
1000
A: Temperature

C

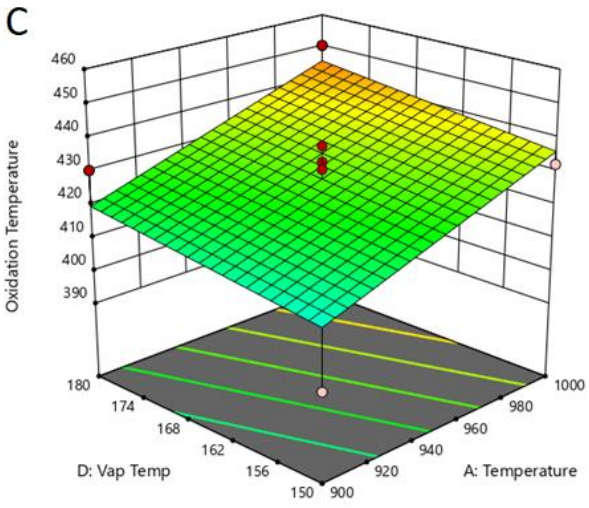
Oxidation Temperature
460
450
440
430
420
410
400
390
180
174
168
162
156
150
D: Vap Temp
900
920
940
960
980
1000
A: Temperature

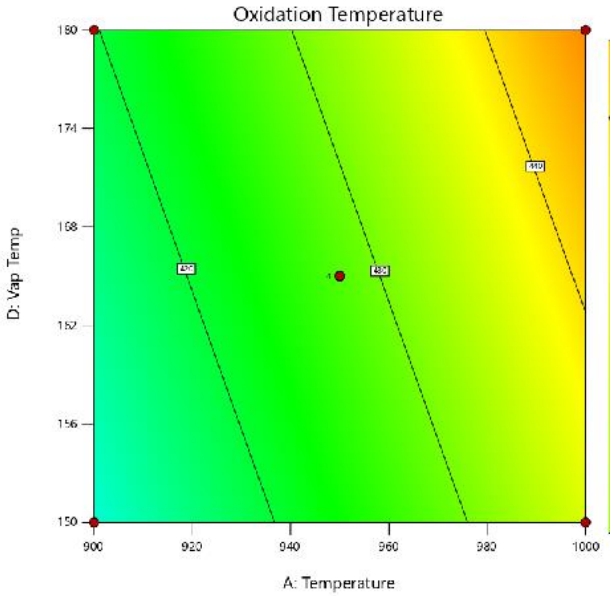
Oxidation Temperature
D: Vap Temp
A: Temperature

D

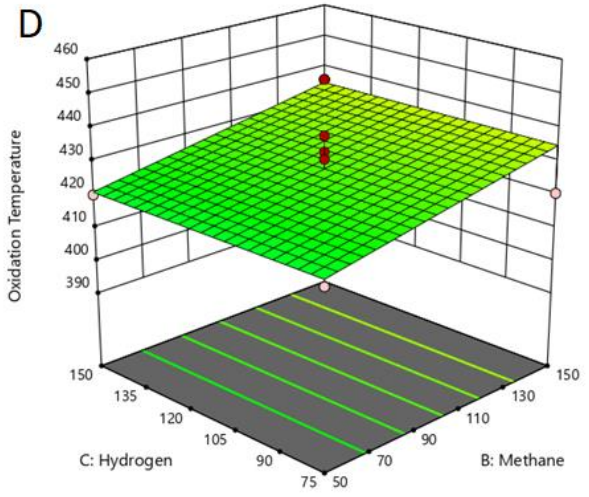
Oxidation Temperature
460
450
440
430
420
410
400
390
150
135
120
105
90
75
C: Hydrogen
50
70
90
110
130
150
B: Methane

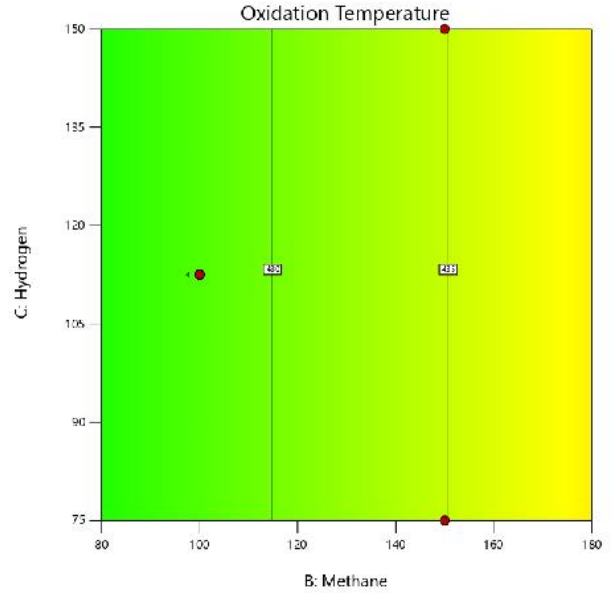
Oxidation Temperature
C: Hydrogen
B: Methane

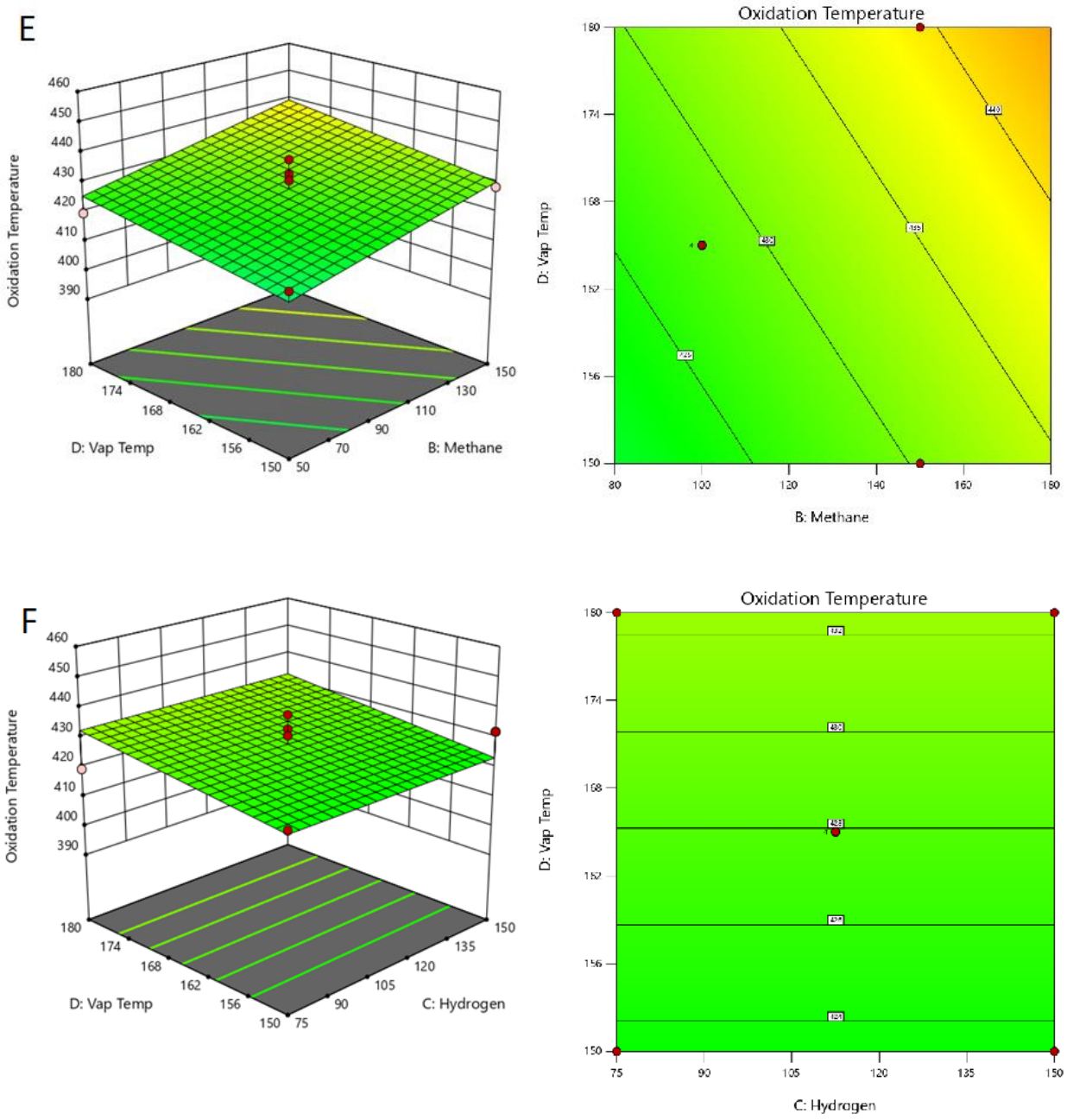

Figure 4.6. Response surface and contour plots of Box-Behnken design for the interactions of the process variables for the production of CNTs in an FCCVD on quantity. The interactions of (A) Synthesis temperature (°C) and Methane flow rate (mL/min); (B) Synthesis temperature (°C) and Hydrogen flow rate (mL/min); (C) Synthesis temperature (°C) and Vaporization temperature (°C); (D) Methane flow rate (mL/min) and Hydrogen flow rate (mL/min); (E)

Methane flow rate (mL/min) and Vaporization temperature (°C); (F) Hydrogen flow rate (mL/min) and Vaporization temperature (°C).

4.2.3 **Response Surface Numerical Optimization**

To determine the best combination of responses, the geometric mean was used as the objective function D.

$$D = (\prod_{i=1}^{n} d_i)^{\frac{1}{n}} \quad (4.3)$$

where d_i – desirability of individual responses and n – number of responses being optimized.

The design expert software was used to solve the desirability as an objective function with limits set within the experimental range (Mohammadian et al., 2018). The two responses were considered in optimization (Khuri & Mukhopadhyay, 2010). Equal weight was assigned to all variables in this optimization while the goals were set at minimal to obtain maximum results using minimum resources. The optimum operating parameters tabulated in Table 4.9 for optimum quantity and oxidation temperature of as-synthesized CNT yarns was described by the model. The experimental result is convergent with the model.

Table 4.9. Optimum operating parameters for the synthesis of CNT yarns in FCCVD reactor with direct spinning.

Factors	Optimum values
Synthesis Temperature (°C)	970
Methane Volumetric flow rate (mL/min)	137.5
Hydrogen Volumetric flow rate (mL/min)	78
Vaporization Temperature (°C)	175
Argon Volumetric flow rate (mL/min)	100
Spinning rate (rpm)	125
Mass of thiophene (mg)	2
Quantity (g)	0.18
Oxidation Temperature (°C)	441.306
Desirability	1

4.3 Concluding remarks

In conclusion, synthesis of CNT yarn in FCCVD with direct spinning is affected by many parameters including Synthesis Temperature, Methane Volumetric flow rate, Hydrogen Volumetric flow rate, Vaporization Temperature, Argon Volumetric flow rate, Spinning rate and sulfur content. Their effect on quantity and oxidation temperature of CNTs produced was

methodically examined using DoE in two stages: 2-level fractional factorial for screening and Box-Benken for RSM. Design of Experiments (DoE) is a viable method for optimizing with a small number of experiments. Synthesis temperature, methane volumetric flow rate, hydrogen volumetric flow rate and vaporization temperature were most influential to the morphology and quality of CNT yarns produced in FCCVD. The developed regression models fitted the data adequately with $R^2 = 0.8365$ for the quantity of CNTs produced and $R^2 = 0.7298$ for the oxidation temperature of as-produced CNTs. They are therefore suitable for the description of the process within the considered ranges of variables.

CHAPTER FIVE

5. EFFECT OF SYNTHESIS TEMPERATURE, HYDROGEN FLOW RATE ON ELECTRICAL PROPERTIES OF AS-SYNTHESIZED CNT YARN

Various parameters have been observed to influence the quality and quantity of CNT yarns produced in FCCVD for the application as a filament in incandescent light bulbs. Thus far in this study, synthesis temperature has been observed to have the most influence on the quality of as-synthesized CNT yarn. Further study to determine its effect on the electrical properties because of the desired application is necessary.

This study is therefore carried out to determine the effect of hydrogen to methane ratio on the electrical properties of as-synthesized CNTs. This chapter examines the effect of synthesis temperature and hydrogen flow rate on the electrical properties of as-synthesized CNT nano yarns. A part of this chapter is based on a paper published in Results in Physics: Igbokwe, E. C., Daramola, M. O., & Iyuke, S. E. (2019). Production of carbon nanotube yarns via floating catalyst chemical vapour deposition: Effect of synthesis temperature on electrical conductivity. *Results in Physics, 15, 102705.*

5.1 Results and Discussions

5.1.1 Effect of synthesis temperature on the electrical conductivity of as-synthesized CNTs

To investigate the effect of synthesis temperature on electrical properties, the temperature was varied from 800 – 1000 ^{o}C at a step change of 100 ^{o}C. The flow rates of methane, argon and hydrogen were kept constant at 100 mL/min, 100 mL/min and 75 mL/min, respectively.

The Raman spectra for the as-synthesized carbon nanotube yarns at temperatures 800, 900, and 1000 °C are similar to the prominence of D and G bands at about 1350 cm^{-1} and 1580 cm^{-1} respectively in the first-order region. The second orders region between 2200 cm^{-1} and 3250 cm^{-1} consist of a broad and asymmetric 2D band at near 2730 cm^{-1}. These are depicted in Figure 5.1. They are consistent with the Raman spectra of CNTs (Dresselhaus et al., 2005).

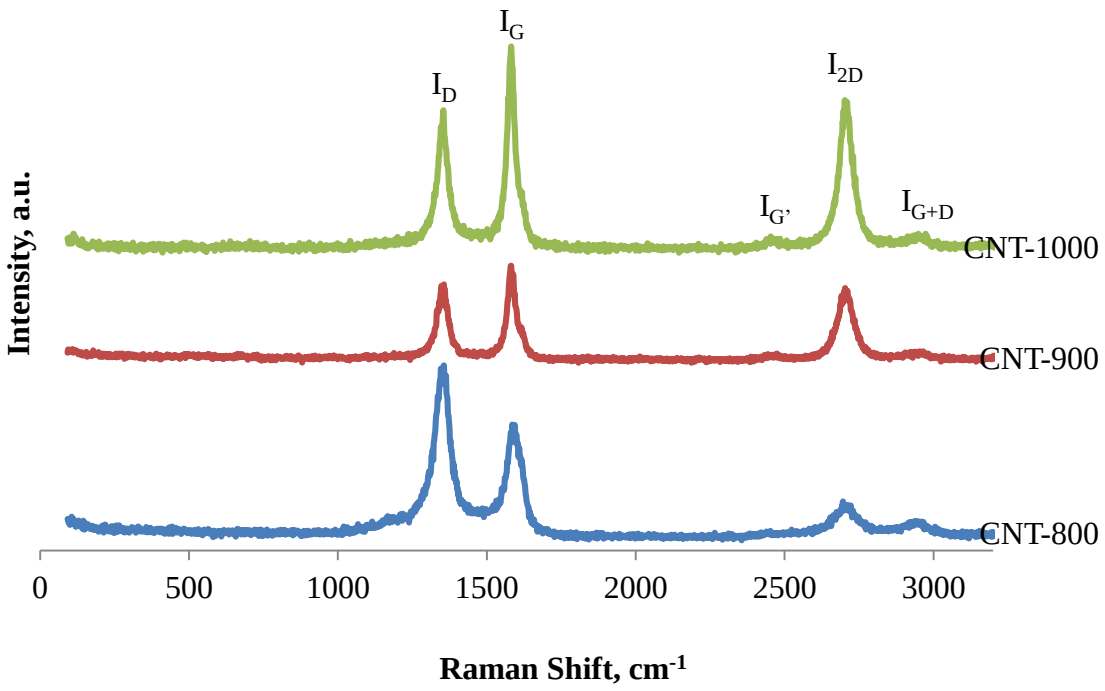

Figure 5.1. Raman spectroscopy spectra of as-synthesized and spun carbon nanotube yarns.

The I_D/I_G ratio indicates the ratio of presence of disordered amorphous carbon to the graphitic carbon atoms disorder (Lehman et al., 2011). It is seen to decrease with an increase in synthesis temperature. It is proposed for use in determining the crystal size (Tuinstra & Koenig, 1970). It is also a measure of graphitization. A decrease in the I_D/I_G ratio could be due to an increase in the number of sp^2 bonds or an increase in the size of its clusters (Ray et al., 2014). An increase in the

intensity of the 2D band with an increase in synthesis temperature, in this case, confirms the decrease of the I_D/I_G ratio with an increase in temperature is due to an increase in the number of sp^2 bonds (Dresselhaus et al., 2010). I_D/I_G ratio of as-synthesized and spun MWCNTs are presented in Table 5.2.

Analysis of the obtained Raman spectroscopy graphs shows CNT-1000 has the sharpest d-band peak of the three spectra with CNT-800 having the broadest base of the band. CNT-1000 is judged the purest sample due to the highest intensity of the 2D-band peak. The 2D band measures purity and quality of MWCNT more accurately than the I_D/I_G ratio given that the 2D-band results from a coupling effect for the two-phonon process, which impurity would otherwise hinder. The peak present around 2450 cm^{-1} in the second-order of the Raman spectra, with CNT-1000 exhibiting the highest intensity in our case, is a strong indication of the structural integrity of the nanotube (Lehman et al., 2011).

Nature of defects found in graphite could be hopping defects caused by deformation on the carbon bonds; on-site defects originating from bonds to other atoms thus forming sp^3 hybridization; or charged impurities initiated by charged atoms adsorbed on the surface of graphene (Venezuela et al., 2011). Electrical properties of CNT such as electron transport and field emissions improve with an increase in sp^2 bonds (Li et al., 2018). D´ band found around 1620 cm^{-1} is responsible for the determination of the nature of defects (Eckmann et al., 2012). Due to the high defect concentration, it is not distinguished from the G-band. The concentration is seen to be highest in CNT-800 because it is not evident. The ratio of I_D/I_{2D} for CNT-900 and CNT-1000 are 1.241 and 1.275, respectively which are approximately 1.3. This indicates the defects are on-site in nature.

Table 5.2. Analysis of as-synthesized CNT yarns

Notation	**Synthesis Temp, (^oC)**	**$FWHM_{002}$, cm^{-1}**	**I_{002} (c.p.s)**	**I_D/I_G**	**I_{2D}/I_G**	**I_{2D}/I_D**	**Electrical conductivity (Sm^{-1})**
CNT-800	800	0.01416	221	1.447934	0.3140	0.2130	0.0065
CNT-900	900	0.01438	348	0.82387	0.9023	0.9833	0.0508
CNT-1000	1000	0.01787	158	0.706145	0.8897	1.0349	0.1673

CNT yarns are clearly identified on the SEM micrographs for the 3 CNTs samples depicted in Figure 5.2 with varying morphology. This could be attributed to the varying levels of iron catalyst sintering and migration at the different synthesis temperatures (Chizari et al., 2014). There are impurities on all the samples. The diameter of the as-synthesized and spun CNT yarns decreases with increase in synthesis temperatures. Theoretical and experimental findings in the literature report increase in diameter of SWCNT and MWCNT with an increase in synthesis temperature. This is in line with the kinetic energy and the diffusion rate of carbon on an iron catalyst as per the kinetic theory of gases (Kuwana & Saito, 2005; Öncel & Yürüm, 2006; Raji et al., 2011). However, this is seen to be contrary for temperatures below 1000 °C which is in line with our findings (Kuwana & Saito, 2007). SEM micrograph also shows CNT-1000 are straight and aligned.

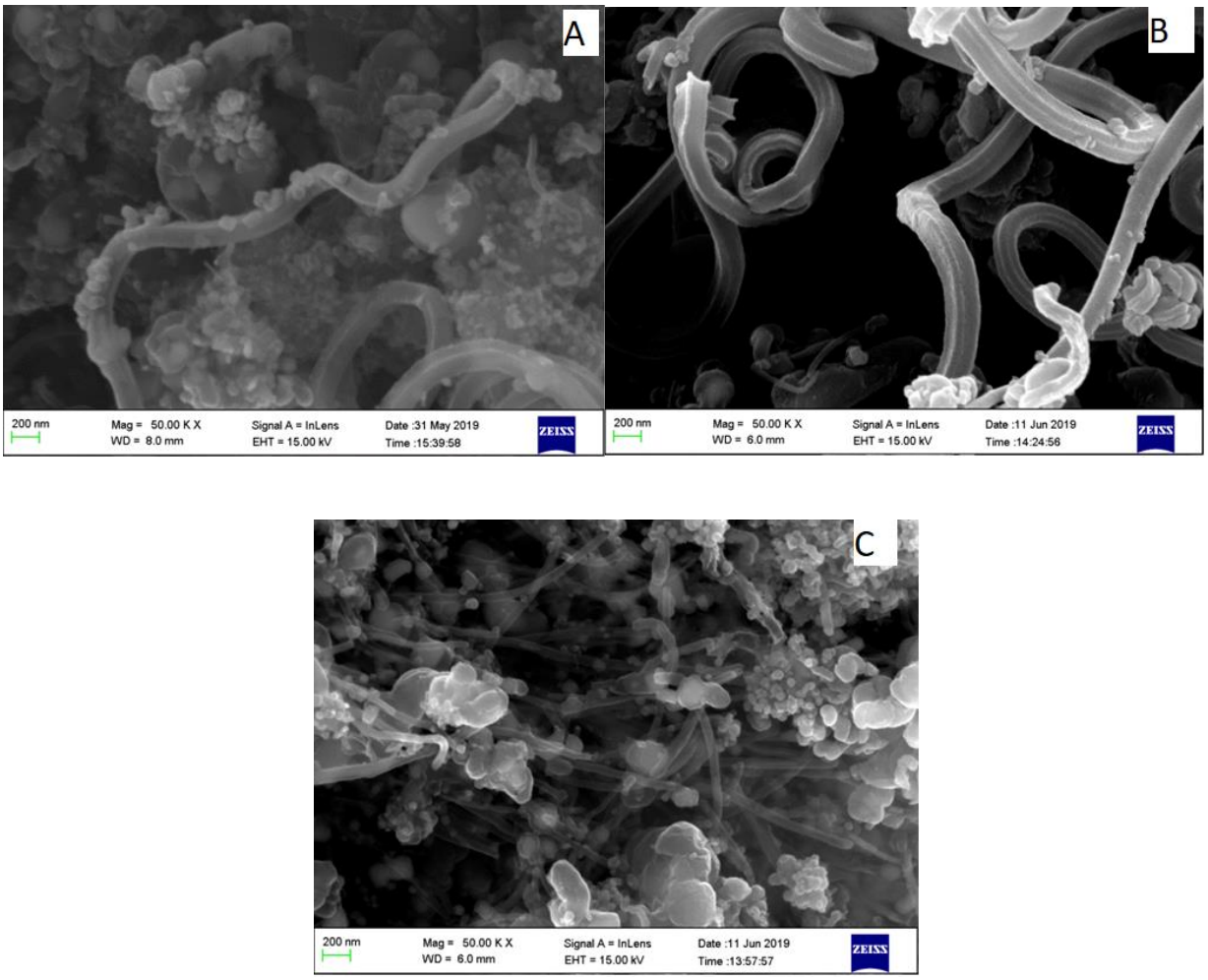

Figure 5.2. SEM micrographs of as-synthesized and spun CNT yarns. A – at 800 °C; B – at 900 °C; C– at 1000 °C.

An X-ray diffraction pattern is a plot of the intensity of X-rays scattered at different angles by a sample. It is used to understand the crystal structure of carbon nanotubes.

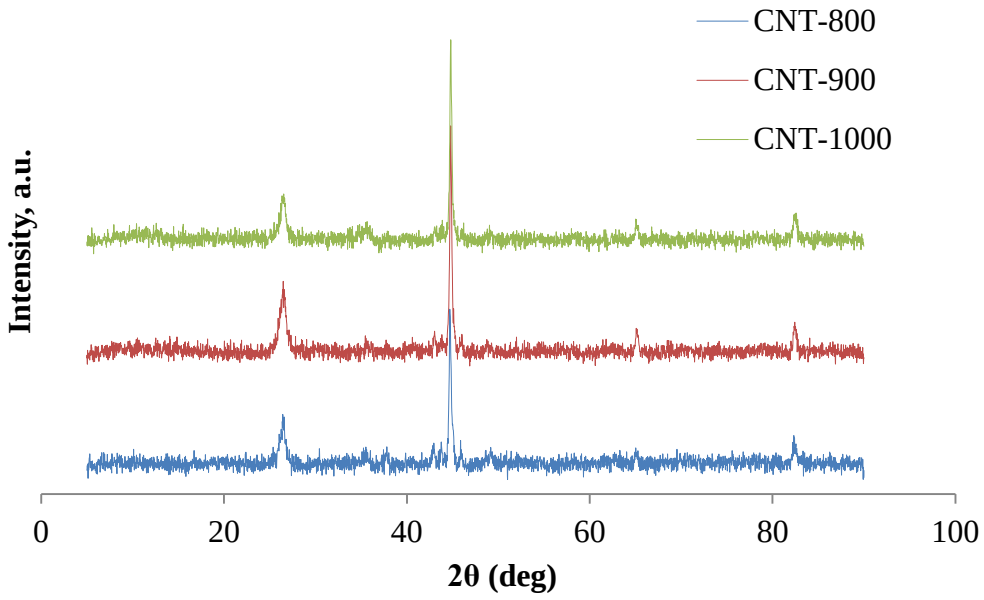

Figure 5.3. XRD patterns of CNT yarns at the various hkl planes

Various peaks owing to the presence of iron from the ferrocene catalyst and other carbonaceous compounds were detected in the CNTs sample irradiated. The diffraction peaks of carbon nanotubes were however found at (001), (002), (100), (004) and (110) corresponding to the atomic pair distribution function PDF 00-058-1638. The (002) diffraction plane is related to the periodicity between the graphene layers and the [(100) and (101)] diffraction planes are related to the periodicity within the graphene layers (Reznik et al., 1995). They are located at 26° and 43° respectively on the 2theta. All the XRD patterns acquired show peaks at equivalent 2θ angular range with equal interplanar distances between the walls. The interplanar distance limit d_{002} = 0.344 nm indicate the as-synthesized carbon materials for all synthesis temperatures are graphite-like (Ermakova et al., 2001). The as-synthesized CNT yarns remain at a higher limit for interplanar distances of graphitic carbon materials due to the maintenance of the sp^3 hybridization structure

by bonding with hydrogen (Ruland, 1965). This is characteristic of filamentous carbon synthesized from methane.

Synthesis temperature is seen to have no detectable effect on the degree of graphitization according to the Maire and Mering formula (Ermakova et al., 2001) since d_{002} =3.44 Å in all three samples

$$d_{002} = 3.354 + 0.086(1 - g) \quad (5.1)$$

where d is interplane distance (d_{002}) in angstroms, g is graphitization percentage.

However, using the Scherrer equation, average crystalline size CNTs can be determined for each sample since they have different full width half maximum (FWHM).

$$D = \frac{n\lambda}{\beta}\cos\theta \quad (5.2)$$

where n is Scherrer constant, λ – wavelength of the x-ray, β – full width half maximum, θ – angle of reflection.

According to the Scherrer equation, the crystal size of nanoparticles is inversely proportional to the full-width-half-maximum of carbon nanotubes. The diameter of the as-synthesized and spun CNT yarns decreases with increasing synthesis temperatures. Larger diameters of CNTs are seen to diminish the nanotube characteristics by increasing the defect density (Collins, 2017; Maffucci et al., 2017).

The distribution of atoms within the lattice determines the peak intensity. Therefore, the x-ray diffraction pattern is the impression of atomic arrangements in an identified material. Cao et al (2001) established that the intensity of the (002) diffraction plane is inverse to the degree of alignment of nanotubes.

$$V_a = \frac{A_{002}}{S_{002}} = \frac{A_{002}}{dI} \quad (5.3)$$

where A_{002} intensity peak area of the (002) diffraction plane from vertically aligned CNTs; S_{002} is the summation of diffraction beams and dI (I_{init} - I_{direct}) is the absorbed intensity of the direct X-ray beam.

An increase in intensity is also associated with an increase in the number of walls in the CNTs (Alhosiny et al., 2013). An increase in the number of walls is associated with an increase in interplanar resistance (Stetter et al., 2010). In this study, CNT-1000 having the least intensity in the XRD pattern also proved to have the least resistance.

Thermogravimetric analysis of the as-synthesized carbon nanotube yarns was carried out to determine the purity, crystallinity, and thermal stability of the nanotubes. The TGA for as-synthesized CNT yarns in Figure 5.4a is typical of MWCNTs. All 3 samples show the comparable oxidation behaviours. All samples showed a slight weight gain before the onset of rapid weight loss. This is attributed to the oxidation of metal particles present on the surface of the as-synthesized samples (Hou et al., 2001). CNT-1000 shows the least oxidation of metal on the surface signifying more catalyst is encapsulated within the nanotubes than CNT-800 and CNT-900. This is confirmed by the SEM images and electron dispersion spectroscopy (Fig 5.5). The composition of iron in the spectrum is seen to decrease with an increase in the synthesis temperature. From the derivative weight curve in Figure 5.4b, it is observed that the as-synthesized and spun MWCNTs exhibit similar oxidation peaks. Flammables like oils on the sample are observed to evaporate at about 50 °C while the wet mass evaporates at about 100 °C. At about 250 °C the amorphous carbons on the surface of the nanotubes are decomposed. The decomposition of carbonaceous compounds is seen at a temperature of about 370 °C for all three samples.

The CNTs synthesized at 800 °C (CNT-800) was thermally stable up to 280 °C with first an increase in weight due to metal catalyst particle oxidation. The rapid oxidation of the sample began at about 540 °C. After the TGA run, about 40% of the sample was left as a residue. CNT-900 showed a slightly higher weight gain making it the highest of the three. This weight gain began at about 290 °C. It remained thermally stable up to 480 °C and oxidation rapidly set in at about 550 °C. The residue of TGA heating in atmospheric air is seen to be about 36% being the lowest of the three samples. In the case of sample CNT-1000, it showed a very slight weight loss before an increase in weight making it the least increase in weight due to oxidation of metal particles on the surface of the as-synthesized CNTs. This indicates that most of the metal catalyst used in the synthesis of CNT-1000 is encapsulated in the CNTs and few left on the surface (Li et al., 2008). This is evident from the TEM images of the samples. Thermal stability is observed up to about 435 °C with rapid oxidation starting at about 560 °C. Approximately 46% of the sample residue remained after TGA analysis at 900 °C. Imperfections on the walls and ends of the nanotubes reduce the oxidation temperatures of as-produced CNTs (Bom et al., 2002). This suggests CNT-800 has the most defects and CNT-1000 the least. The purity of the samples was determined by the percentage of the residue of thermogravimetric analysis carried out under airflow from ambient temperature to 900 °C. Increase in synthesis temperature from 800 °C to 1000 °C resulted in more crystalline nanotubes as shown in the increase in the onset temperature of oxidation temperature as reported by (Lee et al., 2001). The residue of CNT-1000 remained the highest due to oxidative stability probably brought about by the absence of frail edges that could promote unzipping and peeling away of the nanotube walls (Li et al., 2008).

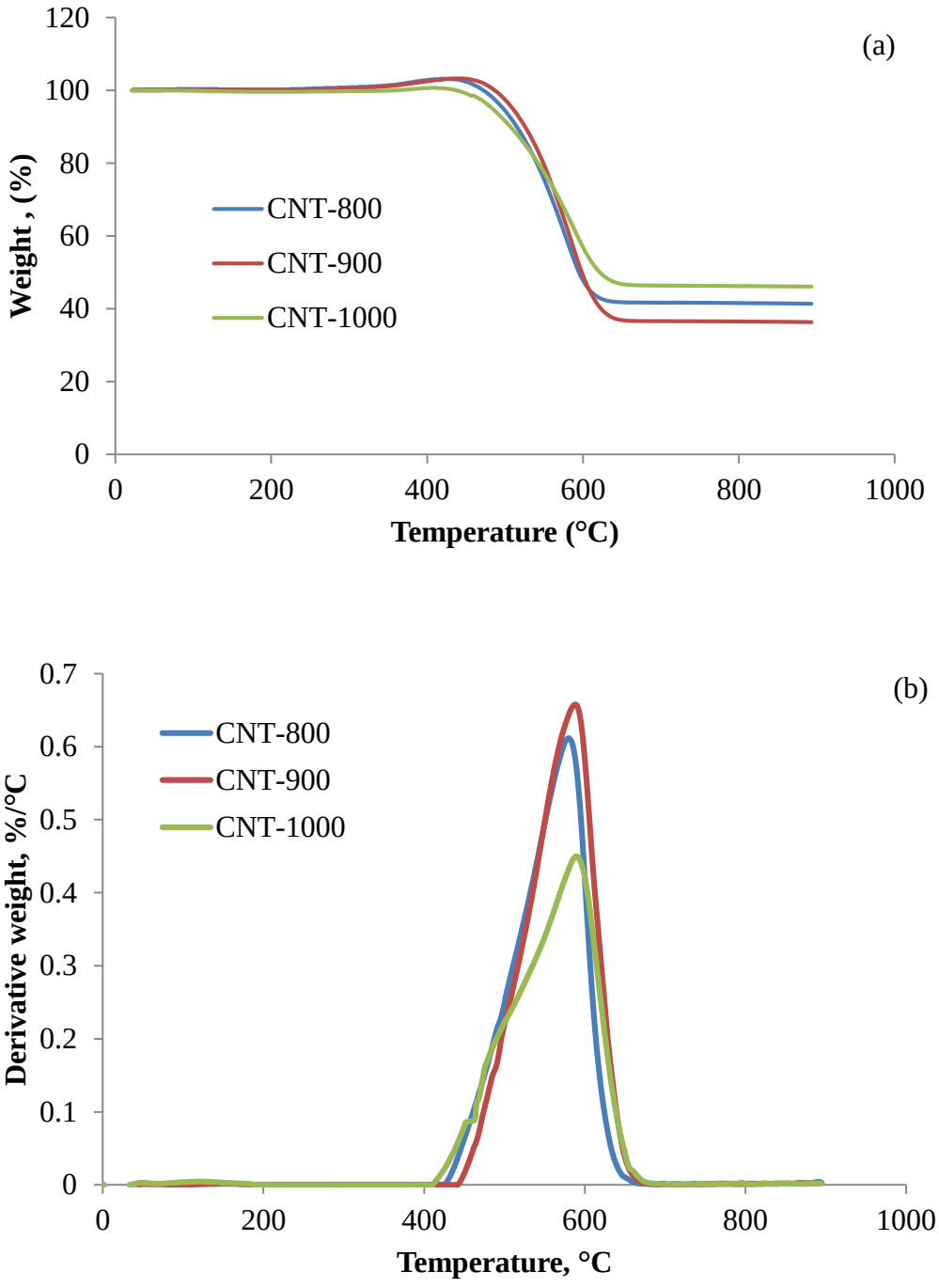

Figure 5.4. (a) weight loss curves for as-synthesized carbon nanotubes in an FCCVD using ferrocene with different temperatures; (b) Temperature effects on oxidation of as-synthesized carbon nanotubes.

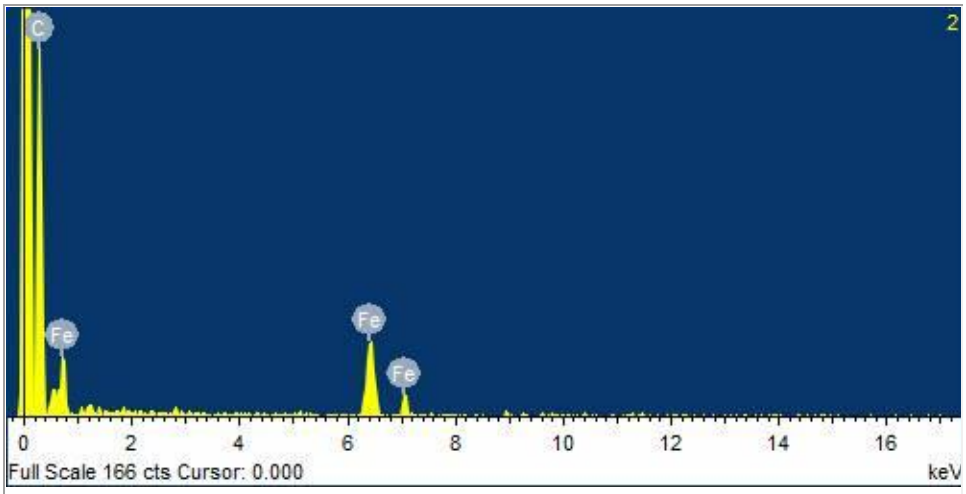

Element	Weight %	Atomic %
C K	82.76	95.71
Fe K	17.24	4.29
Totals	100.00	

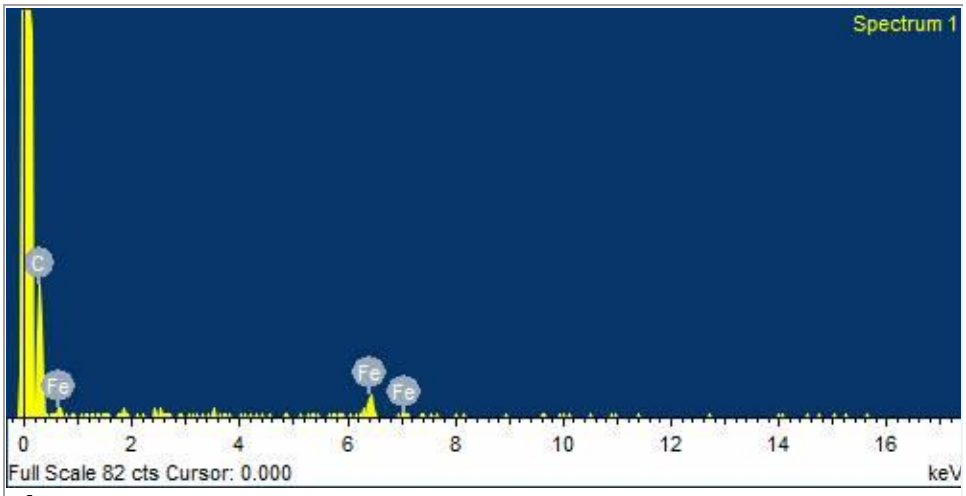

Element	Weight %	Atomic %
C K	89.16	97.45
Fe K	10.84	2.55
Totals	100.00	

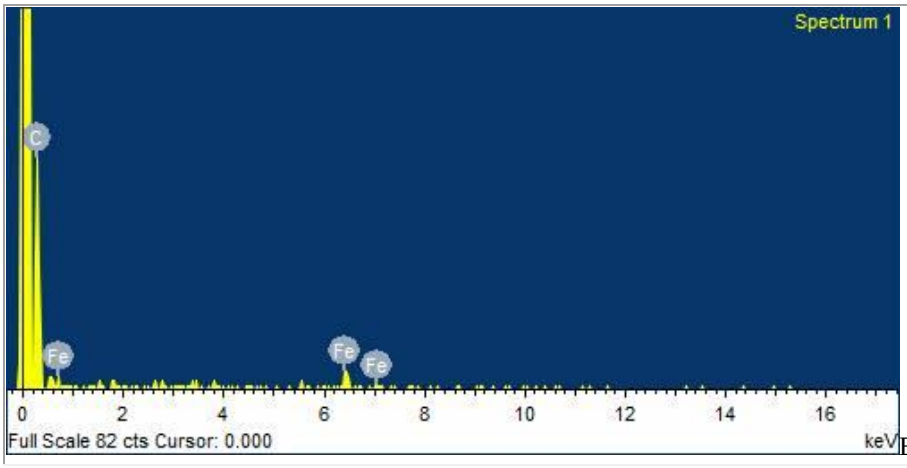

Element	Weight%	Atomic%
C K	92.32	98.24
Fe K	7.68	1.76
Totals	100.00	

Figure 5.5 Energy Dispersive Spectroscopy (EDS) of CNT yarn produced at the synthesis temperature of (a) 800 °C (b) 900 °C (c) 1000 °C showing the decrease in the composition of iron with an increase in synthesis temperature.

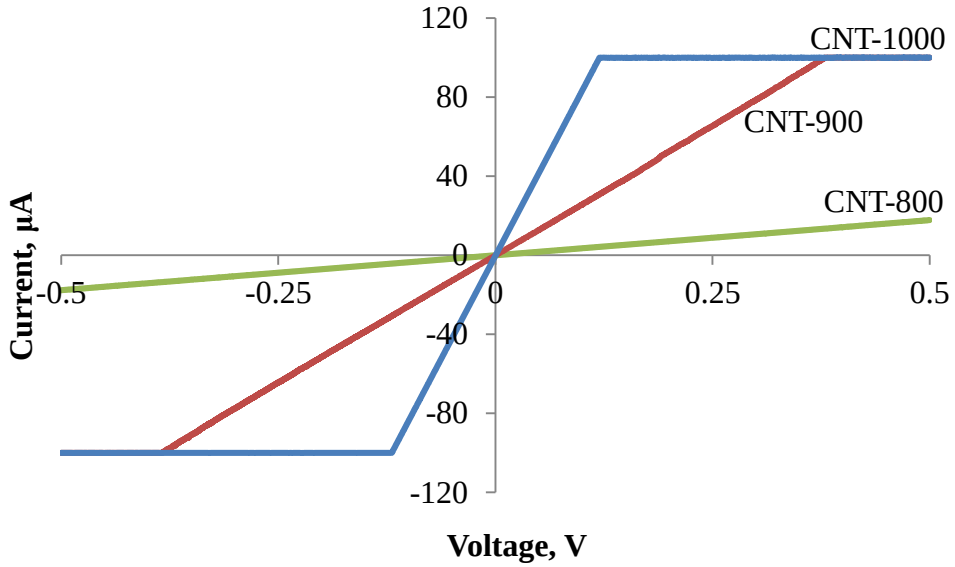

Figure 5.6. Current-voltage relationship of CNTs

Figure 5.6 depicts the relationship between the applied voltage and current for applied voltage −0.5 V to 0.5 V. CNT-800 is seen to have characteristics like a resistor given that it obeys the ohm's law with a precise linear relation between the applied voltage and the current that flows through it (Gutiérrez et al., 2002). However, the resistance is seen to be very high and the conductivity is low Figure 5.5. The resistance of CNT-900 and CNT-1000 are much lower than CNT-800 though they are not constant throughout the measurement (Sze & Ng, 2006; Tans et al., 1998). Resistance increases with increase in temperature indicating that they are semi-conductive in nature as is tungsten wire currently used in incandescent bulbs.

The values of electrical conductivity (Table 5.2) from this study are generally lower than the reported room temperature conductivity of CNTs in the literature (Aberefa et al., 2018; Miao, 2011; Tans et al., 1998). This could be attributed to the lower quality of macroscopic CNTs compared with individual CNTs. Low compact density, impurities and the presence of amorphous carbons could also contribute to low conductivity. However, conductivity is seen to be highest in CNT-1000 indicating that higher temperature within the limits of this study results in better conducting CNT yarn. This finding has been consistent with the findings from the analysis of Raman, XRD, TGA and electron microscopy where we observed higher purity, more aligned, smaller diameter, less defective and more crystalline CNT yarns.

5.1.2 **Effect of Hydrogen**

Experimental runs to determine the effect of hydrogen gas on the quality and quantity of CNT yarns produced in an FCCVD reactor for application as a filament in the incandescent bulb was carried out by varying the ratio of methane and hydrogen. The synthesis conditions are presented

in Table 5.3. Annotations used were in line with the ratio of Hydrogen to methane volumetric flow rates.

Table 5.3. Synthesis conditions for the study on the effect of hydrogen co-feeding

Annotation	**Synthesis Temperature, °C**	**Methane flow rate, mL/min**	**Argon flow rate, mL/min**	**Hydrogen flow rate, mL/min**	**Ratio of hydrogen to methane**
CNT-0	1000	50	100	0	0
CNT-1	1000	50	100	50	1
CNT-2	1000	50	100	100	2
CNT-3	1000	50	100	150	3

Raman spectroscopy was used to determine the changes in the structure of as-synthesized CNT yarns using different hydrogen feed rates. Low laser power was used to acquire spectra because of the presence of iron in the sample which gives off hematite spectra at high laser power. The spectra produced were similar for all the samples as shown in Figure 5.6. The tangential carbon stretching mode seen at about 1580 cm^{-1} confirms the presence of carbon materials in the sample (Yu & Brus, 2001). However, the resonance breathing mode (RBM) usually observed around 100 – 250 cm^{-1} of Raman spectra of single-walled carbon nanotubes (SWCNTs) and some double-walled carbon nanotubes (DWCNTs) are absent in all the spectra. Therefore these spectra are consistent with MWCNTs. I_D/I_G ratio is presented in Table 5.4 is seen to first decrease reaching its minimum point in CNT-1 indicating it is the most graphitized. Comparable observation is made by (Behr et al.,

2010). Further increase in the flow rate of hydrogen increases the concentration of hydrogen in the synthesis environment resulting in less graphitisation of produced CNTs (Losurdo et al., 2011).

The presence of predominantly MWCNT is confirmed from the transmission electron microscopy (TEM) of the as-synthesized CNT yarns (Figure 5.7). Differences in the structure with the flow rate of hydrogen in the FCCVD are however observed in the TEM micrographs. CNT-0 is seen to be made up of thick walls with little or no hollow forming fibrils. In contrast, CNT-1 is seen to have larger diameter tubes with wide hollow and thick straight walls. Behr et al, 2010 found a similar result when hydrogen and methane were used in the ratio of 1 in a catalytic plasma enhanced CVD reactor (Behr et al., 2010). Graphite and CNTs are formed through the formation of iron carbide (Fe_3C) by the ferrocene catalyst in presence of limited supply of hydrogen (Pellegrino et al., 2013). The average length of the CNT-1 nanotube measured using zeta nanosizer is found to be the shortest of the four samples. This can be attributed to the formation of iron carbide which has higher solubility on carbon than in pure iron causing catalyst poisoning (Schulz et al., 2017; Sharma et al., 2009). Subsequent increases in hydrogen co-feeding resulted in less graphitized but longer CNT yarns. Excess hydrogen in the reaction system triggers the modification of the catalyst, acts as an activation agent by promoting carbon source decomposition into more reactive forms and subsequent growth of long CNTs (Ma et al., 2016).

XRD intensity is an inverse measure of the crystallinity of CNTs (Takizawa et al., 2000). XRD intensity of as-synthesized CNT yarns is seen to be very high for samples with no hydrogen co-feeding (Figure 5.9) indicating a high level of disorderliness and low crystallinity. However, co-feeding of hydrogen increases the crystallinity with the maximum value achieved for sample CNT-2. (Li et al., 2017) observed an increase in the alignment of CNT yarn with an increase in the

concentration of hydrogen in the reaction atmosphere up to 15% hydrogen concentration. Further increase in concentration resulted in dishevelled tubes.

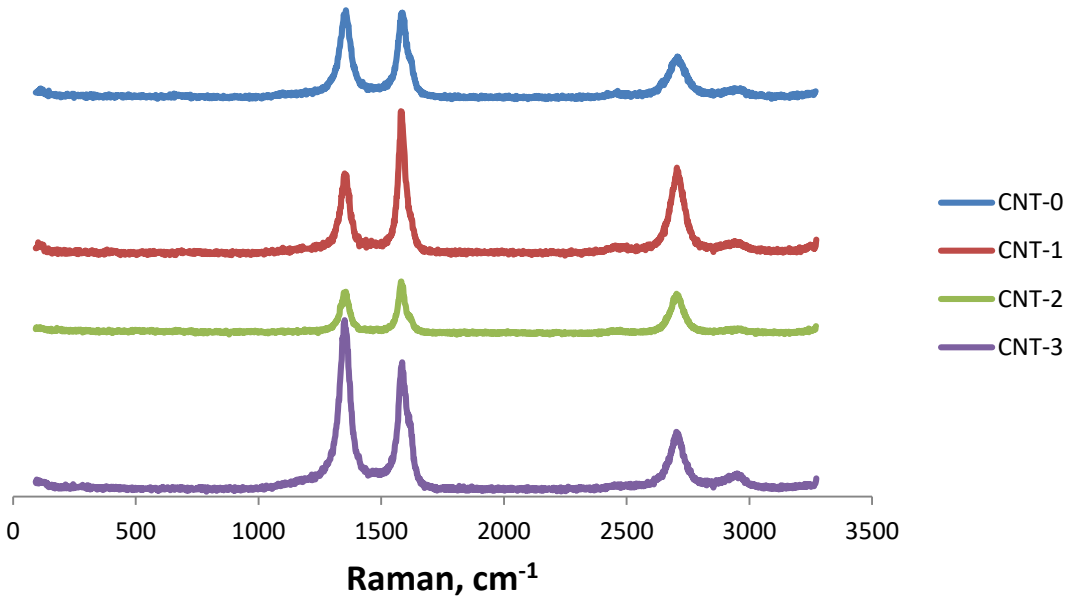

Figure 5.7. Raman spectroscopy showing the effect of hydrogen on as-synthesized CNT yarns

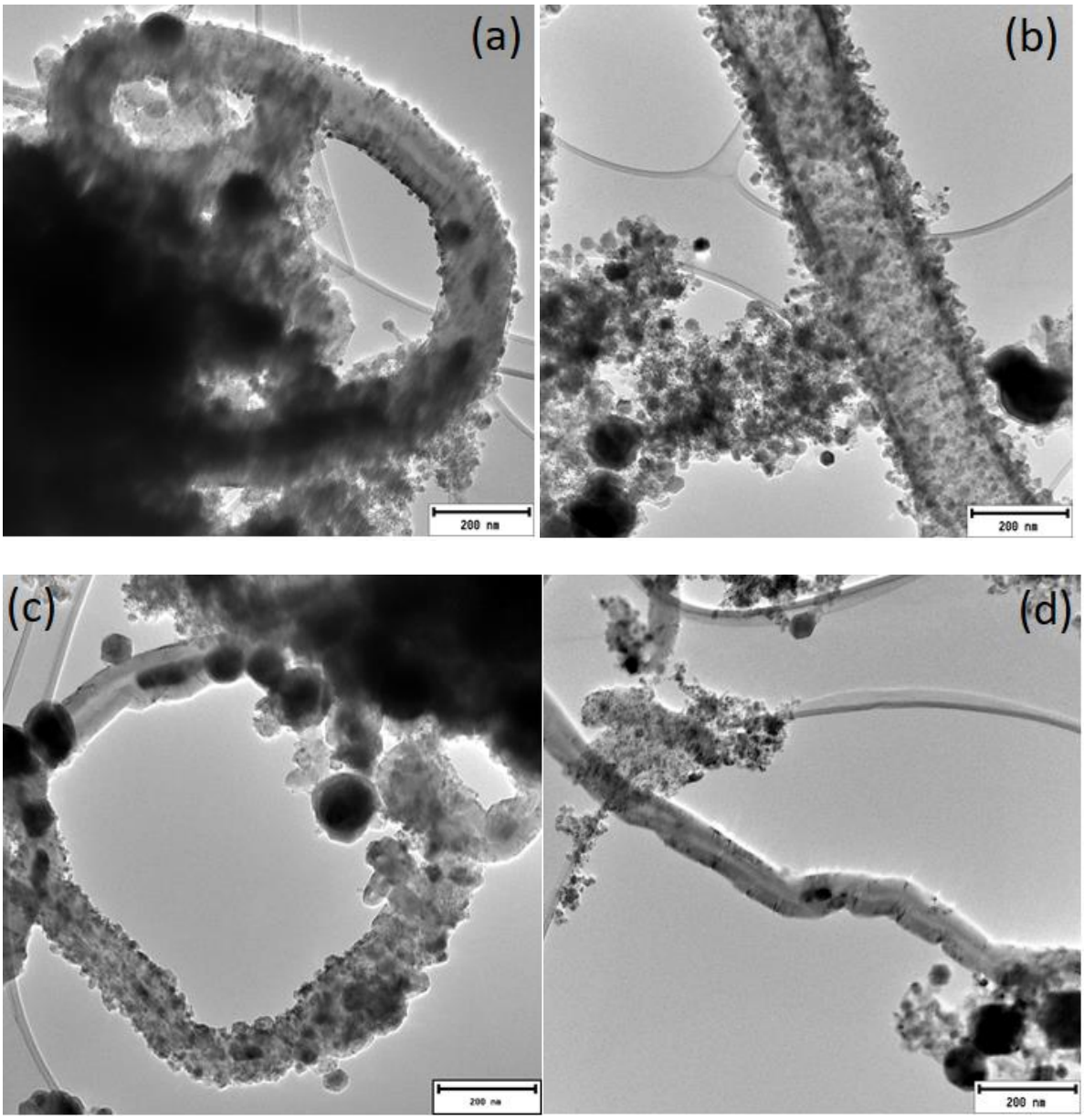

Figure 5.8. TEM of as-synthesized on the effect of hydrogen on the morphology of as-synthesized CNT yarns; (a) CNT-0, (b) CNT-1, (c) CNT-2, and (d) CNT-3

Table 5.4. Values corresponding to the hydrogen flow rate

Annotation	I_D/I_G	Z-ave, nm	XRD Intensity, a.u.
CNT-0	1.184	3075	230
CNT-1	0.577	1603	66
CNT-2	0.824	2893	20
CNT-3	1.314	7320	90

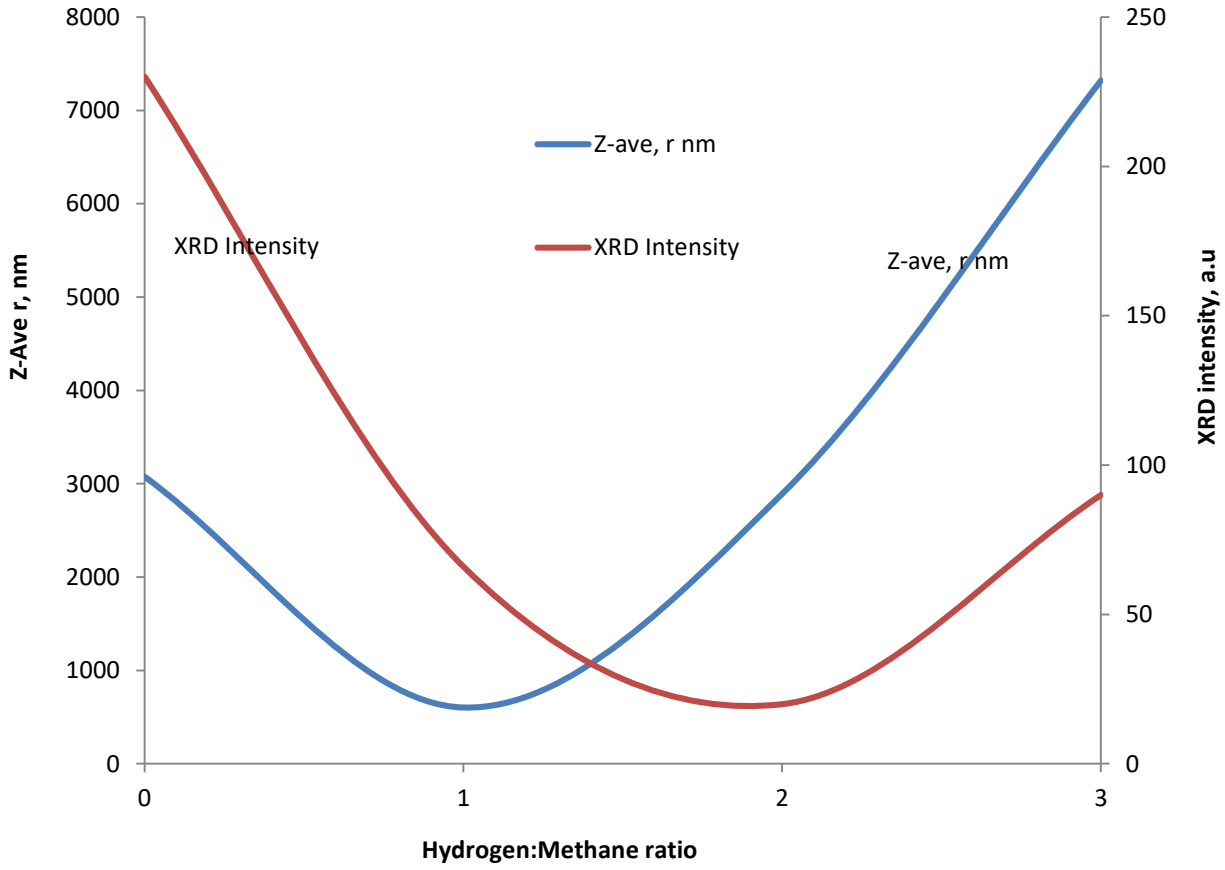

Figure 5.9. Effect of hydrogen flow rate to methane flow rate ratio on the value of XRD intensity and the average length of as-synthesized CNT yarn.

The room temperature current-voltage plot of as-synthesized CNT yarn with varied hydrogen content is presented in Figure 5.10. CNT-0 is seen to have very high ohmic resistance. As-synthesized CNT yarns with hydrogen co-feeding on the other hand, all have non-ohmic diode-type characteristics.

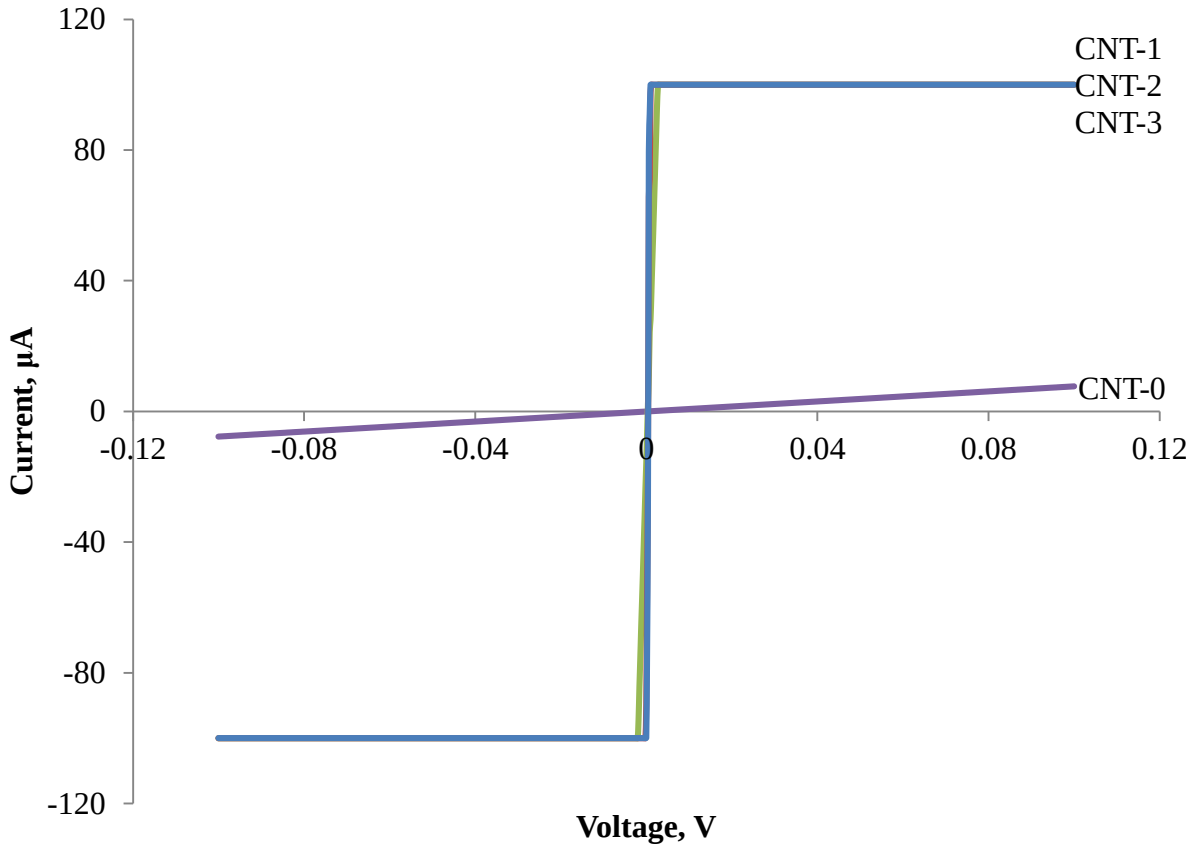

Figure 5.10. Current-voltage relationship of as-synthesized CNTs showing the effect of hydrogen flow rates.

5.2 Concluding remarks

The effect of synthesis temperature and concentration of hydrogen on the quality of as-synthesized CNTs was performed. The following observations were made

- Increase in synthesis temperature improved the general properties of as-synthesized CNT yarns for application as a filament in the incandescent light bulb for the limit of the experimental set-up;
- Higher synthesis temperature produces non-ohmic type resistor consistent with the property of materials used as filament in incandescent light bulbs;
- Synthesis of CNT yarn with hydrogen co-feeding influences the properties of as-synthesized CNT yarns including the degree of graphitization, structure, and length;
- Hydrogen co-feeding on the current-voltage relationship of as-synthesized CNT yarns changed the relationship from ohmic to non-ohmic;
- Hydrogen co-feeding is essential for the synthesis of CNT yarn for application as a filament in incandescent light bulbs.

CHAPTER SIX

6. KINETICS OF PRODUCTION OF CNT YARN IN FCCVD

The catalytic chemical vapour deposition method has been designated to be the most viable method for high yield low-cost CNTs synthesis method. To achieve a large scale and continuous production of CNTs in a CVD, kinetic studies as their formation is a subject of interest. This chapter focuses on developing a kinetic model using the optimum parameters for the synthesis of CNT yarns in an FCCVD achieved in Chapter Four. The derived model is used to determine the amount of CNTs produced for specified concentrations of methane.

6.1 Introduction

A detailed description of the GC set-up is presented in Chapter Three. Assessing the concentration of the exit gases at various flow rates of reactant gases was carried out to determine the effect of residence time on the amount of CNTs produced.

Table 6.1. Reaction gas flow parameters

Methane, mL/min	**Methane, kPa**	**Hydrogen, mL/min**	**Hydrogen, kPa**	**Argon, mL/min**	**Argon, kPa**
20	137.9	16	110.32	20	137.9
40	275.8	32	220.64	40	275.8
60	413.7	48	330.96	60	413.7
100	689.5	80	551.6	100	689.5
140	965.3	112	772.24	140	965.3

6.2 Kinetic model development using an ideal plug flow reactor

An ideal-flow plug flow reactor is assumed in this study. The gases are mixed in the swirled part of the reaction system before it enters into the furnace therefore the gases are assumed to be perfectly mixed in the radial direction. Reactions start immediately at the bottom of the furnace therefore different amount of reactants are found at different lengths of the furnace thus the axial direction is assumed to consist of various thin disks of differential volumes; each thin disk of differential volume has a different composition from the thin disk before and the thin disk after it. Each thin disk is considered as an immeasurably small batch reactor therefore it is considered a separate entity.

Further assumptions made are there are no pressure drops therefore density is constant; the tube diameter is constant throughout the length of the tube and only a single reaction takes place in the unit.

The cross-sectional area, A_c of the circular pipe is considered equal throughout the length of the reactor therefore linear velocity, v is linked to the volumetric flow rate, Q.

$$v = Q/A_c \tag{6.1}$$

While the axial length, z is determined in relation to tube volume as Equation 6.2

$$z = V/A_c \tag{6.2}$$

Material balance for a thin disk of the reactor volume ΔV (Figure 6.1) in an ideal-plug flow can be expressed in Equation 6.3

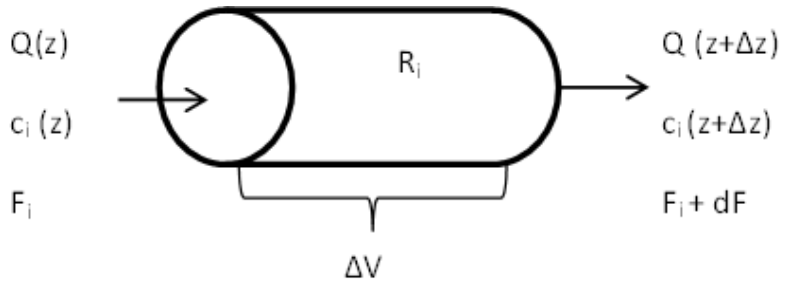

Figure 6.1. Representation of a thin disk of ideal plug flow reactor where the rate of reaction is constant

$$\frac{\partial(c_i \Delta V)}{\partial t} = c_i Q|_z - c_i Q|_{z+\Delta z} + R_i \Delta V \quad (6.3)$$

Where Q is the volumetric gas flow rate; c_j is the molar concentration of component i; R_i is the reaction of component i.

Taking the limits as ΔV tends to zero, and dividing by ΔV

$$\frac{\partial c_i}{\partial t} = -\frac{\partial(c_i Q)}{\partial V} + R_i \quad (6.4)$$

Rearranging Equation 6.4 as a function of velocity v and axial length z,

$$\frac{\partial c_i}{\partial t} = -\frac{\partial(c_i v)}{\partial z} + R_i \quad (6.5)$$

From Equation 6.4, when the time derivative is zero,

$$\frac{\partial(c_i Q)}{\partial V} = R_i \quad (6.6)$$

To design a gas phase reactor, flow rate of gases must be expressed as molar flow rate. Therefore, the mole balance $N_i = c_i Q$ for plug flow reactor can be expressed as Equation 6.7

$$\frac{\partial(N_i)}{\partial V} = R_i \tag{6.7}$$

However, equation of state is an important factor in gas flow as it is a function of temperature, pressure, molar flows, and volumetric flowrate. Therefore, from the ideal gas equation, molar concentration c_i is expressed as Equation 6.8

$$\sum_i c_i = \frac{P}{RT} \tag{6.8}$$

Equation of state for molar flow rates can therefore be expressed as Equation 6.9.

$$\frac{\sum_i N_i}{Q} = \frac{P}{RT} \tag{6.9}$$

Relationship of the volumetric flow rate in the equation of state is expressed as Equation 6.10

$$Q = \frac{RT}{P} \sum_i N_i \tag{6.10}$$

Considering $N_i = c_i Q$, rearranging and substituting into Equation 6.10 concentrations used in the reaction rate expressions are obtained as Equation 6.11.

$$c_i = \frac{N_i}{Q} = \frac{P}{RT} \frac{N_i}{\sum_i N_i} \tag{6.11}$$

For ideal continuous plug-flow reactor operating at steady state, molar material balance for component i is expressed as

$$F_{io} - F_i + G_i = \frac{dN_i}{dt} = 0 \tag{6.12}$$

where F_{io} and F_i are the flow rate of component i at the inlet and the outlet of the reactor; G_i is the product generation rate from component i which is equivalent to the product of reaction rate of component i r_i and volume of the reactor, V. Therefore,

$$F_{io} - F_i + r_i V = 0 \tag{6.13}$$

For thin disk volume dV where there is no change in reaction rate r_i – const. Equation 6.13 becomes

$$F_i - (F_i + dF_i) + r_i V = 0 \tag{6.14}$$

$$dV = \frac{dF_i}{r_i} \tag{6.15}$$

$$V = \int_{F_{io}}^{F_i} \frac{dF_i}{r_i} \tag{6.16}$$

For a single reaction

$$F_i = F_{io}(1 - x_i) \tag{6.17}$$

$$dF_i = -F_{io} dx_i \tag{6.18}$$

$$-r_i = \frac{dx_i}{d(V/F_{io})} \tag{6.19}$$

The reaction rate $-r_{CH_4}$ for the rate equation was determined in relation to CH_4 by taking the slope of the graphical representation of $V/F_{CH_4 o}$ and x_{CH_4}.

6.3 Derivation of Rate Equation

Various steps are involved in the synthesis of CNTs in an FCCVD system with methane hydrocarbon and ferrocene catalyst. The reaction rate equation was derived for the synthesis of CNTs in an FCCVD reactor for the conditions obtained in our optimal conditions in Chapter four above. The general equation for the decomposition of methane in the presence of hydrogen gas used in this study is presented in

$$\mathrm{CH_{4(g)} + H_{2(g)} \xrightarrow{k} C_{(s)} + 3H_{2(g)}} \qquad (6.20)$$

Assumptions (Fogler, 2010; Perry & Green, 2007)

- Langmuir-Hinshelwood mechanism is assumed for the surface reactions - Methane and Hydrogen are both adsorbed on the surface of the catalyst and adsorbed species interact;
- S is the active site
- Steady-state: $-\frac{d[CH_4]}{dt} = 0; -\frac{d[H_2]}{dt} = 0$

Formulation of rival reaction models: Adsorption of methane on the surface of catalysts has been proposed by various authors to be dissociative (Alstrup, 1988; Sharif Zein et al., 2004) and others as molecular (Saraswat et al., 2016; Snoeck et al., 1997). In molecular adsorption, the molecule of methane first adsorbs on the surface of the catalyst before if dissociates via dehydrogenation. On the other hand, in dissociative adsorption molecule of methane dissociates while being adsorbed. In this endeavour, we consider the mechanism of adsorption of methane to be molecular given that two molecules are being adsorbed on the surface of the catalyst (Fogler, 2010). In this work, only five steps were considered therefore the following reaction mechanism is proposed.

Adsorption step:

$$CH_{4\ (g)} + s \underset{k_{-1}}{\overset{k_1}{\rightleftarrows}} CH_4.s \tag{6.21}$$

$$H_{2(g)} + 2s \underset{k_{-2}}{\overset{k_2}{\rightleftarrows}} 2H.s \tag{6.22}$$

Equation 6.21 denotes the molecular adsorption of methane on the catalyst surface while Equation 6.22 signifies hydrogen undergoes dissociative adsorption.

Surface reaction:

$$CH_4.s + 4H.s \underset{k_{-3}}{\overset{k_3}{\rightleftarrows}} C.s + 4H_2.s \tag{6.23}$$

Desorption

$$C.s \underset{k_{-4}}{\overset{k_4}{\rightleftarrows}} C_{(s)} + s \tag{6.24}$$

$$4H_2.s \underset{k_{-5}}{\overset{k_5}{\rightleftarrows}} 4H_{2(g)} + 4s \tag{6.25}$$

where $k_1\ and\ k_{-1}$ are the rate constants for the forward and reverse reactions of methane adsorption on the surface of the catalyst; $k_2\ and\ k_{-2}$ - forward and reverse rate constants for hydrogen adsorption on the surface of the iron catalyst; $k_3\ and\ k_{-3}$ - rate constants for the forward and reverse reactions of the adsorbed reactants on the surface of the catalyst; $k_4\ and\ k_{-4}$ – the rate

constant for the desorption of carbon from the catalyst surface and subsequent growth of CNTs. $k_5\ and\ k_{-5}$ – the rate constant for the desorption of carbon from the catalyst surface.

The rates of adsorption of methane and hydrogen on the surface of iron from ferrocene catalyst are presented in Equations 6.26 to 6.31. The rate of reaction of the adsorbed methane can also be dependent on the pressure of methane (Fogler, 2010; Perry & Green, 2007).

$$r_{forward} = k_1 P_{CH_4} C_v \tag{6.26}$$

$$r_{reverse} = k_{-1}[CH_4.s] \tag{6.27}$$

Rate of adsorption of methane on the active sites is therefore expressed as r_1 in Equation 6.28

$$r_1 = k_1(P_{CH_4} C_v - \frac{[CH_4.S]}{\mathrm{K}_1}) \tag{6.28}$$

where equilibrium constant $K_1 = \frac{k_1}{k_{-1}}$ and C_v is the concentration of the vacant sites on the catalyst surface.

Rate of reaction of the adsorbed hydrogen is dependent on the pressure of hydrogen.

$$r_{forward} = k_2 P_{H_2} C_v \tag{6.29}$$

$$r_{reverse} = k_{-2}[H.s]^2 \tag{6.30}$$

Rate of adsorption of hydrogen on the surface of the catalyst surface is expressed in Equation 6.31

$$r_2 = k_2(P_{H_2} C_v^2 - \frac{[H.S]^2}{K_2}) \tag{6.31}$$

where equilibrium constant of the adsorption of hydrogen on the catalyst surface $K_2 = \frac{k_2}{k_{-2}}$

The rate of surface reaction for the synthesis of CNTs is expressed in Equations 6.32 to 6.34

$$r_{forward} = k_3[CH_4.s][H.s]^4 \quad (6.32)$$

$$r_{reverse} = k_{-3}[C.s][H_2.s]^4 \quad (6.33)$$

The rate of the surface reaction becomes as stated in Equation 6.34

$$r_3 = k_3([CH_4.s][H.s]^4 - \frac{[C.s][H_2.s]^4}{K_3}) \quad (6.34)$$

where equilibrium constant $K_3 = \frac{k_3}{k_{-3}}$

The rate of desorption of the products from the surface of the catalyst is expressed in Equations (6.35) to (6.40).

$$r_{forward} = k_4[C.s] \quad (6.35)$$

$$r_{reverse} = k_{-4}[CNT]C_v \quad (6.36)$$

Rate of desorption of carbon from the catalyst to form CNTs is expressed as Equation 6.37

$$r_4 = k_4([C.s] - \frac{[CNT]C_v}{K_4}) \quad (6.37)$$

The rate of desorption of Hydrogen from the catalyst surface is expressed in Equations (6.38) to (6.40)

$$r_{forward} = k_5[H_2.s]^4 \quad (6.38)$$

$$r_{reverse} = k_{-5}[H_2]^4 C_v^4 \quad (6.39)$$

Equation 6.40 is the rate for the desorption of hydrogen from the catalyst surface

$$r_5 = k_5([H_2.s]^4 - \frac{[H_2]^4 C_v^4}{K_5}) \quad (6.40)$$

where $K_5 = \frac{k_5}{k_{-5}}$

To determine C_v, the site balance is utilized. The total concentration of sites, C_t which is assumed to be constant, is calculated as:

$$C_t = C_v + C_{CH_4.s} + C_{H.s} + C_{H_2.s} + C_{C.s} \quad (6.41)$$

At quasi-equilibrium state, the rates of adsorption, rate of surface reaction and the rate of desorption are all equal which is equal to the rate of decomposition of methane and rate of formation of CNTs (Fogler, 2010). Thus

$$r_1 = r_2 = r_3 = r_4 = r_5 = -r_{CH_4} = r_{CNT} \quad (6.42)$$

A single type of catalyst surface is assumed and the activity on the surface is uniform for the various reaction steps on the catalyst surface.

Model Discrimination:

CASE I: Considering surface reaction as the rate-limiting step: k_3 is comparatively much smaller than k_1, k_2, k_4 and k_5 (Fogler, 2004). Therefore

$$\frac{r_1}{k_1} \cong \frac{r_2}{k_2} \cong \frac{r_4}{k_4} \cong \frac{r_5}{k_5} \cong 0 \tag{6.43}$$

$\frac{r_3}{k_3}$ on the other hand, is very large.

The concentration of the adsorbed methane molecules on the active sites is expressed as Equations 6.44 and 6.45

$$\frac{r_1}{k_1} = \left(P_{CH_4} C_v - \frac{[CH_4.s]}{\mathrm{K}_1}\right) = 0 \tag{6.44}$$

$$CH_4.s = K_1 P_{CH_4} C_v \tag{6.45}$$

Equations (6.46) and (6.47) are used to determine the expression for the concentrations of the catalyst site occupied by $[H.s]$

$$\frac{r_2}{k_2} = \left(P_{H_2} C_v^2 - \frac{[H.s]^2}{K_2}\right) = 0 \tag{6.46}$$

$$[H.s] = C_v \sqrt{(K_2 P_{H_2})} \tag{6.47}$$

From Equation 6.37 the expression for $C_{C.S}$ is determined as in Equation 6.49

$$\frac{r_4}{k_4} = [C.s] - \frac{[CNT]C_v}{K_4} = 0 \tag{6.48}$$

$$[C.s] = \frac{[CNT]C_v}{K_4} \tag{6.49}$$

From Equation 6.40

$$\frac{r_5}{k_5} = [H_2.s]^4 - \frac{[H_2]^4 C_v^4}{K_5} = 0 \tag{6.50}$$

The expression for $C_{H_2.S}$ is derived as Equation 6.51

$$[H_2.s] = \frac{[H_2]C_v}{\sqrt[4]{K_5}} \tag{6.51}$$

Plugging the values of concentration of adsorbed molecules into the expression for the rate surface reaction (Equation 6.34), we obtain Equation 6.52 as

$$r_3 = k_3(K_1 P_{CH_4} C_v C_v^4 (K_2 P_{H_2})^2 - \frac{[CNT]C_v([H_2]C_v)^4}{K_4 K_3 K_5}) \tag{6.52}$$

Simplifying Equation 6.52

$$r_3 = k_3 C_v^5 \left(K_1 P_{CH_4} K_2^2 \, {P_{H_2}}^2 - \frac{[CNT][H_2]^4}{K_4 K_3 K_5}\right) \tag{6.53}$$

The concentration of the vacant sites C_v is determined from Equation 6.41 by plugging in the values of the concentrations of the sites occupied by the molecules

$$C_t = C_v \left(1 + P_{CH_4} K_1 + \sqrt{K}_2 \sqrt{P}_{H_2} + \frac{[H_2]}{\sqrt[4]{K_5}} + \frac{[CNT]}{K_4}\right) \tag{6.54}$$

Therefore C_v is expressed as Equation 6.55

$$C_v = \frac{C_t}{\left(1 + P_{CH_4} K_1 + \sqrt{K}_2 \sqrt{P}_{H_2} + \frac{[H_2]}{\sqrt[4]{K_5}} + \frac{[CNT]}{K_4}\right)} \tag{6.55}$$

Substituting Equation 6.55 into Equation 6.53, we derive Equation 6.56 as the rate equation for the surface reaction.

$$r_3 = k_3\left(\frac{C_t}{1+P_{CH_4}K_1+\sqrt{K}_2\sqrt{P}_{H_2}+\frac{[H_2]}{\sqrt[4]{K_5}}+\frac{[CNT]}{K_4}}\right)^5\left(K_1P_{CH_4}K_2^2\ {P_{H_2}}^2-\frac{[CNT][H_2]^4}{K_4K_3K_5}\right) \quad (6.56)$$

In the initial rates for the decomposition of methane, $-\mathrm{r}_{CH_{4.}0}$, no products are present thus the expression for the rate of decomposition of methane presented as in Equation 6.57

$$-\mathrm{r}_{CH_{4.}0} = k_3\left(\frac{C_t}{1+P_{CH_4}K_1+\sqrt{K}_2\sqrt{P}_{H_2}}\right)^5\left(K_1P_{CH_4}K_2^2\ P_{H_2}^2\right) \quad (6.57)$$

Further simplification gives Equation 6.58

$$-\mathrm{r}_{CH_{4.}0} = k_3\frac{C_t^5K_1P_{CH_4}K_2^2\ P_{H_2}^2}{\left(1+P_{CH_4}K_1+\sqrt{K}_2\sqrt{P}_{H_2}\right)^5} \quad (6.58)$$

Equation 6.58 was solved as a non-linear simultaneous equation using Excel Solver. The objective function, g, applied is $g = \sum_{i=1}^{N}\frac{r_{exp_i}-r_{mod_i}}{r_{exp_i}}$.

CASE II: Considering adsorption of CH_4 on the surface of the catalyst as the rate-limiting step therefore k_1 is very small in comparison to k_2, k_3, k_4, and k_5 which are very large (Fogler, 2004). Therefore,

$$\frac{r_2}{k_2} \cong \frac{r_3}{k_3} \cong \frac{r_4}{k_4} \cong \frac{r_5}{k_5} \cong 0 \quad (6.59)$$

while $\frac{r_1}{k_1}$ is very large.

Bearing in mind the site balance in Equation 6.41

$$C_t = C_v + C_{CH_4.s} + C_{H.s} + C_{H_2.s} + C_{C.s} \quad (6.41)$$

Expression for $C_{CH_4.S}$ is determined from Equation 6.34 and expressed in Equation 6.61.

$$\frac{r_3}{k_3} = [CH_4.s][H.s]^4 - \frac{[C.s][H_2.s]^4}{K_3} = 0 \tag{6.60}$$

$$[CH_4.s] = \frac{[C.s][H_2.s]^4}{[H.s]^4 K_3} \tag{6.61}$$

Equation 6.61 for the $C_{CH_4.S}$still contains expressions for occupied sites. Equations 6.45, 6.49, 6.51 were used to plug into Equation 6.61 resulting in Equation 6.62.

$$[CH_4.s] = \frac{[H_2]^4 \cancel{C_v^4}[CNT]C_v}{\cancel{C_v^4}K_2^2 P_{H_2}^2 K_3 K_5 K_4} = \frac{[H_2]^4[CNT]C_v}{K_2^2 P_{H_2}^2 K_3 K_5 K_4} \tag{6.62}$$

$$C_t = C_v + \frac{[H_2]^4[CNT]C_v}{K_2^2 P_{H_2}^2 K_3 K_5 K_4} + \frac{[H_2]C_v}{\sqrt[4]{K_5}} + \frac{[CNT]C_v}{K_4} + C_v\sqrt{(K_2 P_{H_2})} \tag{6.63}$$

$$C_t = C_v\left(1 + \frac{[H_2]^4[CNT]}{K_2^2 P_{H_2}^2 K_3 K_5 K_4} + \frac{[H_2]}{\sqrt[4]{K_5}} + \frac{[CNT]}{K_4} + \sqrt{(K}_2 P_{H_2})\right) \tag{6.64}$$

$$C_v = \frac{C_t}{1+\frac{[H_2]^4[CNT]}{K_2^2 P_{H_2}^2 K_3 K_5 K_4}+\frac{[H_2]}{\sqrt[4]{K_5}}+\frac{[CNT]}{K_4}+\sqrt{(K_2 P_{H_2})}} \tag{6.65}$$

Substituting the derived expressions for the occupied active sites and vacant sites into the equation for the rate of adsorption of methane on the surface of the iron catalyst (Equation 6.28), the resulting expression in Equation 6.66.

$$r_1 = k_1 C_t \left(\frac{P_{CH_4}}{1+\frac{[H_2]^4[CNT]}{K_2^2 P_{H_2}^2 K_3 K_5 K_4}+\frac{[H_2]}{\sqrt[4]{K_5}}+\frac{[CNT]}{K_4}+\sqrt{(K_2 P_{H_2})}} - \right.$$

$$\left. \frac{[H_2]^4[CNT]}{K_2^2 P_{H_2}^2 K_3 K_5 K_4 K_1 \left(1+\frac{[H_2]^4[CNT]}{K_2^2 P_{H_2}^2 K_3 K_5 K_4}+\frac{[H_2]}{\sqrt[4]{K_5}}+\frac{[CNT]}{K_4}+\sqrt{(K_2 P_{H_2})}\right)} \right) \quad (6.66)$$

In the initial rates for the decomposition of methane, $-\mathrm{r}_{CH_{4.}0}$, no products are present thus the expression for the rate equation for the adsorption of methane presented as Equation 6.67

$$-\mathrm{r}_{CH_{4.}0} = r_1 = \frac{k_1 C_t P_{CH_4}}{1+\sqrt{(K_2 P_{H_2})}} \quad (6.67)$$

$$-\mathrm{r}_{CH_{4.}0} = \frac{k_1' P_{CH_4}}{1+\sqrt{(K_2 P_{H_2})}} \quad (6.68)$$

where $k_1' = k_1 C_t$

The values of $k_1' and\ K_2$ are determined by solving the non-linear simultaneous equation on Excel Solver.

Inputting the values of the kinetic parameters, $k_1' and\ K_2$, Equation 6.68 can be rewritten as Equation 6.69.

$$-\mathrm{r}_{CH_{4.}0} = \frac{1.78*10^{-4} P_{CH_4}}{1+\sqrt{(1.28 P_{H_2})}} \quad (6.69)$$

Equation 6.69 indicates that the rate of decomposition methane and the resultant formation of CNTs is directly proportional to the pressure of methane in the reaction mix. Hydrogen, on the other hand, has an inverse effect on the rate of decomposition of methane.

6.4 Results and Discussion

The initial reaction rate for the decomposition of methane against the initial partial pressure of methane plots for the surface reaction as the rate-limiting step is presented in Figure 6.2

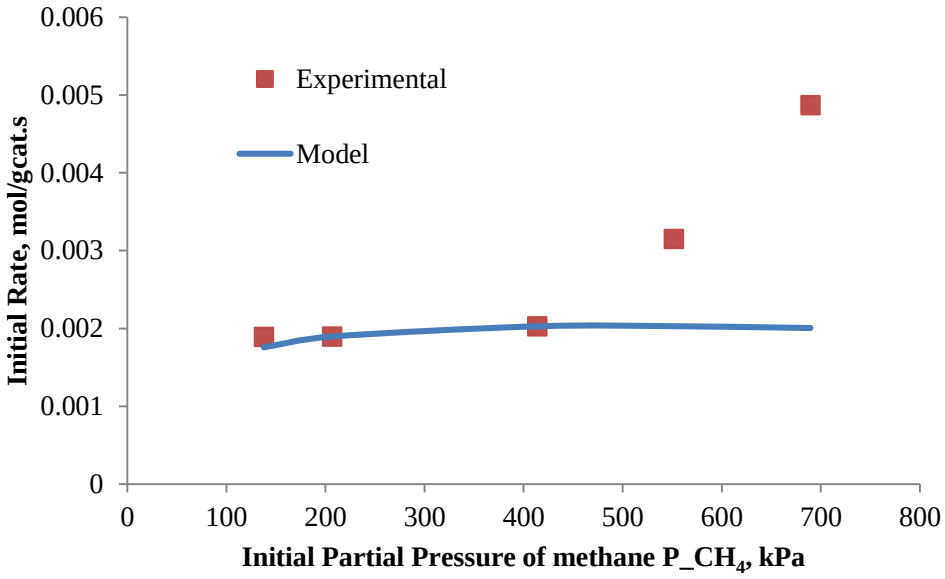

Figure 6.2. A plot of surface reaction limited rate equation showing the initial rate versus the initial partial pressure of methane (markers represent the experimental data while the solid line represents the model in Equation 6.58)

Figure 6.2 shows the model has a linear relationship between the reaction rate and the partial pressure of methane which does not correlate to the experimental data. This indicates the surface reaction is not the rate-limiting step therefore adsorption of methane on the surface of the iron catalyst.

Initial rate plots for the molecular adsorption of methane as the rate-limiting step, consistent with the experimental observations is presented in Figure 6.3.

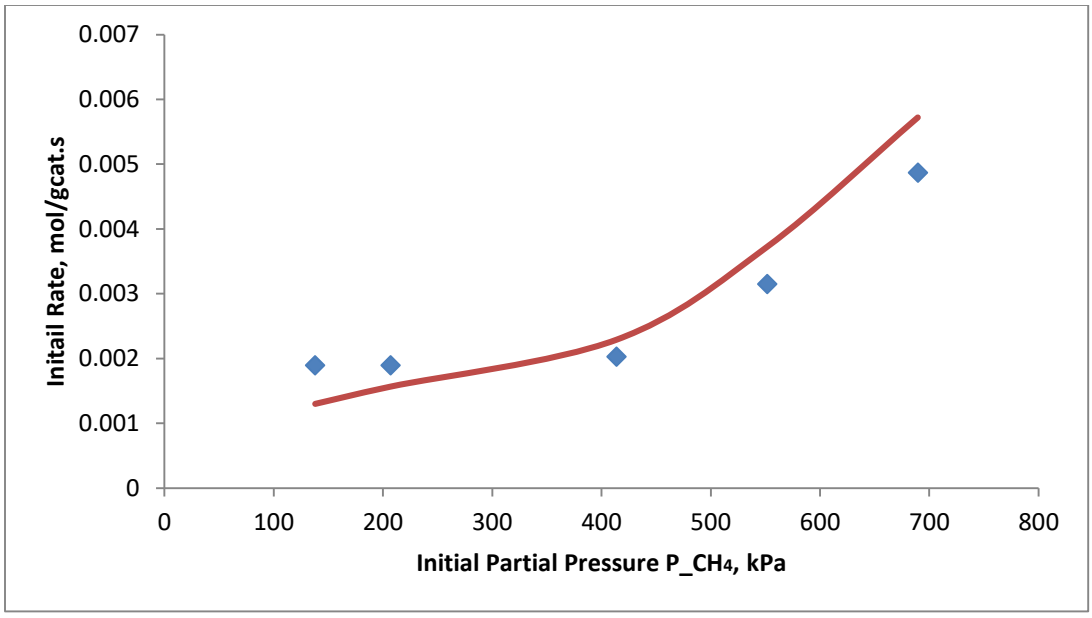

Figure 6.3. A plot of the initial rate of decomposition of methane on the surface of the catalyst against the initial partial pressure of methane (markers are experimental data; solid line represents the model in Equation 6.68)

Figure 6.3 shows that there is a good fit between the experimental data and the model. This indicates adsorption of methane on the surface of the iron catalyst is the rate-limiting step for the production of CNTs. This is in line with the findings of Demicheli et al., (1991) in the study of the carbon formation from a mixture of methane and hydrogen.

The increase in the rate of formation of CNTs initially starts slowly with an initial increase in pressure of methane in both the model and experimental data until a pressure of 400 kPa. However, this initial increase is steeper in the model than in the experimental data. Further increase in pressure of methane elicits a more significant increase in the rate of CNTs production. On the other hand, an increase in pressure of hydrogen decreases the rate of formation of CNTs. This is in line with the conclusion drawn by Ni et al., 2006

Equation 6.68 is determined to be the rate equation for the synthesis of CNTs from methane and hydrogen mixture with adsorption of methane on the surface of iron catalysts as the rate-limiting step. Adsorption of methane on the catalyst surface as the rate-limiting step is, therefore, the most consistent mechanism for the synthesis of CNTs in an FCCVD reactor with methane. Similar conclusions were reported by Saraswat et al., (2016) and Snoeck et al., (1997).

Parameter Identification: Adsorption of methane on the surface of the catalyst is determined as the rate-limiting step with the plot of the initial rates of decomposition of methane against initial partial pressure of methane fitting the experimental rate of reaction obtained. The rate equation presented in Equation 6.66 can be further represented as the rate of formation of CNTs in Equation 6.70. Variables of the rate equation for the synthesis of CNTs are [CNT] and [H_2].

$$\frac{d[CNT]}{dt} = k_1 C_t \left(\frac{P_{CH_4} K_2^2 P_{H_2}^2 \, K_3 K_5 K_4 K_1 - [H_2]^4 [CNT]}{K_2^2 P_{H_2}^2 K_3 K_5 K_4 K_1 \left(1 + \frac{[H_2]^4 [CNT]}{K_2^2 P_{H_2}^2 K_3 K_5 K_4} + \frac{[H_2]}{\sqrt[4]{K_5}} + \frac{[CNT]}{K_4} + \sqrt{K_2 P_{H_2}} \right)} \right) \qquad (6.70)$$

Assuming all consumed methane resulted in the formation of CNTs, from the stoichiometry of the reaction in Equation 6.20 and the ideal gas law, the concentrations of CNTs and hydrogen from the experimental data expressed in pressure values (kPa) were determined using Equations 6.71 and 6.72 respectively.

$$[CNT] * RT = P_{CH_4}(1 - x) \qquad (6.71)$$

$$[\mathrm{H_2}] * RT = 2P_{CH_4} x - P_{H_2} \qquad (6.72)$$

where x is the methane conversion and RT is the product of a gas constant and synthesis temperature.

Equilibrium constants $K_1, K_3, K_4, and\ K_5$ were determined using the Excel solver.

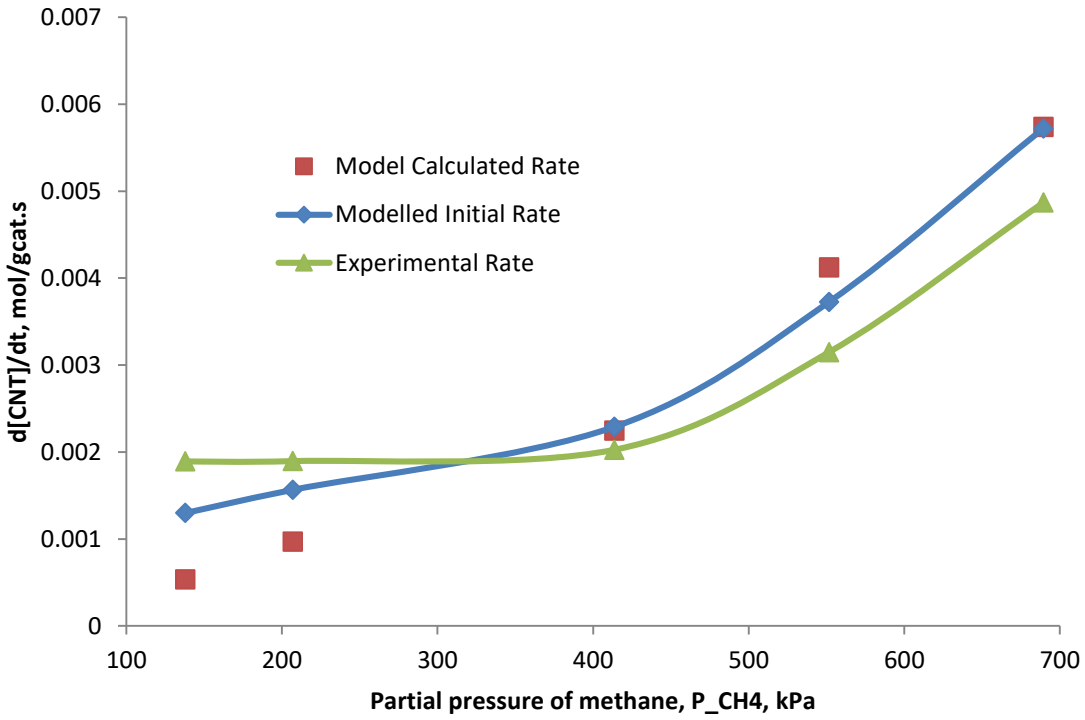

Figure 6.4. A plot of the rate of formation of carbon nanotube against the partial pressure of methane

Figure 6.4 shows that the model predicted for the formation of CNTs in an FCCVD reactor fits well with the experimental data. Statistical analysis presented in Figure 6.5 shows the model can adequately describe the process in the reactor with adjusted R square of 86.1%.

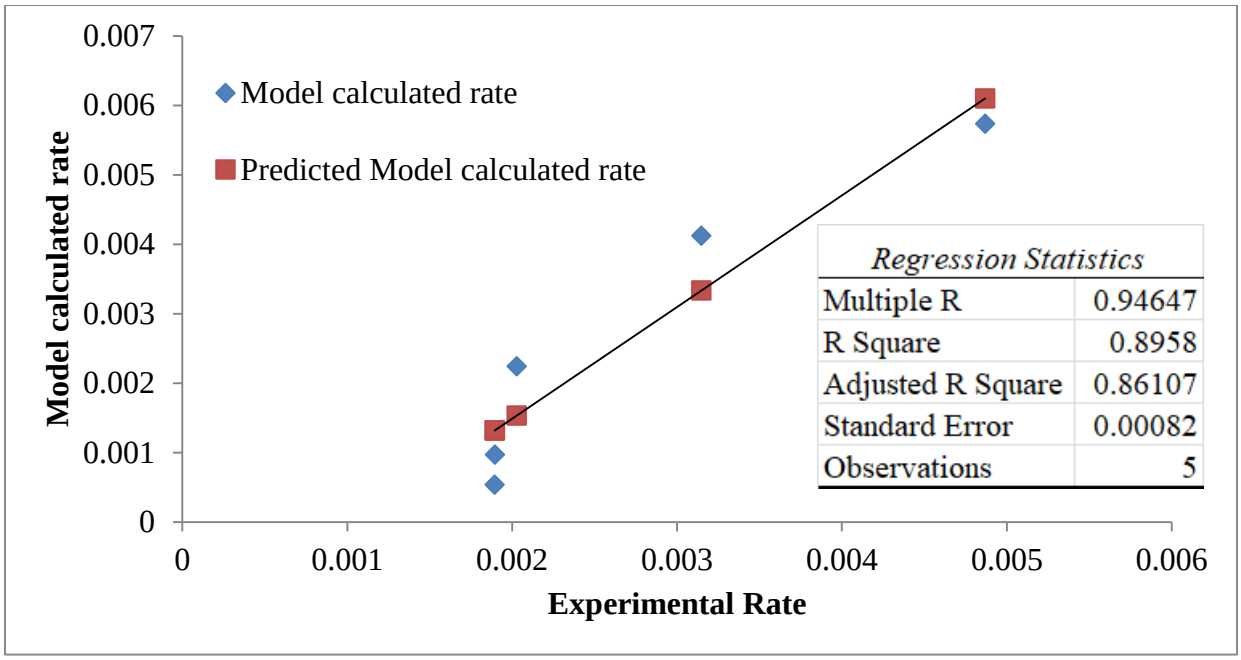

Figure 6.5. Parity plot of the calculated rate over the actual reaction rate with the regression statistics table

Statistical sensitivity analysis: In this statistical analysis, rate as a function of synthesis temperature, partial pressures of methane and hydrogen for the initial rate of decomposition of methane is considered.

$$-\mathrm{r}_{CH_{4.}0} = f(T, P_{CH_4}, P_{H_2}) \qquad (6.73)$$

The specific reaction rate constant is a function of temperature and can be determined through the Eyring and Arrhenius equations (Arrhenius, 1889; Eyring, 1935). However, a wide range of energy activation (60−236 kJ/mol) for the adsorption of methane on the surface of the catalyst has been reported (Alstrup & Tavares, 1993; Kuvshinov et al., 1998; Wert, 1950). The activation energy was estimated in this work. Eyring equation (Equation 6.74) as a form of the Arrhenius equation (Equation 6.71) was used to estimate the pre-exponential factor.

$$k = \frac{k_b T}{h} e^{\frac{\Delta S^*}{R}} e^{-\frac{(\Delta H^* - RT)}{RT}} \quad (6.74)$$

$$k = A e^{\left(-\frac{Ea}{RT}\right)} \quad (6.75)$$

where pre-exponential factor $A = \frac{k_b T}{h} e^{\frac{\Delta S^*}{R}}$ and $E_a^* = (\Delta H^* - RT)$.

k_b – Boltzmann constant, JK^{-1}; h – Planck constant in Js^{-1}; T – Temperature in K; R – gas constant in $JK^{-1}mol^{-1}$; ΔS^* – entropy of activation $Jmol^{-1}K^{-1}$; ΔH^* – enthalpy of activation J/mol; Ea – the energy of activation in $Jmol^{-1}$.

The pre-exponential factor for a heterogeneous gaseous reaction was calculated as dependent on the entropy of activation using the transition state theories (Ptáček et al., 2018; Roduner, 2014). For gaseous heterogeneous reaction, entropy is lost with the attachment of reactant gas to the solid catalyst. Change in entropy is approximated as Equation 6.76 (Horiuti Juro, 1961)

$$\Delta S^* = RIn\ G^{*(a)} - S_{ads} \quad (6.76)$$

where $G^{*(a)}$ – number of active sites available for activation; and S_{ads} – partial molar entropy of adsorbate.

Substituting Equation 6.76 into Equation 6.74

$$k = \frac{k_b T}{h G^{*(a)}} e^{\frac{-S_{ads}}{R}} e^{-\frac{E_a}{RT}} \quad (6.77)$$

$G^{*(a)}$ – is found to be in the range of $4.2*10^{14}$ cm^{-2} (Horiuti Juro, 1961; Miyahara & Kazusaka, 1976)

Value for A is calculated for synthesis temperature, T = 1243 K is calculated to be $6.475 * 10^{-2}\ cm^2 s^{-1}$

The energy of activation is determined from Equation 6.69 by linearizing

$$\ln k = \ln A - \frac{E_a}{RT} \tag{6.78}$$

Expression for activation energy is therefore

$$E_a = RT \ln \frac{A}{k} \tag{6.79}$$

where $k = k'_1$ defined in Equation 6.68.

$$E_a = 8.314 * 1243 \ln \frac{6.475*10^{-2}}{1.78*10^{-4}} = 60949.88\ J/mol \tag{6.80}$$

The energy of activation calculated is in the range of values reported in literature (Douven et al., 2011; Saraswat et al., 2016)

Isothermal and plug flow conditions are assumed in this work. The specific reaction rate constant, k is, however, temperature-dependent according to the Arrhenius equation and written as Equation 6.76. Therefore the rate of the equation is a function of temperature.

$$k'_1 = 6.475 * 10^{-2} e^{\left(-\frac{60949.88}{8.314T}\right)} \tag{6.81}$$

Substituting for the specific rate constant k'_1, (Equation 6.81) into Equation 6.68 to get Equation 6.82.

$$-\mathrm{r}_{CH_4.0} = \frac{6.475*10^{-2} e^{\left(-\frac{7330.99}{T}\right)} P_{CH_4}}{1+\sqrt{(1.28 P_{H_2})}} \tag{6.82}$$

From Equation 6.82, the rate equation is dependent on temperature, partial pressure of methane and partial pressure of hydrogen.

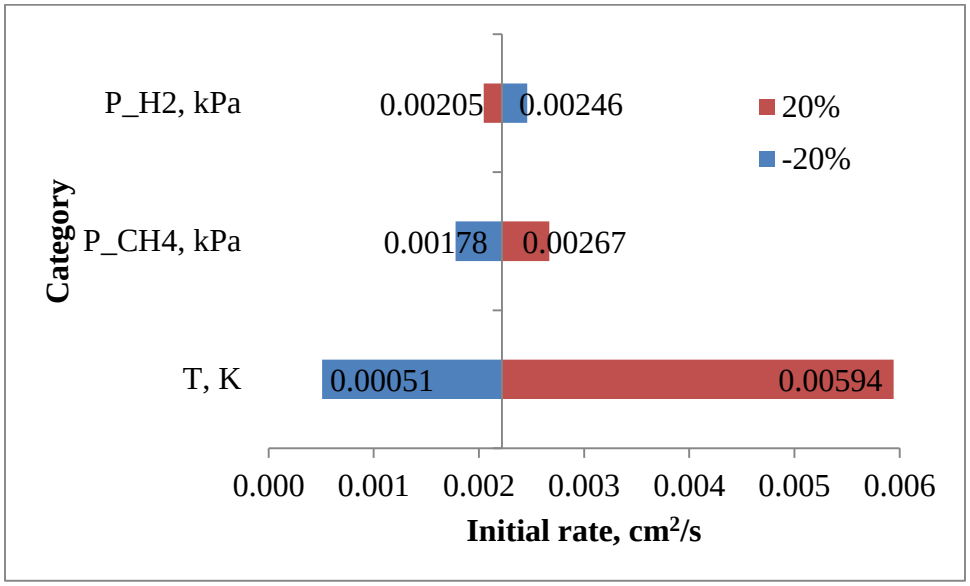

Figure 6.6. Tornado plot for sensitivity analysis of variables on the rate equation

Change in synthesis temperature is seen in Figure 6.6 to be most sensitive confirming results and conclusions drawn from the parametric optimization in Chapter Four. An increase in temperature results in a more significant increase in the rate of reaction than a decrease in temperature of the same magnitude. Change in the partial pressure of methane has a similar impact on the rate of reaction. An increase in methane partial pressure increases the rate of reaction in the same measure as a decrease. The effect of the partial pressure of hydrogen on the rate of reaction is seen as to be inverse to the rate of reaction. A decrease in the partial pressure of hydrogen, however, increases the rate of reaction to a higher level than an increase in partial pressure of the same magnitude.

Temperature and Concentration profile of methane in FCCVD: Partial differential form of energy balance for a reaction in a plug flow system is given as in Equation 6.83 (Merrill & Hamrin, 1970)

$$\frac{\partial T}{\partial z} - \frac{\lambda}{\sum_i F_i C_p}\left[\frac{\partial^2 T}{\partial r^2} + \frac{1}{r}\frac{\partial T}{\partial r}\right] + r_{CH_4}\frac{\Delta H^\circ}{\sum_i F_i C_p} = 0 \qquad (6.83)$$

where z – the axial distance of the reactor, m; λ – thermal conductivity of reaction mixture, W/m.K; ΣFi – molar flow rate of all components in the reaction mixture, mol/s; Cp – specific heat, J/K.kg; ΔH° - the heat of reaction, J/mol.

For radius r, boundary conditions are given as

$$z = 0 \qquad \begin{matrix} T = T_0 \\ x = 0 \end{matrix}$$

$$r = const \qquad \frac{\partial T}{\partial r} = 0$$

Considering these boundary conditions and isothermal plug flow conditions, Equation 6.83 can be simplified

$$\frac{dT}{dz} + \frac{r_{CH_{4,o}}\Delta H^\circ + q}{\sum_i F_i C_p} = 0 \qquad (6.84)$$

where $q = -k\frac{dT}{dz}$ is the rate of heat transfer and $\Delta H^\circ = \Delta H^\circ_{298} + \int_{298}^{T} \Delta C_p \, dT$

Change in temperature with the change in the axial dimension of the reactor is due to the rate of heat transfer along the length of the reactor

From Section 6.2.3, Equation derived as a function of linear velocity, v and axial length, z is given as

$$\frac{\partial c_i}{\partial t} = -v\frac{\partial c_i}{\partial z} + R_i \qquad (6.5)$$

where reaction of component i $R_i = \alpha_i r_i$. α_i- stoichiometric coefficient of component i and r_i – rate law of component i.

At steady state, $\frac{\partial c_i}{\partial t} = 0$, and substituting ordinary differential for partial differential, Equation 6.85 showing the dependency of the extent of conversion of component i on linear velocity, length of the reactor, and reaction rate.

$$\frac{dc_i}{dz} = \frac{\alpha_i}{\nu} r_i \tag{6.85}$$

Considering the initial rate of decomposition of methane derived, in relation to methane as an irreversible first-order reaction, and assuming isothermal conditions, Equation 6.85 can be written as

$$\frac{d[CH_4]}{dz} = -\frac{1}{\nu} k[CH_4] \tag{6.86}$$

Rearranging and taking the integral,

$$\int_{[CH_4,0]}^{[CH_4]} \frac{d[CH_4]}{[CH_4]} = -\frac{k}{\nu} \int_0^L dz \tag{6.87}$$

Integrating, concentration of methane along the reactor tube can be written as

$$[CH_4]_L = [CH_4]_0 e^{-\frac{kL}{\nu}} \tag{6.88}$$

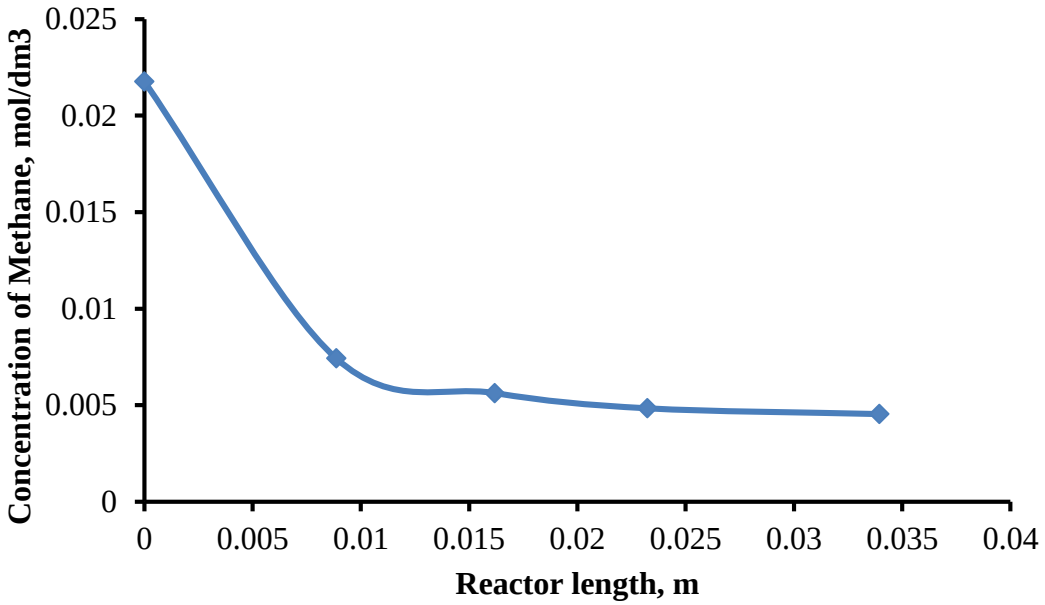

Figure 6.7. Concentration profile of methane along the length of the reactor.

The concentration of methane decreases as an exponential function along the length of the reactor (Figure 6.7). According to the model developed for the FCCVD, two-thirds of the methane concentration decomposes in the first third part of the reactor. Total decomposition of methane in the reactor is shown to be about 80%.

6.5 Concluding remark

Rising interest in the application of CNTs in science and engineering due to their unique properties has made it inevitable to understand the kinetics of its formation. Understanding the kinetics is necessary for large scale production. This chapter focused on the effect of concentration (pressure) of methane with hydrogen co-feeding on the rate of formation of CNTs in FCCVD system is modelled. The kinetic model for the synthesis of CNTs from methane with hydrogen co-feeding is reported in the open literature for the first time with the effect of hydrogen considered.

Adsorption of methane on the surface of the catalyst was found to be the rate-limiting step. The derived model and experimental results fairly fit with high R-squared value of over 86%.

Synthesis temperature was reconfirmed to have the most effect on the rate of production of CNTs. The partial pressure of hydrogen is seen to have an inverse effect on the rate of production of CNTs howbeit less intense than the partial pressure of methane.

CHAPTER SEVEN

7. INCANDESCENT LIGHT EMISSION FROM CARBON NANOTUBE YARNS

7.1 Introduction

This chapter discusses the simple mechanical and electrical properties of as-synthesized CNT yarns produced in an FCCVD reactor with direct spinning. Their light emission studies were carried out in comparison to the light emissions of commercial 60W tungsten wire.

CNT bundles were synthesized via decomposition of methane on ferrocene catalyst in a floating catalyst chemical vapour deposition (FCCVD) reactor. The mode of operation of FCCVD is described in Chapter Three. The synthesis conditions used were the optimal conditions determined and presented in Chapter Four.

Morphology and structure of as-synthesized CNT yarns were determined using TEM, SEM and Raman spectroscopy. These techniques have been described in detail earlier in Chapter Three. The procedures for the electrical, mechanical, and incandescent properties of as-synthesized CNT yarns are described in Chapter Three.

7.2 Results and Discussions

7.2.1 Physico-Chemical Properties of CNT yarn

Raman spectroscopy presented in Figure 7.2 shows the spectra is made up of the D, G, and 2D bands. The D-band defines the degree of disorderliness while the G-band designates the degree of graphitization and the 2D band is measures purity. A high degree of graphitization and high purity

are observed, with the I_D/I_G ratio of ~0.335 and I_{2D}/I_G ratio of ~ 0.566. The absence of resonance breathing mode (RBM) and a shoulder on the G-band show the yarn is predominantly made up of MWCNT (Mevellec et al., 2011). This is evidenced in SEM and TEM micrographs. Figure 7.1 shows micrographs from an electron microscope of as-synthesized CNT yarns made up of long individual CNTs. SEM image of the tip of the yarn is presented in Figure 7.1B showing the CNTs are quite well-aligned.

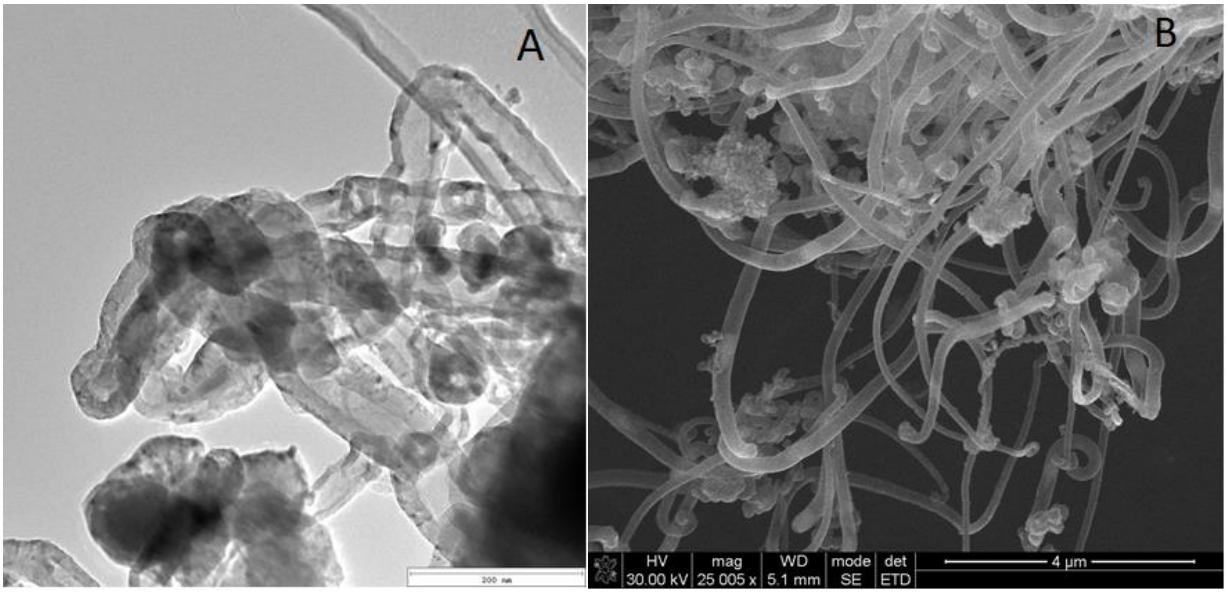

Figure 7.1. Micrographs of as-synthesized CNT yarns (A) TEM micrograph (B) SEM micrograph

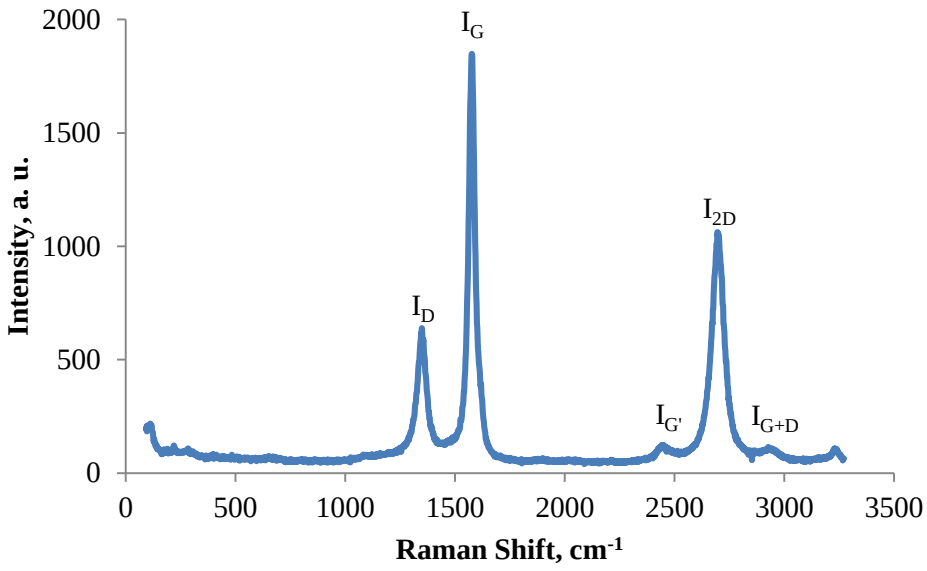

Figure 7.2. Raman spectroscopy of CNT yarn synthesized at optimal synthesis condition

7.2.2 **Mechanical and Electrical Properties**

A representative force-strain curve of as-synthesized CNT yarn of samples tested is presented in Figure 7.3. The stress-softening regime of the curve is nonlinear indicating the yarns do not have strong mechanical bonds holding the individual CNTs together (Abot et al., 2014; Alosh, 2013). This is due to the yarns being formed by weak Van der Waal forces and lack of densification or strong twist in the yarn. The straightening region (up to 0.1% in the strain axis) shows a deep in the graph due to the adjustment of the clamps to the full length of the yarn measured.

Tensile strength and Young's modulus of as-synthesized CNT yarn at break was found to be averagely 10.26 Mpa and 28.74 Mpa respectively. Young modulus values are comparable to values for long MWCNTs found in the literature (Kim et al., 2017), however, the values for tensile strength are a few degrees less. This can be attributed to the poor alignment of as-synthesized CNT yarns.

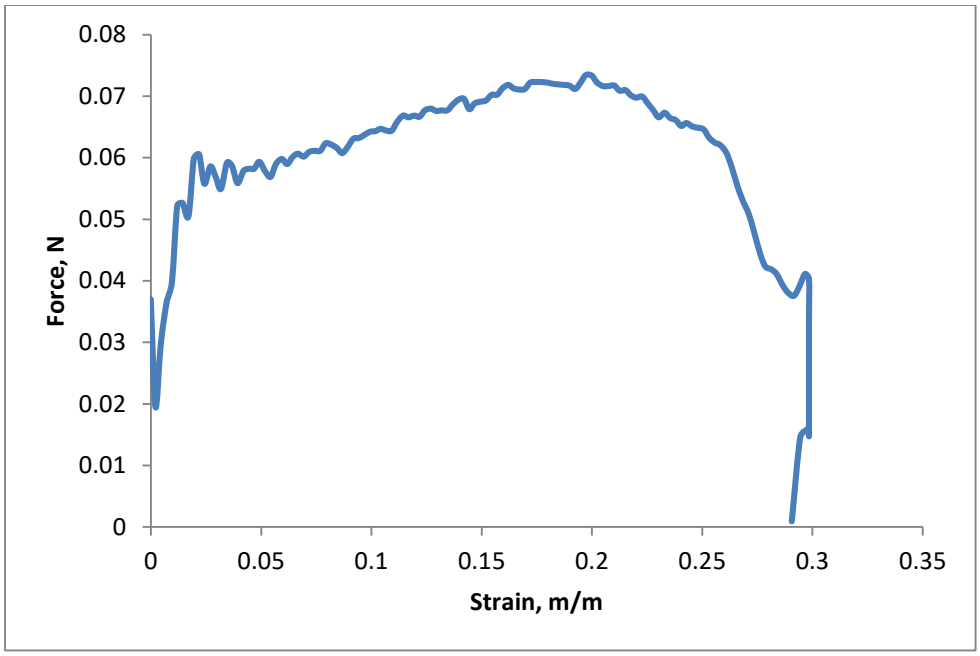

Figure 7.3. Force-strain curve of as-synthesized CNT yarn

I-V graph of a representative sample is presented in Figure 7.4b. The I–V curve is nonlinear indicating a traditional semiconductor transistor and specifically a diode since it has a junction of two layers (Bandaru, 2007). The I–V curve is made up of two regions: the linear region passes through the origin and operates like a resistor with current increasing as voltage increases. On the other hand, the saturation region, where the current does not change with an increase in voltage, operates like a current source (Wang et al., 2018). The resistivity is calculated as described in Igbokwe et al., (2019) and found to be $4.95.10^{-3}$ Ω/cm. This is relatively high resistivity compared to the resistivity of individual long CNTs reported in literature (Li et al., 2004). This could be attributed to the low densification of the yarn.

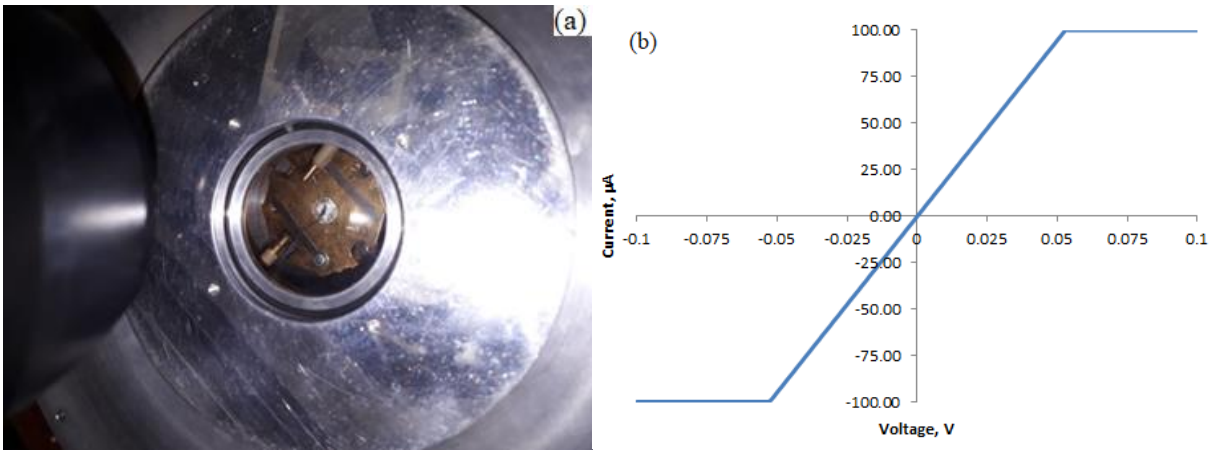

Figure 7.4. Two-point probe electrical conductivity measurement. (a) high field cryogen-free measurement system (Cryogenic Ltd) (b) Current–Voltage (I-V_{bias}) curve of as-synthesized CNT yarns produced at optimum parameters.

7.2.3 **Incandescent properties**

Spectra measurements of as-synthesized CNT yarns and tungsten filament were taken between 400 nm and 800 nm wavelength which is the visible light range (Li et al., 2003). The spectra are presented in Figure 7.6. The onset voltage, the voltage at which a measurable intensity of illumination from the blackbody material can be measured, of CNT yarn in this experiment was 5.2 V while that of Tungsten is 10.5 V (Wei et al., 2004). Commercial 60 W tungsten filaments glowed with more intensity than MWCNT yarn at these respective onset voltages. This could be attributed to low densification of CNT yarn.

Using the formula for power: $P \cong \frac{V^2}{R}$, since the resistance of incandescent materials decreases with an increase in temperature (Li et al., 2003), the electric power consumption of the tungsten is calculated to be over five times more than that of as-synthesized CNT yarn. This lower power consumption could be attributed to the high surface area of CNTs resulting in low onset voltage

(Sharma & Kar, 2014). For a diode, resistance increases but current remains constant therefore power consumption increases.

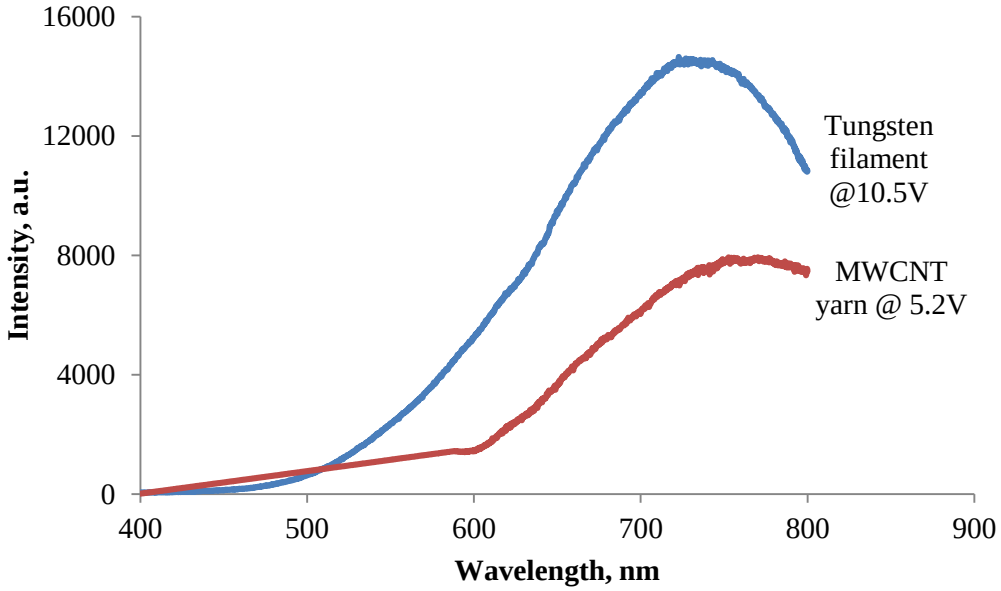

Figure 7.5. Light emission spectra of tungsten filament and MWCNT yarn

This onset voltage obtained in this research is comparable to the onset voltages reported in the literature and tabulated in Table 2.2. Li et al (2003) report an onset voltage of 11 V for MWCNT bundles produced via direct spinning illuminated in a vacuum while Jayasinghe (2011) reports an onset voltage of 3 V for similarly produced and illuminated CNTs. Densification generally resulted in lower onset voltage with values as low as 2.4 V for MWCNT under vacuum (Zhang et al., 2005). Illumination in argon reported in the literature is largely on SWCNT, where onset voltages as low as 1.4 V, is achieved for suspended single SWCNT and 7 V for individual SWCNT on substrates (Mann et al., 2007).

7.3 Concluding remarks

- CNT yarns synthesized in FCCVD at optimum synthesis conditions have been identified to be predominantly MWCNT
- As-synthesized CNT yarn in an FCCVD reactor under the optimum condition emits visible light when current is passed through it at a lower voltage than commercial tungsten filament used in incandescent bulbs;
- Power consumption for the emission of visible light from as-synthesized CNT yarn is significantly lower than commercial tungsten filament used in incandescent bulbs.

CHAPTER EIGHT

8. CONCLUSIONS AND RECOMMENDATIONS

8.1 General conclusions

The demand for increased application of carbon nanotubes necessitates the development of macroscopic nanotube-based materials such as yarns and films with properties similar to the individual nanotubes. The development of a new experimental technique for the production of CNT yarns proving the concept that CNTs can be produced and spun directly into its macroscopic size for predetermined application with potential for cost reduction was established. The set up for simultaneous catalyst pre-treatment, CNT aerosol production and spinning into yarns have the potential for low material consumption, low energy use and infrastructure maximization. The synergistic effect of diverse parameters is anticipated to influence the efficiency and the viability of this process. In line with these, statistical models to understand the main and interactive effects of various parameters in the production of carbon nanotube yarns in an FCCVD reactor using methane as carbon source and ferrocene as catalysts were developed. The model obtained for oxidation temperature was not an excellent representation. This could be attributed to the wide variations in the quality of nanotubes produced in the same CNT aerosol batch. These disparities can be seen within the length single nanotubes.

Characterization and performance evaluation study of the effect of temperature and hydrogen on as-synthesized CNT yarns for application as a filament in incandescent light bulbs indicated resistor-type current-voltage relationship exists for the low resistance yarn similar to that of light-emitting diodes. Hydrogen co-feeding was found to be essential in the production of CNT yarns suitable for application as a filament in incandescent light bulbs.

Rates and mechanisms of the formation of CNT aerosol in the FCCVD reactor using methane carbon source and ferrocene catalyst in an ideal plug flow type reactor were studied. It was determined that they are dependent on the concentrations of methane and hydrogen.

Outstanding light emission characteristics in an argon gas environment of as-synthesized and as-spun CNT yarns from floating catalyst CVD with direct spinning is first reported in the open literature. Application of the FCCVD reactor system with direct spinning ensured the elimination of post-production processes that result in a higher cost of operation from production to application.

8.2 Recommendations

The work presented in this thesis is a proof of concept. Some future works that can be carried out to improve on the results reported in this procedure are as follows:

1. The spinning of CNT yarn in this work was carried out primarily at a right angle ensuring the individual CNTs are largely straight. Winding the as-synthesized CNTs at varied angles from the right angle could result in better interconnections between the individual CNTs. Effects of these varied winding angles of as-synthesized CNT yarn could affect the intensity of emissions and other light emission properties.
2. The resistance of as-synthesized film-like macroscopic CNTs was found to have high resistance therefore they could not glow at the low current that was available for the light emission test. Further work could be carried out to determine the effect of the tightness and thickness of yarns on light emission properties.
3. In this work, we determined the kinetics focusing on the decomposition of methane. Many other products were formed alongside nanotubes. Further work can be carried out to

determine the selectivity for the formation of carbon nanotubes from decomposed methane in the FCCVD above other forms of carbon like carbon onions and other carbonaceous substances.

4. Considering the plug-flow type of the FCCVD system, the residence time is dependent on the flow rate. In this study, argon gas was found to have an insignificant effect on the quantity and properties of as-synthesized CNT yarns. The flow rate of methane was changed; therefore, residence time was changed. However, the effect of residence time cannot be directly deciphered since the concentration of methane increased. It will be interesting to determine the exclusive effect of residence time on CNTs formation by varying the flow rate of argon carrier gas at a constant methane flow rate.
5. Carbon source and carrier gases are introduced into the FCCVD reactor through the vaporizer picking up the vaporized catalyst into the reactor. It is supposed that the higher the flow rate of gases used, the more catalyst vapour is picked up. Determination of the relationship between the gas flow rates and the amount of catalyst picked into the reactor will be essential to regulate the quantity and quality of synthesized CNTs.

REFERENCES

Abdullahi, I., Sakulchaicharoen, N., & Herrera, J. E. (2012). A mechanistic study on the growth of multi-walled carbon nanotubes by methane decomposition over nickel–alumina catalyst. *Diamond and Related Materials*, *23*, 76–82.

Aberefa, O. A., Daramola, M. O., & Iyuke, S. E. (2019). Production and functionalization of carbon nanotubes for application in membrane synthesis for natural gas separation. *Microporous and Mesoporous Materials*, *280*, 26–36. https://doi.org/10.1016/j.micromeso.2018.12.040

Aberefa, O., Bedasie, K., Madhi, S., Daramola, M. O., & Iyuke, S. E. (2018). Production of carbon nanotube yarn from swirled floating catalyst chemical vapour deposition: a preliminary study. *Advances in Natural Sciences: Nanoscience and Nanotechnology*, *9*(3), 1–8. https://doi.org/10.1088/2043-6254/aad5cb

Abot, J. L., Alosh, T., & Belay, K. (2014). Strain dependence of electrical resistance in carbon nanotube yarns. *Carbon*, *70*, 95–102. https://doi.org/10.1016/j.carbon.2013.12.077

Abu Amr, S. S., Aziz, H. A., & Bashir, M. J. K. (2014). Application of response surface methodology (RSM) for optimization of semi-aerobic landfill leachate treatment using ozone. *Applied Water Science*, *4*(3), 231–239. https://doi.org/10.1007/s13201-014-0156-z

Agboola, A. E., Pike, R. W., Hertwig, T. A., & Lou, H. H. (2007). Conceptual design of carbon nanotube processes. *Clean Technologies and Environmental Policy*, *9*(4), 289–311. https://doi.org/10.1007/s10098-006-0083-2

Aguiar-Hualde, J.-M., Magnin, Y., Amara, H., & Bichara, C. (2017). Probing the role of carbon

solubility in transition metal catalyzing single-walled carbon nanotubes growth. *Carbon*, *120*, 226–232. https://doi.org/10.1016/j.carbon.2017.05.035

Alhosiny, N., Badawi, A., & Abdallah, S. (2013). The Effects of CNTs Types on The Structural and Electrical Properties of CNTs / PMMA Nanocomposite Films. *International Journal of Engineering & Technology*, *13*(02), 77–79. https://doi.org/1310302-7676

Allaedini, G., Masrinda Tasirin, S., Aminayi, P., Yaakob, Z., & Zainal MeorTalib, M. (2016). Carbon nanotubes via different catalysts and the important factors that affect their production: A review on catalyst preferences. *Int. J. Nano Dimens*, *7*(3), 186–185. https://doi.org/10.7508/ijnd.2016.03.002

Alosh, T. M. (2013). *Electrical Resistivity Dependence on Mechanical Stresses of Carbon Nanotube Yarns (Doctoral dissertation).* Catholic University of America.

Alstrup, I. (1988). A new model explaining carbon filament growth on nickel, iron, and NiCu alloy catalysts. *Journal of Catalysis*, *109*(2), 241–251. https://doi.org/10.1016/0021-9517(88)90207-2

Alstrup, Ib, & Tavares, M. T. (1993). Kinetics of carbon formation from CH4+ H2 on silica-supported nickel and Ni-Cu catalysts. *Journal of Catalysis*, *139*(2), 513–524.

Alvarenga, J., Jarosz, P. R., Schauerman, C. M., Moses, B. T., Landi, B. J., Cress, C. D., & Raffaelle, R. P. (2010). High conductivity carbon nanotube wires from radial densification and ionic doping. *Applied Physics Letters*, *97*(18), 1–4. https://doi.org/10.1063/1.3506703

Alvarez, N. T., Miller, P., Haase, M. R., Lobo, R., Malik, R., & Shanov, V. (2019). Tailoring physical properties of carbon nanotube threads during assembly. *Carbon*, *144*, 55–62.

https://doi.org/10.1016/j.carbon.2018.11.036

Andrews, R., Jacques, D., Rao, A. M., Rantell, T., Derbyshire, F., Chen, Y., Chen, J., & Haddon, R. C. (1999). Nanotube composite carbon fibers. *Applied Physics Letters*, *75*(9), 1329–1331.

Angulakshmi, V. S., Karthikeyan, S., & Syed Shabudeen, P. S. (2015). Effect of synthesis temperature on the growth of multiwalleded carbon nanotubes from Zeamays oil as evidenced by structural, Raman and XRD analyses. *Rasayan Journal of Chemistry*, *8*(1), 1–7.

Anisimov, A. S., Nasibulin, A. G., Jiang, H., Launois, P., Cambedouzou, J., Shandakov, S. D., & Kauppinen, E. I. (2010). Mechanistic investigations of single-walled carbon nanotube synthesis by ferrocene vapor decomposition in carbon monoxide. *Carbon*, *48*(2), 380–388. https://doi.org/10.1016/j.carbon.2009.09.040

Antunes, E. F., Lobo, A. O., Corat, E. J., Trava-Airoldi, V. J., Martin, A. A., & Veríssimo, C. (2006). Comparative study of first- and second-order Raman spectra of MWCNT at visible and infrared laser excitation. *Carbon*, *44*(11), 2202–2211. https://doi.org/10.1016/j.carbon.2006.03.003

Arjmand, M., Mirkhani, S. A., Pötschke, P., Krause, B., & Sundararaj, U. (2017). Impact of synthesis temperature on structure of carbon nanotubes and morphological and electrical characterization of their polymeric nanocomposites. *AIP Conference Proceedings*, *1914*, 1–6. https://doi.org/10.1063/1.5016698

Arrhenius, S. (1889). On the reaction rate of the inversion of non-refined sugar upon souring. *Z Phys Chem*, *4*, 226–248.

Audier, M., & Coulon, M. (1985). Kinetic and Microscopic Aspects of Catalytic Carbon Growth.

Carbon, *23*(3), 317–323.

Baker, R. (1972). Nucleation and growth of carbon deposits from the nickel catalyzed decomposition of acetylene. *Journal of Catalysis*, *26*(1), 51–62. https://doi.org/10.1016/0021-9517(72)90032-2

Baker, R. T. K. (1989). Catalytic growth of carbon filaments. *Carbon*, *27*(3), 315–323.

Baker, R. T. K., & Harris, P. S. (1978). *In Chemistry and Physics of Carbon, Vol. 14, Walker, P. L., Jr., Thrower, P. A., Eds*. Dekker: New York.

Bandaru, P. R. (2007). Electrical Properties and Applications of Carbon Nanotube Structures. *Journal of Nanoscience and Nanotechnology*, *7*(4), 1239–1267. https://doi.org/10.1166/jnn.2007.307

Baranov, A. V, Bekhterev, A. N., Bobovich, Y. S., & Petrov, V. I. (1987). Interpretation of some singularities in raman-spectra of graphite and glass carbon. *Optika I Spektroskopiya*, *62*(5), 1036–1042.

Barnard, J. S., Paukner, C., & Koziol, K. K. (2016). The role of carbon precursor on carbon nanotube chirality in floating catalyst chemical vapour deposition. *Nanoscale*, *8*(39), 17262–17270. https://doi.org/10.1039/C6NR03895F

Batani, D., Vinci, T., & Bleiner, D. (2014). Laser-ablation and induced nanoparticle synthesis. *Laser and Particle Beams*, *32*(1), 1–7. https://doi.org/10.1017/S0263034613000669

Baughman, R. H. (2002). Carbon Nanotubes — the Route Toward. *Science*, *297*(787), 787–792. https://doi.org/10.1126/science.1060928

Bayat, N., Rezaei, M., & Meshkani, F. (2016). Methane decomposition over Ni-Fe/Al2O3catalysts for production of COx-free hydrogen and carbon nanofiber. *International Journal of Hydrogen Energy*, *41*(3), 1574–1584. https://doi.org/10.1016/j.ijhydene.2015.10.053

Behabtu, N, Green, M., & Pasquali, M. (2008). Carbon nanotube-based neat fibers. *Nano Today*, *3*(5–6), 24–34. https://doi.org/10.1016/S1748-0132(08)70062-8

Behabtu, Natnael, Young, C. C., Tsentalovich, D. E., Kleinerman, O., Wang, X., Ma, A. W. K., Bengio, E. A., Ter Waarbeek, R. F., De Jong, J. J., Hoogerwerf, R. E., Fairchild, S. B., Ferguson, J. B., Maruyama, B., Kono, J., Talmon, Y., Cohen, Y., Otto, M. J., & Pasquali, M. (2013). Strong, light, multifunctional fibers of carbon nanotubes with ultrahigh conductivity. *Science*, *339*(6116), 182–186. https://doi.org/10.1126/science.1228061

Behr, M. J., Gaulding, E. A., Mkhoyan, K. A., & Aydil, E. S. (2010). Effect of hydrogen on catalyst nanoparticles in carbon nanotube growth. *Journal of Applied Physics*, *108*(5), 1–8. https://doi.org/10.1063/1.3467971

Biró, L. P., Lambin, P., Loiseau, A., & Culot, C. (2002). Structure of carbon nanotubes probed by local and global probes. *Carbon*, *40*(10), 1635–1648. https://doi.org/http://dx.doi.org/10.1016/S0008-6223(02)00006-4

Blanchard, F., Reymond, J. P., Pommier, B., & Teichner, S. J. (1982). On the mechanism of the Fischer-Tropsch synthesis involving unreduced iron catalyst. *Journal of Molecular Catalysis*, *17*(2–3), 171–181. https://doi.org/10.1016/0304-5102(82)85028-1

Bodiba, V., Igbokwe, E., Mahangani, N., Aberefa, O., Daramola, M. O., & Iyuke, S. E. (2018). Production of CNT yarns for use as filaments in incandescent bulb: effect of carbon source

and state of catalyst on production of CNT. *IOP Conference Series: Materials Science and Engineering*, *413*(1), 1–7. https://doi.org/10.1088/1757-899X/413/1/012027

Bom, D., Andrews, R., Jacques, D., Anthony, J., Chen, B., Meier, M. S., & Selegue, J. P. (2002). Thermogravimetric Analysis of the Oxidation of Multiwalled Carbon Nanotubes: Evidence for the Role of Defect Sites in Carbon Nanotube Chemistry. *Nano Letters*, *2*(6), 615–619. https://doi.org/10.1021/nl020297u

Bonadiman, R., Lima, M. D., de Andrade, M. J., & Bergmann, C. P. (2006). Production of single and multi-walled carbon nanotubes using natural gas as a precursor compound. *Journal of Materials Science*, *41*(22), 7288–7295. https://doi.org/10.1007/s10853-006-0938-2

Bouts, N., Gaillard, M., Donero, L., El Mel, A. A., Gautron, E., Angleraud, B., Boulmer-Leborgne, C., & Tessier, P. Y. (2017). Growth control of carbon nanotubes using nanocomposite nickel/carbon thin films. *Thin Solid Films*, *630*, 38–47. https://doi.org/10.1016/j.tsf.2016.10.025

Bowers, B. (2011). The end of an incandescent affair. *IEEE Spectrum*, 44–51.

Bradford, P. D., & Bogdanovich, A. E. (2008). Electrical Conductivity Study of Carbon Nanotube Yarns, 3-D Hybrid Braids and their Composites. *Journal of Composite Materials*, *42*(15), 1533–1545. https://doi.org/10.1177/0021998308092206

Bulmer, J. S., Christie, L. M., Anderson, D. P., Petry, J. M., Quinton, B. T., Li, G., Lee, J. H., Wan, H., Ruter-, B., Yost, K., & Barnes, P. N. (2010). Bulk Carbon Nanotube Yarn Conductivity and Strength Enhancement Through High Temperature Annealing. *Carbon*, 628–629.

Cançado, L. G., Takai, K., Enoki, T., Endo, M., Kim, Y. A., Mizusaki, H., Jorio, A., Coelho, L. N., Magalhães-Paniago, R., & Pimenta, M. A. (2006). General equation for the determination of the crystallite size La of nanographite by Raman spectroscopy. *Applied Physics Letters*, *88*(16), 1–4. https://doi.org/10.1063/1.2196057

Cao, A., Xu, C., Liang, J., Wu, D., & Wei, B. (2001). X-ray diffraction characterization on the alignment degree of carbon nanotubes. *Chemical Physics Letters*, *344*, 13–17. https://doi.org/10.1016/S0009-2614(01)00671-6

Chen, K., & Murray, W. A. (1980). Energy , Incandescent Lighting , and 100 Years. *IEEE Transactions on Industry Applications, IA-16*(3), 413–419.

Chiodarelli, N., Masahito, S., Kashiwagi, Y., Li, Y., Arstila, K., Richard, O., Cott, D. J., Heyns, M., De Gendt, S., Groeseneken, G., & Vereecken, P. M. (2011). Measuring the electrical resistivity and contact resistance of vertical carbon nanotube bundles for application as interconnects. *Nanotechnology*, *22*(8), 1–8. https://doi.org/10.1088/0957-4484/22/8/085302

Chipara, D. M., Chipara, A. C., & Chipara, M. (2011). Raman Spectroscopy of Carbonaceous Materials: A Concise Review. *Spectroscopy*, *26*(10), 42–47.

Chizari, K., Vena, A., Laurentius, L., & Sundararaj, U. (2014). The effect of temperature on the morphology and chemical surface properties of nitrogen-doped carbon nanotubes. *Carbon*, *68*, 369–379. https://doi.org/10.1016/j.carbon.2013.11.013

Cho, J., Park, J. H., Kim, J. K., & Schubert, E. F. (2017). White light-emitting diodes: History, progress, and future. *Laser & Photonics Reviews*, *11*(2), 1–17. https://doi.org/10.1002/lpor.201600147

Christen, H. M., Puretzky, A. A., Cui, H., Belay, K., Fleming, P. H., Geohegan, D. B., & Lowndes, D. H. (2004). Rapid Growth of Long, Vertically Aligned Carbon Nanotubes through Efficient Catalyst Optimization Using Metal Film Gradients. *Nano Letters*, *4*(10), 1939–1942. https://doi.org/10.1021/nl048856f

Ci, Punbusayakul, N., Wei, J., Vajtai, R., Talapatra, S., & Ajayan, P. M. (2007). Multifunctional Macroarchitectures of Double-Walled Carbon Nanotube Fibers. *Advanced Materials*, *19*(13), 1719–1723. https://doi.org/10.1002/adma.200602520

Ci, Wei, J., Wei, B., Liang, J., Xu, C., & Wu, D. (2001). Carbon nanofibers and single-walled carbon nanotubes prepared by the floating catalyst method. *Carbon*, *39*(3), 329–335. https://doi.org/10.1016/S0008-6223(00)00126-3

Collins, P. G. (2017). Defects and disorder in carbon nanotubes. In A. V. Narlikar & Y. Y. Fu (Eds.), *Oxford Handbook of Nanoscience and Technology: Frontiers and Advances* (Vol. 1). Oxford University Press. https://doi.org/10.1093/oxfordhb/9780199533053.013.2

Collins, P. G., & Avouris, P. (2002). Intershell Conductance of Multiwalled Carbon Nanotubes. *AIP Conference Proceedings*, *633*, 223–226. https://doi.org/10.1063/1.1514110

Costa, S., Borowiak-Palen, E., Kruszyńska, M., Bachmatiuk, A., & Kaleńczuk, R. J. (2008). Characterization of carbon nanotubes by Raman spectroscopy. *Materials Science-Poland*, *26*(2), 1–9.

Dai, H. (2002). Carbon nanotubes: opportunities and challenges. *Surface Science*, *500*(1–3), 218–241. https://doi.org/10.1016/S0039-6028(01)01558-8

Das, R., Shahnavaz, Z., Ali, M. E., Islam, M. M., & Abd Hamid, S. B. (2016). Can We Optimize

Arc Discharge and Laser Ablation for Well-Controlled Carbon Nanotube Synthesis? *Nanoscale Research Letters*, *11*(1), 1–23. https://doi.org/10.1186/s11671-016-1730-0

Dasgupta, K., Venugopalan, R., Dey, G. K., & Sathiyamoorthy, D. (2008). Novel catalytic route to bulk production of high purity carbon nanotube. *Journal of Nanoparticle Research*, *10*(1), 69–76. https://doi.org/10.1007/s11051-007-9219-5

De Volder, M. F. L. L., Tawfick, S. H., Baughman, R. H., & Hart, A. J. (2013). Carbon Nanotubes: Present and Future Commercial Applications. *Science*, *339*(6119), 535–539. https://doi.org/10.1126/science.1222453

Demicheli, M. C., Ponzi, E. N., Ferretti, O. A., & Yeramian, A. A. (1991). Kinetics of carbon formation from CH4-H2 mixtures on nickel-alumina catalyst. *The Chemical Engineering Journal*, *46*(3), 129–136. https://doi.org/10.1016/0300-9467(91)87004-T

Devaux, X., Tsareva, S. Y., Kovalenko, A. N., Zaramenskih, K. S., McRae, E., & Zharikov, E. V. (2012). Influence of CS2 on the growth of carbon nanotubes. *Physica E*, *44*(6), 1028–1031. https://doi.org/10.1016/j.physe.2010.11.014

Dichiara, A., & Bai, J. (2012). The growth of carbon nanotube multilayers on ceramic μ-particles by catalytic chemical vapour deposition. *Diamond and Related Materials*, *29*, 52–58. https://doi.org/10.1016/j.diamond.2012.07.010

Douven, S., Pirard, S. L., Heyen, G., Toye, D., & Pirard, J. P. (2011). Kinetic study of double-walled carbon nanotube synthesis by catalytic chemical vapour deposition over an Fe-Mo/MgO catalyst using methane as the carbon source. *Chemical Engineering Journal*, *175*(1), 396–407. https://doi.org/10.1016/j.cej.2011.08.066

Dresselhaus, M., Dresselhaus, G., Eklund, P., & Saito, R. (1998). Carbon nanotubes. *Physics World*, *11*(1), 33–38. https://doi.org/10.1088/2058-7058/11/1/32

Dresselhaus, Mildred S, Jorio, A., Hofmann, M., Dresselhaus, G., & Saito, R. (2010). Perspectives on Carbon Nanotubes and Graphene Raman Spectroscopy. *Nano Letters*, *10*(3), 751–758. https://doi.org/10.1021/nl904286r

Dresselhaus, Millie S., Dresselhaus, G., Saito, R., & Jorio, A. (2005). Raman spectroscopy of carbon nanotubes. *Physics Reports*, *409*(2), 47–99. https://doi.org/10.1016/j.physrep.2004.10.006

Ebbesen, T. W., Lezec, H. J., Hiura, H., Bennett, J. W., Ghaemi, H. F., & Thio, T. (1996). Electrical conductivity of individual carbon nanotubes. *Nature*, *382*(6586), 54–56. https://doi.org/10.1038/382054a0

Eckmann, A., Felten, A., Mishchenko, A., Britnell, L., Krupke, R., Novoselov, K. S., & Casiraghi, C. (2012). Probing the Nature of Defects in Graphene by Raman Spectroscopy. *Nano Letters*, *12*(8), 3925–3930. https://doi.org/10.1021/nl300901a

Einarsson, E., Murakami, Y., Kadowaki, M., & Maruyama, S. (2008). Growth dynamics of vertically aligned single-walled carbon nanotubes from in situ measurements. *Carbon*, *46*(6), 923–930. https://doi.org/10.1016/j.carbon.2008.02.021

Endo, M., Takeuchi, K., Igarashi, S., Kobori, K., Shiraishi, M., & Kroto, H. W. (1993). The production and structure of pyrolytic carbon nanotubes (PCNTs). *Journal of Physics and Chemistry of Solids*, *54*(12), 1841–1848. https://doi.org/10.1016/0022-3697(93)90297-5

Energy Information and Security Act of 2007, Subtitle B—Lighting Energy Efficiency.

Engel-Herbert, R., Pforte, H., & Hesjedal, T. (2007). CVD synthesis and purification of single-walled carbon nanotubes using silica-supported metal catalyst. *Materials Letters*, *61*(11–12), 2589–2593. https://doi.org/10.1016/j.matlet.2006.10.004

Ermakova, M. A., Ermakov, D. Y., Chuvilin, A. L., & Kuvshinov, G. G. (2001). Decomposition of methane over iron catalysts at the range of moderate temperatures: The influence of structure of the catalytic systems and the reaction conditions on the yield of carbon and morphology of carbon filaments. *Journal of Catalysis*, *201*(2), 183–197. https://doi.org/10.1006/jcat.2001.3243

Eyring, H. (1935). The Activated Complex and the Absolute Rate of Chemical Reactions. *Chemical Reviews*, *17*(1), 65–77.

Fan, S., Chapline, M. G., Franklin, N. R., Tombler, T. W., Cassell, A. M., & Dai, H. (1999). *Self-Oriented Regular Arrays of Carbon Nanotubes and Their Field Emission Properties*. *283*(January), 512–515.

Fang, S., Zhang, M., Zakhidov, A. A., & Baughman, R. H. (2010). Structure and process-dependent properties of solid-state spun carbon nanotube yarns. *Journal of Physics Condensed Matter*, *22*(33), 1–6. https://doi.org/10.1088/0953-8984/22/33/334221

FAQ : phasing out conventional incandescent bulbs. (2009). In *MEMO/09/368* (Issue September 2009).

Felisberto, M., Tzounis, L., Sacco, L., Stamm, M., Candal, R., Rubiolo, G. H., & Goyanes, S. (2017). Carbon nanotubes grown on carbon fiber yarns by a low temperature CVD method: A significant enhancement of the interfacial adhesion between carbon fiber/epoxy matrix

hierarchical composites. *Composites Communications*, *3*, 33–37. https://doi.org/10.1016/j.coco.2017.01.003

Fogler, H. S. (2004). Chemical reaction engineering. In *The Engineering Handbook, Second Edition*. https://doi.org/10.1201/9781420014389.ch11

Fogler, H. S. (2010). *Essentials of Chemical Reaction Engineering: Essenti Chemica Reactio Engi*. Pearson Education.

Frank, S., Poncharal, P., Wang, Z. L., & Heer, W. A. de. (1998). Carbon Nanotube Quantum Resistors. *Science*, *280*(5370), 1744–1746. https://doi.org/10.1126/science.280.5370.1744

Gao, B., Wang, I.-W., Ren, L., Haines, T., & Hu, J. (2019). Catalytic Performance and Reproducibility of Ni/Al2O3 and Co/Al2O3 Mesoporous Aerogel Catalysts for Methane Decomposition. *Industrial & Engineering Chemistry Research*, *58*(2), 798–807. https://doi.org/10.1021/acs.iecr.8b04223

Gao, Z., & Yuen, M. M. F. (2012). Study of CNT growth termination mechanism: Effect of catalyst diffusion. *13th International Thermal, Mechanical and Multi-Physics Simulation and Experiments in Microelectronics and Microsystems*, 1–5. https://doi.org/10.1109/ESimE.2012.6191723

Gogotsi, Y., Libera, J. A., & Yoshimura, M. (2000). Hydrothermal synthesis of multiwall carbon nanotubes. *Journal of Materials Research*, *15*(12), 2591–2594. https://doi.org/10.1557/JMR.2000.0370

Goh, T. N. (2001). A pragmatic approach to experimental design in industry. *Journal of Applied Statistics*, *28*(3–4), 391–398. https://doi.org/10.1080/02664760120034126

Gommans, H. H., Alldredge, J. W., Tashiro, H., Park, J., Magnuson, J., & Rinzler, A. G. (2000). Fibers of aligned single-walled carbon nanotubes: Polarized Raman spectroscopy. *Journal of Applied Physics*, *88*(5), 2509–2514. https://doi.org/10.1063/1.1287128

Gommes, C., Blacher, S., Bossuot, C., Marchot, P., Nagy, J. B., & Pirard, J.-P. (2004). Influence of the operating conditions on the production rate of multi-walled carbon nanotubes in a CVD reactor. *Carbon*, *42*(8–9), 1473–1482.

Goyenola, C., Stafström, S., Hultman, L., & Gueorguiev, and G. K. (2012). Structural Patterns Arising during Synthetic Growth of Fullerene-Like Sulfocarbide. *The Journal of Physical Chemistry C*, *116*(39), 21124–21131. https://doi.org/10.1021/jp307347t

Gspann, T. S., Smail, F. R., & Windle, A. H. (2014). Spinning of carbon nanotube fibres using the floating catalyst high temperature route: purity issues and the critical role of sulphur. *Faraday Discuss.*, *173*(35), 47–65. https://doi.org/10.1039/c4fd00066h

Guarnieri, M. (2015). Switching the Light: From Chemical to Electrical [Historical]. *IEEE Industrial Electronics Magazine*, *9*(3), 44–47. https://doi.org/10.1109/MIE.2015.2454038

Guellati, O., Janowska, I., Bégin, D., Guerioune, M., Mekhalif, Z., Delhalle, J., Moldovan, S., Ersen, O., & Pham-Huu, C. (2012). Influence of ethanol in the presence of H2 on the catalytic growth of vertically aligned carbon nanotubes. *Applied Catalysis A: General*, *423–424*, 7–14. https://doi.org/10.1016/j.apcata.2012.02.036

Gutiérrez, M. P., Li, H., & Patton, J. (2002). *Thin Film Surface Resistivity*.

Haggenmueller, R., Gommans, H. H., Rinzler, A. G., Fischer, J. E., & Winey, K. I. (2000). Aligned single-wall carbon nanotubes in composites by melt processing methods. *Chemical Physics*

Letters, *330*, 219–225.

Hamad, A. H., Khashan, K. S., & Hadi, A. A. (2016). Laser Ablation in Different Environments and Generation of Nanoparticles. In *Applications of Laser Ablation - Thin Film Deposition, Nanomaterial Synthesis and Surface Modification*. InTech. https://doi.org/10.5772/65241

Harris, M. (2009). Let there be light! *Engineering & Technology*, *10*(6), 18–21.

Haskin, C., & Edwards, G. (2013). Determination of the Concentration of Atmospheric Gases By Gas Chromatography. *McNair Scholars Research Journal*, *6*(1), 37–52.

He, D., Bozlar, M., Genestoux, M., & Bai, J. (2010). Diameter- and length-dependent self-organizations of multi-walled carbon nanotubes on spherical alumina microparticles. *Carbon*, *48*(4), 1159–1170. https://doi.org/10.1016/j.carbon.2009.11.039

Hoecker, C., Smail, F., Pick, M., & Boies, A. (2017). The influence of carbon source and catalyst nanoparticles on CVD synthesis of CNT aerogel. *Chemical Engineering Journal*, *314*, 388–395. https://doi.org/10.1016/j.cej.2016.11.157

Holban, A. M., Grumezescu, A. M., & Andronescu, E. (2016). Inorganic nanoarchitectonics designed for drug delivery and anti-infective surfaces. In *Surface Chemistry of Nanobiomaterials* (pp. 301–327). Elsevier. https://doi.org/10.1016/B978-0-323-42861-3.00010-8

Hong, B. H., Lee, J. Y., Beetz, T., Zhu, Y., Kim, P., & Kim, K. S. (2005). Quasi-Continuous Growth of Ultralong Carbon Nanotube Arrays. *Journal of the American Chemical Society*, *127*(44), 15336–15337. https://doi.org/10.1021/ja054454d

Horiuti Juro. (1961). Activation Free Energy and Activation Energy as Determining Factors.

Journal of the Research Institute for Catalysis Hokkaido University, *9*(3), 211–232.

Hou, G., Wang, G., Deng, Y., Zhang, J., Nshimiyimana, J. P., Chi, X., Hu, X., Chu, W., Dong, H., Zhang, Z., Liu, L., & Sun, L. (2016). Effective enhancement of the mechanical properties of macroscopic single-walled carbon nanotube fibers by pressure treatment. *RSC Advances*, *6*(99), 97012–97017. https://doi.org/10.1039/c6ra21238g

Hou, P., Liu, C., Tong, Y., Xu, S., Liu, M., & Cheng, H. (2001). Purification of single-walled carbon nanotubes synthesized by the hydrogen arc-discharge method. *Journal of Materials Research*, *16*(9), 2526–2529. https://doi.org/10.1557/JMR.2001.0346

Hüsing, N., & Schubert, U. (1998). Aerogels—Airy Materials: Chemistry, Structure, and Properties. *Angewandte Chemie International Edition*, *37*(1–2), 22–45. https://doi.org/10.1002/(SICI)1521-3773(19980202)37

Igbokwe, E. C., Daramola, M. O., & Iyuke, S. E. (2019). Production of carbon nanotube yarns via floating catalyst chemical vapor deposition: Effect of synthesis temperature on electrical conductivity. *Results in Physics*, *15*, 1–7. https://doi.org/10.1016/j.rinp.2019.102705

Iijima, S. (1991). Helical microtubules of graphitic carbon. *Letters to Nature*, *354*, 56–58.

Iyuke, S. E. (2015). *Process for Producing Carbon Nanotubes* (Patent No. US 9,102,525 B2). United States Patent.

Iyuke, S. E., Abdulkareem, S. A., Afolabi, S. A., & Piennar, C. H. v. (2007). Catalytic Production of Carbon Nanotubes in a Swirled Fluid Chemical Vapour Deposition Reactor. *International Journal of Chemical Reactor Engineering*, *5*(1), 1–9. https://doi.org/10.2202/1542-6580.1422

Iyuke, S. E., & Simate, G. S. (2011). Synthesis of Carbon Nanomaterials in a Swirled Floating Catalytic Chemical Vapour Deposition Reactor for Continuous and Large Scale Production. In *Carbon Nanotubes – Growth and Applications* (pp. 35–58).

Jacob, B. (2009). Lamps for improving the energy efficiency of domestic lighting. *Lighting Research & Technology*, *41*(3), 219–228. https://doi.org/10.1177/1477153509339610

Jahanshahi, M., & Dehghani, A. (2013). Fabrication, Purification and Characterization of Carbon Nanotubes: Arc-Discharge in Liquid Media (ADLM). In *Syntheses and Applications of Carbon Nanotubes and Their Composites*. InTech. https://doi.org/10.5772/51116

Jayasinghe, C. (2011). *Synthesis and Characterization of Carbon Nanotube, Threads, Yarns, and Sheets*. University of Cincinnati, Cincinnati, OH.

Jeong, H. J. (2001). Temperature and time dependence of the growth of carbon nanotubes by thermal chemical vapor deposition. *AIP Conference Proceedings*, *590*, 35–38. https://doi.org/10.1063/1.1420051

Jeong, S.-H., Lee, O.-J., Lee, K.-H., Oh, S. H., & Park, C.-G. (2002). Preparation of Aligned Carbon Nanotubes with Prescribed Dimensions: Template Synthesis and Sonication Cutting Approach. *Chemistry of Materials*, *14*(4), 1859–1862. https://doi.org/10.1021/cm011620h

Jiang, K., Fan, S., & Li, Q. (2004). *Light Filament Formed from Carbon Nanotubes and Method for Making Same* (Patent No. US 2004/0051432 A1). United States Patent Application Publication.

Jin, Z., Chu, H., Wang, J., Hong, J., Tan, W., & Li, Y. (2007). Ultralow Feeding Gas Flow Guiding Growth of Large-Scale Horizontally Aligned Single-Walled Carbon Nanotube Arrays. *Nano*

Letters, *7*(7), 2073–2079. https://doi.org/10.1021/nl070980m

José-Yacamán, M., Miki-Yoshida, M., Rendón, L., & Santiesteban, J. G. (1993). Catalytic growth of carbon microtubules with fullerene structure. *Applied Physics Letters*, *62*(6), 657–659. https://doi.org/10.1063/1.108857

Jourdain, V., & Bichara, C. (2013). Current understanding of the growth of carbon nanotubes in catalytic chemical vapour deposition. *Carbon*, *58*, 2–39. https://doi.org/10.1016/j.carbon.2013.02.046

Jung, Y. J., Wei, Vajtai, R., Ajayan, P. M., Homma, Y., Prabhakaran, K., & Ogino, T. (2003). Mechanism of Selective Growth of Carbon Nanotubes on SiO2/Si Patterns. *Nano Letters*, *3*(4), 561–564. https://doi.org/10.1021/nl034075n

Kane, C. L., & Mele, E. J. (1997). Size , Shape , and Low Energy Electronic Structure of Carbon Nanotubes. *Physical Review Letters*, *78*(10), 1932–1935.

Keidar, M. (2007). Factors affecting synthesis of single wall carbon nanotubes in arc discharge. *Journal of Physics D: Applied Physics*, *40*(8), 2388–2393. https://doi.org/10.1088/0022-3727/40/8/S18

Khavarian, M., Chai, S. P., Tan, S. H., & Mohamed, A. R. (2011). Effect of Different Parameters on the Morphology of Carbon Nanotubes Structures Grown by Floating Catalyst Method. *Journal of Applied Sciences*, *11*(13), 2382–2387. https://doi.org/10.3923/jas.2011.2382.2387

Khuri, A. I., & Mukhopadhyay, S. (2010). Response surface methodology. *Wiley Interdisciplinary Reviews: Computational Statistics*, *2*(2), 128–149. https://doi.org/10.1002/wics.73

Kim, H., Wang, M., Lee, S. K., Kang, J., Nam, J.-D., Ci, L., & Suhr, J. (2017). Tensile properties

of millimeter-long multi-walled carbon nanotubes. *Scientific Reports*, *7*(1), 1–7. https://doi.org/10.1038/s41598-017-10279-0

Kim, K.-E., Kim, K.-J., Jung, W. S., Bae, S. Y., Park, J., Choi, J., & Choo, J. (2005). Investigation on the temperature-dependent growth rate of carbon nanotubes using chemical vapor deposition of ferrocene and acetylene. *Chemical Physics Letters*, *401*(4–6), 459–464. https://doi.org/10.1016/j.cplett.2004.11.113

Kim, P., Shi, L., Majumdar, A., & McEuen, P. L. (2001). Thermal Transport Measurements of Individual Multiwalled Nanotubes. *Physical Review Letters*, *87*(21), 215502. https://doi.org/10.1103/PhysRevLett.87.215502

Kociak, M., Kasumov, A. Y., Guéron, S., Reulet, B., Khodos, I. I., Gorbatov, Y. B., Volkov, V. T., Vaccarini, L., & Bouchiat, H. (2001). *Superconductivity in Ropes of Single-Walled Carbon Nanotubes*. https://doi.org/10.1103/PhysRevLett.86.2416

Kozlov, M. E., Capps, R. C., Sampson, W. M., Ebron, V. H., Ferraris, J. P., & Baughman, R. H. (2005). Spinning Solid and Hollow Polymer-Free Carbon Nanotube Fibers. *Advanced Materials*, *17*(5), 614–617. https://doi.org/10.1002/adma.200401130

Krasnikov, D. V., Zabelich, B. Y., Iakovlev, V. Y., Tsapenko, A. P., Romanov, S. A., Alekseeva, A. A., Grebenko, A. K., & Nasibulin, A. G. (2019). A spark discharge generator for scalable aerosol CVD synthesis of single-walled carbon nanotubes with tailored characteristics. *Chemical Engineering Journal*, *372*, 462–470. https://doi.org/10.1016/j.cej.2019.04.173

Kristyan, S. (1997). Kinetics of the heterogeneous catalytic decomposition of methane. *The Canadian Journal of Chemical Engineering*, *75*(1), 229–237.

https://doi.org/10.1002/cjce.5450750131

Kucukayan, G., Ovali, R., Ilday, S., Baykal, B., Yurdakul, H., Turan, S., Gulseren, O., & Bengu, E. (2011). An experimental and theoretical examination of the effect of sulfur on the pyrolytically grown carbon nanotubes from sucrose-based solid state precursors. *Carbon*, *49*(2), 508–517. https://doi.org/10.1016/j.carbon.2010.09.050

Kukovecz, Á., Méhn, D., Nemes-Nagy, E., Szabó, R., & Kiricsi, I. (2005). Optimization of CCVD synthesis conditions for single-wall carbon nanotubes by statistical design of experiments (DoE). *Carbon*, *43*(14), 2842–2849. https://doi.org/10.1016/j.carbon.2005.06.001

Kuo, D.-H., Su, M.-Y., & Chen, W.-R. (2006). Fast Rate Growth of Organized Carbon Nanotubes by CVD Using Iron Pentacarbonyl as Gas-Phase Catalyst. *Chemical Vapor Deposition*, *12*(6), 395–402. https://doi.org/10.1002/cvde.200506408

Kuvshinov, G. G., Mogilnykh, Y. I., & Kuvshinov, D. G. (1998). Kinetics of carbon formation from CH4-H2 mixtures over a nickel containing catalyst. *Catalysis Today*, *42*(3), 357–360. https://doi.org/10.1016/S0920-5861(98)00115-1

Kuwana, K., & Saito, K. (2005). Modeling CVD synthesis of carbon nanotubes: Nanoparticle formation from ferrocene. *Carbon*, *43*(10), 2088–2095. https://doi.org/10.1016/j.carbon.2005.03.016

Kuwana, K., & Saito, K. (2007). Modeling ferrocene reactions and iron nanoparticle formation: Application to CVD synthesis of carbon nanotubes. *Proceedings of the Combustion Institute*, *31*(2), 1857–1864. https://doi.org/10.1016/j.proci.2006.07.097

Lavelle, B. M. (2014). *FAQ: The End of the Light Bulb as We Know It - US News and World*

Report. 2007–2009.

Lawson, J., Grimshaw, S., & Burt, J. (1998). A quantitative method for identifying active contrasts in unreplicated factorial designs based on the half-normal plot. *Computational Statistics and Data Analysis*, *26*(4), 425–436. https://doi.org/10.1016/S0167-9473(97)00040-6

Lee, C. J., Park, J., Huh, Y., & Yong Lee, J. (2001). Temperature effect on the growth of carbon nanotubes using thermal chemical vapor deposition. *Chemical Physics Letters*, *343*(1–2), 33–38. https://doi.org/10.1016/S0009-2614(01)00680-7

Lee, O., Jung, J., Doo, S., Kim, S.-S., Noh, T.-H., Kim, K.-I., & Lim, Y.-S. (2010). Effects of temperature and catalysts on the synthesis of carbon nanotubes by chemical vapor deposition. *Metals and Materials International*, *16*(4), 663–667. https://doi.org/10.1007/s12540-010-0822-0

Lee, S.-H., Park, J., Kim, H.-R., Lee, T., Lee, J., Im, Y.-O., Lee, C.-H., Cho, H., Lee, H., Jun, C., Ahn, Y., Lee, I.-B., & Lee, K. (2016). Synthesis of carbon nanotube fibers using the direct spinning process based on Design of Experiment (DoE). *Carbon*, *100*, 647–655. https://doi.org/10.1016/j.carbon.2016.01.034

Lehman, J. H., Terrones, M., Mansfield, E., Hurst, K. E., & Meunier, V. (2011). Evaluating the characteristics of multiwall carbon nanotubes. *Carbon*, *49*(8), 2581–2602. https://doi.org/10.1016/j.carbon.2011.03.028

Lekawa-Raus, A., Patmore, J., Kurzepa, L., Bulmer, J., & Koziol, K. (2014). Electrical Properties of Carbon Nanotube Based Fibers and Their Future Use in Electrical Wiring. *Advanced Functional Materials*, *24*(24), 3661–3682. https://doi.org/10.1002/adfm.201303716

Li, G., Chakrabarti, S., Schulz, M., & Shanov, V. (2010). The effect of substrate positions in chemical vapor deposition reactor on the growth of carbon nanotube arrays. *Carbon*, *48*(7), 2111–2115. https://doi.org/10.1016/j.carbon.2010.01.054

Li, H., Zhao, N., He, C., Shi, C., Du, X., & Li, J. (2008). Thermogravimetric analysis and TEM characterization of the oxidation and defect sites of carbon nanotubes synthesized by CVD of methane. *Materials Science and Engineering: A*, *473*(1–2), 355–359. https://doi.org/10.1016/j.msea.2007.04.003

Li, P., Jiang, K., Liu, M., Li, Q., Fan, S., & Sun, J. (2003). Polarized incandescent light emission from carbon nanotubes. *Applied Physics Letters*, *82*(11), 1763–1765. https://doi.org/10.1063/1.1558900

Li, S., Yu, Z., Rutherglen, C., & Burke, P. J. (2004). Electrical Properties of 0.4 cm Long Single-Walled Carbon Nanotubes. *Nano Letters*, *4*(10), 2003–2007. https://doi.org/10.1021/nl048687z

Li, W., Dichiara, A., & Bai, J. (2013). Carbon nanotube–graphene nanoplatelet hybrids as high-performance multifunctional reinforcements in epoxy composites. *Composites Science and Technology*, *74*, 221–227. https://doi.org/10.1016/j.compscitech.2012.11.015

Li, Wang, K., Wei, J., Wei, B., Zhu, H., Wang, Z., Luo, J., Liu, W., Zheng, M., & Wu, D. (2007). Luminescence of carbon nanotube bulbs. *Chinese Science Bulletin*, *52*(1), 113–117. https://doi.org/10.1007/s11434-007-2211-8

Li, X., Cheng, Y., Zhao, L., Zhang, Q., & Wang, M. S. (2018). Structural and electrical properties tailoring of carbon nanotubes via a reversible defect handling technique. *Carbon*, *133*, 186–

192. https://doi.org/10.1016/j.carbon.2018.03.029

Li, Y., Zhang, X. B., Tao, X. Y., Xu, J. M., Huang, W. Z., Luo, J. H., Luo, Z. Q., Li, T., Liu, F., Bao, Y., & Geise, H. J. (2005). Mass production of high-quality multi-walled carbon nanotube bundles on a Ni/Mo/MgO catalyst. *Carbon*, *43*(2), 295–301. https://doi.org/10.1016/j.carbon.2004.09.014

Li, Yang, Ji, K., Duan, Y., Meng, G., & Dai, Z. (2017). Effect of Hydrogen Concentration on the Growth of Carbon Nanotube Arrays for Gecko-Inspired Adhesive Applications. *Coatings*, *7*(12), 221. https://doi.org/10.3390/coatings7120221

Liang, W., Bockrath, M., Bozovic, D., Hafner, J. H., Tinkham, M., & Hongkun, P. (2001). Fabry - Perot interference in a nanotube electron waveguide. *Nature*, *411*, 665–669.

Lim, S.-R., Kang, D., Ogunseitan, O. A., & Schoenung, J. M. (2013). Potential Environmental Impacts from the Metals in Incandescent, Compact Fluorescent Lamp (CFL), and Light-Emitting Diode (LED) Bulbs. *Environmental Science & Technology*, *47*(2), 1040–1047. https://doi.org/10.1021/es302886m

Liu, K., Jiang, K., Feng, C., Chen, Z., & Fan, S. (2005). A growth mark method for studying growth mechanism of carbon nanotube arrays. *Carbon*, *43*(14), 2850–2856.

Liu, K., Sun, Y., Zhou, R., Zhu, H., Wang, J., Liu, L., Fan, S., & Jiang, K. (2010). Carbon nanotube yarns with high tensile strength made by a twisting and shrinking method. *Nanotechnology*, *21*(4), 045708. https://doi.org/10.1088/0957-4484/21/4/045708

Liu, P., Liu, L., Wei, Y., Liu, K., Chen, Z., Jiang, K., Li, Q., & Fan, S. (2009). Fast high-temperature response of carbon nanotube film and its application as an incandescent display.

Advanced Materials, *21*(35), 3563–3566. https://doi.org/10.1002/adma.200900473

Liu, Q., Ren, W., Chen, Z.-G., Liu, B., Yu, B., Li, F., Cong, H., & Cheng, H.-M. (2008). Direct synthesis of carbon nanotubes decorated with size-controllable Fe nanoparticles encapsulated by graphitic layers. *Carbon*, *46*(11), 1417–1423. https://doi.org/10.1016/j.carbon.2008.06.021

Liu, W. W., Adam, T., Aziz, A., Chai, S. P., Mohamed, A. R., & Hashim, U. (2013). A Study on the Effect of Calcination Temperature on the Graphitization of Carbon Nanotubes Synthesized by the Decomposition of Methane. *Advanced Materials Research*, *832*(3), 56–61. https://doi.org/10.4028/www.scientific.net/AMR.832.56

Losurdo, M., Giangregorio, M. M., Capezzuto, P., & Bruno, G. (2011). Graphene CVD growth on copper and nickel: role of hydrogen in kinetics and structure. *Physical Chemistry Chemical Physics*, *13*(46), 20836. https://doi.org/10.1039/c1cp22347j

Lu, X., Ausman, K. D., Piner, R. D., & Ruoff, R. S. (1999). Scanning electron microscopy study of carbon nanotubes heated at high temperatures in air. *Journal of Applied Physics*, *186*(1999), 186–189. https://doi.org/10.1063/1.370715

Lunk, H. J. (2015). Incandescent lighting and powder metallurgical manufacturing of tungsten wire. *ChemTexts*, *1*(1), 1–12. https://doi.org/10.1007/s40828-014-0003-8

Ma, Y., Dichiara, A. B., He, D., Zimmer, L., & Bai, J. (2016). Control of product nature and morphology by adjusting the hydrogen content in a continuous chemical vapor deposition process for carbon nanotube synthesis. *Carbon*, *107*, 171–179. https://doi.org/10.1016/j.carbon.2016.05.060

Macisaac, D., Kanner, G., & Anderson, G. (1999). Basic physics of the incandescent lamp (lightbulb). *The Physics Teacher*, *37*(9), 520–525. https://doi.org/10.1119/1.880392

Maffucci, A., Maksimenko, S. A., & Miano, G. (2017). *Electrical Conductivity of Carbon Nanotubes : Modeling and Characterization Department of Electrical Engineering and Information School of Electrical Engineering Tel Aviv University* , (Issue October 2016). https://doi.org/10.1007/978-3-319-29746-0

Magrez, A., Seo, J. W., Smajda, R., Mionić, M., & Forró, L. (2010). Catalytic CVD synthesis of carbon nanotubes: Towards high yield and low temperature growth. *Materials*, *3*(11), 4871–4891. https://doi.org/10.3390/ma3114871

Mann, D., Kato, Y. K., Kinkhabwala, A., Pop, E., Cao, J., Wang, X., Zhang, L., Wang, Q., Guo, J., & Dai, H. (2007). Electrically driven thermal light emission from individual single-walled carbon nanotubes. *Nature Nanotechnology*, *2*(1), 33–38. https://doi.org/10.1038/nnano.2006.169

Martin, J., Adana, D. D. R. de, & Asuero, A. G. (2017). Fitting Models to Data: Residual Analysis, a Primer. In *Uncertainty Quantification and Model Calibration*. InTech. https://doi.org/10.5772/68049

Maser, W. K., Benito, A. M., & Martínez, M. T. (2002). Production of carbon nanotubes: the light approach. *Carbon*, *40*(10), 1685–1695. https://doi.org/10.1016/S0008-6223(02)00009-X

Massart, D. L., Dijkstra, A., & Kaufman, L. (1978). Chapter 11 Survey of experimental optimization methods. In *Techniques and Instrumentation in Analytical Chemistry* (Vol. 1, pp. 213–218). Elsevier. https://doi.org/10.1016/S0167-9244(08)70055-6

Matthews, M. J., Pimenta, M. A., Dresselhaus, G., Dresselhaus, M. S., & Endo, M. (1999). Origin of dispersive effects of the Raman D band in carbon materials. *Physical Review B*, *59*(10), R6585–R6588. https://doi.org/10.1103/PhysRevB.59.R6585

Matulka, R., & Wood, D. (2013). *The History of the Light Bulb | Department of Energy*. Department of Energy. https://www.energy.gov/articles/history-light-bulb

McRae, E., Devaux, X., Tsareva, S. Y., Kovalenko, A. N., Zaramenskih, K. S., & Zharikov, E. V. (2013). On the effect of sulphur on the formation of carbon nanotubes and multibranched carbon nanostructures. *Journal of Physics: Conference Series*, *416*, 012003. https://doi.org/10.1088/1742-6596/416/1/012003

Merrill, L. S., & Hamrin, C. E. (1970). Conversion and Temperature Profiles for Complex Reactions in Laminar and Plug. *AlChE Journal*, 194–198.

Mevellec, J. Y., Bergeret, C., Cousseau, J., Buisson, J. P., Ewels, C. P., & Lefrant, S. (2011). Tuning the raman resonance behavior of single-walled carbon nanotubes via covalent functionalization. *Journal of the American Chemical Society*, *133*(42), 16938–16946. https://doi.org/10.1021/ja2062677

Meyyappan, M. (2004). *Carbon Nanotubes Science and Applications*. CRC Press.

Miao, M. (2011). Electrical conductivity of pure carbon nanotube yarns. *Carbon*, *49*(12), 3755–3761. https://doi.org/10.1016/j.carbon.2011.05.008

Miao, M., McDonnell, J., Vuckovic, L., & Hawkins, S. C. (2010). Poisson's ratio and porosity of carbon nanotube dry-spun yarns. *Carbon*, *48*(10), 2802–2811. https://doi.org/10.1016/j.carbon.2010.04.009

Mittal, G., Dhand, V., Rhee, K. Y., Park, S. J., & Lee, W. R. (2015). A review on carbon nanotubes and graphene as fillers in reinforced polymer nanocomposites. *Journal of Industrial and Engineering Chemistry*, *21*, 11–25. https://doi.org/10.1016/j.jiec.2014.03.022

Miyahara, K., & Kazusaka, A. (1976). Number of Active Sites and Turnover Number For Heterogeneous Catalysis. *Journal of the Research Institute for Catalysis Hokkaido University*, *24*(1), 65–70.

Mohammadian, N., Ghoreishi, S., Hafeziyeh, S., Saeidi, S., & Dionysiou, D. (2018). Optimization of Synthesis Conditions of Carbon Nanotubes via Ultrasonic-Assisted Floating Catalyst Deposition Using Response Surface Methodology. *Nanomaterials*, *8*(5), 316. https://doi.org/10.3390/nano8050316

Mohammed, I. A., Bankole, M. T., Abdulkareem, A. S., Ochigbo, S. S., Afolabi, A. S., & Abubakre, O. K. (2017). Full factorial design approach to carbon nanotubes synthesis by CVD method in argon environment. *South African Journal of Chemical Engineering*, *24*, 17–42. https://doi.org/10.1016/j.sajce.2017.06.001

Moisala, A., Nasibulin, A. G., Brown, D. P., Jiang, H., Khriachtchev, L., & Kauppinen, E. I. (2006). Single-walled carbon nanotube synthesis using ferrocene and iron pentacarbonyl in a laminar flow reactor. *Chemical Engineering Science*, *61*(13), 4393–4402. https://doi.org/10.1016/j.ces.2006.02.020

Moisala, A., Nasibulin, A. G., & Kauppinen, E. I. (2003). The role of metal nanoparticles in the catalytic production of single-walled carbon nanotubes - A review. *Journal of Physics Condensed Matter*, *15*(42), S3011. https://doi.org/10.1088/0953-8984/15/42/003

Mongwe, T. H. (2018). *Synthesis of carbon nano-onions and their application in photovoltaic cells*. University of the Witwatersrand, Johannesburg.

Montgomery, D. C. (2005). Experiments with random factors. *Design and Analysis of Experiments. 6th Edition. John Wiley and Sons. Inc*, 495.

Moothi, K., Simate, G. S., Falcon, R., Iyuke, S. E., & Meyyappan, M. (2015). Carbon Nanotube Synthesis Using Coal Pyrolysis. *Langmuir*, *31*(34), 9464–9472. https://doi.org/10.1021/acs.langmuir.5b01894

Mukesh, T., & Jha, A. K. (2017). *A Review on : Carbon Nanotubes Are Vital for Plant Growth*. *5*, 1–9. https://doi.org/10.11648/j.ajaf.s.2017050501.11

Muñoz, E., Maser, W. K., Benito, A. M., Martínez, M. T., de la Fuente, G. F., Maniette, Y., Righi, A., Anglaret, E., & Sauvajol, J. L. (2000). Gas and pressure effects on the production of single-walled carbon nanotubes by laser ablation. *Carbon*, *38*(10), 1445–1451. https://doi.org/10.1016/S0008-6223(99)00277-8

Muñoz, E., Maser, W. K., Benito, A. M., Martínez, M. T., de la Fuente, G. F., Righi, A., Sauvajol, J. L., Anglaret, E., & Maniette, Y. (2000). Single-walled carbon nanotubes produced by cw CO2 -laser ablation: study of parameters important for their formation. *Applied Physics A: Materials Science & Processing*, *70*(2), 145–151. https://doi.org/10.1007/s003390050026

Nagelkerke, N. J. D. (1991). A Note on a General Definition of the Coefficient of Determination. In *Biometrika* (Vol. 78, Issue 3).

Naha, S., & Puri, I. K. (2008). A model for catalytic growth of carbon nanotubes. *Journal of Physics D: Applied Physics*, *41*(6), 1–6. https://doi.org/10.1088/0022-3727/41/6/065304

Nasibulin, A. G., Pikhitsa, P. V, Jiang, H., & Kauppinen, E. I. (2005). Correlation between catalyst particle and single-walled carbon nanotube diameters. *Carbon*, *43*(11), 2251–2257. https://doi.org/https://doi.org/10.1016/j.carbon.2005.03.048

Ni, L., Kuroda, K., Zhou, L. P., Kizuka, T., Ohta, K., Matsuishi, K., & Nakamura, J. (2006). Kinetic study of carbon nanotube synthesis over Mo/Co/MgO catalysts. *Carbon*, *44*(11), 2265–2272. https://doi.org/10.1016/j.carbon.2006.02.031

Nikolaev, P., Bronikowski, M. J., Bradley, R. K., Rohmund, F., Colbert, D. T., Smith, K. a, & Smalley, R. E. (1999). Gas-phase catalytic growth of single-walled carbon nanotubes from carbon monoxide. *Chemical Physics Letters*, *313*(1–2), 91–97. https://doi.org/Doi 10.1016/S0009-2614(99)01029-5

Novoselova, I. A., Oliinyk, N. F., Volkov, S. V., Konchits, A. A., Yanchuk, I. B., Yefanov, V. S., Kolesnik, S. P., & Karpets, M. V. (2008). Electrolytic synthesis of carbon nanotubes from carbon dioxide in molten salts and their characterization. *Physica E: Low-Dimensional Systems and Nanostructures*, *40*(7), 2231–2237. https://doi.org/10.1016/j.physe.2007.10.069

Öncel, Ç., & Yürüm, Y. (2006). Carbon nanotube synthesis via the catalytic CVD method: A review on the effect of reaction parameters. *Fullerenes Nanotubes and Carbon Nanostructures*, *14*(1), 17–37. https://doi.org/10.1080/15363830500538441

Onoji, S. E., Iyuke, S. E., Igbafe, A. I., & Daramola, M. O. (2017). Hevea brasiliensis (rubber seed) oil: modeling and optimization of extraction process parameters using response surface methodology and artificial neural network techniques. *Biofuels*, *7269*, 1–15. https://doi.org/10.1080/17597269.2017.1338122

Pellegrino, L., Daghetta, M., Pelosato, R., Citterio, A., & Carlo, V. M. (2013). Searching for Rate Determining Step of CNT Formation : The Role of Cementite. *CHEMICAL ENGINEERING TRANSACTIONS*, *32*(Iii), 739–744. https://doi.org/10.3303/CET1332124

Peng, B., Locascio, M., Zapol, P., Li, S., Mielke, S. L., Schatz, G. C., & Espinosa, H. D. (2008). Measurements of near-ultimate strength for multiwalled carbon nanotubes and irradiation-induced crosslinking improvements. *Nature Nanotechnology*, *3*(10), 626–631. https://doi.org/10.1038/nnano.2008.211

Perincek, O., & Colak, M. (2013). Use of Experimental Box-Behnken Design for the Estimation of Interactions Between Harmonic Currents Produced by Single Phase Loads. *International Journal of Engineering Research and Applications*, *3*(2), 158–165.

Perry, R. H., & Green, D. W. (2007). *Perry's chemical engineers' handbook, 8th illustrated ed*. New York: McGraw-Hill.

Petit, P., & Loiseau, A. (2003). Carbon nanotubes: from science to applications. *Comptes Rendus Physique*, *4*(9), 967–974. https://doi.org/10.1016/j.crhy.2003.10.021

Pirard, S. L., Douven, S., Bossuot, C., Heyen, G., & Pirard, J.-P. (2007). A kinetic study of multi-walled carbon nanotube synthesis by catalytic chemical vapor deposition using a Fe–Co/Al2O3 catalyst. *Carbon*, *45*(6), 1167–1175.

Plata, D. L., Meshot, E. R., Reddy, C. M., Hart, A. J., & Gschwend, P. M. (2010). Multiple Alkynes React with Ethylene To Enhance Carbon Nanotube Synthesis, Suggesting a Polymerization-like Formation Mechanism. *ACS Nano*, *4*(12), 7185–7192. https://doi.org/10.1021/nn101842g

Prasek, J., Drbohlavova, J., Chomoucka, J., Hubalek, J., Jasek, O., Adam, V., & Kizek, R. (2011). Methods for carbon nanotubes synthesis - Review. *Journal of Materials Chemistry*, *21*(40), 15872–15884. https://doi.org/10.1039/c1jm12254a

Ptáček, P., Šoukal, F., & Opravil, T. (2018). Introduction to the Transition State Theory. In *Introducing the Effective Mass of Activated Complex and the Discussion on the Wave Function of this Instanton* (pp. 27–45). InTech. https://doi.org/10.5772/intechopen.78705

Puretzky, A. A., Geohegan, D. B., Jesse, S., Ivanov, I. N., & Eres, G. (2005). In situ measurements and modeling of carbon nanotube array growth kinetics during chemical vapor deposition. *Applied Physics A: Materials Science and Processing*, *81*(2), 223–240. https://doi.org/10.1007/s00339-005-3256-7

Qian, W., Liu, T., Wei, F., Wang, Z., & Li, Y. (2004). Enhanced production of carbon nanotubes: combination of catalyst reduction and methane decomposition. *Applied Catalysis A: General*, *258*(1), 121–124.

Raji, K., Thomas, S., & Sobhan, C. B. (2011). A chemical kinetic model for chemical vapor deposition of carbon nanotubes. *Applied Surface Science*, *257*(24), 10562–10570. https://doi.org/10.1016/j.apsusc.2011.07.051

Rakić, T., Kasagić-Vujanović, I., Jovanović, M., Jančić-Stojanović, B., & Ivanović, D. (2014). Comparison of Full Factorial Design, Central Composite Design, and Box-Behnken Design in Chromatographic Method Development for the Determination of Fluconazole and Its Impurities. *Analytical Letters*, *47*(8), 1334–1347. https://doi.org/10.1080/00032719.2013.867503

Ramirez, A., Royo, C., Latorre, N., Mallada, R., Tiggelaar, R. M., & Monzón, A. (2014). Unraveling the growth of vertically aligned multi-walled carbon nanotubes by chemical vapor deposition. *Materials Research Express*, *1*(4), 1–16. https://doi.org/10.1088/2053-1591/1/4/045604

Ray, S. C., Tetana, Z. N., Erasmus, R., Mathur, A., & Coville, N. J. (2014). Carbon spheres for energy applications: Raman and X-ray photoemission spectroscopy studies. *International Journal of Energy Research*, *38*(4), 444–451. https://doi.org/10.1002/er.3079

Reich, S., Thomsen, C., & Maultzsch, J. (2008). *Carbon nanotubes: basic concepts and physical properties*. John Wiley & Sons.

Ren, Z. F., Huang, Z. P., Xu, J. W., Wang, J. H., Bush, P., Siegal, M. P., & Provencio, P. N. (1998). *Synthesis of Large Arrays of Well-Aligned Carbon Nanotubes on Glass*. *282*(November), 1105–1108.

Reznik, D., Olk, C. H., Neumann, D. A., & Copley, J. R. D. (1995). X-ray powder diffraction from carbon nanotubes and nanoparticles D. *The American Physical Society Physical Review B*, *52*(1), 116–124.

Rodiles, X., Reguero, V., Vila, M., Alemán, B., Arévalo, L., Fresno, F., O'Shea, V. A. d. la P., & Vilatela, J. J. (2019). Carbon nanotube synthesis and spinning as macroscopic fibers assisted by the ceramic reactor tube. *Scientific Reports*, *9*(1), 2–11. https://doi.org/10.1038/s41598-019-45638-6

Roduner, E. (2014). Understanding catalysis. *Chemical Society Reviews*, *43*(24), 8226–8239. https://doi.org/10.1039/c4cs00210e

Ruland, W. (1965). X-ray studies on the carbonization and graphitization of acenaphthylene and bifluorenyl. *Carbon*, *2*(4), 365–378. https://doi.org/10.1016/0008-6223(65)90007-2

Sahle-Demessie, E., Zhao, A., & Salamon, A. W. (2011). A Study of Aged Carbon Nanotubes by Thermogravimetric Analysis. In *PerkinElmer, Inc. Shelton, CT 06484 USA A* (pp. 1–5).

SAinfo, & BuaNews. (2011). *SA to phase out inefficient bulbs by 2016*. Brand South Africa. https://www.brandsouthafrica.com/governance/sustainable/lightbulbs-071211

Salvetat-delmotte, J., & Rubio, A. (2002). *Mechanical properties of carbon nanotubes : a fiber digest for beginners*. *40*, 1729–1734.

Salvetat, J.-P., Bonard, J.-M., N.H.Thomson, A.J.Kulik, Forro, L., Benoit, W., & Zuppiroli, L. (1999). Mechanical properties of carbon nanotubes. *Applied Physics A Materials Science & Processing*, *69*, 255–260. https://doi.org/10.1007/s003399900114

Santangelo, S., Messina, G., Donato, M. G., Lanza, M., Milone, C., & Pistone, A. (2006). Low-frequency Raman study of hollow multiwalled nanotubes grown by Fe-catalyzed chemical vapor deposition. *Journal of Applied Physics*, *100*(10), 104311–104315. https://doi.org/10.1063/1.2386951

Saraswat, S. K., Sinha, B., Pant, K. K., & Gupta, R. B. (2016). Kinetic study and modeling of homogeneous thermocatalytic decomposition of methane over a Ni–Cu–Zn/Al2O3 catalyst for the production of hydrogen and bamboo-shaped carbon nanotubes. *Industrial & Engineering Chemistry Research*, *55*(45), 11672–11680.

Schauer, M. W., & White, M. A. (2015). Tailoring Industrial Scale CNT Production to Specialty Markets. *MRS Proceedings*, *1752*, 103–109. https://doi.org/10.1557/opl.2015.90

Scheibe, B., Borowiak-Palen, E., & Kalenczuk, R. J. (2010). Oxidation and reduction of multiwalled carbon nanotubes — preparation and characterization. *Materials Characterization*, *61*(2), 185–191. https://doi.org/10.1016/j.matchar.2009.11.008

Schleich, J., Mills, B., & Dütschke, E. (2014). A Brighter Future? Quantifying the Rebound Effect in Energy Efficient Lighting. *Energy Policy*, *Elsevier*, *72*, 35–42. https://doi.org/10.1016/j.enpol.2014.04.028

Schulz, M. J., Hou, G., Ng, V., Rabiee, M., Cahay, M., Chaudhary, S., Lindley, D., Chauhan, D., Paine, M., Vijayakumar, D., Xu, C., Yin, Z., Haworth, K., Liu, Y., Sundaram, M., Li, W., Mast, D., & Shanov, V. N. (2017). Science to commercialization of carbon nanotube sheet and yarn. *WSEAS Transactions on Applied and Theoretical Mechanics*, *12*, 41–50.

See, C. H., & Harris, A. T. (2007). A review of carbon nanotube synthesis via fluidized-bed chemical vapor deposition. *Industrial and Engineering Chemistry Research*, *46*(4), 997–1012. https://doi.org/10.1021/ie060955b

Sekoai, P. T., Ayeni, A. O., & Daramola, M. O. (2017). Parametric Optimization of Biohydrogen Production from Potato Waste and Scale-Up Study Using Immobilized Anaerobic Mixed Sludge. *Waste and Biomass Valorization*, *0*(0), 1–13. https://doi.org/10.1007/s12649-017-0136-2

Shah, K. A., & Tali, B. A. (2016). Synthesis of carbon nanotubes by catalytic chemical vapour deposition: A review on carbon sources, catalysts and substrates. *Materials Science in Semiconductor Processing*, *41*, 67–82. https://doi.org/10.1016/j.mssp.2015.08.013

Sharif-Zein, S. H., Mohamed, A. R., Talpa Sai, P. S., Zein, S. H. S., Mohamed, A. R., & Sai, P. S.

T. (2004). Kinetic Studies on Catalytic Decomposition of Methane to Hydrogen and Carbon over Ni/TiO 2 Catalyst. *Industrial & Engineering Chemistry Research*, *43*(16), 4864–4870. https://doi.org/10.1021/ie034208f

Sharma, & Kar, K. K. (2014). Carbon nanotube coated carbon fiber based composite filaments for luminescent bulbs. *Materials Letters*, *137*, 150–152. https://doi.org/10.1016/j.matlet.2014.09.003

Sharma, Renu, Moore, E., Rez, P., & Treacy, M. M. J. J. (2009). Site-Specific Fabrication of Fe Particles for Carbon Nanotube Growth. *Nano Letters*, *9*(2), 689–694. https://doi.org/10.1021/nl803180e

Sharma, Ritu, Sharma, A. K., & Sharma, V. (2015). Synthesis of carbon nanotubes by arc-discharge and chemical vapor deposition method with analysis of its morphology, dispersion and functionalization characteristics. *Cogent Engineering*, *2*(1), 1–10. https://doi.org/10.1080/23311916.2015.1094017

Sharon, M., Apte, P. R., Purandare, S. C., & Zacharia, R. (2005). Application of the Taguchi Analytical Method for Optimization of Effective Parametersof the Chemical Vapor Deposition Process Controlling the Production of Nanotubes/Nanobeads. *Journal of Nanoscience and Nanotechnology*, *5*(2), 288–295. https://doi.org/10.1166/jnn.2005.035

Shin, K. Y., Su, H. C., & Tsai, C. H. (2006). In situ growth of single-walled carbon nanotubes by bimetallic technique with/without dielectric support for nanodevice applications. *Journal of Vacuum Science & Technology B: Microelectronics and Nanometer Structures*, *24*(1), 358–361. https://doi.org/10.1116/1.2151223

Shirazi, Y., Tofighy, M. A., Mohammadi, T., & Pak, A. (2011). Effects of different carbon precursors on synthesis of multiwall carbon nanotubes: Purification and Functionalization. *Applied Surface Science*, *257*(16), 7359–7367. https://doi.org/10.1016/j.apsusc.2011.03.146

Simate, G. S., Moothi, K., Meyyappan, M., Iyuke, S. E., Ndlovu, S., Falcon, R., & Heydenrych, M. (2014). Kinetic model of carbon nanotube production from carbon dioxide in a floating catalytic chemical vapour deposition reactor. *RSC Advances*, *4*(19), 9564–9572. https://doi.org/10.1039/c3ra47163b

Sivakumar, V. M., Abdullah, A. Z., Mohamed, A. R., & Chai, S. P. (2011). Optimized parameters for carbon nanotubes synthesis over Fe and Ni catalysts VIA methane CVD. *Reviews on Advanced Materials Science*, *27*(1), 25–30.

Snoeck, J.-W., Froment, G. F., & Fowles, M. (1997). Kinetic Study of the Carbon Filament Formation by Methane Cracking on a Nickel Catalyst. *Journal of Catalysis*, *169*(1), 250–262. https://doi.org/10.1006/jcat.1997.1635

Snoeck, J. W., Froment, G. F., & Fowles, M. (1997). Filamentous carbon formation and gasification: Thermodynamics, driving force, nucleation, and steady-state growth. *Journal of Catalysis*, *169*(1), 240–249. https://doi.org/10.1006/jcat.1997.1634

Somani, P., & Umeno, M. (2007). Importance of Transmission Electron Microscopy for Carbon Nanomaterials Research. *Modern Research and Educational Topics in Microscopy*, *3*, 634–642.

Song, W., Kinloch, I. A., & Windle, A. H. (2003). Nematic Liquid Crystallinity of Multiwall Carbon Nanotubes. *Science*, *302*(5649), 1363–1363.

https://doi.org/10.1126/science.1089764

Song, W., & Windle, A. H. (2005). Isotropic - Nematic Phase Transition of Dispersions of Multiwall Carbon Nanotubes. *Macromolecules*, *38*, 6181–6188. https://doi.org/10.1021/ma047691u

Stadermann, M., Sherlock, S. P., In, J. Bin, Fornasiero, F., Park, H. G., Artyukhin, A. B., Wang, Y., De Yoreo, J. J., Grigoropoulos, C. P., Bakajin, O., Chernov, A. A., & Noy, A. (2009). Mechanism and kinetics of growth termination in controlled chemical vapor deposition growth of multiwall carbon nanotube arrays. *Nano Letters*, *9*(2), 738–744. https://doi.org/10.1021/n1803277g

Stetter, A., Vancea, J., & Back, C. H. (2010). Conductivity of multiwall carbon nanotubes: Role of multiple shells and defects. *Physical Review B*, *82*(11), 115451.

Su, M., Zheng, B., & Liu, J. (2000). A scalable CVD method for the synthesis of single-walled carbon nanotubes with high catalyst productivity. *Chemical Physics Letters*, *322*(5), 321–326. https://doi.org/10.1016/S0009-2614(00)00422-X

Sumpter, B. G., Huang, J., Meunier, V., Romo-Herrera, J. M., Cruz-Silva, E., Terrones, H., & Terrones, M. (2009). A theoretical and experimental study on manipulating the structure and properties of carbon nanotubes using substitutional dopants. *International Journal of Quantum Chemistry*, *109*(1), 97–118. https://doi.org/10.1002/qua.21893

Sundaram, R. M., & Windle, A. H. (2017). One-step purification of direct-spun CNT fibers by post-production sonication. *Materials and Design*, *126*, 85–90. https://doi.org/10.1016/j.matdes.2017.04.011

Suriani, A. B., Asli, N. A., Salina, M., Mamat, M. H., Aziz, A. A., Falina, A. N., Maryam, M., Shamsudin, M. S., Md Nor, R., Abdullah, S., & Rusop, M. (2013). Effect of Iron and Cobalt Catalysts on The Growth of Carbon Nanotubes from Palm Oil Precursor. *IOP Conference Series: Materials Science and Engineering*, *46*(012014), 1–6. https://doi.org/10.1088/1757-899X/46/1/012014

Sze, S. M., & Ng, K. K. (2006). *Physics of semiconductor devices*. John wiley & sons.

Ta, B. Q., Haugen, T. B., Hoivik, N., Halvorsen, E., & Aasmundtveit, K. E. (2013). Local synthesis of carbon nanotubes in silicon microsystems: The effect of temperature distribution on growth structure. *Materials*, *6*(8), 3160–3170. https://doi.org/10.3390/ma6083160

Takizawa, M., Bandow, S., Yudasaka, M., Ando, Y., Shimoyama, H., & Iijima, S. (2000). Change of tube diameter distribution of single-wall carbon nanotubes induced by changing the bimetallic ratio of Ni and Y catalysts. *Chemical Physics Letters*, *326*(3–4), 351–357. https://doi.org/10.1016/S0009-2614(00)00817-4

Tang, Z. K., Zhang, L., Wang, N., Zhang, X. X., Wen, G. H., Li, G. D., Wang, J. N., Chan, C. T., & Sheng, P. (2001). *Superconductivity in 4 Angstrom Single-Walled Carbon Nanotubes* (Vol. 292).

Tans, S. J., Verschueren, A. R. M., & Dekker, C. (1998). Room-temperature transistor based on a single carbon nanotube. *Nature*, *393*, 669–672.

Tripathi, P., Durbach, S., & Coville, N. (2017). Synthesis of Multi-Walled Carbon Nanotubes from Plastic Waste Using a Stainless-Steel CVD Reactor as Catalyst. *Nanomaterials*, *7*(10), 1–17. https://doi.org/10.3390/nano7100284

Tsentalovich, D. E., Headrick, R. J., Mirri, F., Hao, J., Behabtu, N., Colin, C., Young, C. C., & Pasquali, M. (2017). Influence of Carbon Nanotube Characteristics on Macroscopic Fiber Properties. *ACS Applied Materials & Interfaces*, *9*(41), 36189–36198. https://doi.org/10.1021/acsami.7b10968

Tuinstra, F., & Koenig, J. L. (1970). Raman Spectrum of Graphite. *The Journal of Chemical Physics*, *53*(3), 1126–1130. https://doi.org/10.1063/1.1674108

Vanyorek, L., Loche, D., Katona, H., Casula, M. F., Corrias, A., Kónya, Z., Kukovecz, Á., & Kiricsi, I. (2011). Optimization of the Catalytic Chemical Vapor Deposition Synthesis of Multiwall Carbon Nanotubes on FeCo(Ni)/SiO 2 Aerogel Catalysts by Statistical Design of Experiments. *The Journal of Physical Chemistry C*, *115*(13), 5894–5902. https://doi.org/10.1021/jp111860x

Venezuela, P., Lazzeri, M., & Mauri, F. (2011). Theory of double-resonant Raman spectra in graphene: Intensity and line shape of defect-induced and two-phonon bands. *Physical Review B - Condensed Matter and Materials Physics*, *84*(3), 1–28. https://doi.org/10.1103/PhysRevB.84.035433

Vida-simiti, I., Cluj-napoca, U. T., Chicinas, I., Cluj-napoca, U. T., Batin, G., & Cluj-napoca, U. T. (2004). Applications of scanning electron microscopy (SEM) in nanotechnology and nanoscience. *Romanian Journal Physics*, *49*(9), 955–965.

Vigolo, B., Penicaud, A., Coulon, C., Sauder, C., Pailler, R., Journet, C., Bernier, P., & Poulin, P. (2000). Macroscopic Fibers and Ribbons of Oriented Carbon Nanotubes. *Science*, *290*(5495), 1331–1334.

Walsh, K., Spazzoli, R., Du Bois, T., Filby, S., & Reeders, C. (2019). *Cost Benefit Analysis of technology-neutral regulations to introduce minimum energy performance standards for general lighting*.

Wang, A. (2014). *Spinning Methods for Carbon Nanotube Fibers*. University of Cincinnati.

Wang, J. L., Gu, M., Zhang, X., & Song, Y. (2009). Thermal conductivity measurement of an individual fibre using a T type probe method. *Journal of Physics D: Applied Physics*, *42*(10), 1–7. https://doi.org/10.1088/0022-3727/42/10/105502

Wang, W. F., Cheng, K. Y., Wu, M. C., & Hsieh, K. C. (2018). Analyses of current-voltage characteristics using derivative methodology. *Solid-State Electronics*, *149*, 15–22. https://doi.org/10.1016/j.sse.2018.08.002

Wasel, W., Kuwana, K., Reilly, P. T. A., & Saito, K. (2007). Experimental characterization of the role of hydrogen in CVD synthesis of MWCNTs. *Carbon*, *45*(4), 833–838. https://doi.org/10.1016/j.carbon.2006.11.013

Wei, Chen, Q., Peng, L.-M., Cui, R., & Li, Y. (2009). Tensile Loading of Double-Walled and Triple-Walled Carbon Nanotubes and their Mechanical Properties. *The Journal of Physical Chemistry C*, *113*(39), 17002–17005. https://doi.org/10.1021/jp902471q

Wei, J. Q., Sun, J. L., Wu, D. H., Guo, J. H., Luo, J. Bin, Wang, K. L., Jin-Quan, W., Jia-Lin, S., De-Hai, W., Ji-Hua, G., Jian-Bin, L., & Kun-Lin, W. (2006). Properties of the incandescent light emitted from double-walled carbon nanotube filament. *Chinese Physics*, *15*(11), 2731–2734. https://doi.org/10.1088/1009-1963/15/11/045

Wei, J., Zhu, H., Wu, D., & Wei, B. (2004). Carbon nanotube filaments in household light bulbs.

Applied Physics Letters, *84*(24), 4869–4871. https://doi.org/10.1063/1.1762697

Wei, X., Wang, M. S., Bando, Y., & Golberg, D. (2011). Thermal stability of carbon nanotubes probed by anchored tungsten nanoparticles. *Science and Technology of Advanced Materials*, *12*(4), 0–6. https://doi.org/10.1088/1468-6996/12/4/044605

Wert, C. A. (1950). Diffusion coefficient of C in α-iron. *Physical Review*, *79*(4), 601–605. https://doi.org/10.1103/PhysRev.79.601

Widagdo, S. (2006). Incandescent light bulb: Product design and innovation. *Industrial and Engineering Chemistry Research*, *45*(25), 8231–8233. https://doi.org/10.1021/ie060391b

Wirth, C. T., Zhang, C., Zhong, G., Hofmann, S., & Robertson, J. (2009). Diffusion- and Reaction-Limited Growth of Carbon Nanotube Forests. *ACS Nano*, *3*(11), 3560–3566. https://doi.org/10.1021/nn900613e

Wood, R. F., Pannala, S., Wells, J. C., Puretzky, A. A., & Geohegan, D. B. (2007). Simple model of the interrelation between single- and multiwall carbon nanotube growth rates for the CVD process. *Physical Review B - Condensed Matter and Materials Physics*, *75*(23), 1–8. https://doi.org/10.1103/PhysRevB.75.235446

Wortmann, T., & Fatikow, S. (2009). Carbon Nanotube Detection by Scanning Electron Microscopy. *MVA2009 IAPR Conference on Machine Vision Applications*, 370–373.

Xia, W., Su, D., Birkner, A., Ruppel, L., Wang, Y., Wöll, C., Qian, J., Liang, C., Marginean, G., Brandl, W., & Muhler, M. (2005). Chemical vapor deposition and synthesis on carbon nanofibers: Sintering of ferrocene-derived supported iron nanoparticles and the catalytic growth of secondary carbon nanofibers. *Chemistry of Materials*, *17*(23), 5737–5742.

https://doi.org/10.1021/cm051623k

Xu, Y., Ma, Y., Liu, Y., Feng, S., He, D., Haghi-Ashtiani, P., Dichiara, A., Zimmer, L., & Bai, J. (2018). Evolution of Nanoparticles in the Gas Phase during the Floating Chemical Vapor Deposition Synthesis of Carbon Nanotubes. *Journal of Physical Chemistry C*, *122*(11), 6437–6446. https://doi.org/10.1021/acs.jpcc.8b00451

Yadav, M. D., Patwardhan, A. W., Joshi, J. B., & Dasgupta, K. (2019). Kinetic study of multi-walled carbon nanotube synthesis by thermocatalytic decomposition of methane using floating catalyst chemical vapour deposition. *Chemical Engineering Journal*, *377*, 1–9. https://doi.org/10.1016/j.cej.2018.09.056

Yeong, K. S., & Thong, J. T. L. (2004). Effects of adsorbates on the field emission current from carbon nanotubes. *Applied Surface Science*, *233*, 20–23. https://doi.org/10.1016/j.apsusc.2004.03.222

Yu, M.-F., Lourie, O., Dyer, M. J., Moloni, K., Kelly, T. F., & Rouff, R. S. (2013). Strenght and Breaking Mechanism of Multiwalled Carbon Nanotubes Under Tensile Load. *Science*, *287*(January), 637–640. https://doi.org/10.1126/science.287 .5453.637

Yu, Zhixin, Chen, D., Tøtdal, B., Zhao, T., Dai, Y., Yuan, W., & Holmen, A. (2005). Catalytic engineering of carbon nanotube production. *Applied Catalysis A: General*, *279*(1–2), 223–233. https://doi.org/10.1016/j.apcata.2004.10.032

Yu, Zhonghua, & Brus, L. (2001). Rayleigh and Raman scattering from individual carbon nanotube bundles. *Journal of Physical Chemistry B*, *105*(6), 1123–1134. https://doi.org/10.1021/jp003081u

Zeng, Q., Li, Z., & Zhou, Y. (2006). Synthesis and Application of Carbon Nanotubes. *Journal of Natural Gas Chemistry*, *15*(3), 235–246. https://doi.org/10.1016/S1003-9953(06)60032-7

Zhang, M., Atkinson, K., & Baughman, R. H. (2004). Multifunctional Carbon Nanotube Yarns by Downsizing an Ancient Technology. *Science*, *306*(5700), 1358–1361. https://doi.org/10.1126/science.1104276

Zhang, M., Fang, S., Zakhidov, A. A., Lee, S. B., Aliev, A. E., Williams, C. D., Atkinson, K. R., & Baughman, R. H. (2005). Materials science: Strong, transparent, multifunctional, carbon nanotube sheets. *Science*, *309*(5738), 1215–1219. https://doi.org/10.1126/science.1115311

Zhang, S., Koziol, K. K. K., Kinloch, I. A., & Windle, A. H. (2008). Macroscopic fibers of well-aligned carbon nanotubes by wet spinning. *Small*, *4*(8), 1217–1222. https://doi.org/10.1002/smll.200700998

Zhang, S., & Kumar, S. (2008). Carbon nanotubes as liquid crystals. *Small*, *4*(9), 1270–1283. https://doi.org/10.1002/smll.200700082

Zhang, Wang, D.-G., Huang, J.-Q., Zhou, W.-P., Luo, G.-H., Qian, W.-Z., & Wei, F. (2010). Dry spinning yarns from vertically aligned carbon nanotube arrays produced by an improved floating catalyst chemical vapor deposition method. *Carbon*, *48*(10), 2855–2861. https://doi.org/10.1016/j.carbon.2010.04.017

Zhang, X., Jiang, K., Feng, C., Liu, P., Zhang, L., Kong, J., Zhang, T., Li, Q., & Fan, S. (2006). Spinning and Processing Continuous Yarns from 4-Inch Wafer Scale Super-Aligned Carbon Nanotube Arrays. *Advanced Materials*, *18*(12), 1505–1510. https://doi.org/10.1002/adma.200502528

Zhang, Xiefei, Li, Q., Tu, Y., Li, Y., Coulter, J. Y., Zheng, L., Zhao, Y., Jia, Q., Peterson, D. E., & Zhu, Y. (2007). Strong carbon-nanotube fibers spun from long carbon-nanotube arrays. *Small*, *3*(2), 244–248. https://doi.org/10.1002/smll.200600368

Zhang, Y., Zou, G., Doorn, S. K., Htoon, H., Stan, L., Hawley, M. E., Sheehan, C. J., Zhu, Y., & Jia, Q. (2009). Tailoring the Morphology of Carbon Nanotube Arrays: From Spinnable Forests to Undulating Foams. *ACS Nano*, *3*(8), 2157–2162. https://doi.org/10.1021/nn9003988

Zhao, X., & Shin, Y. C. (2013). Femtosecond laser ablation of aluminum in vacuum and air at high laser intensity. *Applied Surface Science*, *283*, 94–99.

Zhao, Y., Wei, J., Vajtai, R., Ajayan, P. M., & Barrera, E. V. (2011). Iodine doped carbon nanotube cables exceeding specific electrical conductivity of metals. *Scientific Reports*, *1*(c), 1–5. https://doi.org/10.1038/srep00083

Zhao, Z. G., Li, F., Liu, C., & Cheng, H. M. (2005). Light emission and degradation of single-walled carbon nanotube filament. *Journal of Applied Physics*, *98*(4), 1–4. https://doi.org/10.1063/1.1996852

Zheng, B., Li, Y., & Liu, J. (2002). CVD synthesis and purification of single-walled carbon nanotubes on aerogel-supported catalyst. *Applied Physics A: Materials Science & Processing*, *74*(3), 345–348. https://doi.org/10.1007/s003390201275

Zhong, X.-H., Li, Y.-L., Liu, Y., Qiao, X., Feng, Y., Liang, J., Jin, J., Zhu, L., Hou, F., & Li, J. (2010). Continuous Multilayered Carbon Nanotube Yarns. *Advanced Materials*, *22*(6), 692–696. https://doi.org/10.1002/adma.200902943

APPENDIX

Appendix A: Materials and Methods

A1. Operation of the floating catalyst chemical vapour deposition reactor (FCCVD)

Figure A1: Floating catalyst chemical vapour deposition reactor with direct spinning set-up in operation

Loading the catalyst:

- It is ensured that the vaporizer pot is cool.
- The bolts and nuts are unscrewed and stored away. Appropriate personal protective equipment is worn.
- The vaporizer is manually cleaned out of the residual catalyst and returned CNT particles.
- The required amount of catalyst is weighed out and poured into the vaporizer.
- The lid is closed and the nuts are screwed tight.
- A picture of the vaporizer is presented in Figure A2

Figure A2: Vaporizer pot on a hotplate

Gas supply, mixing, and flow

- Rotameter flow meters with a gas mixer are shown in Figure A3…
- All gases are equipped with an in-line, single-stage pressure regulator, needle flow control valve, and shut off toggle valve.

- All gases mix and enter the reactor system through a single line.
- The mixed gas pressure is a free flow to atmospheric ~100 kpa.
- The maximum flow rate of each gas is 150 mL/min.
- The operating pressure of the reactor is atmospheric and monitored by a pressure gauge
- The desired flow of each gas is adjusted with the rotameter needle valve.

Figure A3: Control panel showing (a) pressure gauge for pressure monitoring (b) rotameter for methane gas, argon gas, and hydrogen gas channelled through to the vaporizer via a single pipe monitored by a pressure gauge.

Reaction system

- The reaction takes place in the furnace section depicted in Figure A4;
- The reactant gases are supplied to the vertical furnace from the bottom to top;
- A long pipe passes through the from furnace section into the vaporizer to the collector;

- Clean out is carried out using a flush down system.

Figure A4: Furnace section with pipe encased by tube.

Flushing the system

- The operating temperature of the furnace ranged between 800 °C – 1000 °C (maximum operating temperature of the furnace).
- Inert gas – Argon is used as a carrier gas to reduce the heat load on the reactor tube.
- Dry N_2 gas was used to flush the system to reduce the presence of O_2 and avoid the explosion from O_2/H_2 interaction as argon gas is expensive.

- Although the reactor is open at one end, the system is equipped with cyclones containing soapy water to dissolve gases and reduce the possibility of the presence of O_2 in the system after flushing.
- The gas sensor is installed and ensured to be properly working.
- Figure A5 shows the picture of cyclones

Figure A5: Cyclone system of FCCVD

Assembly and disassembly of the reactor

- Collecting synthesis products requires the dissembling of the upper part of the reactor system shown in Figure A6
- Screws and bolts are unscrewed and the cover removed and kept in a box;
- The spindle is extracted and the CNT yarn collected;
- CNT is further collected from the wall of the stainless steel pipe above the furnace;
- The wall is cleaned out through the furnace and down into the vaporizer and collected
- The spindle is replaced and the bolt replaced
- The top is replaced and the bolts and nuts are replaced and screwed tight in place.
- Nitrogen is passed to ensure no leakages and blockages.

Figure A6: Upper part of FCCVD reactor set up

Table A1: HAZOP performed for the FCCVD reactor system.

	Guide Word	**Deviation**	**Cause**	**Consequences**	**Action Required**
Vaporizer	No	No heating	- Hotplate was not turned on	- Poor catalyst supply	- Ensure hotplate is on and increase heating rate
	Low	The low temperature in the vaporizer	- No proper contact of hotplate with the vaporizer - Faulty thermocouple	- Poor quality of catalyst supplied	- Establish contact between hotplate and vaporizer pot - Use another thermocouple
	High	The high temperature in the vaporizer	- The high heating rate of the hotplate	- Incorrect synthesis conditions	- Monitor hot plate
	No	No catalyst	- No catalyst in the vaporizer	- No product yield	- Supply catalyst to the vaporizer

			- Blockage at the swirled section		- Unblock swirled section
Reactor	No	No flowrate of methane	- Gas exhausted - Gas valve not open	- CNT yield only from the carbon in ferrocene, thus low yield	- Ensure gas availability - Ensure gas flow indicated on the flowmeter
		No flowrate of Argon	- Gas exhausted - Gas valve not open	- Flame in reactor - Poor quality product	- Ensure gas availability - Ensure gas flow indicated on the flowmeter
		No heating	- Spoilt heating coil - Poor contact	- No reaction	- Replace the heating coil in the furnace - Check for proper contact

	More of	The high flow rate of gases	- Flowmeter speed too high	- Incorrect reaction conditions	- Ensure proper settings of the flow meter
	High	The high temperature in the reactor	- Overheating reactor	- Incorrect synthesis condition	- Ensure the correct setting of thermocouple
Cyclone System	No	Malfunction	- A build-up of CNT in cyclone	- Pressure build-up - Blocked reactor exit	- Clean cyclone - Drain cyclone

Appendix B: Calibration of GC

The calibration of GC for CH_4 and H_2 was carried out by external method within the explosion limits. Various standardized concentrations in a thermal conductivity detector (TCD) of the GC. The standard gas used was comprised of 60% methane, 10% hydrogen, and 30% carbon dioxide. A quantitative relationship between methane content and the area of the peak is proportional. Standard gas was diluted stepwise in nitrogen gas for preparation of 0.4%, 1.0%, 2.0%, 4.0%, 8.0% and 10.0%. 10 mL of prepared gas samples were injected slowly into GC equipped with the Hayesep Q column. Nitrogen gas (99.998%) was used as the carrier gas. Initial temperature, oven temperature TCD temperature were maintained at 35 °C, 80 °C, and 250 °C respectively with a ramp rate of 20 °C/min. The equivalent contents (EC) of gases in the diverse concentrations of standard gas injected into the GC are obtained as in Equations B1 – B3.

$$EC = \frac{10\ ml * Conc\ \%}{60\%}$$ for methane B1

$$EC = \frac{10\ ml * Conc\ \%}{10\%}$$ for hydrogen B2

$$EC = \frac{10\ ml * Conc\ \%}{30\%}$$ for carbon dioxide B3

The chromatography of standard gas (Figure B1) shows peaks for Hydrogen, methane, and carbon dioxide with a retention time of 1.34, 7.16, and 19.17 min respectively.

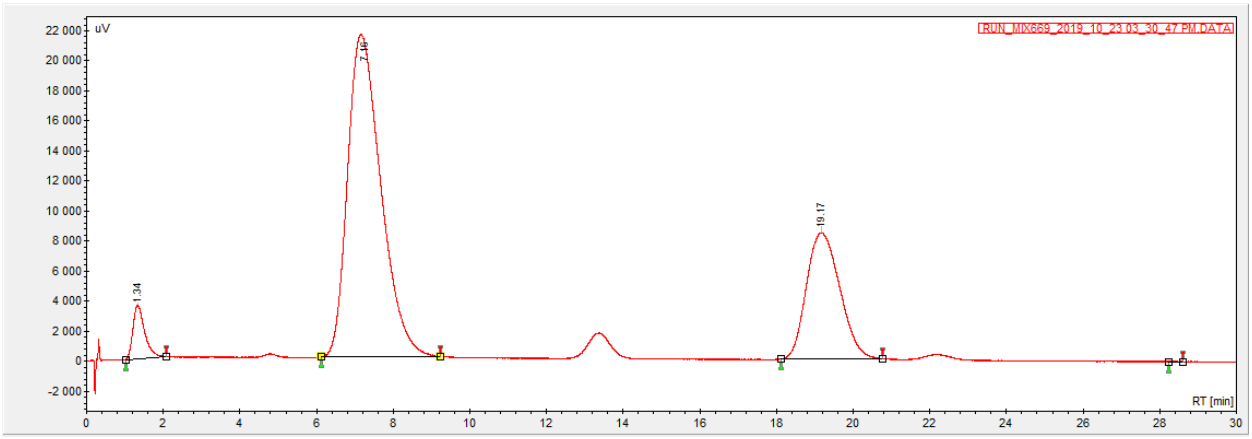

Figure B1: Chromatograph of standard gas.

The quantitative relationships between compositions for each component and the corresponding peak areas obtained from the GC analysis are expressed in the calibration equations presented in Table B1.

Table B1 GC calibration equations

Component	Calibration Equation	R-squared
Methane	y = 93.8535x - 10.8845	0.9928
Hydrogen	y = 1.0659x + 14.9065	0.9916

Carbon dioxide	y = 0.1447x + 7.6919	0.9801

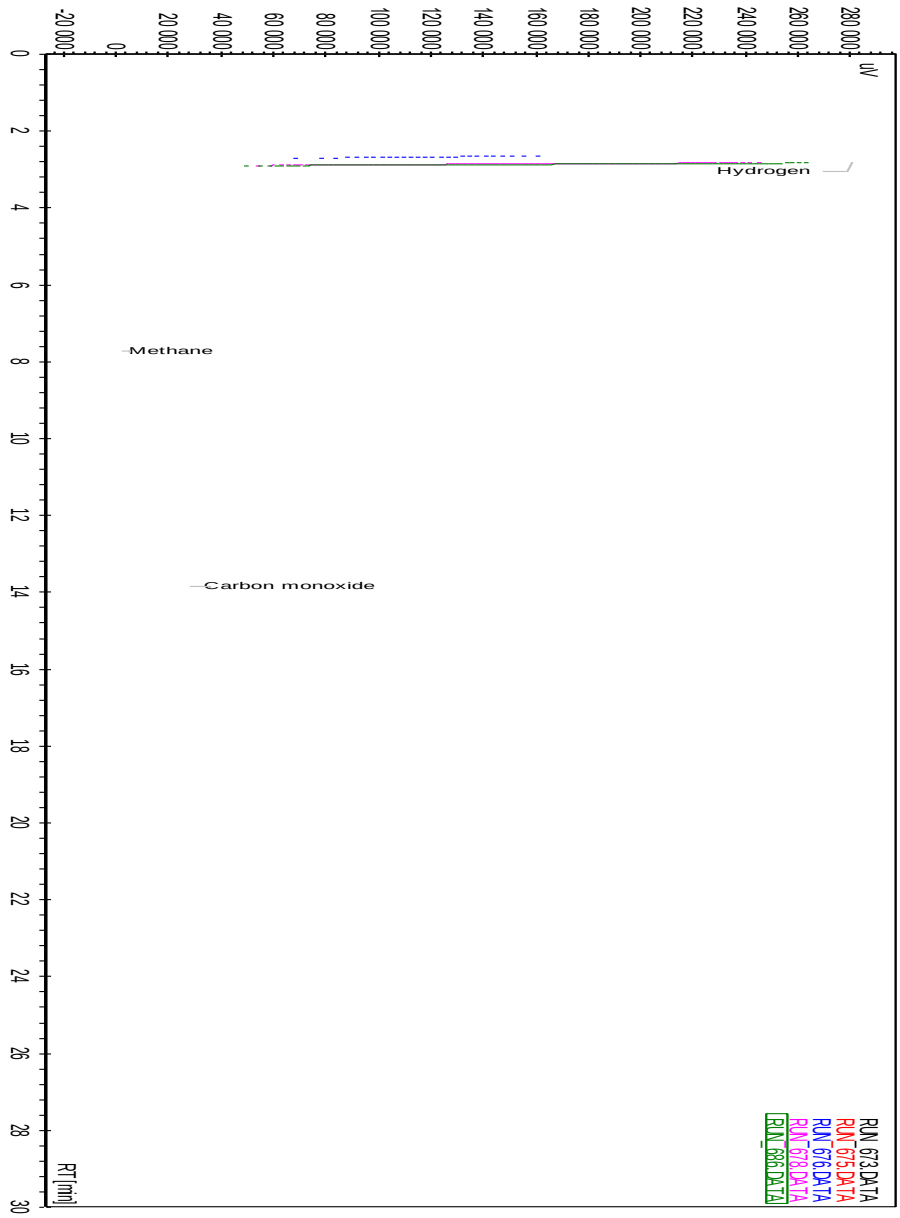

Figure B2 Integrated TCD analysis of the representative results obtain at various flow rates of methane in the FCCVD synthesis of CNT.

The results presented from specific runs for the methane flow rates. The integration tool provides the exit time of each component from the column – retention time [min]; volume percentage of an absolute measure of exit gas – the amount [%]; area occupied by component's peak – area [uV/min]. The value of exit gas of each component was determined from the area of the peak.

Table A 2: Summary of integrated data from GC for each flow rate

Methane flow rate, mL/min	**Gases**	**Retention time [min]**	**Amount [%]**	**Area, [uV/min]**
20	Hydrogen	2.42	86.23	19366.1
	Methane	7.66	5.45	1224.4
40	Hydrogen	2.54	95.51	56424.6
	Methane	7.68	1.19	701.2
60	Hydrogen	2.57	96.24	82662.7
	Methane	7.60	0.68	586.3
100	Hydrogen	2.77	95.27	129693.3
	Methane	7.69	0.18	250.5
140	Hydrogen	2.79	89.99	137344.2
	Methane	7.72	0.11	163.4

Appendix C: Copy of Publications from this Thesis

Results in Physics 15 (2019) 102705

Contents lists available at ScienceDirect

Results in Physics

journal homepage: www.elsevier.com/locate/rinp

Production of carbon nanotube yarns via floating catalyst chemical vapor deposition: Effect of synthesis temperature on electrical conductivity

E.C. Igbokwe, M.O. Daramola*, S.E. Iyuke

School of Chemical and Metallurgical Engineering, Faculty of Engineering and the Built Environment, University of the Witwatersrand, Wits 2050 Johannesburg, South Africa

ARTICLE INFO

Keywords:
CNT yarns
Temperature
CNTs
Incandescent bulbs
Physicochemical properties

ABSTRACT

Effect of synthesis temperature on the structure, morphology and crystallinity of as-synthesized CNT yarns via direct spinning was studied using Raman spectroscopy, x-ray powder diffraction (XRD) and thermogravimetric analysis (TGA). Effects of synthesis temperature on purity, morphology and thermal stability were related to the conductivity of the CNT yarns. It was observed that increase in synthesis temperature increased the sp^2 content of the as-synthesized carbon nanotubes yarns as indicated by the decrease in I_D/I_G ratio and increase in oxidation temperature. Current-Voltage (I-V) relationship for the CNT yarns synthesized at 1000 °C indicates an increase in resistivity with increased applied voltage, indicating promising potential of the produced yarns as filaments for incandescent bulbs.

Introduction

Extraordinary properties exhibited by carbon nanotubes, made up of one or more graphene sheets rolled up into concentric seamless cylinder [1], have intensified interest of researchers to explore the material in a wide range of applications [2]. The properties of CNTs such as electrical and thermal conductivity; mechanical strength; and chemical stability are controlled by the morphology (e.g. length, diameter, number of walls) and arrangements of carbon on the graphene sheets [3]. To date, large scale production of CNTs yarns with specific properties for processing into their macroscopic level with properties comparable to the individual CNT for effective application is still a challenge, and multiple post-treatment steps could be required to achieve this [4].

However, floating catalyst chemical vapour deposition (FC-CVD), one of the methods to synthesize carbon nanotube is the most scalable technique at viable production cost. FC-CVD is widely used in the industry for continuous production of CNTs with the catalyst and hydrocarbon introduced into the furnace synchronously [5,6]. Thermal decomposition of metallocene e.g. ferrocene or nickelocene forms supersaturated metallic vapour and subsequently facilitates the formation of metal nanoparticles in the reactor [7–9]. Very little catalyst deactivation occurs in this method since both hydrocarbon and catalyst are introduced at the same time. In addition, post synthesis treatment is not required with this method as there are no substrates involved. Consequently, production of yarn in this study employed the use of FCCVD reactor equipped with spinning device. In addition ferrocene was used as catalyst because of its stability, non-toxicity and low-cost [8].

Formation of macroscopic CNT is attributed to the van der Waals attractions existing between the forming CNTs [10]. Factors influencing the morphology and quality of CNTs are carbon source, catalyst type, synthesis temperature, flow rates of carbon source and the carrier gases and the composition of carrier gases [11]. Complexities stemming from the convergence of many parameters influencing the physical and chemical properties, orientation and building blocks interactions of individual CNTs in the bulk, result in fundamental difficulties in determining the influence of each factor on the various parameters [12–15]. Normally, transmission electron microscopy (TEM) is used to verify formation of CNT yarns in the as-synthesized sample thus size, morphology, and defects for individual nanotubes could be determined by TEM imaging. Statistically, TEM is not an adequate representation of the properties of samples as it works in very high magnification and presents single nanoscale object. Powder XRD gives an average description of the atomic structure of the sample set. Complete and quantitative analysis of bulk CNT materials consisting of crystallites, particles, and domains can be carried out by XRD. Although carbon nanotubes are generally not referred to as crystalline materials, they scatter X-ray at specific angles making their structural information to be captured using the atomic pair distribution function (PDF) [16,17].

* Corresponding author.
E-mail address: Michael.Daramola@wits.ac.za (M.O. Daramola).

https://doi.org/10.1016/j.rinp.2019.102705
Received 23 July 2019; Received in revised form 14 September 2019; Accepted 25 September 2019
Available online 28 September 2019

Raman spectroscopy is a simple, non-destructive technique for characterization of CNTs as it gives information on the crystal structure at molecular level [18–20]. However, it is more sensitive to morphological changes at the molecular level than electron microscopy and XRD [21]. Raman spectra of highly uniform carbon structures consist of two features: the tangential in-plane stretching vibration of C-C bonds, G-band located at about 1580 cm^{-1} in the first order and 2D-band at between 2600 cm^{-1} and 2700 cm^{-1}in the second order [22]. The D-band found in the first order is known as structural disorder band indicates the presence of irregularities in the structure is found at about 1350 cm^{-1} [23]. In multi-walled carbon nanotubes (MWCNT) the excitation of the D-band can sometimes be attributed to the variability or complexity of the structure and not necessarily defects. The relative intensities of G and 2D-bands point to layer numbers [24] – the higher the 2D band, the lower the layer number. The radial breathing mode (RBM) is detected, in the first order, at about 150 cm^{-1} − 350 cm^{-1} in SWCNT and MWCNT with innermost diameter of 1–2 nm [25].

In this study, as-synthesized CNT yarns were obtained at synthesis temperature of 800 °C, 900 °C and 1000 °C, annotated as CNT-800, CNT-900 and CNT-1000, respectively. Raman, XRD and TGA techniques were used to analyze the samples. Information gleaned from the morphology, purity and crystallinity of the samples were used to decipher the effect synthesis temperature on electrical properties of the samples towards the application of yarns as filaments in incandescent bulbs. Measurement of the electrical conductivity of as-produced CNT yarns was taken for confirmation.

Experimental

Materials and synthesis of CNT yarn

Argon gas (99.999%), hydrogen (99.9%) and methane gas (99%) were supplied by Afrox (South Africa). Ferrocene (98%) was acquired from Sigma Aldrich (South Africa). No alterations were made to the materials. They were used as supplied.

An upward flow vertical swirling floating catalyst chemical vapour deposition (FCCVD) reactor was employed in the synthesis of the yarns (see Fig. 1 for the schematic of the FCCVD reactor used). It consists of a 650 mm long stainless steel tube with 450 mm of it encased in a furnace. The lower end of the tube is inserted into a vapourizer separated by a swirled mixer section and the other end to the motor controlled spinning spindle, cyclones and exhaust. Temperature controller and PT-100 thermocouples are used to regulate and monitor the temperatures in the vaporizer and furnace tube respectively. Gases from the gas lines are passed to the furnace through the vapourizer where it picks up ferrocene catalyst vapour. The CNT aerosol formed in the furnace, was carried past the furnace and spun onto the rotating spindle.

During the synthesis of the CNT yarns, Ferrocene was first introduced into the vapourizer section of the FCCVD. Nitrogen gas was passed through the reactor to create an inert environment and check for leaks. The vapourizer was heated with a hot plate and the temperature monitored. The furnace set value was programmed to desired temperature and allowed to ramp and hold at that temperature. Pre-determined flow rates of gases were passed from the gas lines into the heated vapourizer where ferrocene was carried alongside the gases into the furnace through the swirled mixer maintained at a temperature of 250 °C by a heating tape to avoid recrystallization. The gas flow rates were controlled and monitored by rotameters. The direct spinning of the yarn was carried out on the spindle controlled by the motor at 50 rpm spin rates. The reaction was continued until the ferrocene in the vapourizer was exhausted. The system was allowed to cool and the spun yarns were collected from the spindle.

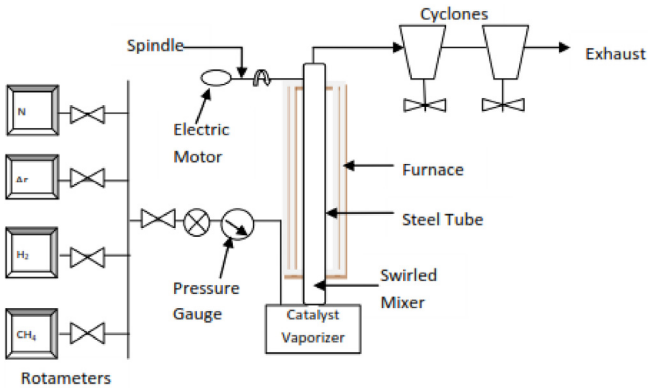

Fig. 1. Schematic of floating catalyst chemical vapour deposition FCCVD reactor.

The flow rates of methane, argon and hydrogen were kept constant at 100 ml/min, 100 ml/min and 75 ml/min, respectively, and the temperature was varied from 800 to 1000 °C at a step change of 100 °C.

Characterization of the as-synthesized CNT yarns

Bruker XRD D2 Phaser was used to investigate the change in the crystallinity of CNT yarns due to change in synthesis temperature. The XRD pattern of as-produced CNT yarns was generated by the Cu-Kα radiation source with wavelength λ = 1.5406 Å. DIFFRAC.EVA software was used to match the Miller indices (*hkl*). The structure of the as-synthesized carbon nanotube yarns was examined by a Raman spectrometer (Jobin Yvon T64000) equipped with an Ar ion laser (514.5 nm) with very low laser power (0.04 mW) to avoid localized heating. Raman spectroscopy is a non-destructive method of analysis, sensitive to both crystalline and molecular structure commonly used in characterization of carbon materials [18,19].

Thermogravimetric analysis of the as-synthesized yarns was carried out under 25 ml/min air gas flow using a thermogravimetric analyzer (model SDT Q600). For each analytical run, approximately 5 mg of sample was placed in an aluminum crucible and loaded into the instrument. A second crucible was also placed in empty to serve as reference. The loaded sample was heated from ambient temperature to 900 °C at a heating rate of 10 °C/min. An increase in weight is observed in all the samples prior to a sharp decrease following the on-set of oxidation.

A scanning electron microscope (SEM) and transmission electron microscope (TEM) were employed to investigate the purity and morphology of the as-produced carbon nanotubes. SEM samples were prepared by mounting small amount of as-synthesized CNT yarns onto a carbon tape stuck on an aluminum stub. The samples were then coated with double layers of 10 nm 60/40 gold/palladium in a Sputtercoater (EmiTech K550X Sputtercoater) and viewed in an in a scanning electron microscope (FEI Nova600 FIB-SEM) operated at 30 kV. TEM analysis of the as-synthesized CNT yarn samples was carried out using a transmission electron microscope (FEI Tecnai T12 TEM) operated at 120 kV. Samples were prepared for TEM analysis by placing a little sample into a vile, adding 5 ml methanol and sonicated until well dispersed. Using a pipette, samples were retrieved and a drop was placed on the copper grid. It was allowed to dry before transferring it onto the sample holder and subsequently loaded into the instrument by inserting the sample holder.

Electrical conductivity of the as-synthesized CNT yarns was obtained using a high field cryogen free measurement system (Cryogenic Ltd) relating to a two-probe method test at room temperature. Small amount of sample containing nanoyarns was pressed to form a tin film mat covering 5 mm × 5 mm surface on the sample holder, was mounted using a nonconductive double sided tape. Contact between the sample holder and the yarn was made by applying conductive silver paint from the four corners of the thin film onto the sample holder. After the paint dried, sample holder was mounted and a two-point probe was used to take measurements at room temperature. Measurements at various

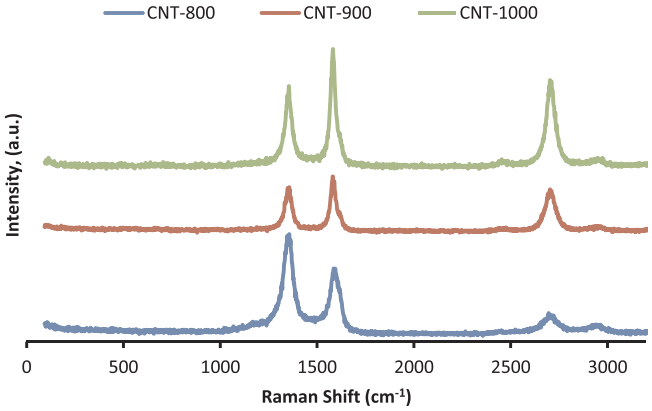

Fig. 2. Raman spectra of the as-synthesized and spun carbon nanotube yarns.

voltages were taken between −0.1 V to 0.1 V and −2 V to 2 V with 5 μV steps passing through the sample in each measurement.

Results and discussion

Effect of temperature on purity of the as-synthesized CNT yarns

The Raman spectra for the as-synthesized carbon nanotube yarns at temperatures 800 °C, 900 °C and 1000 °C shown in Fig. 2 are similar with the prominence of D and G bands at about 1350 cm^{-1} and 1580 cm^{-1} respectively in the first order region. The second orders region between 2200 cm^{-1} and 3500 cm^{-1} consist of broad and asymmetric 2D band at near 2730 cm^{-1}.

I_D/I_G ratios of as-synthesized and spun MWCNT yarns are presented in Table 1. The I_D/I_G ratio indicates the ratio of presence of disordered amorphous carbon to the graphitic carbon atoms disorder [18]. It is seen to decrease with increase in synthesis temperature. It is a measure of graphitization. Decrease in I_D/I_G ratio could be as a result of an increase in the number of sp^2 bonds or increase in the size of its clusters [26]. Increase in the intensity of the 2D band, with an increase in synthesis temperature in this case, confirms the decrease of I_D/I_G ratio with increase in temperature is due to an increase in the number of sp^2 bonds [27]. Electrical properties of CNT such as electron transport and field emissions improve with increase in sp^2 bonds [28].

Analysis of the obtained Raman spectroscopy graphs shows CNT-1000 has the sharpest d-band peak of the three spectra with CNT-800 having the broadest base of the band. CNT-1000 is judged the purest sample due to the highest intensity of the 2D-band peak. The 2D band is measures purity and quality of MWCNT more accurately than I_D/I_G ratio given that the 2D-band results from a coupling effect for two-phonon process, which impurity would otherwise hinder [22]. Analysis of XRD pattern of samples indicates the as-synthesized carbon materials for all synthesis temperatures are graphite-like with the interplanar distance limit d_{002} = 0.344 nm due to the maintenance of the sp^3 hybridization structure by bonding with hydrogen in filamentous carbon synthesized from methane [29,30]. Therefore, synthesis temperature is seen to have no detectable effect on the degree of graphitization according to the Maire and Mering formula [29].

$$d = 3.354 + 0.086\,(1-g), \tag{1}$$

Table 1
Results from Raman and XRD analysis.

Notation	Synthesis Temperature (°C)	$FWHM_{002}$, (cm^{-1})	I_{002} (a.u.)	I_D/I_G
CNT-800	800	0.01416	221	1.447934
CNT-900	900	0.01438	348	0.82387
CNT-1000	1000	0.01787	158	0.706145

where d is interplane distance (d_{002}) in Angstroms, g is graphitization percentage.

However, using Scherrer equation, average crystalline size CNT can be determined for each sample since they have different full width at half maximum (FWHM) [31].

$$D = k\lambda/\beta\cos\theta \tag{2}$$

where D – crystalline size, k – is Scherrer constant, λ – wavelength of the x-ray, β – full width half maximum, θ – angle of reflection in radian.

According to Eq. (2), the crystal size of nanoparticles (D) is inversely proportional to full width half maximum (β) of carbon nanotubes which is seen in Table 1 to increase with increase in synthesis temperature therefore the diameter of the as-synthesized and spun CNT yarns decreases with increase in synthesis temperatures. This is confirmed by the SEM micrographs in Fig. 6. Larger diameter of CNT is seen to diminish the nanotube characteristics by increasing the defect density [32,33]. These are consistent with the electrical properties of the samples.

Effect of temperature on the morphology of the as-synthesized CNT yarns

The morphology of as-produced CNT yarns was determined using x-ray diffraction and electron microscopy. The distribution of atoms within the lattice determines the peak intensity in x-ray diffraction pattern. Cao et al. established that intensity of the (0 0 2) diffraction plane is inverse to degree of alignment of nanotubes [34].

$$V_a = \frac{A_{002}}{S_{002}} = \frac{A_{002}}{dI} \tag{3}$$

where A_{002} intensity peak area of the (0 0 2) diffraction plane from vertically aligned CNTs; S_{002} is the summation of diffraction beams and dI (I_{init} - I_{direct}) is the absorbed intensity of the direct X-ray beam.

Increase in intensity is also associated with increase in the number of walls in the CNT [35]. Increase in the number of walls is associated with increase in interplanar resistance [36]. Fig. 3 shows the value of intensity on all the diffraction peaks of carbon nanotubes found at (0 0 1), (0 0 2), (1 0 0), (0 0 4) and (1 1 0) corresponding to the atomic pair distribution function (PDF) number 00–058-1638. The (0 0 2) diffraction plane is related to the periodicity between the graphene layers and the [(1 0 0) and (1 0 1)] diffraction planes are related to the periodicity within the graphene layers [37]. They are located at 26° and 43° respectively on the 2-theta scale. The low intensity observed in the CNT-800 could be attributed to the formation of thick fibrils with low to no hollows, thereby making them straight and more aligned than CNT-900. CNT-1000 on the other hand, possesses more long straight tubes with narrower diameter giving it low intensity. These observations are supported by the images from SEM and TEM where CNT-900 is seen to be made of curled and bent nanotubes. Intensity of CNT-1000 is seen to

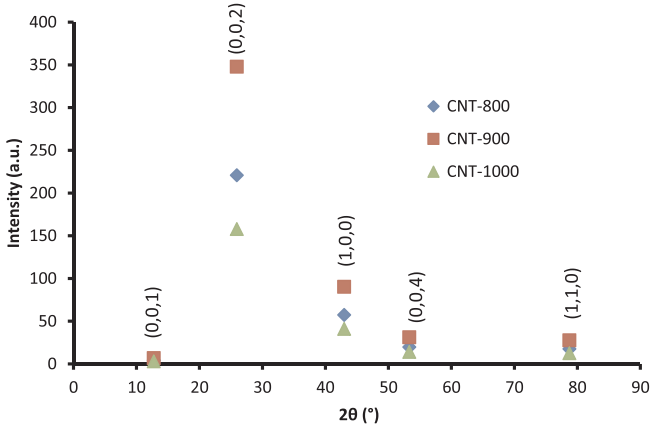

Fig. 3. XRD patterns of CNT yarns at the various hkl planes.

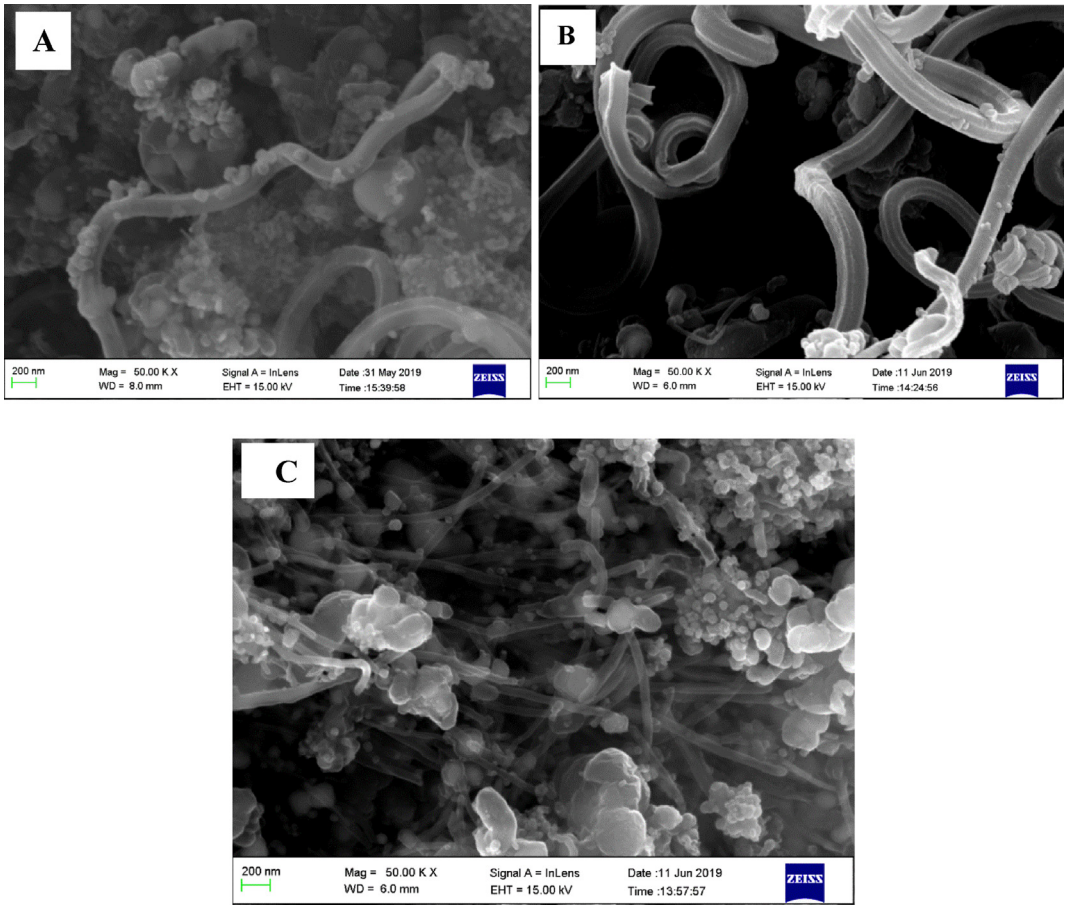

Fig. 4. SEM micrographs of as-synthesized and spun CNT yarns. A – at 800 °C; B – at 900 °C; C– at 1000 °C.

be consistently lowest in all the diffraction planes indicating CNT-1000 has the best alignment and least interplanar resistance. Electrical properties of the samples corroborate these findings with CNT-1000 having the least resistance of the three samples.

Nature of defects found in graphite could be hopping defects caused by deformation on the carbon bonds; on-site defects originating from bonds to other atoms thus forming sp^3 hybridization; or charged impurities initiated by charged atoms adsorbed on the surface of graphene [38]. Ó band observed at 1620 cm^{-1} is responsible for the determination of the nature of defects. It is more distinguished from the G-band in purer samples [39]. The concentration is highest in CNT-800 because it is not evident on the spectrum and most evident in CNT-1000 spectrum. The ratio of $I_D/I_Ó$ for CNT-900 and CNT-1000 were 1.241 and 1.275, respectively, indicating the defects are on-site in nature.

From the SEM micrographs in Fig. 4, it is evident that there are impurities on all the samples. CNT-800 and CNT-900 have larger diameter than CNT-1000. Theoretical and experimental findings in literature report increase in diameter of SWCNT and MWCNT with increase in synthesis temperature in line with the kinetic energy and the diffusion rate of carbon on iron catalyst increases in accordance with the kinetic theory of gases [40–42]. However this is seen to be contrary for temperatures below 1000 °C which is in line with our findings [43]. SEM micrograph also shows CNT-1000 are straight and aligned. This is in tandem with the XRD analysis and TEM micrographs in Fig. 5.

The peak present around 2450 cm^{-1} in the second order of the Raman spectra, with CNT-1000 exhibiting the highest intensity in our case, is a strong indication of the structural integrity of the nanotube [18].

There is a slight broadening of the (0 0 2) peak width in CNT-1000 which could be an indication of a slight decrease in crystallite size as

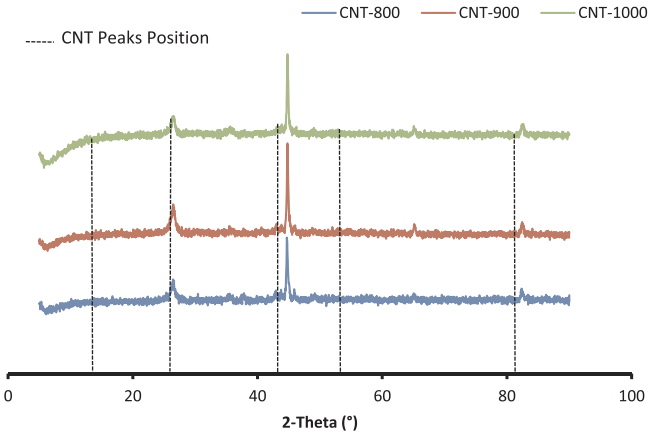

Fig. 5. The XRD spectra of the as-synthesized CNT yarns.

seen in Fig. 5. Broadening of peak width is inversely proportional to crystallite size. Therefore, CNT-1000 possesses the lowest crystallite size. Kleinsmith reports initial increase in external nanotube diameter with increase in temperature and a subsequent decrease in the diameter with further increase in temperature [44]. Decrease in crystallite size could be attributed to the lowering of partial pressure of the carbon source with increase in temperature because the CVD was not completely closed during the production. This in turn facilitates the growth of carbon nanotube on the smaller but more reactive catalyst particles [45,46]. This could perhaps explains the partial reduction in the number of nanotube walls [47] achieved as a result of synthesis temperature in this case. It can be concluded that synthesis of CNT yarns at

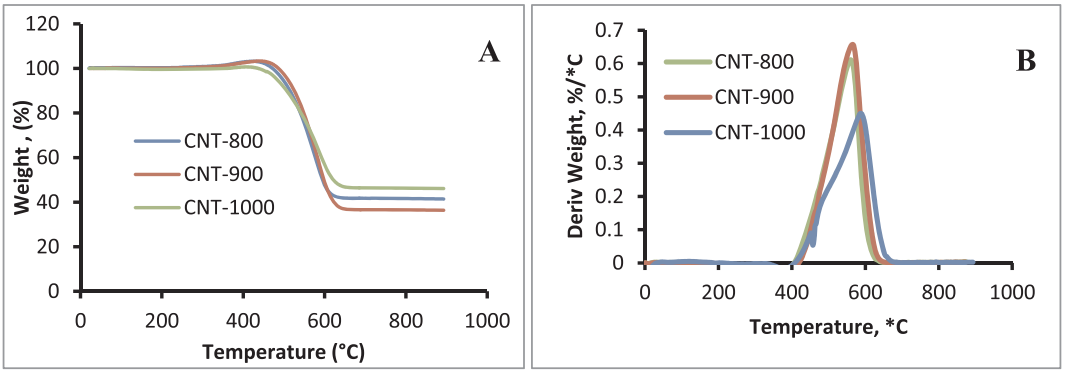

Fig. 6. (A) weight loss curves for as-synthesized carbon nanotubes in a FCCVD using ferrocene with different temperatures. (B) Derivative weight loss curve.

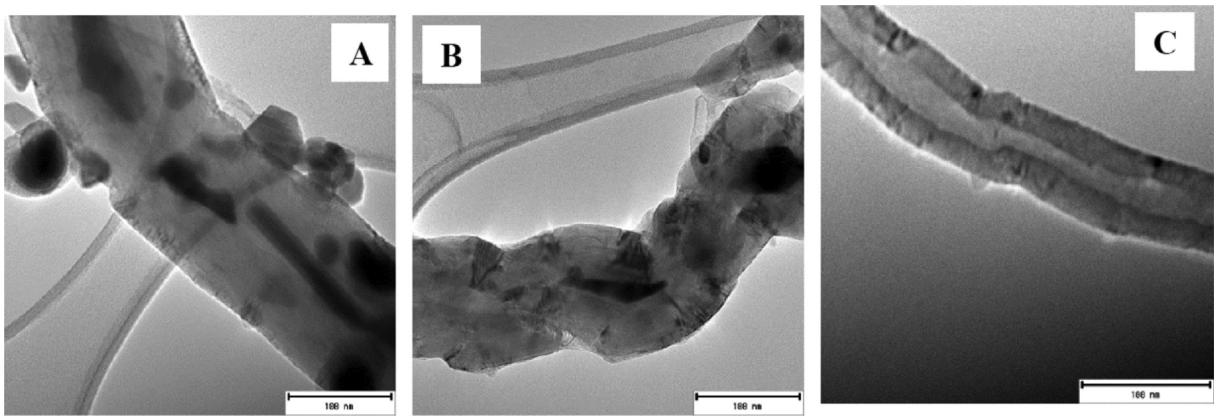

Fig. 7. TEM images of the as-synthesized CNT yarns at 800 °C (A), 900 °C (B) and 1000 °C (C).

1000 °C resulted in fewer walls. This is confirmed from the TEM micrographs presented in Fig. 7 where the tube inner diameter in CNT-1000 is wide yet the outer diameter is smallest of the three samples with XRD analysis giving the interplanar distance as equal for all samples. It should be noted that the images were captured at the highest magnification. However, the number of wall in the multi-walled CNT yarns could not be determined and the accurate distance between the walls could not be estimated as well. Notwithstanding, it is however evident the diameter decreases with increase in synthesis temperature.

The (1 0 0) peak relates to curvature of the carbon nanotubes, its helicity or twisting along the length of the nanotubes [47]. Based on the diagram in Fig. 5, there is no appreciable change with temperature therefore we can conclude that the helic angle is unchanged and there was no unzipping of the carbon nanotube into nanoribbons.

Effect of temperature on thermal decomposition of the as-synthesized CNT yarn

Thermal quality of CNT yarns was determined by the peak temperature position of the derivative mass loss curve from thermogravimetric analysis (TGA) in Fig. 6b. Lanza et al. found impurities including catalyst residues have little or no effect on the DTG peak temperature [48]. From the DTG graph in Fig. 6b, it could be observed that the curves are asymmetrical indicating the presence of impurities [49]. CNT-1000 curve is the most asymmetrical of the 3 samples which could indicate the presence of amorphous carbon on the surface of the nanotubes. Though highest oxidation temperature was still maintained as seen on the DTG curve and Table 2.

Defects on the surface of the nanotube outer walls and fringe edges provided initiation sites for oxidation reactions [50], therefore they are related to intensities from Raman spectroscopy [51]. The 2D band of Raman spectroscopy is regarded as a long-range order indicator

Table 2
Thermal and electrical properties.

Sample Notation	I_{2D}/I_G	I_{2D}/I_D	Oxidation onset temperature (°C)	Electrical conductivity (Sm^{-1})
CNT-800	0.3140	0.2130	578	0.0065
CNT-900	0.9023	0.9833	586	0.0508
CNT-1000	0.8897	1.0349	588	0.1673

responsible for the coupling effects necessary for two-phonon processes. Increase in average inter-defect distances increases the overall crystalline density in MWCNT. This is sensitive to I_{2D}/I_G and I_{2D}/I_D where the higher the intensity ratios, the higher the crystallinity of the nanotubes. From intensity ratios in Table 2, CNT-1000 exhibits the most graphitic ordering and highest crystallinity degree. This agrees with the finding from TGA and subsequently the electrical conductivity.

Effect of temperature on conductivity of as-synthesized CNT yarns

The electrical conductivity of each sample at room temperature was calculated as described [52] and presented below.

The gradient of the linear IV graph obtained for CNT-800 is Ohmic in nature therefore it was used to estimate the resistance of each sample in accordance with Ohm's law,

$$R = 1/\text{gradient since } R = V/I \quad (4)$$

where R is the resistance of the sample (Ω), V is voltage, (V) and I is current (A).

For the non-resistors IV relationships are not linear as observed in CNT-900 and CNT-1000, therefore they are not constant but exponential. At room temperature, they behave like a diode. Thus, Maxwell-Boltzmann statistics could be used to predict the current

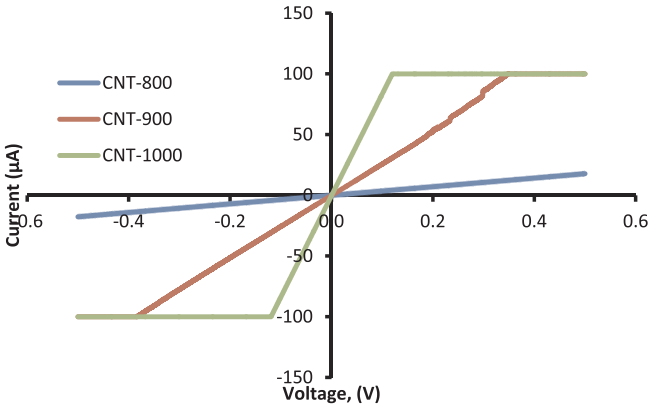

Fig. 8. I-V characteristics of as-synthesized CNT yarns.

density at the junction [53].

$$I \approx I_o e^{eV/kT} \tag{5}$$

where I is current through the diode; I_o is leakage current; e is the electronic charge (1.6×10^{-19}) V, the bias voltage; k is the Boltzmann's constant (1.38×10^{-23} J/K); T is the absolute temperature. Since IV is recorded at room temperature, absolute temperature is taken to be 298 K. Value of e/kT is calculated to be [1.6×10^{-19}/(298 x1.38×10^{-23})] equals 38.91

$$I \approx I_o e^{38.91V} \tag{6}$$

$$\frac{dI}{dV} = 38.91 e^{38.91V} \tag{7}$$

At the junction, $\frac{dI}{dV} = 38.9I$, therefore dynamic resistance R $= \frac{dV}{dI} = \frac{1}{38.9I}$

Cut in voltage for CNT-900 diode is 0.3501 V and for CNT-1000 diode is 0.1199 V. Total resistance increased due to contacts between the silver paste and the substrate and between the probe and the silver paste. The derivative of the current voltage relationship can then be expressed as:

$$\frac{dI}{dV} = 1/\left[R_s + \frac{R_j R_c}{R_j + R_c}\right] I \tag{8}$$

where Rs is the load resistance in the measurement equipment; Rj is resistance at the junction; and Rc is the contact resistance. Therefore, increase in contact resistance increases the overall resistance.

$$R = R_s + \frac{R_j R_c}{R_j + R_c} \tag{9}$$

The resistivity of each sample was determined by the correlation between resistance, cross-sectional area and length of the test samples expressed thus:

$$\rho = \mathrm{RA/L} \tag{10}$$

where ρ is resistivity (Ω · m); A is the crosssectional area of the CNT mat calculated to be 25 mm^2; and L is the length of the mat measured as 5 mm.

The electrical conductivity of each sample is therefore found by the formula:

$$\sigma = 1/\rho \tag{11}$$

where ρ is the resistivity of the sample and σ is the electrical conductivity of the sample (Sm^{-1}).

The characteristic electrical conductivity of each sample is shown in Table 2. The values are generally lower than the reported conductivity of CNT in literature [50,51,54,55]. This could be attributed to lower quality of macroscopic CNT compared with individual CNTs. Low compact density, impurities and the presence of amorphous carbon could also contribute to low conductivity. Conductivity is seen to be highest in CNT-1000, indicating that higher temperature within the limits of this study results in better conducting CNT yarn. This finding has been consistent with the findings from the analyses conducted using Raman, XRD, TGA, SEM and TEM where CNT yarns with higher purity, more aligned CNTs, smaller diameter, and higher crystallinity were obtained.

Fig. 8 depicts the relationship between applied voltage and current. Measurements were taken from −0.5 V to 0.5 V applied. CNT-800 behaves like a resistor given that it obeys the ohm's law with a precise relation between the applied voltage and the current that flows through it. These are usually not semiconductors. CNT-900 and CNT-1000, on the other hand, exhibits the properties of diodes [56], indicating that they are semi-conductive in nature as the tungsten wire currently used in incandescent bulbs.

Conclusion

As-synthesized CNT yarns were produced in a FCCVD via direct spinning. Changes in physical properties, morphology, and crystallinity were observed via Raman spectroscopy, X-ray diffraction and thermogravimetric analysis. Their influence on electrical properties of the CNT yarns for application as filaments in incandescent bulbs has been highlighted. Transmission Electron Microscopy and Scanning Electron Microscopy were employed to confirm some of these findings. Increase in synthesis temperature of CNT yarns, within the scope of this study, was seen to improve the overall quality of as-synthesis yarns and thus the electrical conductivity of as-synthesized yarns.

Author statement

All authors conceptualized the idea and EI carried out the experiments. MOD and EI analysed data, interpreted the data, and wrote the manuscript. SEI reviewed it before submission.

Declaration of Competing Interest

There is no conflict of interest.

Acknowledgements

The authors acknowledge the National Research Foundation (NRF), South Africa for financial assistance through grant No: NRFCPRR106053. We are grateful to Dr. Rudolph Erasmus for his assistance with Raman spectral collection and his valuable contribution in the analysis and to the workshop staff of the School of Chemical and Metallurgical Engineering for their support with the fabrication and continued maintenance of the FCCVD reactor.

Appendix A. Supplementary material

Supplementary data to this article can be found online at https://doi.org/10.1016/j.rinp.2019.102705.

References

[1] De Volder MFL, Tawfick SH, Baughman RH, Hart AJ. Carbon nanotubes: Present and future commercial applications. Science (80-.) 2013;339(6119):535–9.
[2] Zhang D, Miao M, Niu H, Wei Z. Core-spun carbon nanotube yarn supercapacitors for wearable electronic textiles. ACS Nano 2014;8(5):4571–9.
[3] Mittal G, Dhand V, Rhee KY, Park SJ, Lee WR. A review on carbon nanotubes and graphene as fillers in reinforced polymer nanocomposites. J Ind Eng Chem 2015;21:11–25.
[4] Jourdain V, Bichara C. Current understanding of the growth of carbon nanotubes in catalytic chemical vapour deposition. Carbon NY 2013;58:2–39.
[5] Zhang Q, et al. Dry spinning yarns from vertically aligned carbon nanotube arrays produced by an improved floating catalyst chemical vapor deposition method. Carbon NY 2010;48(10):2855–61.

[6] Singh C, Shaffer MSP, Windle AH. Production of controlled architectures of aligned carbon nanotubes by an injection chemical vapour deposition method. Carbon NY 2003.
[7] Hoecker C, Smail F, Pick M, Weller L, Boies AM. The dependence of CNT aerogel synthesis on sulfur-driven catalyst nucleation processes and a critical catalyst particle mass concentration. Sci. Rep. 2017;7(1).
[8] Barreiro A, et al. Thermal decomposition of Ferrocene as a method for production of single-walled carbon nanotubes without additional. Carbon Sources 2006.
[9] Hou G, et al. The effect of a convection vortex on sock formation in the floating catalyst method for carbon nanotube synthesis. Carbon NY 2016;102:513–9.
[10] He D, Bozlar M, Genestoux M, Bai J. Diameter- and length-dependent self-organizations of multi-walled carbon nanotubes on spherical alumina microparticles. Carbon NY 2010.
[11] Bodiba V, Igbokwe E, Mahangani N, Aberefa O, Daramola MO, Iyuke SE. Production of CNT yarns for use as filaments in incandescent bulb: effect of carbon source and state of catalyst on production of CNT. IOP Conf. Ser. Mater. Sci. Eng. 2018;413(1).
[12] Zhang X, et al. Spinning and processing continuous yarns from 4-inch wafer scale super-aligned carbon nanotube arrays. Adv Mater 2006;18(12):1505–10.
[13] Vilatela JJ, Windle AH. Yarn-like carbon nanotube fibers. Adv Mater 2010;22(44):4959–63.
[14] Lekawa-Raus A, Patmore J, Kurzepa L, Bulmer J, Koziol K. Electrical properties of carbon nanotube based fibers and their future use in electrical wiring. Adv Funct Mater 2014;24(24):3661–82.
[15] Motta M, Li YL, Kinloch I, Windle A. Mechanical properties of continuously spun fibers of carbon nanotubes. Nano Lett 2005;5(8):1529–33.
[16] Billinge SJL, Kanatzidis MG. Beyond crystallography: the study of disorder, nanocrystallinity and crystallographically challenged materials with pair distribution functions. Chem Commun 2004(7):749.
[17] Sloan J. Structural studies of multiwall carbon nanotubes by neutron diffraction. Phys Rev B – Condens Matter Mater Phys 1999;59(3):1665–8.
[18] Lehman JH, Terrones M, Mansfield E, Hurst KE, Meunier V. Evaluating the characteristics of multiwall carbon nanotubes. Carbon NY 2011;49(8):2581–602.
[19] Shi JH, Yang BX, Goh SH. Covalent functionalization of multiwalled carbon nanotubes with poly(styrene-co-acrylonitrile) by reactive melt blending. Eur Polym J 2009.
[20] Mevellec JY, Bergeret C, Cousseau J, Buisson JP, Ewels CP, Lefrant S. Tuning the raman resonance behavior of single-walled carbon nanotubes via covalent functionalization. J Am Chem Soc 2011;133(42):16938–46.
[21] Bernard S, Beyssac O, Benzerara K, Findling N, Tzvetkov G, Brown GE, et al. Raman and XRD study of anthracene-based cokes and saccharose-based chars submitted to high-temperature pyrolysis. Carbon NY 2010.
[22] Reich S, Thomsen C. Raman spectroscopy of graphite. Philos Trans R Soc A 2004;362:2271–88. https://doi.org/10.1098/rsta.2004.1454.
[23] Castiglioni C, Mapelli C, Negri F, Zerbi G. Origin of the D line in the Raman spectrum of graphite: a study based on Raman frequencies and intensities of polycyclic aromatic hydrocarbon molecules. J Chem Phys 2001;114(2):963–74.
[24] Ferrari AC. Raman spectroscopy of graphene and graphite: Disorder, electron–phonon coupling, doping and nonadiabatic effects. Solid State Commun 2007;143(1–2):47–57.
[25] Jorio A, Pimenta MA, GSouza-Filho A, Saito R, Dresselhaus G, Dresselhaus MS. Characterizing carbon nanotube samples with resonance Raman scattering. New J Phys 2003;139.
[26] Ray SC, Tetana ZN, Erasmus R, Mathur A, Coville NJ. Carbon spheres for energy applications: Raman and X-ray photoemission spectroscopy studies. Int J Energy Res 2014;38(4):444–51.
[27] Dresselhaus MS, Jorio A, Hofmann M, Dresselhaus G, Saito R. Perspectives on carbon nanotubes and graphene Raman spectroscopy. Nano Lett 2010;10(3):751–8.
[28] Li X, Cheng Y, Zhao L, Zhang Q, Wang M. Structural and electrical properties tailoring of carbon nanotubes via a reversible defect handling technique. Carbon NY 2018;133:186–92.
[29] Ermakova MA, Ermakov DY, Chuvilin AL, Kuvshinov GG. Decomposition of methane over iron catalysts at the range of moderate temperatures: the influence of structure of the catalytic systems and the reaction conditions on the yield of carbon and morphology of carbon filaments. J Catal 2001;201(2):183–97.
[30] Ruland W. X-ray studies on the carbonization and graphitization of acenaphthylene and bifluorenyl. Carbon NY 1965;2(4):365–78.
[31] Langford JI, Wilson AJC. Scherrer after sixty years: a survey and some new results in the determination of crystallite size. J Appl Crystallogr 1978;11(2):102–13.
[32] Collins PG. Defects and disorder in carbon nanotubes. Oxford Handb Nanosci Technol Front Adv 2017;1:1–73.
[33] Maffucci A, Maksimenko SA, Miano G. Electrical conductivity of carbon nanotubes: Modeling and Characterization Department of Electrical Engineering and Information School of Electrical Engineering Tel Aviv University, no. January. 2017.
[34] Cao A, Xu C, Liang J, Wu D, Wei B. X-ray diffraction characterization on the alignment degree of carbon nanotubes. Chem Phys Lett 2001.
[35] Alhosiny N, Badawi A, Abdallah S. The effects of CNTs types on the structural and electrical properties of CNTs/PMMA nanocomposite films. Int J Eng Technol IJET-IJENS 2013;02:77–9.
[36] Stetter A, Vancea J, Back CH. Conductivity of multiwall carbon nanotubes: Role of multiple shells and defects 2010;vol. 82, no. 11.
[37] Reznik D, Olk CH, Neumann DA, Copley JRD. X-ray powder diffraction from carbon nanotubes and nanoparticles D. Am Phys Soc Phys Rev B 1995;52(1):116–24.
[38] Venezuela P, Lazzeri M, Mauri F. Theory of double-resonant Raman spectra in graphene: Intensity and line shape of defect-induced and two-phonon bands. Phys Rev B – Condens Matter Mater Phys 2011;84(3):1–28.
[39] Eckmann A, et al. Probing the nature of defects in graphene by Raman spectroscopy. Nano Lett 2012;12(8):3925–30.
[40] Kuwana K, Saito K. Modeling CVD synthesis of carbon nanotubes: nanoparticle formation from ferrocene. Carbon NY 2005;43(10):2088–95.
[41] Öncel Ç, Yürüm Y. Carbon nanotube synthesis via the catalytic CVD method: a review on the effect of reaction parameters. Fullerenes Nanotub Carbon Nanostruct 2006;14(1):17–37.
[42] Raji K, Thomas S, Sobhan CB. A chemical kinetic model for chemical vapor deposition of carbon nanotubes. Appl Surf Sci 2011;257(24):10562–70.
[43] Kuwana K, Saito K. Modeling ferrocene reactions and iron nanoparticle formation: application to CVD synthesis of carbon nanotubes. Proc Combust Inst 2007;31(2):1857–64.
[44] Kleinsmith JN. The effect of temperature and crystallite size on the growth and morphology of carbon nanotubes; 2005.
[45] Hoogenraad MS. Growth and utilization of carbon fibrils. Universiteit Utrecht, Faculteit Scheikunde; 1995.
[46] Vanyorek L, et al. Optimization of the catalytic chemical vapor deposition synthesis of multiwall carbon nanotubes on FeCo(Ni)/SiO 2 aerogel catalysts by statistical design of experiments. J Phys Chem C Apr. 2011;115(13):5894–902.
[47] Misak HE, Asmatulu R, O'Malley M, Jurak E, Mall S. Functionalization of carbon nanotube yarn by acid treatment. Int J Smart Nano Mater 2014;5(1):34–43.
[48] Lanza M, Santangelo S, Messina G, Galvagno S, Milone C. Crystalline quality evaluation of carbon nanotubes by kinetic analysis in quasi-isothermal conditions. ChemPhysChem 2010;11(9):1925–31.
[49] Santangelo S, Lanza M, Milone C. Evaluation of the overall crystalline quality of amorphous carbon containing multiwalled nanotubes. J Phys Chem C 2013;117(9):4815–23.
[50] Bom D, et al. Thermogravimetric analysis of the oxidation of multiwalled carbon nanotubes: evidence for the role of defect sites in carbon nanotube chemistry. Nano Lett 2002;2(6):615–9.
[51] Ajayan PM, Ebbesen TW, Ichihashi T, Iijima S, Tanigaki K, Hiura H. Opening carbon nanotubes with oxygen and implications for filling. Nature 1993;362(6420):522–5.
[52] Gutiérrez MP, Li H, Patton J. Thin film surface resistivity in partial fulfillment of course requirements for mate 210 experimental methods in materials engineering fall 2002 professor G. Selvaduray; 2002. pp. 0–24.
[53] Sze SM, Ng KK. Physics of semiconductor devices. 1981.
[54] Aberefa O, Bedasie K, Madhi S, Daramola MO, Iyuke SE. Production of carbon nanotube yarn from swirled floating catalyst chemical vapour deposition: a preliminary study. Adv Nat Sci Nanosci Nanotechnol 2018;9(3).
[55] Miao M. Electrical conductivity of pure carbon nanotube yarns. Carbon NY Oct. 2011;49(12):3755–61.
[56] Tans SJ, Verschueren ARM, Dekker C. Room-temperature transistor based on a single carbon nanotube. Nature 1998;393(7):669–72.

Production of CNT yarns for use as filaments in incandescent bulb: effect of carbon source and state of catalyst on production of CNT

IOP Conf. Series: Materials Science and Engineering **413** (2018) 012027 doi:10.1088/1757-899X/413/1/012027

Production of CNT yarns for use as filaments in incandescent bulb: effect of carbon source and state of catalyst on production of CNT

Veronica Bodiba, Ezinne Igbokwe, Ndanganeni Mahangani, Oluseyi Aberefa, Michael Olawale Daramola*, Sunny E. Iyuke

School of Chemical and Metallurgical Engineering, Faculty of Engineering and the Built Environment, University of the Witwatersrand, Wits 2050, Johannesburg, South Africa.

*Corresponding author e-mail address: Michael.Daramola@wits.ac.za

Abstract. Presence of highly aligned carbon nanotubes (CNTs) bundles is a prerequisite to producing good quality CNTs that will retain their original good electrical and mechanical properties when spun into yarn. In this study, effects of carbon source and state of catalyst on the CNT yield and quality during the production of CNTs were investigated. CNTs were produced in a Swirled Continuous CVD reactor using acetylene and methane as carbon sources and ferrocene as a catalyst to investigate the effect of carbon source and the production was carried out with the state of the catalyst altered to investigate effect of state of catalyst on the yield and quality of the CNTs. The quality and purity of the produced CNTs were checked with Raman and Scanning electron microscopy (SEM) provides information on the morphology of the produced CNTs. SEM images of the produced CNTs using acetylene gas reveal the presence of more nanoballs than those produced using methane under the similar conditions. However, amount of CNTs produced using methane is very low compared to the amount obtained when acetylene was used. The CNT yield from methane was enhanced when ferrocene (catalyst) was dissolved in cyclopentane. Results from SEM and Raman Spectroscopy indicates CNT bundles with longer lengths and reduced number of nanoballs when methane was used together with ferrocene dissolved in cyclopentane as compared to using ferrocene in a solid state.

1. Introduction

To maximize the excellent mechanical, electrical and thermal properties possessed by CNTs in the nanoscale in fabrication of components, devices and other applications has increased efforts and interest in production macroscopic assemblies of CNTs. Research aimed at optimizing the production of well aligned, good quality and quantity CNTs to meet the requirements for spinning into yarns are currently on top gear. The catalytic chemical vapor deposition (CCVD) is currently the most viable process for the synthesis of carbon nanotubes. The influence of numerous growth parameters on the resulting nanotubes characteristics, such as diameter, length, number of graphene layers, defect density etc., has been studied [1,2].

Generally, nano-sized transition metal particles, e.g., nickel, iron, cobalt, molybdenum and copper, have been successfully used in CCVD either in oxide or metallic forms or as mixtures [1,2]. The solubility of carbon in catalyst particles determines the ability of metal to catalytically decompose gaseous carbon-containing molecules. As Moisala et al. highlighted in their review, the solubility of carbon in iron and nickel significantly increases for metal particles with a diameter of less than approximately 10 nm [1]. Seidel and co-workers investigated the difference of the carbon nanotubes growth behaviour when Fe, Co, and Ni catalysts were used [3].

The authors observed that the order of the lowest growth temperatures agrees with the order of the bulk melting points of the three transition metals (Ni, 1,450 °C; Co, 1,490 °C; Fe, 1,540 °C). For binary compounds, e.g., cobalt–molybdenum [4], iron–molybdenum [5] and iron–cobalt [6,7], the yield of carbon

nanotubes has been observed to increase significantly. However, the precise catalyst composition has a great influence on the final product. $Fe_{1-x}Co_x$ alloys are among the most efficient catalysts for the synthesis of multi-walled carbon nanotubes [6,7]. The resulting yield, as well as the nanotubes characteristics, strongly depends on the parameter x.

Most used carbon precursors in CVD method are methane, carbon monoxide, acetylene, ethylene, benzene and toluene [8]. It has been discovered that the use of unsaturated hydrocarbons as carbon precursors results in high yield deposition rate as compared to the use of saturated hydrocarbons [9]. Saturated hydrocarbons are favoured for the growth of single walled carbon nanotubes (SWCNTs) because they synthesize graphitized filaments with fewer walls than when using unsaturated hydrocarbons. Furthermore, excessive carbon precursor concentration or hydrocarbon self-pyrolysis are some of the causes of catalyst poisoning during high temperature processing. This can be avoided by limiting carbon precursor feed rate to the catalyst particles by controlling partial pressure of carbon precursor and choosing the carbon precursor according to the decomposition rate [10].

Obtaining high quality nanoyarns that will exhibit the same electrical and mechanical properties as the original carbon nanotubes (CNTs) bundles from which they are made has been a great challenge, possibly due to inconsistence in the results reported in literature on the production of high quality CNTs, intermediates for nanoyarn production. Against this background, effects of carbon source and state of catalyst on the CNT yield and quality during the production of CNTs in a Swirled Continuous CVD reactor were investigated in this study.

2.Experimental

CNTs were produced in a swirled continuous CVD reactor using acetylene and methane as carbon sources and ferrocene as a catalyst to investigate the effect of carbon source on the yield and quality of produced CNTs. During the production, 10 g of ferrocene ($F_e(CO)_5$) catalyst was vaporizer at 300ºC in the vapourizer attached to the reactor and the vapourized catalyst was carried to the reaction zone, where acetylene or methane and H_2 gas were introduced, by argon gas. The flow rate of the carbon source, the argon gas and the H_2 gas into the reactor were 150 ml/min, 150 ml/min and 50 ml/min, respectively. The reaction zone (inside the CVD reactor) was maintained at reaction temperature of 850ºC and the reaction was run for 12 minutes. The temperature at the reaction zone was measured with a PT-100 thermocouple and controlled with PID controller built with the reactor. To gain insight into the effect of temperature on the yield and quality of produced CNTs, the reaction temperature was varied from 850ºC to 950ºC at a step change of 50ºC.

To investigate the effect of changing the state of catalyst from solid state to liquid state on the quality and yield of CNTs produced in the reactor, 10 g of ferrocene powder was dissolved in 10 ml of cyclopentane. The liquid solution was vaporizer at 300ºC in the vapourizer attached to the reactor and the vapourized catalyst was carried to the reaction zone, where acetylene or methane and H_2 gas were introduced, by argon gas. The flow rate of the carbon source, the argon gas and the H_2 gas into the reactor were 150 ml/min, 150 ml/min and 50 ml/min, respectively. The reaction zone (inside the CVD reactor) was maintained at reaction temperature of 850ºC and the reaction was run for 12 minutes. Figure 1 depicts the experimental set-up used in the investigation. The yield of the produced CNTs was calculated by measuring the amount of CNT collected after the production. The quality of the produced CNTs was checked using scanning electron microscope (SEM) equipped with energy-dispersive X-ray spectroscopy (EDS) for morphology and elemental composition; and Raman spectroscopy to check the degree of defect and graphitic formation. The results obtained from the characterization were compared to obtain logical conclusions.

Figure 1: An experimental set-up for CNT production.

3. Results and discussion

Figure 2 depicts the CNT yield obtained when acetylene and methane were used as the carbon sources. The use of acetylene displayed a higher yield compared to methane at the various temperatures studied. For both the maximum CNT yield was recorded at 900°C, where the CNT yield with acetylene at this temperature is about 14.5 times higher than that of methane. Acetylene gives high yield because it is easier to break carbon chains in unsaturated hydrocarbons than in saturated hydrocarbons [11]. The SEM images of CNTs produced are presented in Figure 3. From the images, it is evident that CNTs produced with acetylene contain more of nanoballs than the nanotubes and the length of the nanotubes is short, making production of good quality yarns from these nanotubes a mirage. However, better CNT bundles with fewer nanoballs were obtained when methane was used as a carbon source. The CNTs from methane contain a substantial number of nanotubes with reasonable length and excellent spinnable array required to produce yarns.

EDX could be employed to determine the purity and elemental composition of the produced CNTs from different carbon sources. Elemental compositions of the produced CNTs obtained from EDX are shown in Figure 4. The major component of the products obtained from the CVD using acetylene and methane as carbon sources are carbonaceous in nature (see Figure 4). Acetylene products contain more carbon but the accompanying SEM images indicate the quality of the product. Methane has more impurities from the iron based catalyst but this can be easily purified. The ratio of the intensities of the D and G bands is a suitable identification of the quality of bulk samples. Therefore, from the Raman spectra in Fig 5, it is evident that the use of methane produces CNTs with a fewer structural defects as compared to the CNTs from acetylene. There is also an indication that the methane source produced mostly single-walled carbon nanotubes (SWCNT) and double-walled carbon nanotubes (DWCNT). Both SWCNT and DWCNT show higher differences in intensities of D and G bands [12]. The presence of radial breathing mode (RBM) seen in Fig 5b is a strong indication of the presence of SWCNT in CNTs produced from methane carbon source [13].

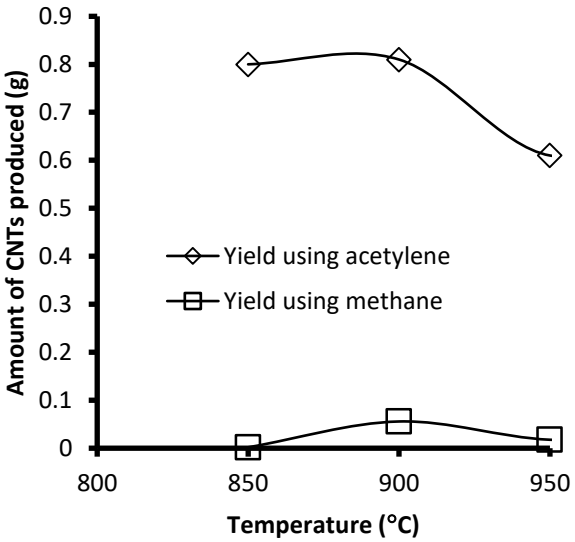

Figure 2: CNT production yield using various carbon sources-(methane and acetylene).

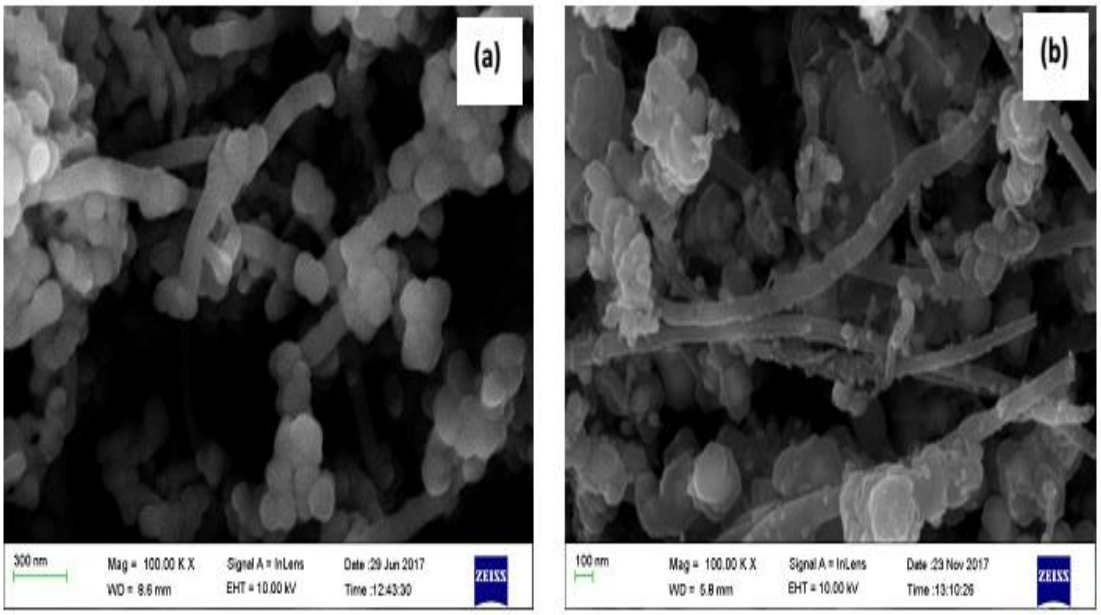

Figure 3: SEM images of CNT produced from (a) Acetylene (b) Methane

(a)

Element	Weight%	Atomic%
C K	89.08	94.37
O K	5.55	4.41
Fe L	5.37	1.22
Totals	100.00	

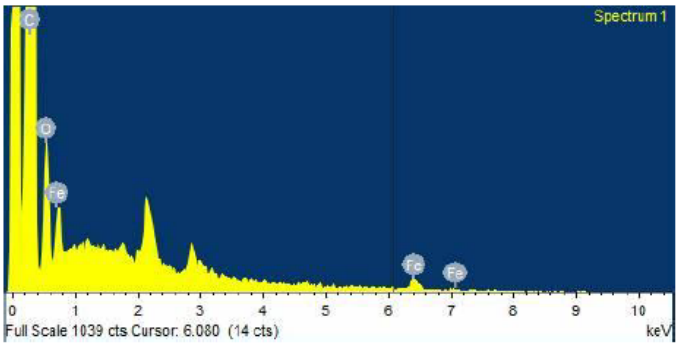

(b)

Element	Weight%	Atomic%
C K	78.43	90.31
O K	7.02	6.07
Si K	0.09	0.05
Fe K	14.46	3.58
Totals	100.00	

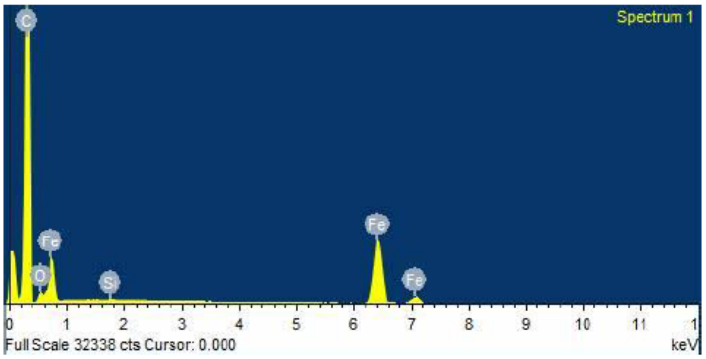

Figure 4: Energy Dispersive X-ray spectroscopy (EDX) of CNT produced from (a) Acetylene and (b) Methane

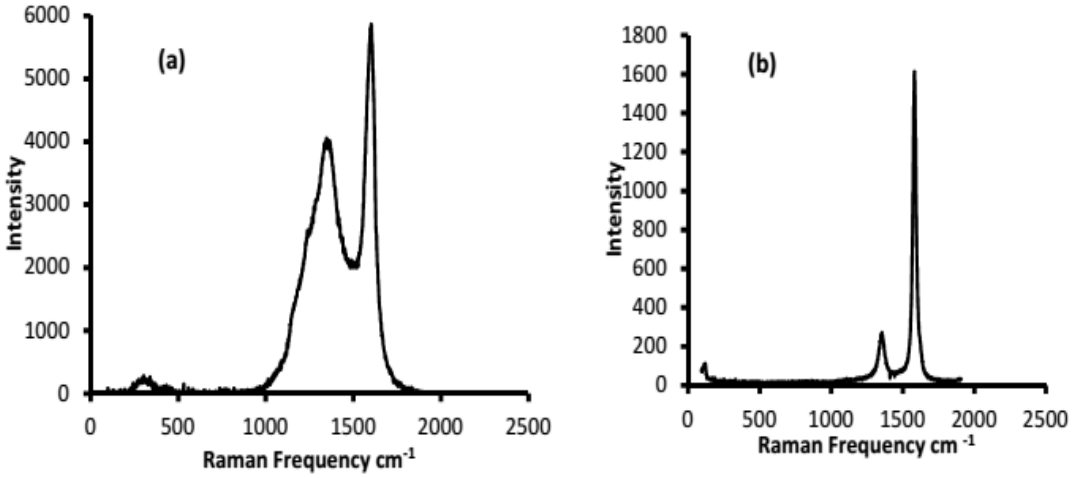

Figure 5: Raman spectroscopy of a) Acetylene and b) Methane

Fig 6 shows a significant improvement in the yield of CNT produced from ferrocene dissolved in cyclopentane. The maximum yield occurred at 900℃ for both the ferrocene in solid state and the ferrocene in liquid state. When ferrocene was dissolved in cyclopentane, the CNT yield was 6.8 times

higher than the CNT yield when ferrocene was in solid state. The higher yield could be attributed to the participation of cyclopentane in the reaction since it is a hydrocarbon, thereby enhancing the carbon concentration in the reaction [14]. Comparing the SEM images of the produced CNT bundles when the catalyst was in solid state (Fig 7a) with the SEM image when it was dissolved in cyclopentane (Fig 7b) reveals that there is presence of CNTs together with nanoballs in Fig 7a while **F**ig 7b shows a better formation of CNTs characterized with long array of spinnable multi-walled and single-walled CNTs with a few number of nanoballs. These types of CNTs formed when ferrocene was dissolved in cyclopentane will result in the formation of high quality CNT yarns would possess the same quality as the original CNTs.

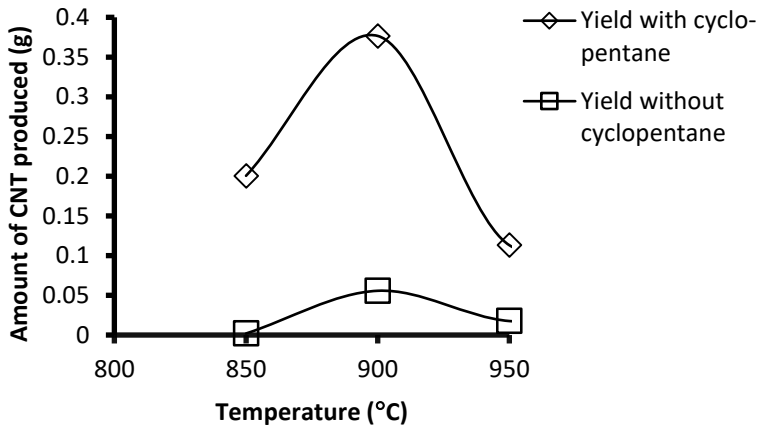

Figure 6: CNT yield with varying state of catalyst using methane as carbon source.

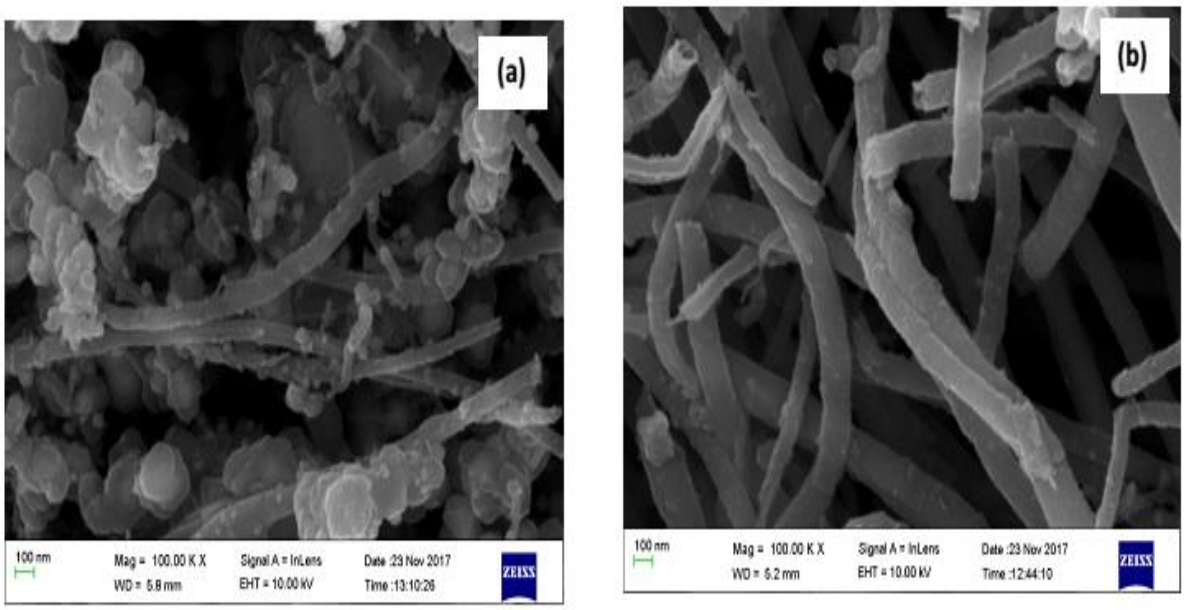

Figure 7: SEM images for CNT bundles produced at various conditions: (a) Methane used as a carbon source with ferrocene in a solid state and (b) Methane used as a carbon source with ferrocene dissolved in cyclopentane.

4.Conclusion

In this study, effect of carbon source and the state of catalyst on the yield and quality of CNTs has been investigated. Results of the investigation reveal that using acetylene as a carbon source yielded higher

amount of CNTs compared to using methane gas. However, the quality of CNTs produced when methane gas is used is far better than when acetylene gas is used. In addition, pre-dissolution of the ferrocene catalyst in cyclopentane prior to vapourization enhances the quality and yield of CNTs produced as compared to non-dissolution of the catalyst prior to vapourization.

Acknowledgments

Research is supported by the National Research Foundation of South Africa grant No. NRF-CPRR106053.

References

[1] Moisala, A., Nasibulin, A.G., Kauppinen, E.I. The role of metal nanoparticles in the catalytic production of single-walled carbon nanotubes - a review [J]. J. Phys.: Condens. Matter, 2003, 14: S3011-S3035.
[2] Dupuis, A.C. The catalyst in the CCVD of carbon nanotubes - a review [J]. Prog. Mater. Sci., 2005, 50:929-961
[3] Seidel, R., Duesberg, G.S., Unger, E., Graham, A.P., Liebau, M., Kreupl, F. Chemical vapor deposition growth of single-walled carbon nanotubes at 600 °C and a simple growth model. J. Phys. Chem. B, 2004,108:1888-1893.
[4] Alvarez, W.E., Kitiyanan, B., Borgna, A., Resasco, D.E. Synergism of Co and Mo in the catalytic production of single-wall carbon nanotubes by decomposition of CO[J]. Carbon, 2001,39:547-558.
[5] Harutyunyan, A.R., Pradhan, B.K., Kim, U.J., Chen, G., Eklund, P.E. CVD synthesis of single wall carbon nanotubes under "soft" conditions [J]. Nano Lett., 2002, 2:525-530.
[6] Flahaut, E., Govindaraj, A., Peigney, A., Laurent, Ch., Rousset, A., Rao, C.N.R. Synthesis of single-walled carbon nanotubes using binary (Fe, Co, Ni) alloy nanoparticles prepared in situ by the reduction of oxide solid solutions [J]. Chem. Phys. Lett., 1999, 300: 236-242.
[7] Magrez, A., Seo, J.W., Mikó, Cs., Hernadi, K., Forró, L. Growth of carbon nanotubes with alkaline earth carbonate as support [J]. J. Phys. Chem. B, 2005,109: 10087-10091.
[8] Behabtu, N., Green, M. J., Pasquali, M. Carbon nanotube-based neat fibers [J]. Nano Today, 2008, 3(5–6):24–34.
[9] Awasthi, K., Srivastava, A., & Srivastava, O. N. Synthesis of carbon nanotubes [J]. Journal of Nanoscience and Nanotechnology, 2005, 5(10):1616-1636.
[10] Eatemadi, A., Daraee, H., Karimkhanloo, H., Kouhi, M., Zarghami, N., Akbarzadeh, A., Abasi, M., Younes Hanifehpour Y., Joo, S. W. Carbon nanotubes: properties, synthesis, purification, and medical applications [J]. Nanoscale research letters, 2014, 9(1): 393.
[11] Baker R.T.K. and Harris, P.S. Chemistry and Physics of Carbon [B]. J.P.L. Walker and P.A. Thrower (eds.), Deeker, New York : Basel , 1978.
[12] Costa, S., Borowiak-Palen, E., Kruszyńska, M., Bachmatiuk, A., Kaleńczuk, R. J. Characterization of carbon nanotubes by Raman spectroscopy [J]. Materials Science-Poland,2008, 26 (2): 433-441
[13] Dresselhaus, M.S., Dresselhaus, G., Saitoc, R. and Joriod A. Raman spectroscopy of carbon nanotubes [J]. Physics Reports, 2005, 409:47–99.
[14] Weissker, U., Silke, H., Albrecht, L. & Bernd, B. Carbon nanotubes filled with ferromagnetic materials. Materials, 2010, 3:4383-4427.

Production of CNT Yarns from Methane Gas for Use as Filaments in Incandescent Bulbs: Thermodynamic Properties of As-spun CNT Yarns

Production of CNT Yarns from Methane Gas for Use as Filaments in Incandescent Bulbs: Thermodynamic Properties of As-spun CNT Yarns.

N. Mahagani [1], E. Igbokwe [1], O. Aberefa [1], V. Bodiba [1] M.O. Daramola [1*] and S. E. Iyuke [2]

[1] School of Chemical and Metallurgical Engineering, University of the Witwatersrand, South Africa.
[2] Petroleum Training Institution, Effurum Delta State, Nigeria
* Corresponding Author; Michael.Daramola@wits.ac.za

Abstract
Energy efficiency is a minimal cost energy resource. It is critical in bridging the gap via reducing overall demand, allowing electricity supply to be expanded to meet increasing demand in a timely and sustainable way. Incandescent bulbs with tungsten filaments convert only about 10% of the input energy into light with the rest wasted as heat and resultant carbon dioxide gas emissions. This results in high energy and environmental inefficiency. Carbon nanotubes (CNT) yarns as filaments for replacement of tungsten in incandescent bulbs represent an economic option boosting high energy and environmental efficiency. In this study, CNT yarns were produced from methane, an abundant greenhouse gas currently flared in Africa. Synthesis of CNT yarns were carried out in a Floating Catalyst Chemical Vapour Deposition (FC-CVD) reactor using ferrocene as the catalyst with direct spinning of CNT into yarn. The quality and morphology of the produced yarns at different temperatures (900 – 1000^{o}C) were determined using Scanning Electron Microscope (SEM) and Raman Spectroscopy. The optimum temperature to produce CNT yarns was found to be at reactor temperature of 950^{o}C. The thermodynamics associated with the production of the as-spun CNT yarns were determined by Thermogravimetric Analysis (TGA) and Differential Scanning Calorimetry (DSC). Heat capacity of CNT yarns was calculated based on the measured heat flow at thermal stable state. A polynomial regression of the form: $Cp=0.002T^2 – 0.4512T+66.099$ was proposed for the prediction of the thermodynamic values. Change in thermodynamic quantities of yarn such as entropy and enthalpy were determined based on the heat capacities calculated from fitted polynomial models using relationship of thermodynamic function.

Key words: Carbon nanotube yarn, Kinetic, Themodynamics,

1. Introduction
Since their rediscovery by Iijima [1], carbon nanotubes (CNTs) are identified as fascinating materials due to their remarkable electrical and mechanical properties. Currently, there is a great effort by researchers to fabricate CNT yarn in order to make use of CNTs remarkable properties. These properties make CNT yarn suitable material to consider in different application, such as, incandescent lamp filament [2], supercapacitor [3], artificial muscles [4], solar cell [5], and many more.

Surfactant-based coagulation spinning, direct spinning, forest spinning, and liquid crystalline spinning are the four most studied methods of manufacturing yarn from CNTs. Surfactant-based

coagulation involves injecting a binder which is polymeric between CNTs to produce a yarn [6]. During the direct spinning method, CNTs and yarns get produced at the same time [7]. In forest spinning, CNTs that are grown on a substrate get drawn and twisted to form a yarn [8]. Liquid-crystalline spinning involves spinning the suspension of CNTs to form a wet-crystalline suspension [9]. Out of all four methods, direct spinning method was found to be advantageous for continuous mass production. It was also found to be the most effective method in producing yarn with good mechanical and electrical properties [6;10].

Studies of thermodynamic properties of a material provide important information for classification of the energy state of the material, sorption, functionalization, calculation of equilibria, etc. Therefore, thermophysical quantities need to be considered when studying material. Thermophysical quantities of individual CNTs has gained interest and their study are been reported in open literature. The source of calculating these thermodynamic properties is by obtaining experimental heat capacities. Heat capacities of material are required in areas such as physics, chemical engineering and in chemistry to determine phase transition, mass balance, entropy and enthalpy. Heat capacities of SWCNTs were found to be higher than that of MWCNTs at a temperature below 275 K. However, at a temperature above 275 K MWCNTs have higher heat capacities than SWCNTs [11]. A study by Muratov showed that the heat capacity of MWCNTs is almost the same as that of graphite at a temperature of 298.15 K, though heat capacity of graphite is slightly higher [12]. As far as could be ascertained, no heat capacities and other thermodynamic properties of CNT yarn reported in open literature until now. Hence this study focused on the thermodynamic properties of yarn produced at different reactor temperatures using the direct spinning method. Effect of production temperature on the thermophysical quantities of the yarn was also investigated.

2. Methodology

2.1 CNT yarn synthesis

A continuous catalytic chemical vapor deposition (CCVD) reactor was used to synthesize CNT yarn. The reactor was equipped with a motor and spindle (Fig.1) to directly spin the CNTs into yarn. Before each experiment, Nitrogen gas (purity: 99.999%) was used to purge the system to remove any contaminants as well as to detect any gas leak around the system. 7 g of Ferrocene (purity: 98%) was used as catalyst, CH_4 gas (purity: 99%) was used as carbon precursor at a constant flow rate of 125 ml/min. CH_4 gas was chosen as carbon precursor because it produces high quality CNTs as compared to other carbon precursors [13]. At the start of each experiment, ferrocene powder was heated in a vaporiser simultaneously with heating the reactor using the furnace to the desired temperature (900 to 1000^{o}C). During the reaction, CH_4 gas was fed into the reaction zone and Argon gas (99.999%) at a constant flow rate of 150 ml/min was used to carry vaporised ferrocene into the reaction zone in the reactor. The electric motor at the reactor outlet was switched on to turn the spindle at a speed of 10 rpm. Each experiment was conducted for 15 mins. CNT yarn was collected from the spindle after the system has cooled down.

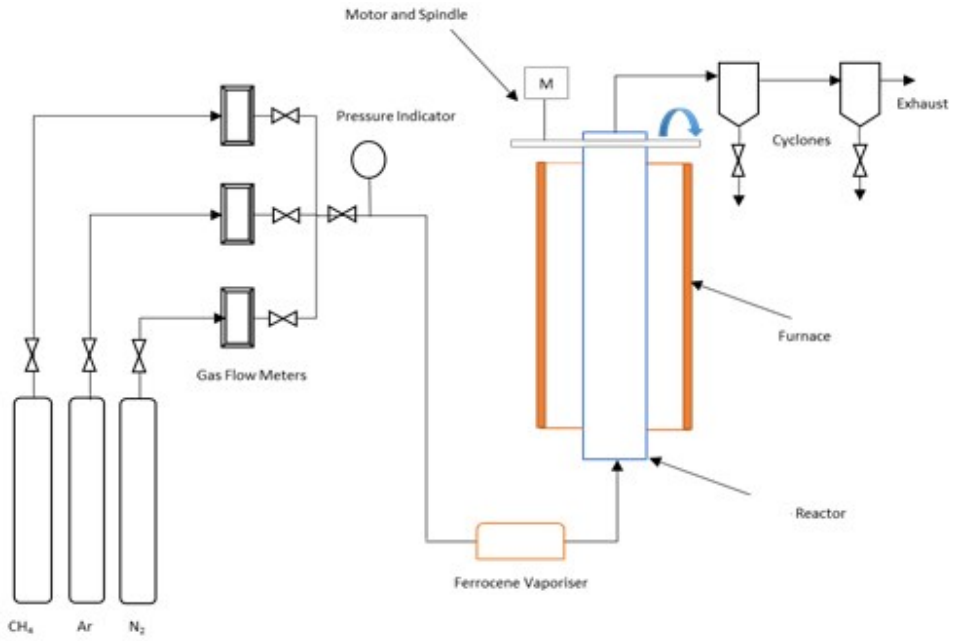

Figure 1**:** Process Flow Diagram of experimental set-up to produce CNT yarn

2.2 CNT yarn Characterization

Yarn morphology was obtained via SEM using FEI QUANTRA 200 ESEM equipped with Energy-dispersive X-ray spectroscopy (EDS) and operated at a voltage of 30 kV. A small amount of yarn sample was attached on the aluminium stud with an aid of double-sided carbon tape. Gold-palladium was used to coat the mounted sample before the microscope was used to capture images of the coated sample.
A Horiba LabRam HR equipped with Olympus BX41 microscope was used to determine the degree of crystallinity of the sample. Raman scattering in the sample was excited at wavelength of 514.5 nm using Lexel argon ion laser. Backscattered light was collected using a 100x objective, which was spread using a 600 lines mm^{-1} grating, on top of liquid nitrogen cooled charge couple device detector. In order to prevent localised heating, the laser at the sample was approximately 0.4 mW.

2.3 Thermophysical measurement of CNT yarn

The Thermogravimetry and heat flow measurements of yarn samples were carried out using thermogravimetric analyser (TGA) equipped with Differential Scanning calorimeter (DSC), model SDT600. Two platinum crucibles were used during the analysis, one for loading sample and the other one was left empty for reference. For each measurement, the initial mass of the sample was about 10 mg. The loaded sample is heated from ambient temperature to a temperature of 900^{o}C at a heating ramp of 10^{o}C per minute. Nitrogen gas was allowed to flow to the system at a flow rate of 50 ml per minute throughout the measurement.

The heat capacity (C_P) of the sample was determined by the dimensional relationships, dividing the heat flow by the rate of heating the sample using equation (1) [14]:

$$\frac{\Delta Q/\tau}{\Delta T/\tau} = \frac{\Delta Q}{\Delta T} = C_p \quad (1)$$

Specific heat capacity ($C_{p,m}$) was expressed in terms of heat flow acquired from the DSC curve using Equation (2):

$$C_{p,m} = \frac{1}{m}\frac{\Delta Q}{\Delta T} = \frac{1}{m}.C_p \quad (2)$$

Where:

m = initial sample mass,

$\frac{\Delta Q}{d\tau}$ = heat flow obtained from DSC curve and

$\frac{dT}{d\tau}$ = heating rate

The following thermodynamic functions of CNT yarn were also calculated:

Enthalpy Change using Equation (3):

$$\Delta H = H[T] - H[25] = \int_{25}^{T} C_{p,m} dT \quad (3)$$

Entropy Change using Equation (4):

$$\Delta S = S[T] - S[25] = \int_{25}^{T} \frac{C_{p,m}}{T} dT \quad (4)$$

Whereby 25°C was the initial sample temperature.

3. Result and discussions

3.1 Morphology and crystallinity of CNT yarn

SEM images in Figure 1 depict the formation of a continuous fibrous structure. The diameter of the yarn produced at 900°C, 950°C and 1000°C was approximately 6.5 µm, 12 µm and 25 µm, respectively. These values are greater than that of CNTs which is <100 nm. Therefore, all fibrous structures have a similar structure as a yarn. Comparing the yarn produced at various temperatures, 900°C to 1000°C, Figure 1 indicates that yarn produced at 950°C has a higher degree of alignment with smooth and continuous surface as compared to the yarns produced at 900°C and 1000°C. In addition, increasing reactor temperature from 900°C to 950°C produced CNT yarn with less disorder. These findings agree with other studies that showed that increase in reaction temperature produced high quality yarn [15] and CNTs [16,17]. However, further increase in reactor temperature from 950°C to 1000°C resulted in low quality yarn as compared to those at 950°C but better than those at 900°C. These results agree with the Raman shift results as indicated in Figure 3 and Table 1.

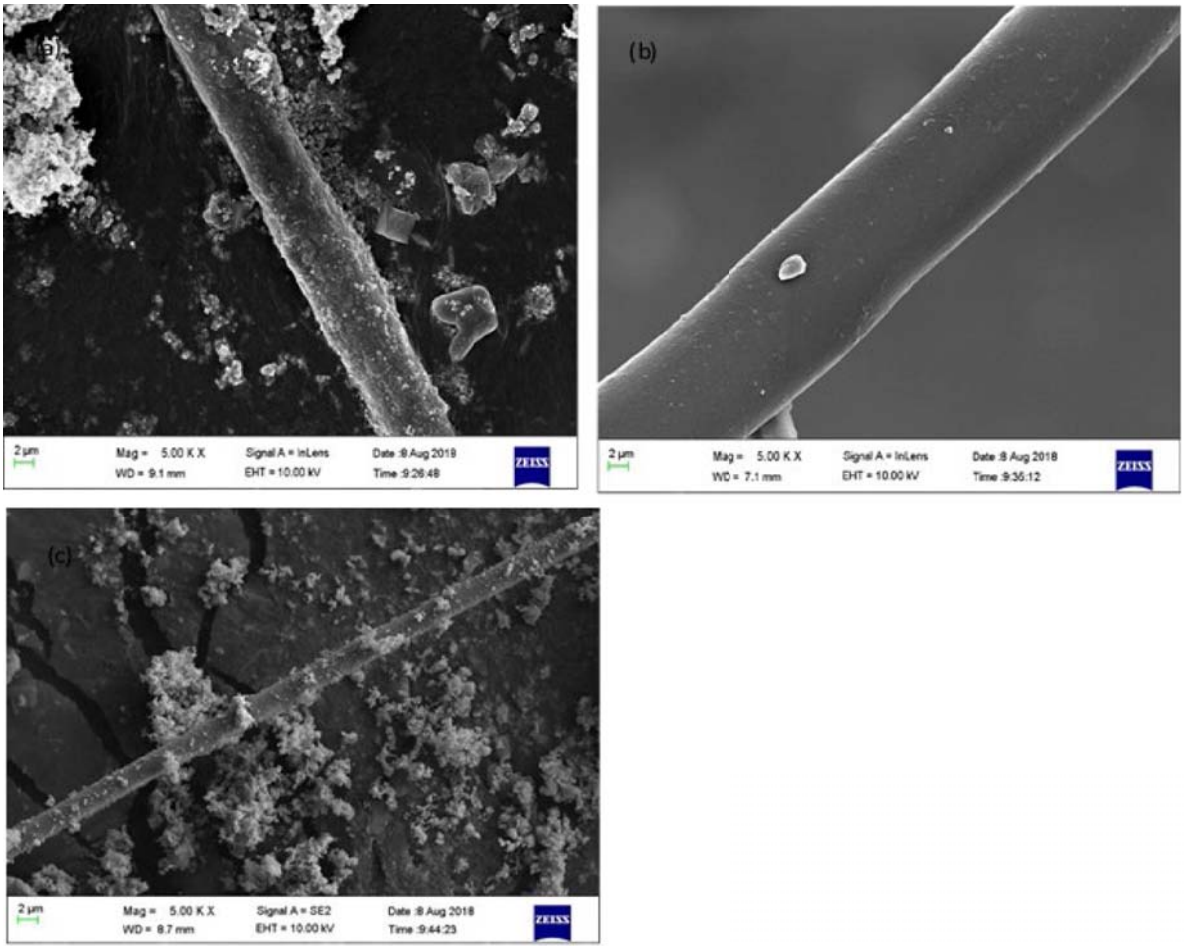

Figure 2: SEM images of CNT yarn produced at reactor temperature of (a) 900ºC (b) 950ºC (c) 1000ºC

Figure 3 shows the spectra of the elemental composition of the produced structure as obtained from EDX. All three spectra indicate that the samples are composed of Carbon, oxygen, and iron impurities. Iron impurities are a result of iron-based catalyst (ferrocene) that was used during synthesis. Therefore, the major components in the samples are carbonaceous in nature. These results only confirm that the fiber shown in Figure 2 is made mainly of carbon. In overall, the reactor temperature of 950ºC shows to be the best temperature of producing yarn with good qualities. Poor quality obtained at 900ºC could be attributed to the incomplete nucleation of CNTs at the reactor temperature of 900ºC for CNT yarn production. In addition, reactor temperature of 1000ºC seems to be too high for production of yarn resulting in destruction of the CNTs [18]. This pattern was also observed by other researchers [19]. Edzatty et al. (2016) studied the effect of different reactor temperature (700 to 900ºC) on the production of carbon nanomaterial and found the best temperature to be 800ºC.

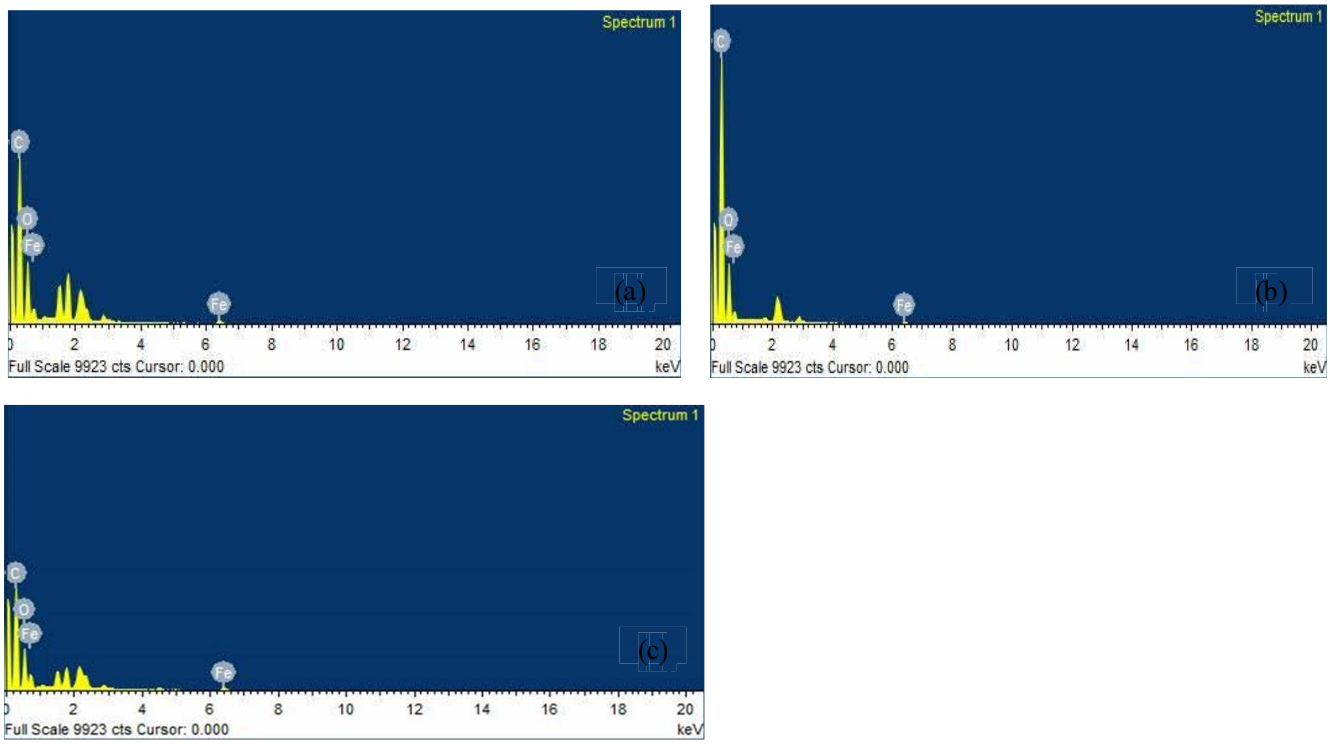

Figure 3: Energy Dispersive X-ray (EDX) of CNT yarn produced at reactor temperature of (a) 900ºC (b) 950ºC (c) 1000ºC

Figure 4 depicts the Raman Spectra of CNT yarn produced at reactor temperature of 900ºC, 950 and 1000ºC. The Raman spectra revolves around assigning, the G-band (between 1579 cm^{-1} and 1581 cm^{-1}) which represents graphitisation degree of CNT yarn, and the D-band (between 1100 to 1500 cm^{-1}) which shows the structural defects of CNT yarn [20]. Figure 4 shows the D-band and G-band at 1300 cm^{-1} and 1590 cm^{-1}, respectively. The I_D/I_G ratio represents the relative intensity of deformation and graphitisation of the CNT yarn [21]. As indicated in Table 1, CNT yarn produced at reactor temperature of 900ºC, 950ºC and 1000ºC have a ratio of 0.36, 0.18 and 0.29, respectively. These values indicate that the CNT yarn maintains a remarkable crystallinity structure as the reactor temperature increases from 900 to 950ºC then the crystallinity gets slightly deformed when the temperature increased further to 1000ºC.

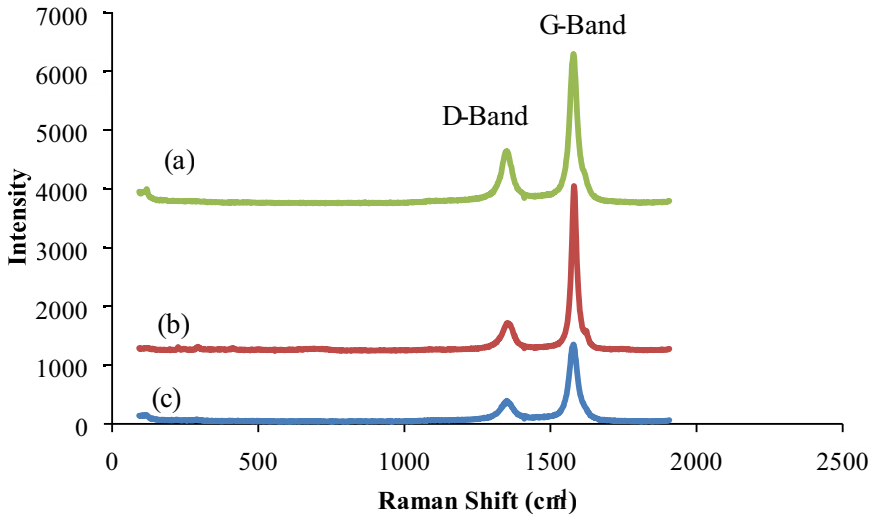

Figure 4: Raman shift of CNTs yarn produced at (a) 900°C; (b) 950°C and (c) 1000°C.

Table 1: ID/IG ratio of CNT yarn produced at 900°C, 950°C and 1000°C.

Graph	Reactor Temperature [°C]	ID/IG
(a)	900	0.36
(b)	950	0.18
(c)	1000	0.29

3.2 Thermophysical quantities of CNT yarn

Figure 5 represented TGA/DSC curve for CNT yarn produced at best reactor temperature (950°C). From the graph shown in Figure 5, the area of weight stability was identified i.e. where no phase change, decomposition or association occurred. Yarn produced at reactor temperature of 950°C is thermally stable at temperatures between 200°C and 330°C as depicted in Figure 5. The thermal stability of the samples was determined based on the weight % curve. The corresponding heat flow of the sample at thermal stable state was used to determine heat capacities of the sample [22,23,24]. Equation (2) was used to calculate heat capacities of yarns based on the heat flow of yarn at their thermal stable state. Figure 6 represents the heat capacities of yarn produced at reactor temperature of 950°C

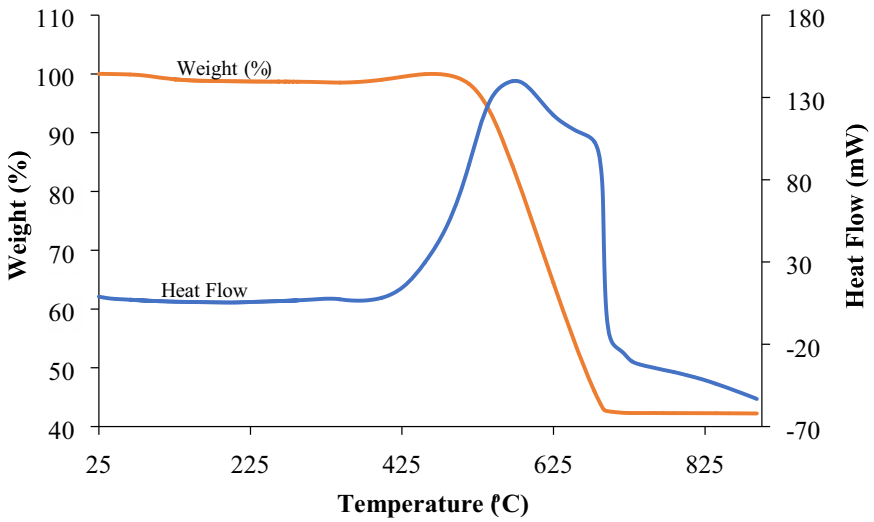

Figure 5: TGA curve of CNT yarn produced at 950°C

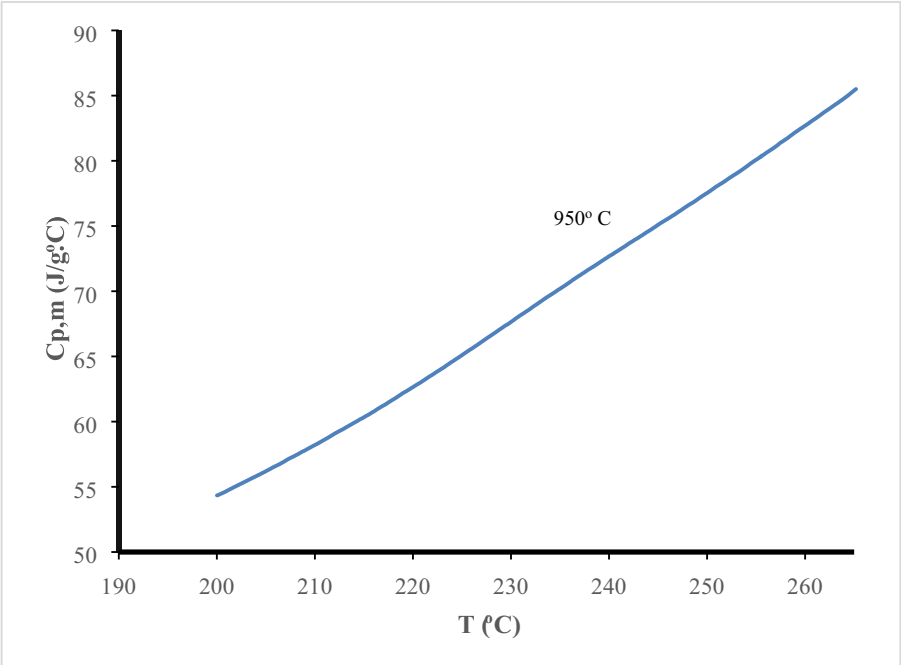

Figure 6: Heat capacities of yarn produced at 950°C

Analysis from Figure 6 indicates that heat capacities of the sample increase with the increase in experimental temperature. At the stable DSC temperature of the yarn, a polynomial equation of specific heat capacities was obtained using Least Square Estimation method. Equation (5) was

obtained as polynomial model to predict the heat capacities of CNT yarn that is produced at reactor temperature of 950ºC.

$$C_{p,m}[J.\ g^{-1}°C^{-1}] = 0.002T^2 - 0.4512T + 66.099 \quad (5)$$

Equation (5) was used to determine smoothed specific heat capacities of yarn produced at reactor temperature of 950ºC. At DSC temperature of 200ºC, the specific heat capacity of yarn was found to be 55 .9 J/ºC.g which is higher than the specific heat capacity of both MWCNTs and SWCNTs which were reported to be 1.1852 J/K.g [25] and 1.02 J/K.g [26], respectively. The heat capacities of yarn and CNTs are expected to be different because of their difference in diameter and purity. From the calculated specific heat capacities, thermodynamic function such as change in Entropy (ΔS) and Change in Enthalpy (ΔH) was determined and shown in Figure 7. Change in entropy increases with the increase in temperature, indicating the degree of disorder of material increases with temperature. Change in enthalpy increased with the increase in temperature, indicating the heat content of material increased with increase in temperature. This behaviour is in agreement with other studies for CNTs [11; 25].

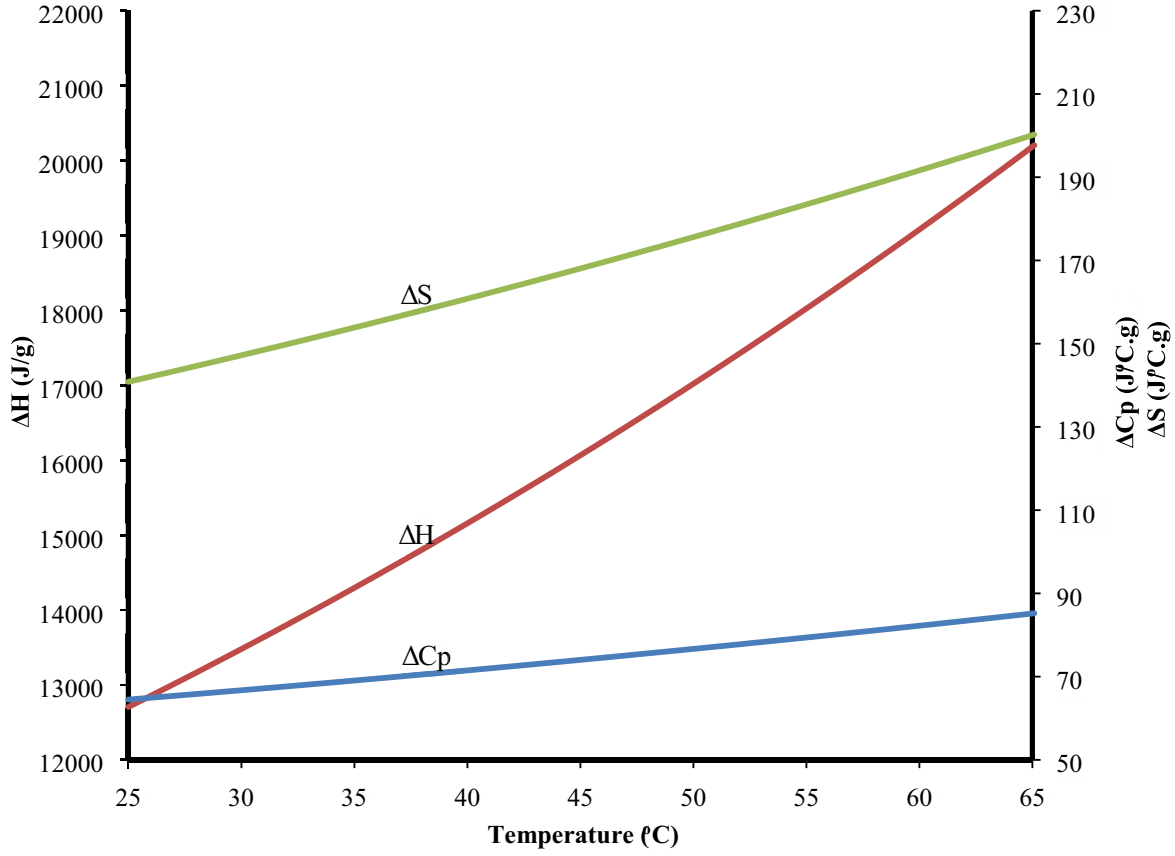

Figure 7: Thermodynamic property of CNT yarns and calculated heat capacities

4. Conclusion

CNT yarn was successfully produced using direct spinning method at reactor temperatures of 900^{o}C, 950^{o}C and 1000^{o}C. The SEM micrographs revealed that yarn produced at 950^{o}C has high degree of CNT alignment as compared to the yarn produced at reactor temperature of 900^{o}C or 1000^{o}C. Since the reactor temperature of 950^{o}C yields yarn with good qualities, their thermodynamic properties were studied in this article. The TGA curve of the CNT yarn show that the yarn was stable at a TGA experimental temperature range of 200 and 330^{o}C. The heat flow of sample at thermal stable state was used to calculate the heat capacities of the sample. The heat capacities of CNT yarn increase with the increase in experimental temperature. The function of heat capacities with respect to the experimental temperature was developed. Thermodynamic functions such as change in entropy and change in enthalpy of the best as-produced yarn were derived based on the established heat capacity equation. Further studies should consider thorough studies on CNT yarn purification and results obtained thereof should be compared with the as-produced yarn.

Acknowledgements

The authors are grateful to NRF for its financial support through the grant number NRF-CPRR106053.

Reference

[1] A Iijima, S. (1991). Helical microtubules of graphitic carbon. *Nature*, 354(6348), 56.
[2] Jiang, Kaili, Qunqing Li, and Shoushan Fan. "Nanotechnology: Spinning continuous carbon nanotube yarns." Nature 419.6909 (2002): 801.
[3] Dalton, A. B., Collins, S., Munoz, E., Razal, J. M., Ebron, V. H., Ferraris, J. P., Coleman, J.N., Kim, B.G. & Baughman, R. H. (2003). Super-tough carbon-nanotube fibres. Nature, 423(6941), 703.
[4] Aliev, A. E., Oh, J., Kozlov, M. E., Kuznetsov, A. A., Fang, S., Fonseca, A. F., ... & Zhang, M. (2009). Giant-stroke, superelastic carbon nanotube aerogel muscles. Science, 323(5921), 1575-1578.
[5] Jeon, I., Matsuo, Y., & Maruyama, S. (2018). Single-walled carbon nanotubes in solar cells. Topics in Current Chemistry, 376(1), 4.
[6] Vigolo, B. (2000). Macroscopic Fibers and Ribbons of Oriented Carbon Nanotubes. Science, 290(5495), 1331-1334.
[7] Li, Y. (2004). Direct Spinning of Carbon Nanotube Fibers from Chemical Vapor Deposition Synthesis. Science, 304(5668), 276-278.
[8] Zhang, M. (2004). Multifunctional Carbon Nanotube Yarns by Downsizing an Ancient Technology. Science, 306(5700), 1358-1361.
[9] Ericson, L. M. (2004). Macroscopic, Neat, Single-Walled Carbon Nanotube Fibers. Science, 305(5689), 1447-1450.
[10] Koziol, K., Vilatela, J., Moisala, A., Motta, M., Cunniff, P., Sennett, M., & Windle, A. (2007). High-performance carbon nanotube fiber. Science, 318(5858), 1892-1895.
[11] Nan, Z., Wei, C., Yang, Q., & Tan, Z. (2009). Thermodynamic properties of carbon nanotubes. Journal of Chemical & Engineering Data, 54(4), 1367-1370.
[12] Muratov, V. B., Vasil'ev, O. O., Kulikov, L. M., Garbuz, V. V., Nesterenko, Y. V., & Duda, T. I. (2012). Thermodynamic properties of multiwalled carbon nanotubes. Journal

of Superhard Materials, 34(3), 173-178.
[13] Bodiba, V., Igbokwe, E., Mahangani, N., Aberefa, O., Daramola, M. O., & Iyuke, S. E. (2018, September). Production of CNT yarns for use as filaments in incandescent bulb: effect of carbon source and state of catalyst on production of CNT. In IOP Conference Series: *Materials Science and Engineering* (Vol. 413, No. 1, p. 012027).
[14] Perry, R. H. & Green, D. W. (1984). Perry's Chemical engineers' handbook. Japan: *McGraw-Hill*.
[15] Aberefa, O., Bedasie, K., Madhi, S., Daramola, M. O., & Iyuke, S. E. (2018). Production of carbon nanotube yarn from swirled floating catalyst chemical vapour deposition: a preliminary study. *Advances in Natural Sciences: Nanoscience and Nanotechnology*, 9(3), 035009.
[16] Iyuke, S. E., & Simate, G. S. (2011). Synthesis of carbon nanomaterials in a swirled floating catalytic chemical vapour deposition reactor for continuous and large-scale production. In *Carbon Nanotubes-Growth and Applications*. InTech.
[17] Muataz, A. A., Ahmadun, F., Guan, C., Mahdi, E., & Rinaldi, A. (2006). Effect of reaction temperature on the production of carbon nanotubes. *Nano*, 1(03), 251-257.
[18] Khavarian, M., Chai, S.P., Tan, S.H., & Mohamed, A.R. (2011). Effect of Different Parameters on the Morphology of Carbon Nanotubes Structures Grown by Floating Catalyst Method. *Journal of Applied Sciences*, 11: 2382-2387.
[19] Edzatty, A. N., Syazwan, S. M., Norzilah, A. H., & Jamaludin, S. B. (2016, July). Effect of reactor temperature on direct growth of carbon nanomaterials on stainless steel. In *AIP Conference Proceedings* (Vol. 1756, No. 1, p. 090003). AIP Publishing.
[20] Potgieter‐Vermaak, S., Maledi, N., Wagner, N., Van Heerden, J. H. P., Van Grieken, R., & Potgieter, J. H. (2011). Raman spectroscopy for the analysis of coal: a review. *Journal of Raman Spectroscopy*, 42(2), 123-129.
[21] Tsoufis, T., Xidas, P., Jankovic, L., Gournis, D., Saranti, A., Bakas, T., & Karakassides, M. A. (2007). Catalytic production of carbon nanotubes over Fe–Ni bimetallic catalysts supported on MgO. *Diamond and Related Materials*, 16(1), 155-160.
[22] Harabor, A., Rotaru, P., & Harabor, N. A. (2013). Thermal and spectral behavior of (Y, Eu) VO4 powder. *Journal of Thermal Analysis and Calorimetry*, 111(2), 1211-1219.
[23] Degeratu, S., Rotaru, P., Manolea, G., Manolea, H., & Rotaru, A. (2009). Thermal characteristics of Ni–Ti SMA (shape memory alloy) actuators. *Journal of Thermal Analysis and Calorimetry*, 97(2), 695-700.
[24] Morîntale, E., & Harabou, A. (2013). Use of heat flows from DSC curve for calculation of specific heat of the solid materials. *Physics AUC*, 23, 89-94.
[25] Kabo, G. J., Paulechka, E., Blokhin, A. V., Voitkevich, O. V., Liavitskaya, T., & Kabo, A. G. (2016). Thermodynamic properties and similarity of stacked-cup multiwall carbon nanotubes and graphite. *Journal of Chemical & Engineering Data*, 61(11), 3849-3857.
[26] Pradhan, N. R., Duan, H., Liang, J., & Iannacchione, G. S. (2009). The specific heat and effective thermal conductivity of composites containing single-wall and multi-wall carbon nanotubes. *Nanotechnology*, 20(24), 245705.